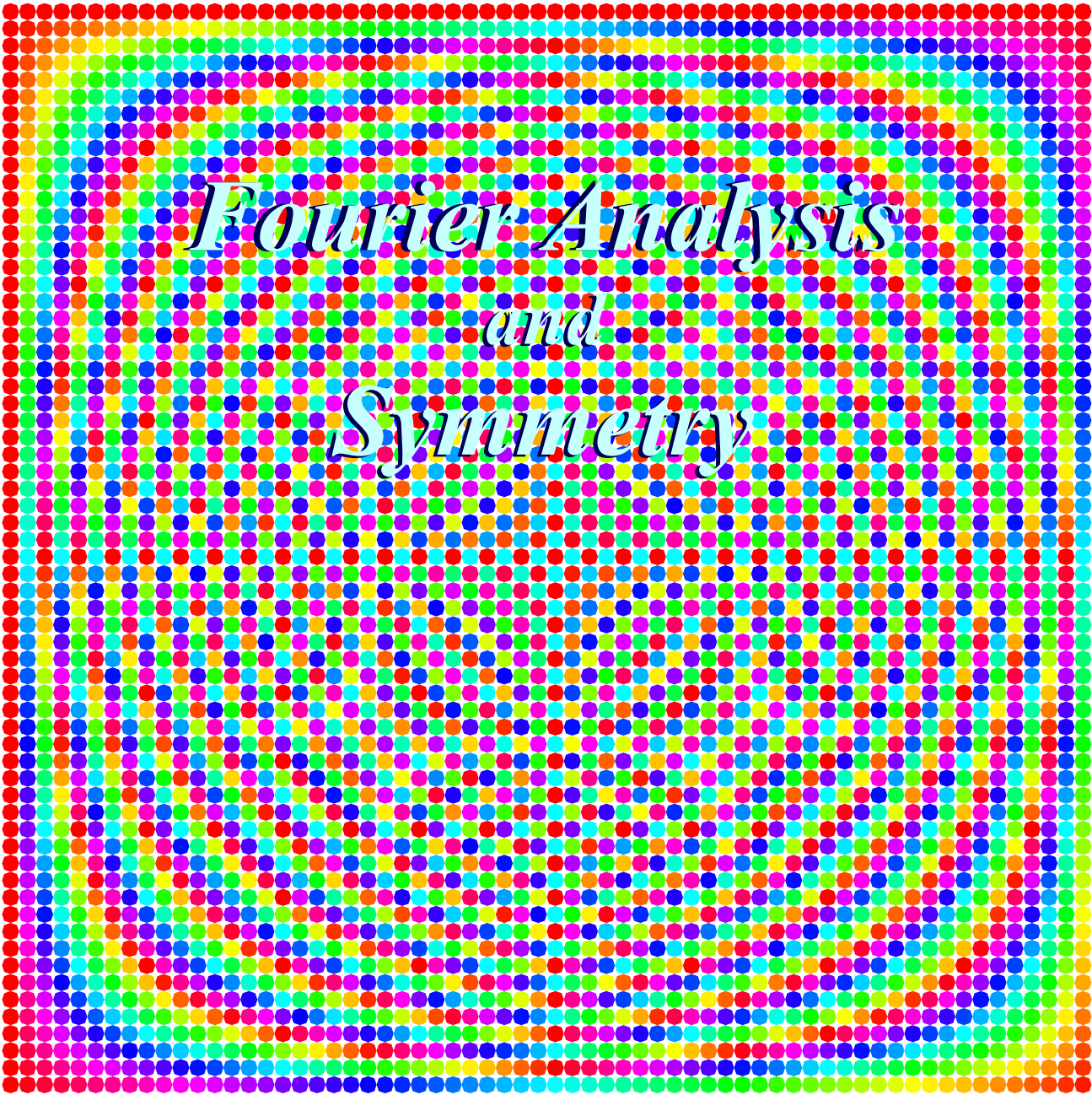# Quantum Theory for the Computer Age
Unit 3

Fourier Analysis
and
Symmetry

Unit 3 Fourier Analysis and Symmetry

Unit 2 discussed quantum $e^{i(k \cdot r - \omega t)}$-wave propagation in space and time and introduced wavevector and frequency ($c\mathbf{k},\omega$)-space while deriving the basic Einstein relativistic transformations and Planck-deBroglie quantum relations. But, what are $e^{i(k \cdot r - \omega t)}$-waves? One answer comes from understanding relations between space-time ($\mathbf{x},ct$) and ($c\mathbf{k},\omega$)-space known as Fourier transformations. Unit 3 begins with discussions of Fourier $\langle ⊠ | ⊠ \rangle$ transformation matrices and shows their connection to translational symmetry. This with Planck's axiom gives the quantum equation of motion known as Schodinger's time equation, the evolution operator, and its generator, the quantum Hamiltonain operator, the *sine qua non* of Schrodinger theory. Unit 3 continues with a detailed description of quantum beats and revivals using symmetry analysis. The final chapter describes 2-state and spin-1/2 systems while introducing U(2) symmetry analysis.
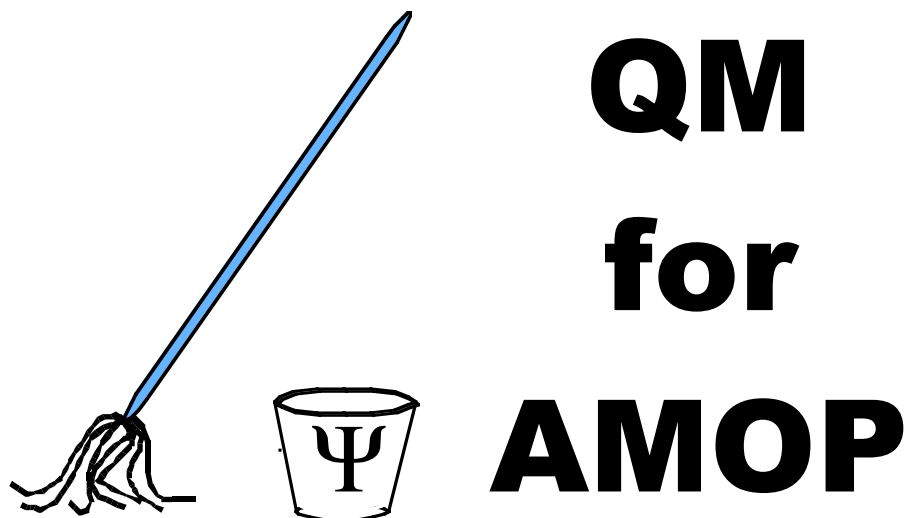
W. G. Harter

Department of Physics
University of Arkansas
Fayetteville

Unit 3 Fourier Analysis and Symmetry

QM
for
AMOP

Chapter 7
Fourier Transformation Matrices

W. G. Harter

REVIEW TOPICS & FORMULAS FOR UNIT 3 ....**34**

Expressing arbitrary wavefunctions or states in terms of spectral components or plane waves is known as Fourier analysis. Fourier transformation matrices relate space and time (coordinate) bases to wavevector and frequency (Energy-momentum) bases of plane waves. Fourier analysis comes in different flavors depending on whether various bases are discretely numbered or continuous. Chapter 7 compares the continuous coordinate bases of Bohr rotor states to the fully continuous plane wave states of an unbounded continuum. Then a discrete "quantum-dot" sytsem is introduced in which both coordinates and wavevectors are discrete. The later is the basis for the introduction of Fourier symmetry analysis in the following Chapter 8 and time evolution in Chapter 9. Discrete symmetry in space and time helps to clarify quantum beats and "revivals" which all quantum systems will exhibit to some degree.

Unit 3 Fourier Analysis and Symmetry

Chapter 7. Fourier Transformation Matrices

We have noted that a quantum experiment cannot move at all unless two or more frequency components can interfere with each other. A single (mono-chromatic) wave $\Psi = \psi e^{-i\omega t}$ is not enough to make anything happen. Such a Ψ-system is a stationary state and appears to be dead. What we can observe is determined by the absolute square $\Psi^*\Psi$, which kills the single oscillating phase.

Similarly, a wave $\Psi = \psi e^{ikx}$ with a single momentum component appears to be a uniform cloud of random counts in space. To obtain any structure in the quantum world, that is, atoms, molecules, solids, people, and so forth, we need *many* momentum components in our matter waves.

The mathematics used to deal with multiple frequency or momentum components is called *Fourier analysis* after Jean Baptiste Fourier, a French artillery officer turned mathematician. This section will review the fundamentals of Fourier theory relevant to quantum theory using the Dirac notation. Fourier analysis has several flavors depending on whether its coordinates and parameters, that is space-time and wavevector-frquency are discrete or continuous and whether x or k are bounded or unbounded. We consider several distinct cases in turn. Each has different forms for its completeness and orthonormality axioms-3 to 4.

7.1 Continuous but bounded x. Discrete but unbounded k

One of the most famous and widely used wavefunction systems in quantum theory are the one-dimensional (1-D) *Bohr orbitals* $\psi_k(x) = \langle x \mid k \rangle$. Examples are sketched in Fig. 7.1.1.

$$\psi_{k_m}(x) = \langle x|k_m \rangle = \frac{e^{ik_m x}}{\sqrt{norm.}} = \psi_{k_m}(x+L) \tag{7.1.1}$$

These can be thought of as a set of waves on a ring of circumference L. The basic waves have just the right wavevectors k_m to put integral numbers of whole wavelengths along L and thereby repeat the wave again after each complete L-revolution. Such requirements are known as *periodic boundary conditions*.

$$\psi_{k_m}(x) = \psi_{k_m}(x+L) = \frac{e^{ik_m x}}{\sqrt{norm.}} = \frac{e^{ik_m(x+L)}}{\sqrt{norm.}} = \psi_{k_m}(x)e^{ik_m L} \tag{7.1.2}$$

The boundary conditions lead to wavevector *quantization conditions*.

$$e^{ik_m L} = 1, \text{ or: } k_m = \frac{2\pi}{L}m, \text{ where: } m = 0, \pm 1, \pm 2, \pm 3, \dots \pm \infty \tag{7.1.3}$$

The allowed wavevectors, while still infinite in number, are forced to be *discrete*.

This is a very common feature of quantum theory for which it owes its name *quantum*, but it happens to classical waves, too. A bounded continuum leads to an unbounded but discrete set of allowed waves. For another example, cavity modes in the Hall of Mirrors in Sec. 6.3 (d) acquire discrete frequencies as soon as the doors are shut. If an indiscrete type of wave is put in a cage, then it is forced to be discrete. (Perhaps, this is just another sad anthropomorphic metaphor.)
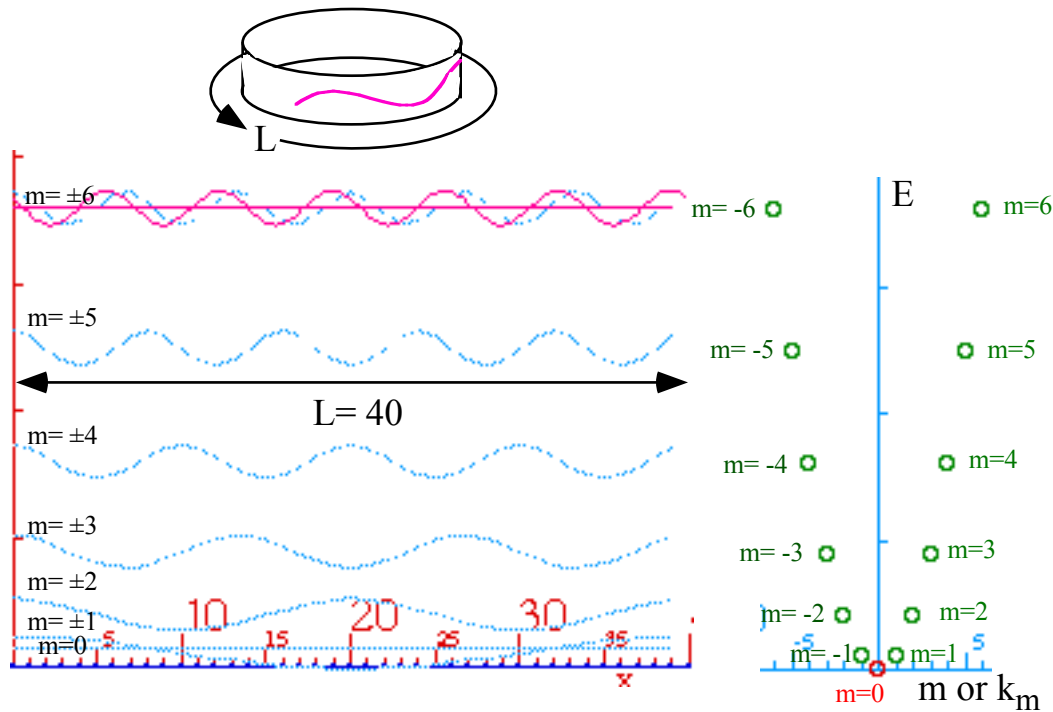
Fig. 7.1.1 Sketches of Bohr orbitals confined to 1-D L-interval and quantum energies (for m=0 to 6).

The resulting amplitudes must satisfy Axioms 1-4. In particular, the orthonormality axiom-3 requires $\langle k_1|$ $k_1\rangle=1$ but $\langle k_1| k_2\rangle =0$, and so forth, or that the following Kronecker delta representation.

$$\langle k_m| k_n\rangle=\delta_{m\,n} \qquad (7.1.4a)$$

Completeness axiom-4 requires that $| k_n\rangle \langle k_n|$ sum up to a unit operator or an *x*-Dirac-delta expression.

$$\Sigma| k_n\rangle \langle k_n| =\mathbf{1}, \text{ or:} \qquad \Sigma\langle x | k_n\rangle \langle k_n| x'\rangle = \langle x | x'\rangle=\delta(x\text{-}x'). \qquad (7.1.4b)$$

(a) Orthonormality axiom-3

Using the integral form (2.1.2) of the completeness relation sum we get the following.

$$\delta_{mn} = \langle k_m|k_n\rangle= \int_{-L/2}^{L/2} dx \langle k_m|x\rangle\langle x|k_n\rangle= \int_{-L/2}^{L/2} dx \frac{e^{-ik_m x}}{\sqrt{norm.}} \frac{e^{ik_n x}}{\sqrt{norm.}} \qquad (7.1.5)$$

The conjugation axiom-2 was used to write

$$\langle k_m|x\rangle = \langle x|k_m\rangle^* = \frac{e^{-ik_m x}}{\sqrt{norm.}} \qquad (7.1.6)$$

After integrating, this determines the *normalization constant norm.* as follows.

$$\delta_{mn} = \int_{-L/2}^{L/2} dx \frac{e^{-ik_m x}}{\sqrt{norm.}} \frac{e^{ik_n x}}{\sqrt{norm.}} = \int_{-L/2}^{L/2} dx \frac{e^{-i(k_m-k_n)x}}{norm.} = \frac{e^{-i(k_m-k_n)x}}{-i(k_m-k_n)norm.}\Bigg|_{-L/2}^{L/2}$$

$$= \frac{e^{-i(k_m-k_n)L/2} - e^{i(k_m-k_n)L/2}}{-i(k_m-k_n)norm.} = \frac{2\sin\left[(k_m-k_n)L/2\right]}{(k_m-k_n)norm.} \qquad (7.1.8)$$

Using the quantization conditions (7.1.3) gives the desired *norm.* value and satisfies axiom-3.

$$\delta_{mn} = \frac{2\sin\pi(m-n)}{\frac{2\pi}{L}(m-n)\,norm.} = \begin{cases} 0 \;\; if\!:\; m \neq n \\ \dfrac{L}{norm.} \;\; if\!:\; m = n \end{cases} , \;\; or\!:\; norm. = L. \qquad (7.1.9)$$

Normalized wave amplitudes are therefore

$$\psi_{k_m}(x) = \langle x|k_m\rangle = \frac{e^{ik_m x}}{\sqrt{L}} \; . \qquad (7.1.10)$$

(b) Completeness axiom-4

Completeness axiom-4 has a Dirac-delta form in the mixed discrete-continuous wave space.

$$\delta(x-x') = \sum_{m=-\infty}^{m=+\infty} \langle x|k_m\rangle\langle k_m|x'\rangle \qquad (7.1.11)$$

We test it with amplitudes (7.1.10) using orthonormality (7.1.4) and conjugation (7.1.5).

$$\int_{-L/2}^{L/2} dx\,\delta(x-x') = \int_{-L/2}^{L/2} dx \sum_{n=-\infty}^{n=+\infty} \frac{e^{ik_n x}}{\sqrt{L}}\frac{e^{-ik_n x'}}{\sqrt{L}} = \sum_{n=-\infty}^{n=+\infty} \frac{e^{-ik_n x'}}{\sqrt{L}} \int_{-L/2}^{L/2} dx\,\frac{e^{ik_n x}}{\sqrt{L}} \qquad (7.1.12)$$

The last integral is a representation of a Kronecker delta $\delta_{0,n}$. Recall that $k_0 = 0$ and use (7.1.4).

$$\int_{-L/2}^{L/2} dx\,\frac{e^{ik_n x}}{\sqrt{L}} = \sqrt{L}\int_{-L/2}^{L/2} dx\,\frac{e^{-ik_0 x}}{\sqrt{L}}\frac{e^{ik_n x}}{\sqrt{L}} = \sqrt{L}\,\langle k_0|k_n\rangle = \sqrt{L}\delta_{0\,n}$$

$$\int_{-L/2}^{L/2} dx\,e^{ik_n x} = L\delta_{0\,n}\;. \qquad (7.1.13)$$

Then (7.1.12) is consistent with (7.1.11) and (7.1.10) and the definition of Dirac's delta.

$$\int_{-L/2}^{L/2} dx\,\delta(x-x') = \int_{-L/2}^{L/2} dx \sum_{n=-\infty}^{n=+\infty} \frac{e^{ik_n x}}{\sqrt{L}}\frac{e^{-ik_n x'}}{\sqrt{L}} = \sum_{n=-\infty}^{n=+\infty} e^{-ik_n x'}\delta_{0\,n} = e^{-ik_0 x'} = 1 \qquad (7.1.14)$$

(c) Fourier series representation of a state

With completeness one can quickly derive a representation of arbitrary state $|\Psi\rangle$ if you know its complex wavefunction $\Psi(x) = \langle x|\Psi\rangle$. Formally, you just operate on $|\Psi\rangle$ with the unit $\mathbf{1} = \Sigma|k_m\rangle\langle k_m|$.

$$\langle x|\Psi\rangle = \sum_{m=-\infty}^{m=+\infty} \langle x|k_m\rangle\langle k_m|\Psi\rangle = \sum_{m=-\infty}^{m=+\infty} \frac{e^{ik_m x}}{\sqrt{L}}\langle k_m|\Psi\rangle$$

$$= \sum_{m=-\infty}^{m=+\infty} e^{ik_m x}\,\Psi_m \qquad (7.1.15a)$$

where the Fourier coefficient Ψ_m is given by the following integral (Use x-completeness $\mathbf{1} = \int dx|x\rangle\langle x|$.)

$$\Psi_m = \frac{\langle k_m|\Psi\rangle}{\sqrt{L}} = \frac{1}{\sqrt{L}}\int_{-L/2}^{L/2} dx\,\langle k_m|x\rangle\langle x|\Psi\rangle = \frac{1}{\sqrt{L}}\int_{-L/2}^{L/2} dx\,\frac{e^{-ik_m x}}{\sqrt{L}}\langle x|\Psi\rangle$$

$$= \frac{1}{L}\int_{-L/2}^{L/2} dx\,e^{-ik_m x}\,\Psi(x) \qquad (7.1.15b)$$

The only requirement is that the function be *periodic* in L, that is, $\Psi(x) = \Psi(x+L)$.

(d) Bohr dispersion relation and energies

In Fig. 7.1.1 the waves with higher k_m have higher energy E_m and are drawn higher according to the E-values given by the *Bohr dispersion function* first drawn in Fig. 5.6.3.

$$E_m = \hbar\omega_m = \frac{(\hbar k_m)^2}{2M} \text{ , where: } p_m = \hbar k_m = \hbar\frac{2\pi}{L}m \text{ .} \qquad (7.1.16)$$

This is just a non-relativistic approximation for energy that neglects the rest energy Mc^2 and higher order terms in (5.2.5b). It is kinetic energy only, that is $KE = \frac{1}{2}Mu^2 = p^2/2M$ with the momentum $p=p_m$ and wavevector $k=k_m$ quantized by conditions (7.1.3). The dispersion function is then a simple parabola of discrete values as shown on the right hand side of Fig. 7.1.1. Note that each energy value E_m , except E_0, has two orthogonal wavefunctions $\psi_{\pm km}$ or states $|\pm k_m\rangle$ corresponding to pairs of oppositely moving wavevectors $\pm k_m$ on either side of the dispersion parabola. The $|\pm k_m\rangle$ are called *degenerate states* because they share a single energy E_m. Such degenerate pairs are each an example of a U(2) two-state system. As long as the degeneracy remains, any unitary linear combination of the two states is also an eigenstate with the same frequency and energy $E=h\nu$.

(e) Sine and cosine Fourier series worth remembering

A function defined by Fourier series (7.1.15) repeats after its fundamental wavelength $L=2\pi/k_1$ or period $T=2\pi/\omega_1$. So do the real and imaginary parts that are series of sine or cosine functions of mth spatial overtone argument $k_m x$ or m^{th} overtone frequency argument $\omega_m t$. Moving wave terms use both: $(k_m x - \omega_m t)$.

Let us consider wave functions with *zero-DC-bias* or zero *(k=0)*-Fourier component: $0=\Psi_0=\int\Psi$. The integrals and derivatives of unbiased functions may also be unbiased. An example of a series of unbiased functions starts with the *alternating Dirac delta function adel(x)* shown at the top of Fig. 7.1.2. Its integrals and derivatives are useful series worth remembering because they are easy to compute and visualize. Compare this function to the simple delta pulse train (5.3.2) shown in Fig. 5.3.2.

The first integral of *adel(x)* is a *square wave* function *box(x)* shown next in line in Fig. 7.1.2. Below it is a *saw-tooth* wave *saw(x)* and then a *parabolic amplitude* wave *paw(x)*. Each wave has an overall scale factor attached so plots that are not delta-like end up with comparable amplitudes.

Wave *paw(x)* looks like a sine wave but isn't quite. The derivative of a genuine sine wave is a cosine wave that looks just like a sine wave but is moved back by $\pi/2$. The derivative of *paw(x)* is *saw(x)*, which is moved back, but it looks nothing like good old *paw(x)*! Subsequent derivatives only accentuate the differences between *sin(x)* and *paw(x)*. Differentiation amplifies little blips or bends (It differentiates!) while integration does the opposite by smoothing out sharp corners or other differences.

There are at least two famous physics topics that make use of functions that are derivatives or integrals of each other. Classical mechanics in one dimension is one such topic where the functions of *acceleration a(t)*, *velocity v(t)*, and *position x(t)*, are each the integral of one above or the derivative of the one below. Classical electrostatics is another topic in which the *charge-density* $\rho(x)$, *electric field E(x)*, and *potential* $\Phi(x)$, are so related. (Various conventions may put $\pm$signs and scale factors onto these relations.)

$$y = \frac{1}{10}\left(\cos x + \frac{1}{1}\cos 3x + \frac{1}{1}\cos 5x + \frac{1}{1}\cos 7x + \frac{1}{1}\cos 9x + \frac{1}{1}\cos 11x \cdots \quad + \frac{1}{1}\cos 23x + \frac{1}{1}\cos 25x\right)$$

adel(x)

$$y = \frac{\sqrt{\pi}}{\sqrt{2}}\left(\sin x + \frac{1}{3}\sin 3x + \frac{1}{5}\sin 5x + \frac{1}{7}\sin 7x + \frac{1}{9}\sin 9x + \frac{1}{11}\sin 11x \quad + \frac{1}{23}\sin 23x + \frac{1}{25}\sin 25x\right)$$

box(x)

$$y = \frac{\sqrt{\pi}}{\sqrt{2}}\left(\cos x + \frac{1}{3^1}\cos 3x + \frac{1}{5^1}\cos 5x + \frac{1}{7^1}\cos 7x + \frac{1}{9^1}\cos 9x + \frac{1}{11^1}\cos 11x + \quad + \frac{1}{23^1}\cos 23x + \frac{1}{25^1}\cos 25x\right)$$

saw(x)

$$y = \frac{\sqrt{\pi}}{\sqrt{2}}\left(\sin x + \frac{1}{3^1}\sin 3x + \frac{1}{5^1}\sin 5x + \frac{1}{7^1}\sin 7x + \frac{1}{9^1}\sin 9x + \frac{1}{11^1}\sin 11x + \quad + \frac{1}{23^1}\sin 23x + \frac{1}{25^1}\sin 25x\right)$$

paw(x)
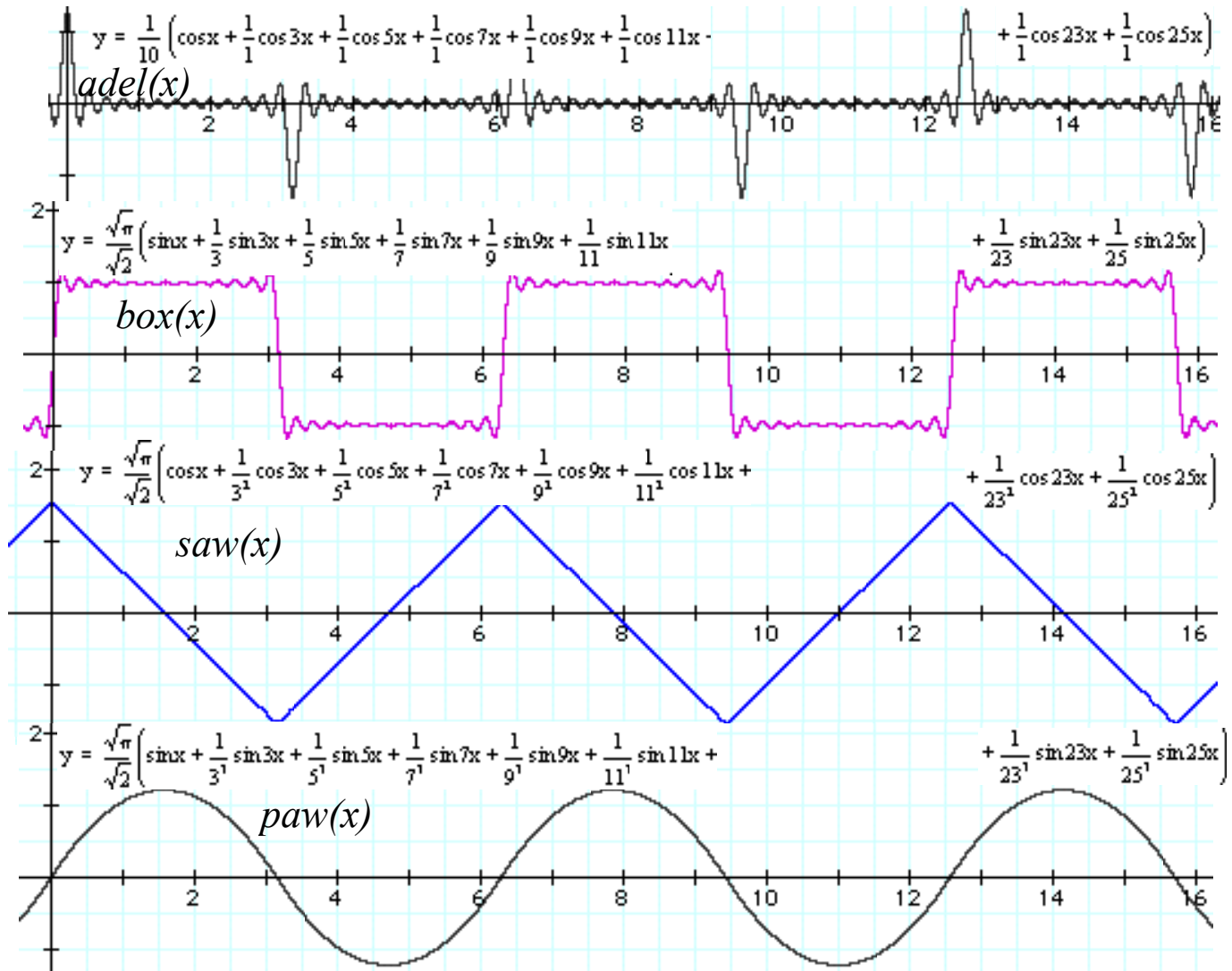
Fig. 7.1.2 Fourier series sharing simple integral or derivative relations to each other.

Some more or less extreme examples of charge and field distributions are sketched in Fig. 7.1.3 on the following page. The first set in Fig. 7.1.3(a) is due to alternating charge layers. The field is that of a series of alternating parallel-plate capacitors. By taking a derivative of the alternating chasrge layers we make the dipole layer distribution shown in the top of the middle Fig. 7.1.3(b). The final example in Fig. 7.1.3(c) actually has a Dirac-delta potential lattice, one of many favorite models for nano science these days. We shall be modeling periodic potentials, too. The preceding gives you some feeling how difficult it may be to actually *produce* some of these exotic potentials! Seldom is theory so easy and the lab so hard.

Also it is worth considering these as time-pulse series. As we will explain later, you may taper the Fourier series amplitudes gradually to zero and thereby replace the sharp and wrinkled deltas and squares by smoother Gauassian or Lorentzian features that are useful spectroscopic models. Of course, you may taper them right back to single term series of one sine or one cosine wave each!

Following page: Fig. 7.1.3 Exotic 1-D electric charge and field distributions.

(a)

**Charge
Density
ρ*(x)***

del(x)

**Electric
Field
E*(x)***

box(x)

Boxcar E-field

**Potential
Φ*(x)***

saw(x)

Sawtooth potenial function

(b) *-(d/dx)del(x)*

**Charge
Density
ρ*(x)***

Dirac-delta derivative (dipole layer lattice)

**Electric
Field
E*(x)***

-dell(x)

Dirac-delta E-field function

**Potential
Φ*(x)***

box(x)

Boxcar Potential field

(c) *-(d/dx)²del(x)*

**Charge
Density
ρ*(x)***

Dirac-delta double derivative (quadrupole layer lattice)

-(d/dx)del(x)

**Electric
Field
E*(x)***

Dirac-delta derivative field lattice

dell(x)

Dirac-delta Potential function

δ(x-π)   δ(x-3π)   δ(x-5π)

−δ(x-0)   −δ(x-2π)   −δ(x-4π)   −δ(x-6π)

7.2 Continuous and unbounded x. Continuous and unbounded k

In the preceding cases all wavevectors are restricted by the quantization condition (7.1.3).

$$k_m = \frac{2\pi}{L} m \, , \text{ where: } m = 0, \pm 1, \pm 2, \pm 3, ... \pm \infty \qquad (7.1.3)_{\text{repeated}}$$

If you let the "cage" become infinitely large ($L \to \infty$) then the wavevector set becomes finer and finer and approaches a *continuum*. The trick is to replace each sum over index *m* by an integral over a continuous *k*-value. If it is done right the wave functions will take a continuous form in *both x and k*.

$$\psi_k(x) = \langle x | k \rangle = \frac{e^{ikx}}{\sqrt{norm.}} \, , \qquad (7.2.1a)$$

We need to verify *k*-orthonormality relations based on wavevector Dirac-delta δ*(k′,k)*-functions.

$$\langle k' | k \rangle = \delta\left(k' - k\right) = \int_{-\infty}^{\infty} dx \langle k' | x \rangle \langle x | k \rangle = \int_{-\infty}^{\infty} dx \, \psi_{k'}(x)^* \psi_k(x) \, , \qquad (7.2.1b)$$

We also need the usual *x*-completeness relations based on spatial Dirac-delta δ*(x′,x)*-functions.

$$\langle x' | x \rangle = \delta\left(x' - x\right) = \int_{-\infty}^{\infty} dk \langle x' | k \rangle \langle k | x \rangle = \int_{-\infty}^{\infty} dk \, \psi_k(x')^* \psi_k(x) \qquad (7.2.1c)$$

It seems that orthonormality and completeness relations are two sides of the same coin. Orthonormality (7.2.1b) for the *k*-states { $|k\rangle...|k'\rangle$..} expresses completeness for the *x*-states $|x\rangle$, and completeness (7.2.1c) of the *k*-states $|k\rangle$ expresses orthonormality for the *x*-states { $|x\rangle...|x'\rangle$..}.

The Dirac notation is extremely efficient but can be confusing. There is a world of difference between the states { $|k\rangle...|k'\rangle$..} of perfectly monochromatic plane waves and the Dirac position states { $|x\rangle...|x'\rangle$..} of perfectly localized particles. Recall that we said that an $|x\rangle$ state was physically unrealizable; crushing a particle into a single position-*x* would cost infinite energy. Technically, a $|k\rangle$ state is unrealizable, too, since it requires an infinite amount of real estate; we have to let its cage dimension *L* be infinite, but that seems easier than the extreme solitary confinement needed to make an $|x\rangle$ state. If space is cheaper than energy, then $|k\rangle$ is easier to approach than $|x\rangle$. Lasers easily make approximate $|k\rangle$'s by being stable and coherent, but producing approximate $|x\rangle$'s for extremely short pulses requires more difficult engineering.

Use caution to not abuse this notation, though it is easily done. It should be obvious why the following rendition of (7.2.1a) is a dreadful mistake.

$$\langle k | k \rangle = \frac{e^{ikk}}{\sqrt{norm.}} = \frac{e^{ik^2}}{\sqrt{norm.}} \qquad \text{(Dirac abuse. Very BAD mistake!)}$$

Letters *x* and *k* denote <u>very</u> different bases which must not to be confused.

(a) Fourier integral transforms

To achieve the limit of infinite real estate ($L \to \infty$) we replace sums over $k_m = \frac{2\pi}{L} m$ such as

$$S = \sum_{m=-\infty}^{m=+\infty} \Phi_{k_m} = \sum_{m=-\infty}^{m=+\infty} \Delta m \, \Phi_{k_m} \, , \text{ where: } \Delta m = 1 \, . \qquad (7.2.2)$$

Integrals over *k* with differential $\Delta k_m = \frac{2\pi}{L} \Delta m = \frac{2\pi}{L} \to dk$ or: $\frac{\Delta m}{\Delta k_m} = \frac{L}{2\pi}$ are used as follows.

$$S = \sum_{m=-\infty}^{m=+\infty} \Delta m\, \Phi_{k\,m} = \sum_{m=-\infty}^{m=+\infty} \frac{\Delta m}{\Delta k_m} \Delta k_m\, \Phi_{k\,m} \quad \text{becomes} \rightarrow \frac{L}{2\pi} \int_{-\infty}^{+\infty} dk \Phi(k) \qquad (7.2.3)$$

This, by itself, blows up as we let ($L \rightarrow \infty$), but so do the normalization denominators $\sqrt{norm.} = \sqrt{L}$, and they cancel. Finally, the Fourier series (7.1.15a) becomes a finite integral.

$$\langle x | \Psi \rangle = \sum_{m=-\infty}^{m=+\infty} \frac{e^{ik\,m^x}}{\sqrt{L}} \langle k_m | \Psi \rangle \quad \text{becomes} \rightarrow \frac{L}{2\pi} \int_{-\infty}^{+\infty} dk \frac{e^{ikx}}{\sqrt{L}} \langle k_m | \Psi \rangle = \int_{-\infty}^{+\infty} dk \frac{e^{ikx}}{\sqrt{2\pi}} \frac{\sqrt{L}}{\sqrt{2\pi}} \langle k_m | \Psi \rangle$$

The trick is to renormalize the k-bases so $\dfrac{\sqrt{L}}{\sqrt{2\pi}} \langle k_m |$ becomes $\rightarrow \langle k |$ letting the L's cancel.

$$\langle x | \Psi \rangle = \int_{-\infty}^{+\infty} dk \frac{e^{ikx}}{\sqrt{2\pi}} \langle k | \Psi \rangle = \int_{-\infty}^{+\infty} dk \langle x | k \rangle \langle k | \Psi \rangle , \qquad (7.2.4a)$$

The newly "normalized" plane wave function $\psi_k(x) = \langle x | k \rangle$ is defined as follows.

$$\langle x | k \rangle = \frac{e^{ikx}}{\sqrt{2\pi}} \qquad (7.2.4b)$$

This $\langle x | k \rangle$ is the *kernal* of a *Fourier integral transform*. An inverse follows by converting (7.1.15b).

$$\frac{\langle k_m | \Psi \rangle}{\sqrt{L}} = \frac{1}{L} \int_{-L/2}^{L/2} dx\, e^{-ik\,m^x} \langle x | \Psi \rangle \quad \text{becomes} \rightarrow \langle k | \Psi \rangle = \frac{\sqrt{L}}{\sqrt{2\pi}} \frac{\sqrt{L}}{L} \int_{-\infty}^{+\infty} dx\, e^{-ikx} \langle x | \Psi \rangle ,$$

$$\langle k | \Psi \rangle = \int_{-\infty}^{+\infty} dx \frac{e^{-ikx}}{\sqrt{2\pi}} \langle x | \Psi \rangle = \int_{-\infty}^{+\infty} dx \langle k | x \rangle \langle x | \Psi \rangle , \qquad (7.2.4c)$$

Here the *inverse kernal* $\langle k | x \rangle$ is simply the conjugate of $\langle x | k \rangle$ as required by conjugation axiom-2.

$$\langle k | x \rangle = \frac{e^{-ikx}}{\sqrt{2\pi}} = \langle x | k \rangle^* . \qquad (7.2.4d)$$

(b) Fourier coefficients: Their many names

The efficiency of the Dirac notation (provided it isn't abused!) should be clear by now. The simple bra-ket $\langle x | k \rangle$ stands for so many different mathematical and physical objects. Let's list some.

(1) $\langle x | k \rangle$ is a *scalar product* of bra $\langle x |$ and ket $| k \rangle$

(2) $\langle x | k \rangle$ is an *x-wavefunction* for a state $| k \rangle$ of definite momentum $p = \hbar k$.

(3) $\langle k | x \rangle = \langle x | k \rangle^*$ is an *k-wavefunction* for a state $| x \rangle$ of definite position x .

(4) $\langle x | k \rangle$ is a unitary *transformation matrix* from position states to momentum states.

(5) $\langle x | k \rangle$ is the *kernal* of a Fourier transform between position states and momentum states.

As beautiful and compact as it is, the continuum functional Fourier analysis is merely an infinite and unbounded abstraction that lets us use calculus to derive formulas in special cases. Its validity as a limiting case for experimental and numerical analysis should always be questioned. Laboratory and computer experiments, on the other hand, invariably deal with finite and bounded spaces, and it these that we turn to in the next section. We finish this section by relating square-wave Fourier transforms to square-wave Fourier series of the preceding section to help clarify discrete-*vs.*-continuum relations.

(c) Time: Fourier transforms worth remembering

Fourier time-frequency (time-per-time) transforms resemble space-k-vector (space-per-space) transforms (7.2.4). But, a negative sign is put in the exponent so the time phasor turns clockwise.

$$\langle t \mid \Psi \rangle = \int_{-\infty}^{+\infty} d\omega \frac{e^{-i\omega t}}{\sqrt{2\pi}} \langle \omega | \Psi \rangle = \int_{-\infty}^{+\infty} d\omega \langle x | \omega \rangle \langle \omega | \Psi \rangle \qquad (7.2.5a) \qquad\qquad \langle t | \omega \rangle = \frac{e^{-i\omega t}}{\sqrt{2\pi}} \ (7.2.5b)$$

$$\langle \omega | \Psi \rangle = \int_{-\infty}^{+\infty} dt \frac{e^{i\omega t}}{\sqrt{2\pi}} \langle t | \Psi \rangle = \int_{-\infty}^{+\infty} dt \langle \omega | t \rangle \langle t | \Psi \rangle \qquad (7.2.5c) \qquad\qquad \langle \omega | t \rangle = \frac{e^{i\omega t}}{\sqrt{2\pi}} = \langle t | \omega \rangle^*$$

Consider, for example, a single square bump of amplitude B and duration $T/2$. Its Fourier transform (7.2.5c) is an *elementary diffraction function sin ω/ω* that is plotted in Fig. 7.2.1.

$$\langle \omega | \Psi \rangle = \int_{-T/4}^{+T/4} dt \frac{e^{i\omega t}}{\sqrt{2\pi}} B = B \frac{e^{i\omega T/4} - e^{-i\omega T/4}}{i\omega\sqrt{2\pi}} = \frac{2B\sin(\omega T/4)}{\omega\sqrt{2\pi}} \qquad (7.2.6)$$

It is the first approximation to an optical diffraction function for a single square aperture.

The Fourier amplitude due to multiple square humps is a combination of finer and finer elementary diffraction patterns. Three half-humps give the following frequency function plotted in Fig. 7.2.2(a).

$$\langle \omega | \Psi \rangle = \frac{1}{\sqrt{2\pi}} \left[A \int_{-3T/4}^{-T/4} dt\, e^{i\omega t} + B \int_{-T/4}^{+T/4} dt\, e^{i\omega t} + A \int_{+T/4}^{+3T/4} dt\, e^{i\omega t} \right]$$

$$= A \frac{e^{-i\omega T/4} - e^{i3\omega T/4}}{i\omega\sqrt{2\pi}} + B \frac{e^{i\omega T/4} - e^{-i\omega T/4}}{i\omega\sqrt{2\pi}} + A \frac{e^{i3\omega T/4} - e^{i\omega T/4}}{i\omega\sqrt{2\pi}} \qquad (7.2.7)$$

$$= \frac{2(B-A)\sin(\omega T/4)}{\omega\sqrt{2\pi}} + \frac{2A\sin(3\omega T/4)}{\omega\sqrt{2\pi}}$$

The frequency functions in Fig. 7.2.3 are the result of a lot more bumps. Each one consists of a series of spikes corresponding to the Fourier series amplitudes *1, 1/3, 1/5, 1/7,...* for the fundamental $\omega = 2\pi/T$ and odd-overtones *3ω, 5ω, 7ω, ...*, respectively, for the *box(x)* function in Fig. 7.1.2. This is an even box function in Fig. 7.2.3 so the series amplitudes alternate sign as *1, -1/3, 1/5, -1/7,...* as shown. The very last example is an unbiased funtion with no DC *(ω=0)*-Fourier component.

The "ringing" between the peaks is generally considered to be a nuisance. One way to get rid of ringing is to turn on the square wave more gradually. Fig. 7.2.4 shows the Fourier transform of a wave that has been turned on and off by a Gaussian (*exp-$(x/a)^2$*). This *windowing* kills the ringing. The width of each frequency peak varies inversely with the width a of the Gaussian window.
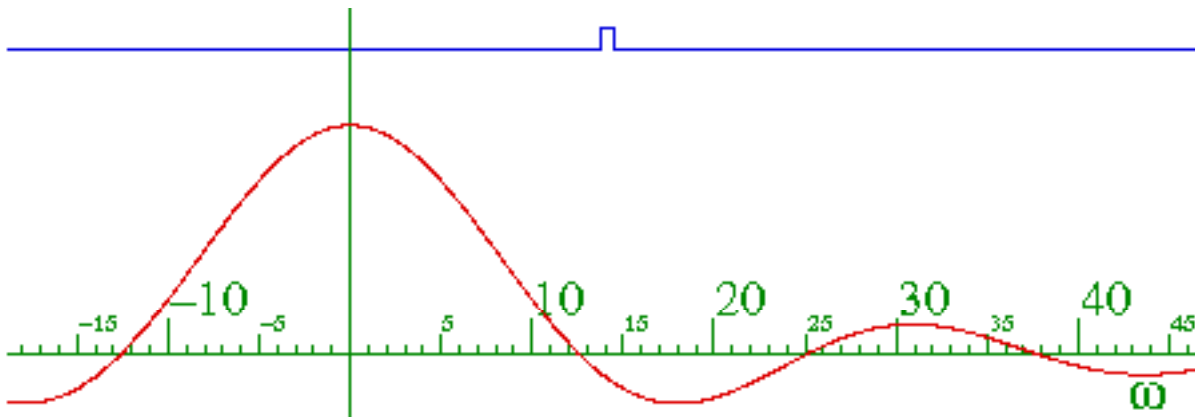
Fig.7.2.1 Elementary diffraction function: Fourier transform of single half square wave.

(a)

(b)
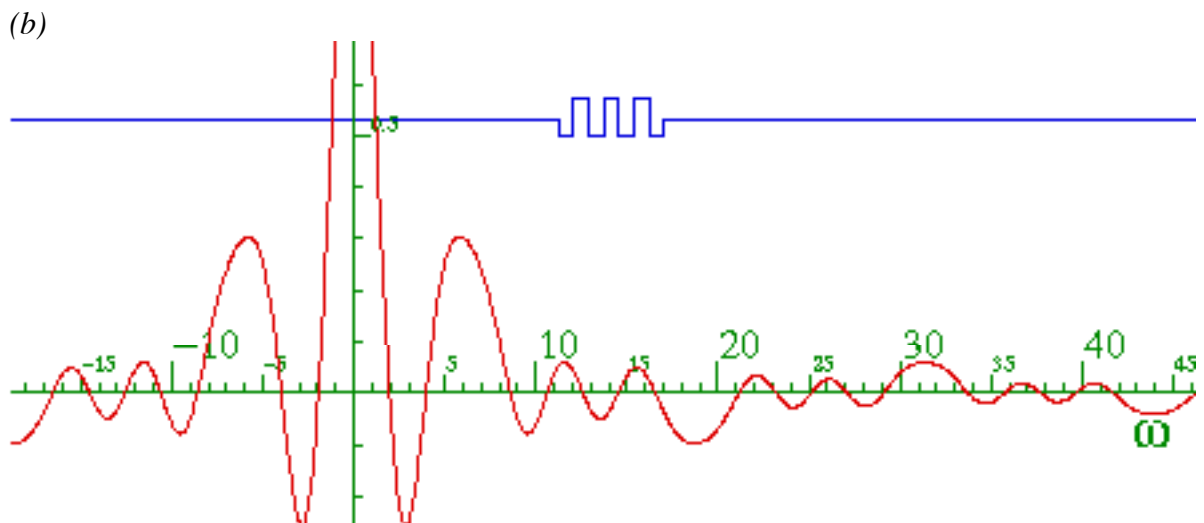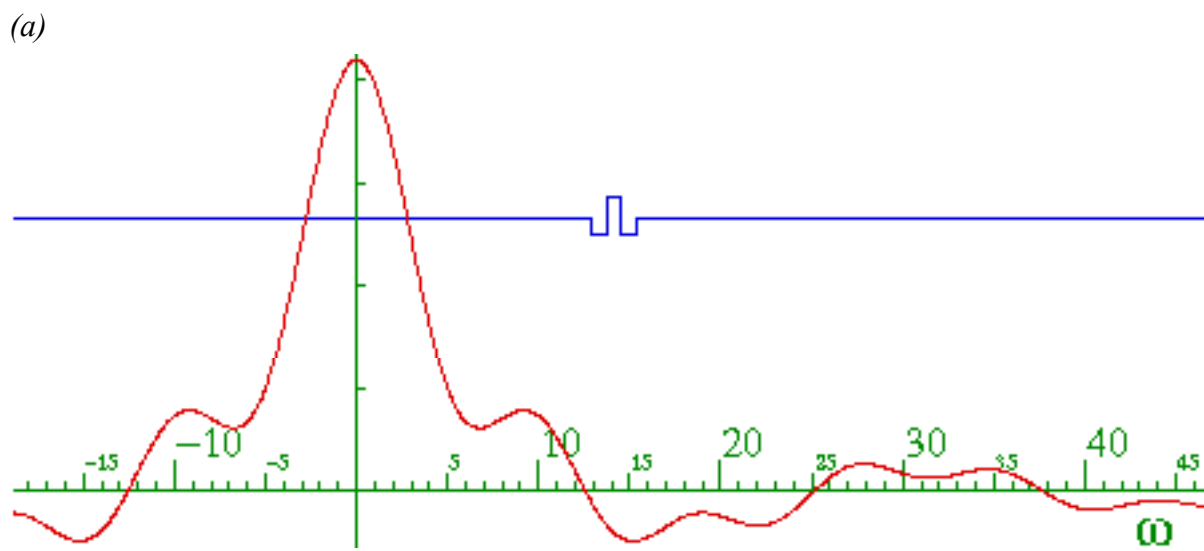
Fig. 7.2.2 Fourier transform of (a) three half- square waves. (b) seven half -square waves.

(a)
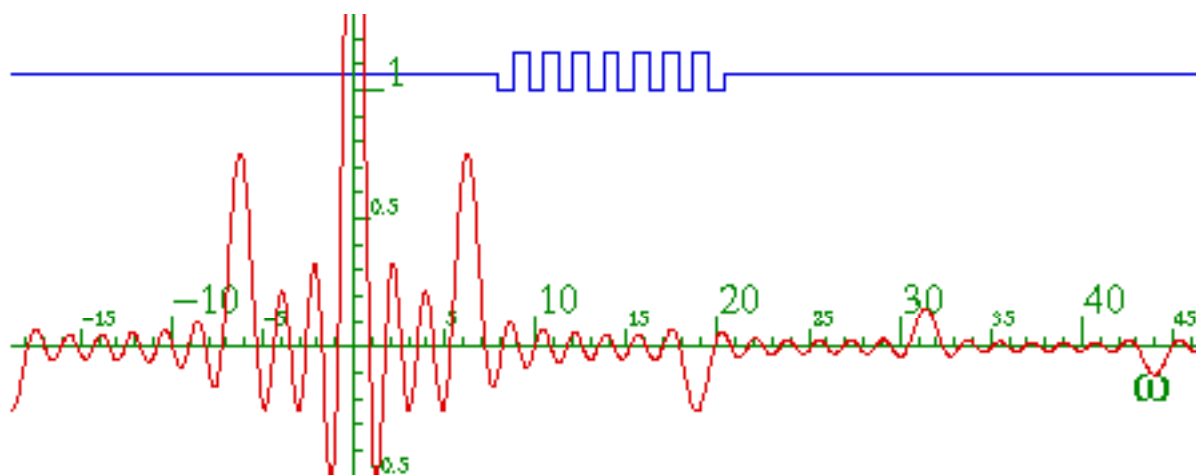
(b)
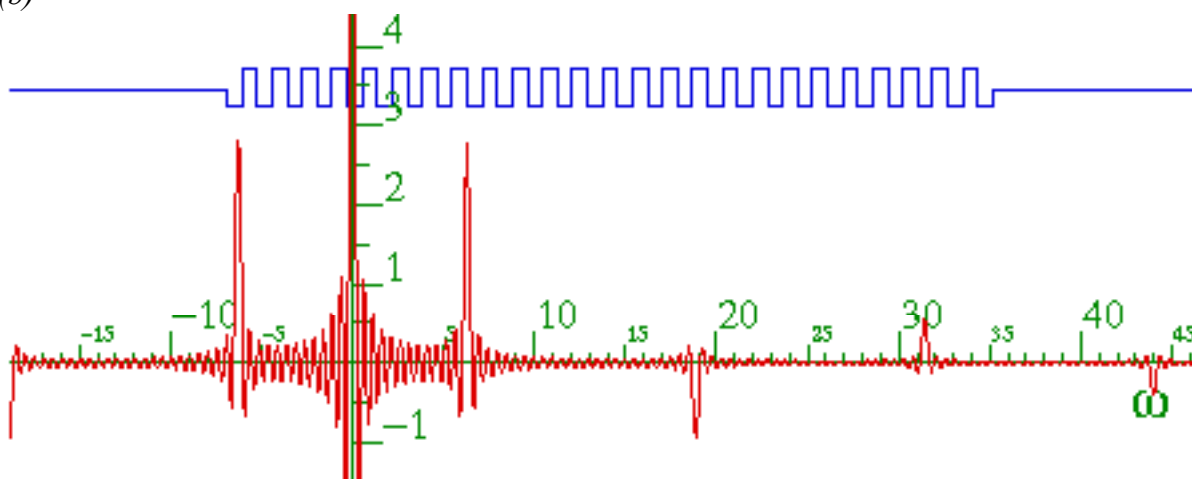
(c)
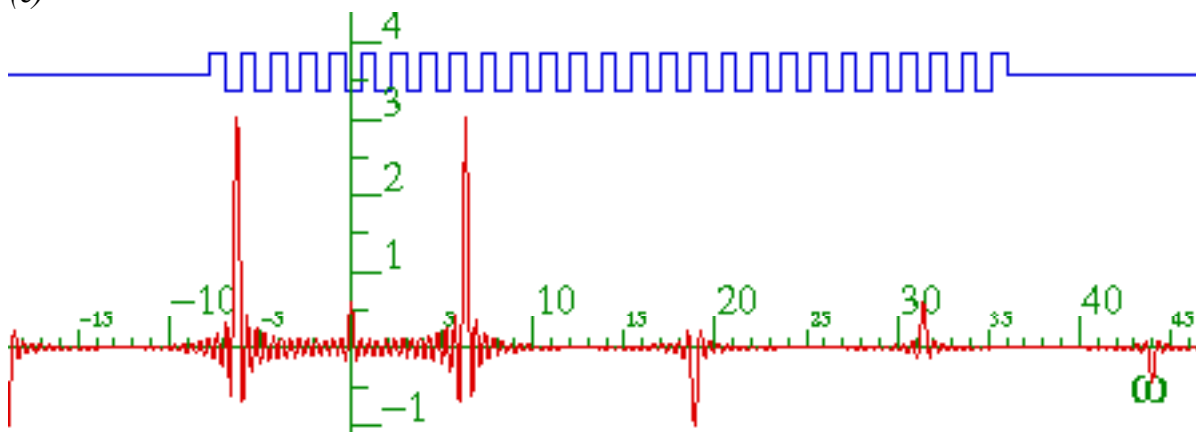
Fig. 7.2.3 Fourier transforms of square half-bumps (a) fifteen (b) forty-nine (c) fifty one .
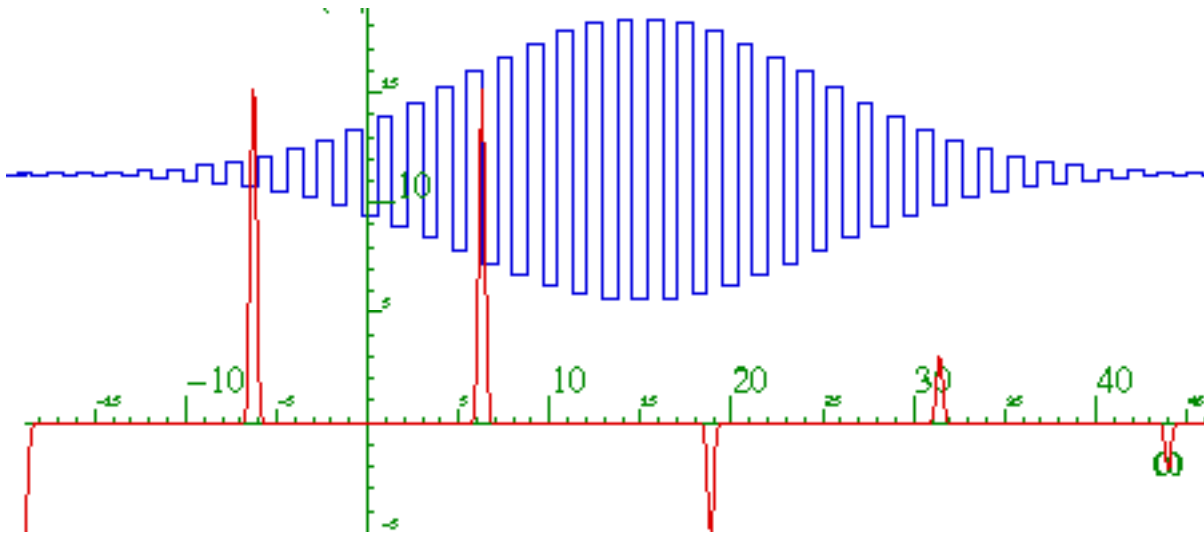
Fig. 7.2.4 Fourier transform of windowed square waves.

The idea of the Fourier integral, as opposed to Fourier series, is that <u>any</u> function, periodic or otherwise can be approximated by sines and cosines from a frequency *continuum*. Fourier series require that the function be periodic and repeat itself perfectly after some fixed period of time. The Fourier integral is supposed to be an enduring and time-invariant frequency map that provides the predestination of a time function forever and ever!

One should be suspicious of something that requires an infinite continuum of perfect frequency oscillators to be behind the scenes running your life. Pure sines and cosines are forever functions but we, like our world, certainly are not so enduring. Consider Fourier integrals as a cute limit-taking tool but not ultimately realistic.

Consider the fictitious function of time shown in Fig. 2.6.6. It is only periodic for awhile, but like most of us, cannot maintain the pace forever and finally gets in trouble with the hereafter.
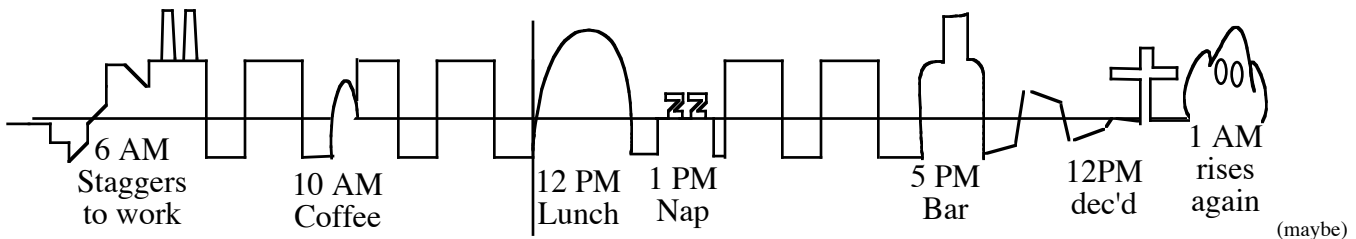
Fig. 7.2.5 A day in the life of a real function.

Now we go on to a practical Fourier analysis that is both finite and discrete.

7.3 Discrete and bounded x. Discrete and bounded k

This is the most restrictive case, but also, due to practical considerations mentioned previously, the one that actually gets used the most these days. However, in spite of its practical value it is not always treated as carefully as the more "mathematically sophisticated" continuum case (b). It should be!

We begin by supposing that space itself is periodic as in case (a) but further is divided into N discrete pieces or points. So the only x-values allowed are the following N values

$$\{ x_0=0, x_1=a , x_2=2a , x_3=3a, ... , x_{N-1}=(N-1)a, x_N =0\} \tag{7.3.1a}$$

and there are only N position states are the following. The last $|N\rangle$ state is the same as the first $|0\rangle$ state.

$$\{ |0\rangle, |1\rangle , |2\rangle , |3\rangle, ... , |N-1\rangle , |N\rangle =|0\rangle\} \tag{7.3.1b}$$

Fig. 7.3.1 shows ways to visualize this as N beads on a ring of length $L = Na$ that wraps around so that the *N-th* bead is the same as the *zero-th*. (Zero-based numbering is the modern computing standard.) Otherwise, we invoke the so-called *periodic* or *Born-VonKarman* boundary conditions and imagine our 1-D world repeats like a computer game outside its boundaries. As shown in Fig. 7.3.1, there is a distance *a* between the lattice of beads. It is called the *lattice spacing a*.
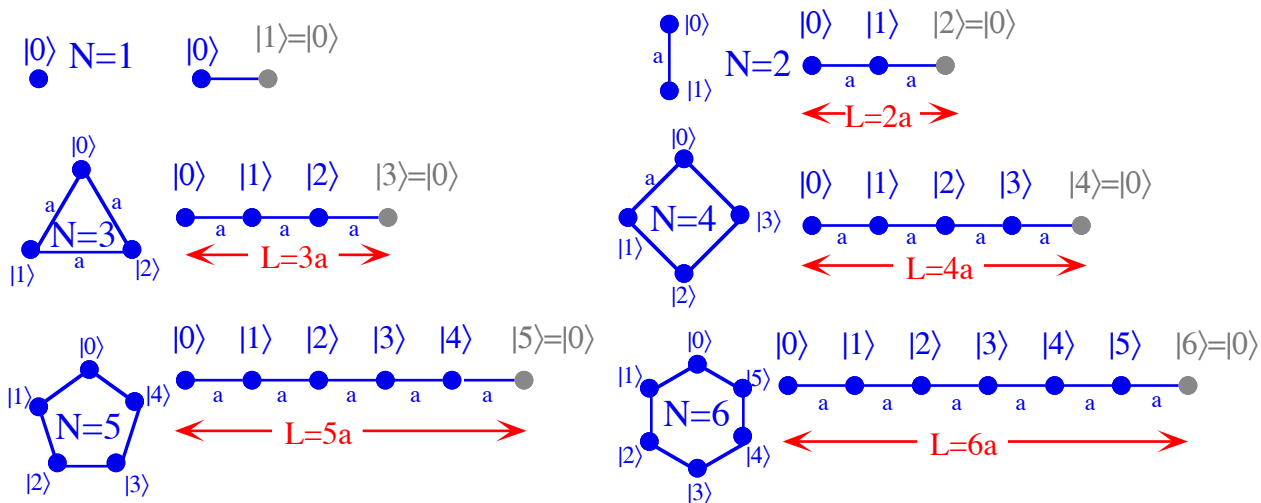
Fig. 7.3.1 Finite coordinate spaces for N-cyclic (C_N) discrete systems (N = 1, 2, ...,6...)

These *ideal quantum dots* will be among our first examples of 2-state, 3-state, ..., and 6-state systems. By studying them carefully, it will be possible to learn important principles which will greatly help later study of molecules and solids which have N-states with large-N but the same basic theory. Also, the quantum dots might have hidden inventions that could make you wealthy!

The basic wavefunctions that live on the discrete dots or beads are a subset of the continuum wavefunctions e^{ikmx} of (2.6.1), as though N equally spaced points of (2.6.1) were extracted and plotted over each lattice point x_p where

$$x_p = p a =p L/N \ . \ (p = 0, 1, 2, 3, ..., N-1) \tag{7.3.2}$$

The basic wavefunctions are given explicitly below.

$$\psi_{k_m}(x_p) = \langle x_p | k_m \rangle = \frac{e^{ik_m x_p}}{\sqrt{N}} = \psi_{k_m}(x_p + L) \qquad (7.3.3)$$

The only change from (7.1.1) is the use of a discrete coordinate x_p defined in (7.3.2) above. Also, the normalization constant has been set to the dimension N since all N exponentials $e^{ik_m x}$ contribute unit magnitude ($|e^{ik_m x}|^2 = 1$) in the normalization sum.

$$\langle k_m | k_m \rangle = \sum_{p=0}^{N-1} \langle k_m | x_p \rangle \langle x_p | k_m \rangle = \sum_{p=0}^{N-1} \frac{e^{-ik_m x_p}}{\sqrt{N}} \frac{e^{ik_m x_p}}{\sqrt{N}} = N \frac{1}{\sqrt{N}} \frac{1}{\sqrt{N}} = 1 \qquad (7.3.4)$$

The quantization conditions due to periodicity requirement (7.3.3) over "cage" length $L=Na$ are similar to (7.1.3) but now expressed in terms of the discrete number N and spacing a of lattice points.

$$e^{ik_m L} = 1 \text{ , or: } k_m = \frac{2\pi}{L} m = \frac{2\pi}{Na} m \qquad (7.3.5a)$$

Wave amplitude at lattice point p is a power-p of $(e^{i2\pi/N})$, the N-th root of unity (normalized, of course)

$$\psi_{k_m}(x_p) = \langle x_p | k_m \rangle = \frac{e^{ik_m x_p}}{\sqrt{N}} = \frac{1}{\sqrt{N}} \left(e^{i2\pi/N} \right)^{mp} \qquad (7.3.5b)$$

All N roots, together, form N-polygons in the complex plane as shown in Fig. 7.3.2. The allowed wave amplitudes in Fig. 7.3.2 resemble the "ring" coordinate positions in Fig. 7.3.1. The complex $z_{m,p}=exp(ik_m x_p)$ are the N-th roots of unity $(z^N=1)$ introduced in a complex arithmetic review (App 1.A).
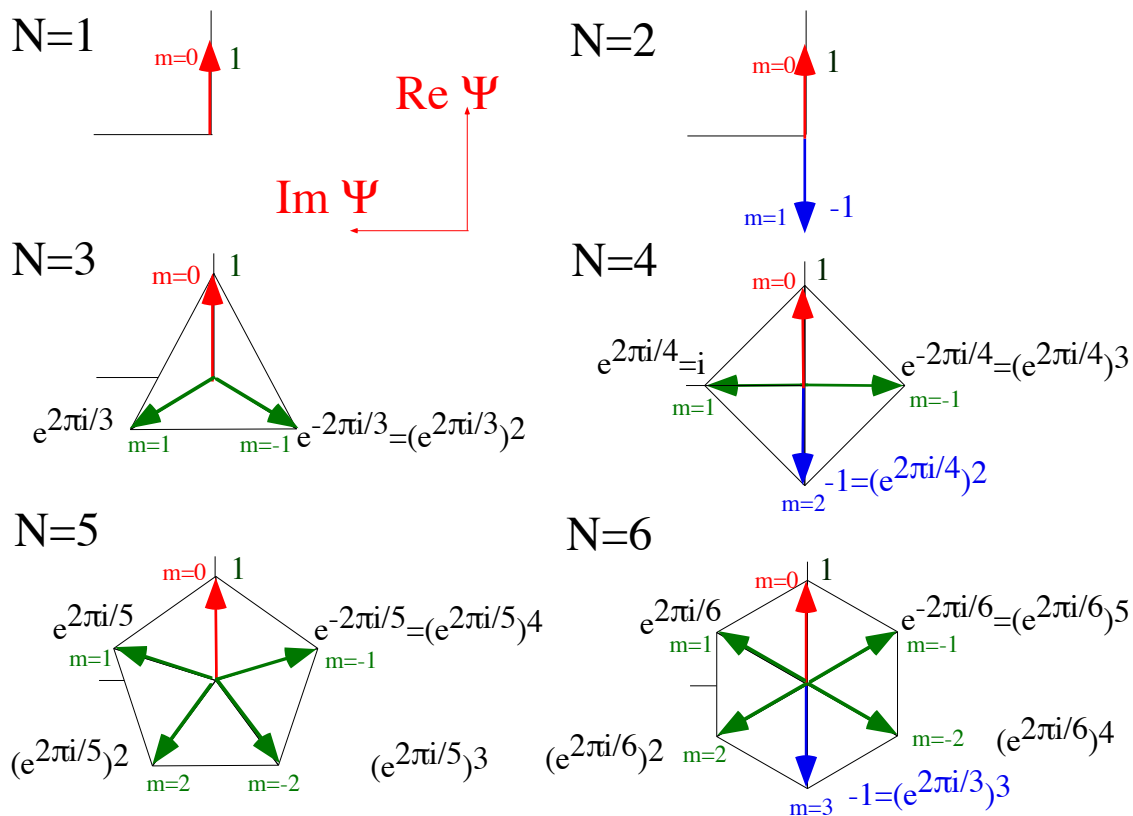
Fig. 7.3.2 Discrete wave amplitudes allowed for N-cyclic (C_N) systems (N = 1, 2, ...,6...)

(a) N-nary counting for N-state systems

Fig. 7.3.2 shows different counting schemes for *odd-N* and *even-N*. In the unbounded cases the *k*-values go from $-\infty$ to $+\infty$. Here, letting *m* count from *-N* to *+N* <u>over</u>-counts and gives *2N+1* states when we know there are only *N*. We could let *m* count from *0* to *N-1*, just like the lattice points. Or, we let *m* count from *-(N-1)/2* to *+(N-1)/2*, (*odd-N*) and from *-(N-2)/2* to *+(N)/2* (*even-N*) as shown below.

It helps to think of *N*-state cyclic system as an *N-nary* computer element. Ever since 1950, we have become accustomed to binary (*N=2*) data storage in 2-bit registers. Inevitably, someone will discover how to make *N*-state registers. Until then, we imagine them. For an *N*-state register the quantum counting index *m* is defined only by an *integer modulo-N* or *(m)$_N$*.

$$(m)_N := m \ modulo \ N \qquad\qquad (7.3.6)$$

For example, for *N=6* in Fig. 7.3.2, all the following values of the quantum index *m* in a given line below have the same value modulo-6.

$$\begin{aligned}
&\ldots = (-9)_6 = (-3)_6 = \underline{(3)_6} = (\ 9\ )_6 = (15)_6 = \ldots = \ 3 \ mod \ 6 \\
&\ldots = (-8)_6 = \underline{(-2)_6} = (4)_6 = (10)_6 = \ldots \ \ = -2 \ mod \ 6 \\
&\ldots = (-7)_6 = \underline{(-1)_6} = (5)_6 = (11)_6 = \ldots \ \ = -1 \ mod \ 6 \\
&\ldots = (-6)_6 = \underline{(\ 0)_6} = (6)_6 = (12)_6 = \ldots \ \ = \ 0 \ mod \ 6 \qquad (7.3.7) \\
&\ldots = (-5)_6 = \underline{(\ 1)_6} = (7)_6 = (13)_6 = \ldots \ \ = \ 1 \ mod \ 6 \\
&\ldots = (-4)_6 = \underline{(\ 2)_6} = (8)_6 = (14)_6 = \ldots \ \ = \ 2 mod \ 6 \\
&\ldots = (-3)_6 = \underline{(\ 3)_6} = (9)_6 = (15)_6 = \ldots \ \ = \ 3 mod \ 6 \\
&\ldots = (-8)_6 = \underline{(-2)_6} = (\ 4)_6 = (10)_6 = \ldots \qquad = -2 \ mod \ 6
\end{aligned}$$

How do we choose a k_m number label? We choose the underlined ones with the smallest *|m|* and pick the positive one if two are equal. This choice {*m=-2,-1,0,1,2,3*} of *N=6 m*-values is used in Fig. 7.3.2.

(b) Discrete orthonormality and completeness

Orthonormality relations for wave states reduce to finite geometric sums.

$$\langle k_m{}'|k_m\rangle = \sum_{p=0}^{N-1} \frac{e^{-ik_{m'}x_p}}{\sqrt{N}} \frac{e^{ik_m x_p}}{\sqrt{N}} = \frac{1}{N}\sum_{p=0}^{N-1} e^{i(k_m - k_{m'})x_p} \ , \ \text{where:} \ x_p = p\ a \quad (7.3.8a)$$

Substituting *(7.3.2)* and *(7.3.5)* gives

$$\langle k_m{}'|k_m\rangle = \sum_{p=0}^{N-1} z^p = \frac{1+z+z^2+\ldots+z^{N-1}}{N} \ , \ \text{where:} \ z = e^{i(k_m - k_{m'})a} = e^{i2\pi(m-m')/N}$$

The geometric sum yields a result that satisfies k_m-orthonormality axiom-3.

$$\langle k_m{}'|k_m\rangle = \frac{1}{N}\frac{1-z^N}{1-z} = \frac{1}{N}\frac{1-e^{i2\pi(m-m')}}{1-e^{i2\pi(m-m')/N}} = \delta_{mm'} \qquad (7.3.8b)$$

The k_m-completeness axiom-4 (or x_p- orthonormality) is satisfied for these wave states, as well.

$$\langle x_p{}'|x_p\rangle = \sum_{m=0}^{N-1} \langle x_p{}'|k_m\rangle\langle k_m|x_p\rangle = \sum_{m=0}^{N-1} \frac{e^{ik_m x_p{}'}}{\sqrt{N}}\frac{e^{-ik_m x_p}}{\sqrt{N}} = \frac{1}{N}\sum_{m=0}^{N-1} e^{i(x_p{}'-x_p)k_m} = \delta_{pp'} \quad (7.3.9)$$

(c) Discrete Fourier transformation matrices

Below are shown Fourier transformation matrices and discrete x_p-wavefunctions (7.3.5b)

$$\langle k_m|x_p\rangle = \psi_{k_m}(x_p)^* = e^{-ik_m x_p}/\sqrt{N} \qquad (7.3.10a)$$

They are drawn as complex phasor amplitudes for the cyclic N-state systems (C_N) for $N = 1, 2, 3, 4, 5,$ and 6.

Also drawn over the phasors is the Re-part of the "Bohr's ghost" continuum x-wavefunctions

$$\langle k_m|x\rangle = \psi_{k_m}(x)^* = e^{-ik_m x}/\sqrt{L} \qquad (7.3.10b)$$

Recall (7.1.10) or Fig. 7.1.1. "Bohr's ghosts" match the discrete waves (7.3.10a) with phasor clocks.
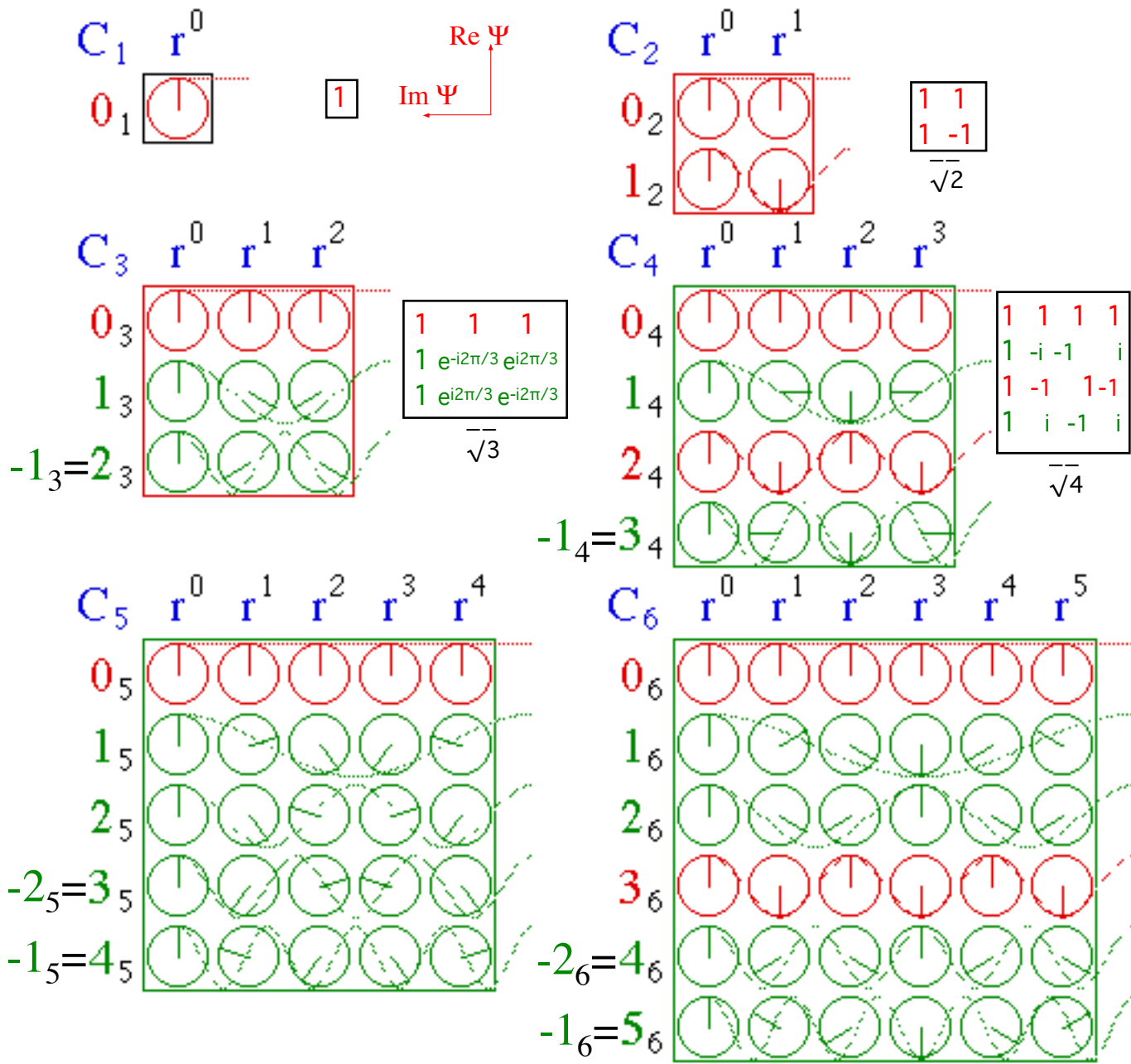
7.3.3 Discrete Fourier transformation matrices for N-cyclic (C_N) systems (N = 1, 2, ...,6...)

(d) Intoducing aliases and Brillouin zones

It is important to see the relation between the continuum waves and their "course-grained" images thatves with integral wave-numbers of *m mod N* whole wavelengths within each $\langle k_m |$-row of phasors. We might as well call them "row-waves" or "bra-waves." Note also, that the same wave shape exists in the <u>columns</u> or kets $|x_p\rangle$. Each "ket-wave" $|x_p\rangle$ represents a δ-position state or "pulse" localized at point x_p. The inverse Fourier transformation $\langle k_m | x_p\rangle$ relates $|x_p\rangle$ to a bra-wave$\langle k_m |$. As required by conjugation axiom-2, namely, $\langle k_m | x_p\rangle = \langle x_p | k_m\rangle^*$, the relation is the same as between $|k_m\rangle$ and $\langle x_p |$, except for conjugation.

For low wave number like, say $(m_N)=(1)_6$ or $(2)_6$, it is easy to see the "Bohr's-ghost wave" mirrored in the phasors as in the second and third row of the C_6 matrix in Fig. 7.3.1. Note however, that these phasors are set so the phase of the one to the right is clockwise (that is it appears <u>ahead)</u> of the one to the left. This means, if the phasors turned clockwise, that the one to the right is feeding energy into the one to its left, so the wave would be moving <u>right-to-left</u> with wave momentum <u>minus</u> $(1)_6$ or <u>minus</u> $(2)_6$, respectively. But, they're conjugated bras so their clocks go backwards and so the labels are OK, after all.

For high wave number like, say $(m_N)=(4)_6$ or $(5)_6$, it is not so easy to see the "Bohr's-ghost wave" mirrored in the phasors as in the fifth and sixth row of the C_6 matrix in Fig. 7.3.1. But, you can see *alias* waves of negative wave momentum $(m_N)=(-2)_6$ or $(-1)_6$, respectively, that is <u>oppositely</u> moving waves of low wavenumber. Recall that (*4 mod 6*) equals (*-2 mod 6*) and (*5 mod 6*) equals (*-1 mod 6*).

Right in the middle row of the *even-N* matrix is a wave that isn't going in either direction. In the C_6 matrix it is the $(3)_6$ wave. Since (*3 mod 6*) equals (*-3 mod 6*) this is a good old push-me-pull-you standing wave with all real amplitudes of (*1, -1, 1, -1, 1, -1*). This can only happen for even-*N* and is known as a *first Brillouin zone boundary* wave in solid-state physics.

All cases have a zero-momentum wave (0_N) at the top of the transformation matrix. This is called the *Brillouin zone center* wave in solid-state physics. Indeed, it is centered at the bottom of the dispersion plot in Fig. 2.6.1. Its phasor settings are the same as that of a higher (N_N), or $(2N_N)$, or $(3N_N)$, ...etc. wave. However, this *N*-state system does not count higher than *N-1* without recycling.

Consider, for example, a *k₋₁₁* wave of wavevector *(-11)₁₂* (with minus-eleven-kinks-modulo-12) as plotted in Fig. 7.3.4 (a). Since *(–11)-mod-12* equals *(+1)-mod-12* (that is, *(-11)₁₂=(+1)₁₂*) it follows that the wave shown has the same effect as a *(+1)₁₂* wave. Indeed, the twelve masses in Fig. 7.3.4(a) line up on a single-kink *(k=1)*-wave moving positively, while the *(k=-11)*-wave moves negatively. (See *WaveIt* movie.) This is an example of aliasing. In a C_{12} lattice, *(k=-11)* is an alias for *(k=+1)*.

Fig. 7.3.4(b) shows the *k*-space with a typical frequency dispersion function plotted above it. The difference between any two alias wavevectors such as *(k=+1)* and *(k=-11)* is a *reciprocal lattice vector k₁₂* or *(12)₁₂=(0)₁₂*. The reciprocal lattice vector k_{12} also spans the first Brillouin-zone from *(-6)₁₂* to *(+6)₁₂* as shown at the bottom of the figure. An important idea here is that a wavevector *k*-space must have the same *N*-fold periodic symmetry as the coordinate *x*-space. Moving across row of a $\langle k_m | x_p\rangle$ matrix gives the same variation as moving up the corresponding column since $\langle k_m | x_p\rangle$ is unitary. Both are *N*-fold periodic!

(a)

⬤ -*Motion of wave state k_{-11} same as wave state $k_{-11}+k_{12} = k_{+1}$*

(b)

100.0%

Reciprocal lattice vector k_{12}

$\omega = 2.00$
1.73
1.41
1.00
0.52
0.00

k_m

Wavevector k (in units of $2\pi/L$)

1st Brillouin Zone
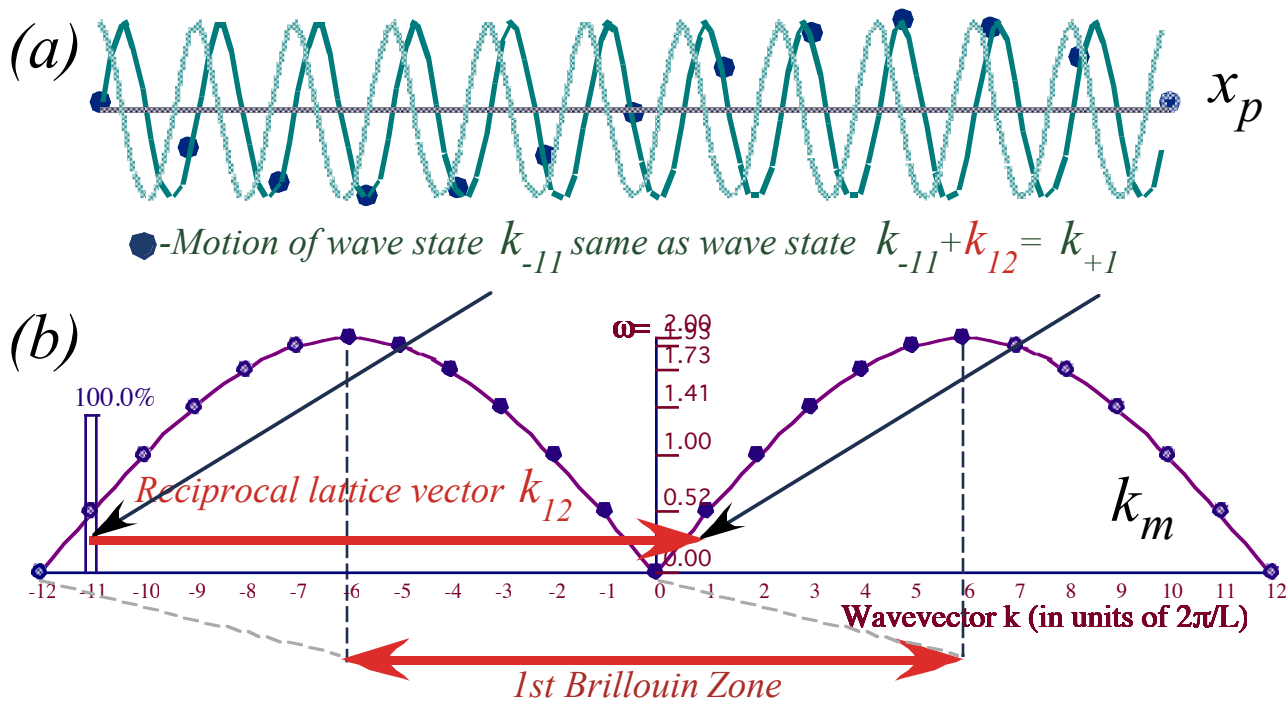
Fig. 7.3.4 (a) (-11)-wave has the same effect as its alias (+1)-wave. (b) Difference is zone vector k_{12}.

To appreciate the symmetry of a Fourier transfom matrix, it may help to examine some larger ones. For example, Fig. 7.3.5 shows the Fourier matrix for $N=24$. Phase of each amplitude $\langle k_m | x_p \rangle$ is color coded so it can be more easily spotted. Symmetry patterns should now be more evident. Remember, that these patterns repeat forever in all directions right and left or up and down in a great checkerboard quilt!

This beginning discussion of discrete wave analysis should make it clear that there is considerable physical and mathematical complexity hiding in these "simple" Fourier structures. Indeed, this is a key to understanding fundamental quantum symmetry properties and techniques which are generally labeled by a mathematical misnomer as "group theory." We shall explore some more of this shortly.
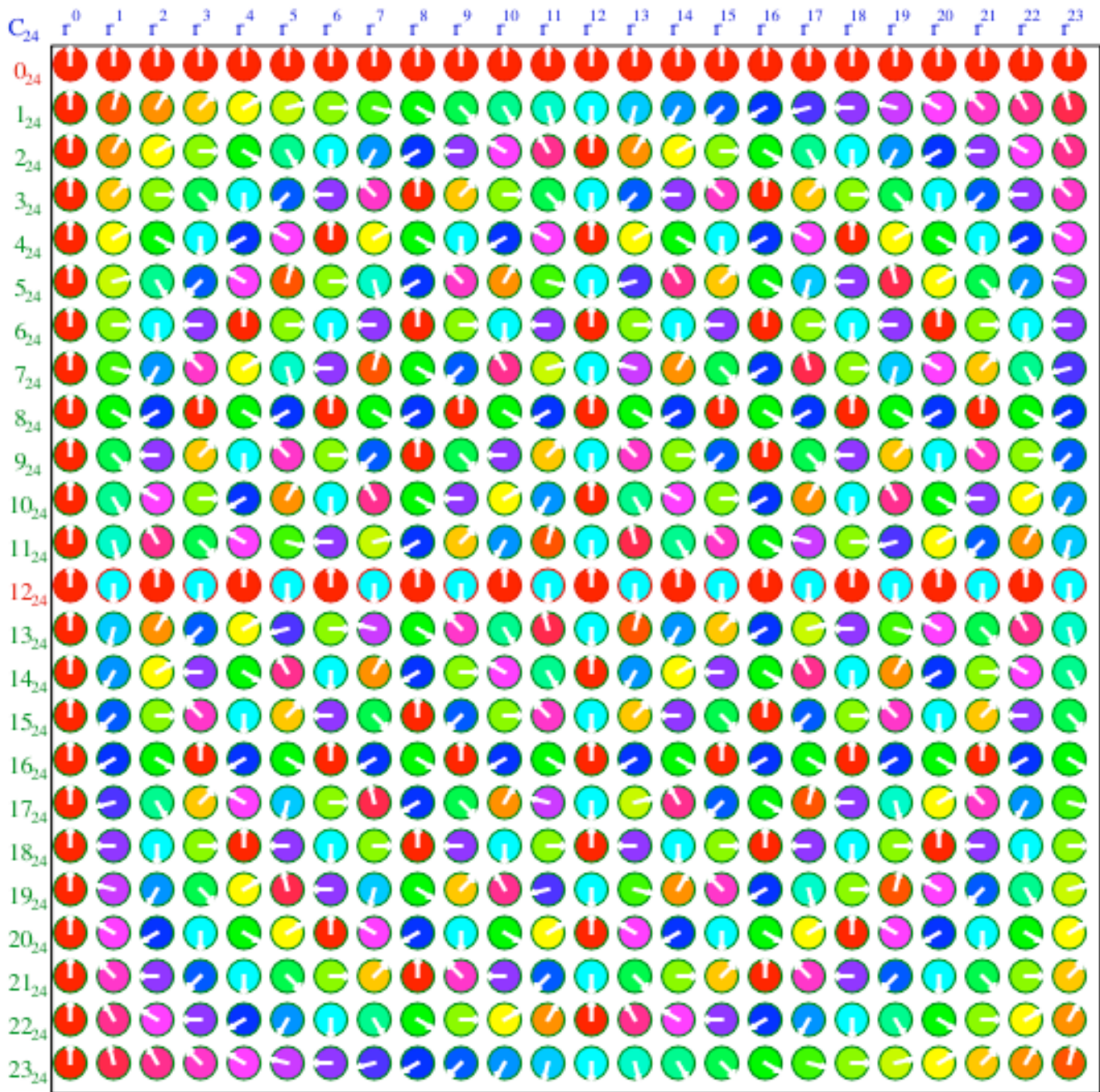
Fig. 7.3.5 Phase color coded Fourier transformation matrix for N=24.

Problems for Chapter 7

Bohring problems

7.1.1. For a Bohr ring of fixed circumference $L = 1nm$ consider the following wavefunction $\Psi(x) = \langle x|\Psi\rangle$ distributions around the ring at $t=0$, and deduce the amplitudes $\langle m|\Psi\rangle$ of each of the eigenstates $|m\rangle$ for $m=0,\pm1,\pm2,..$ Let the eigenfrequencies be $\nu_m = (0, 1, 4, . ., m^2, .)MHz$.

(a) $\Psi(x) = const.$.   (b) $\Psi(x) = const.(1+\cos 2\pi x/L)$.

(c) $\Psi(x) = const.$ for $-L/4 < x < L/4$ and $\Psi(x) = 0$ elsewhere.

For each case evaluate *const.* assuming one particle occupies the ring.

(d) For each case (a) to (c) answer: "Is it a stationary state?" If not, calculate, plot, and discusss the wavefunctions of each case at time $t = 1\mu sec$, and at $0.5\mu sec$.

Continuously boring problems

7.2.1. For an infinite line $(-\infty < x < \infty)$ consider the following wavefunction $\Psi(x) = \langle x|\Psi\rangle$ distributions along the line. Calculate, plot, and discusss the amplitude functions $\langle k|\Psi\rangle$ of each of the eigenstates $|k\rangle$ for $(-\infty < k < \infty)$. Let the eates $|k\rangle$ for $(-\infty < k < \infty)$. Let the eigenfrequencies be $\nu_k = (kL/2\pi)^2 MHz$. (Let unit length be $L = 1nm$.)

(a) $\Psi(x) = const.$.   (b) $\Psi(x) = const.(1+\cos 2\pi x/L)$ . .

(c) $\Psi(x) = const.$ for $-L/4 < x < L/4$ and $\Psi(x) = 0$ elsewhere.

Evalu per unit length ($L = 1nm$.).

(d) For each case (a) to (c) answer: "Is it a stationary state?" If not, calculate, plot, and discusss the wavefunctions of each case at time $t = 1\mu sec$, and at $0.5\mu sec$.

Continuously discrete or discretely continuous?

7.3.1. Ch.7 contains discussion of 1D Fourier wave systems with (a) Continuous x and discrete k, (b) Continuous x and continuous k, and (c) Discrete x and discrete k. Using physical models of each to discuss how physically relizeable these are. Is there a 4th possibility? Discuss.

Aliases on the move

7.3.2. Consider the two aliases (-11) and (+1) in Fig. 7.3.4. Discuss whether a dispersion function $\omega(k)$ should repeat periodically. Should the period be the zone vector k_{12}? For computation use $\omega(k)=|\sin(\pi k/12)|$ as plotted where $k=0, \pm1, \pm2, \pm3 ,\ldots$ in units of $2\pi/L$. Use $V_{phase} = \omega/k$ and $V_{group} = d\omega/dk$.

(a) Is the phase velocity the same for the two alias states (-11) and (+1)? Compute and discuss why or why not.

(a) Is the group velocity the same for the two alias states (-11) and (+1)? Compute and discuss why or why not.

QM
for
AMOP

Chapter 8
Fourier Symmetry Analysis

W. G. Harter

Fourier analysis is most useful when there is a symmetry G in which all the coordinate points are indistinguishable. For an unbounded x-continuum, G is an infinite translational symmetry group labeled T. For a bounded x$_p$-ring of "quantum dots" the symmetry G is an N-cyclic rotation group labeled C$_N$. In Chapter 8 a fictitious hexagonal beam analyzer with C$_6$ symmetry is considered. The transfer matrix eigensolutions of such a device are found using a modern form of Fourier analysis known as group representation theory or symmetry analysis, one of the most powerful tools in quantum theory. The symmetry of the bounded Bohr x-ring continuum is also discussed.

Chapter 8. Fourier Symmetry Analysis

From where do the wavefunctions like $\Psi = e^{i(kx - \omega t)}$ come? One answer to this involves the concept of *symmetry analysis* and *group representation theory*. These sound like big names for what is still regarded as a pretty scary mathematical subject. However, the basic ideas of this powerful tool are actually quite simple as we hope to show now. Most of the needed algebraic work has been done in Ch. 3 regarding spectral decomposition. The physical ideas of Fourier analysis and Bohr ring waves are in Ch. 7. Symmetry group representation theory is really just a beautiful generalization of *Fourier analysis* that gives eigensolutions of "difficult" operators using simple properties of commuting symmetry operators.

8.1. Introducing Cyclic Symmetry: A C_6 example

A ring of quantum dots was introduced in Section 7.3 as a model for finite Fourier analysis. The Fourier tranformation matrix was discussed with examples for *N=1, 2, 3, 4, 5,* and *6*. The idea of cyclic symmetry C_N was broached as a property of the matrices in Fig. 7.3.3 and Fig. 7.3.5. Here that idea is put on a more solid footing.

(a) Cyclic symmetry C_N: A 6-quantum-dot analyzer

Suppose someone invents some beam analyzer that takes an *N*-state beam and sorts it into *N* beams arrayed around a circular device as imagined in Fig. 8.1.1 for *N=6*. Let each beam path entering the device contain particles in one of *N* states $\{|0\rangle, |1\rangle, |2\rangle, ... , |N-1\rangle\}$ after which the device does things which causes the beams to interfere or be otherwise modified before recombining and counting.
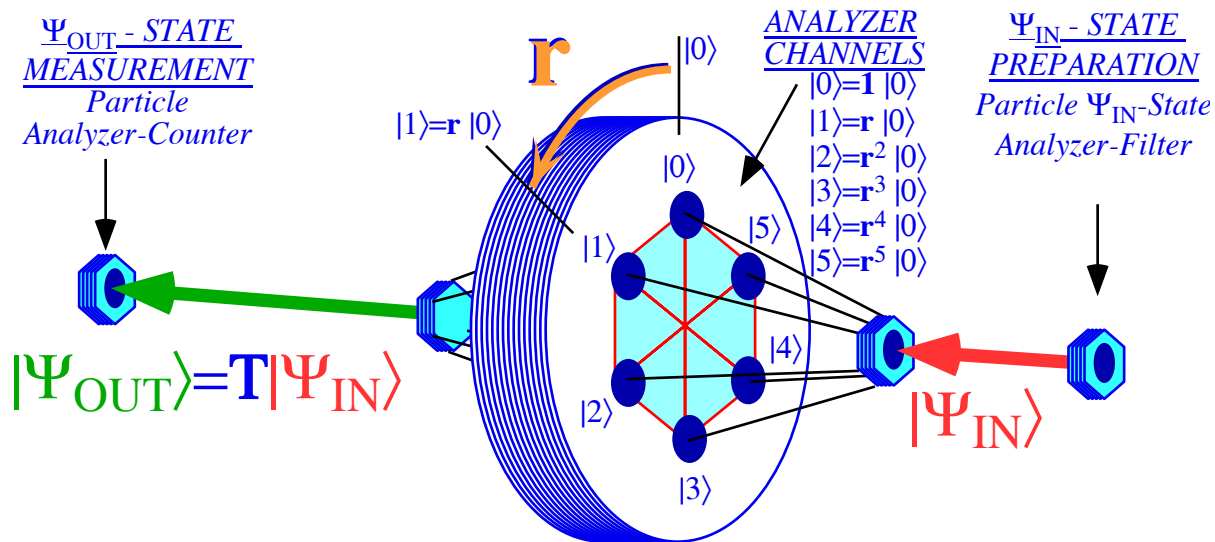
Fig. 8.1.1 Generic N-state (C_N) beam analyzer experiment with (N = 6) channels

We are intentionally being vague about the nature of the states. (After all, this device hasn't even been invented yet!) Let us just say they are some kind of hyper-polarization states. (Put a prefix like 'hyper' on something ordinary and people stop asking questions.) The point is that by just knowing the symmetry of a device it is possible to work out a lot of the quantum mechanics without knowing so much of the underlying

details. It is a lot like the photon polarization and electron spin problems discussed in Chapter 1. Electron and photon "spin" are physically quite different but use much of the same mathematical theory.

By *symmetry*, we mean any operators $\mathbf{r}$, $\mathbf{r}^2$,... that do not alter the analyzer experiment no matter how many times you apply them. In particular, suppose a *60°* rotational operator $\mathbf{r}$ indicated in Fig. 8.1.1. could be done some night by the lab janitor, so when the physicists show up the next morning all their experiments work the same as the day before.

However, it is important to state what we mean the janitor's $\mathbf{r}$-operation to do. He could just rotate the whole lab building by *60°*. That, indeed, is a symmetry, but not one we will discuss until later. Besides, a rotation like that happens every four hours as the Earth turns; no janitor needed! This is called the *symmetry of isotropy of space*. It is a *continuous* or *Lie symmetry* for which *60°* has no special significance.

Instead, what we have in mind for the janitor to do is rotate just the analyzer in the center of Fig. 8.1.1 by *60°* as indicated in the figure. Well, that analyzer looks pretty heavy, so, instead we'll ask that the janitor just rotate the little input source and the little output counter both by minus *60°*, which is operation $\mathbf{r}^{-1} = \mathbf{r}^5$. This does the same as a whole-Earth/lab rotation by *-60°* (which no one detects) followed by a positive *60°* rotation of the big analyzer to "upright" leaving input and output devices behind at *-60°*.

It is important to understand that all transformations are *relative transformations*; something gets moved or mapped relative to something else. You've probably heard it quoted, "Everything's relative!" Well, that's often garbage, but here it isn't. Rotations, Lorentz transformations, and our analyzer operators $\mathbf{T}$ (Recall Fig. 1.6.1), and $\mathbf{r}$ in Fig. 8.1.1 are all mappings of one vector or thing relative to another.

By the way, our helpful suggestion to the janitor won't help much if the input and output devices are big analyzers, too. It was noted in Chapter 1 that filters and counters are analyzers set in certain ways. But, the analyzer in Fig. 8.1.1 is a more powerful one than heretofore discussed. (And, isn't better always bigger?) So let's assume that the janitor can easily do $\mathbf{r}^{-1} = \mathbf{r}^5$ to the smaller input and output devices whose in and out states are written as follows in Dirac notation,

$$|\Psi_{\text{OUT} (r^{-1})}\rangle = \mathbf{r}^{-1}|\Psi_{\text{OUT}}\rangle \ , \qquad\qquad |\Psi_{\text{IN} (r^{-1})}\rangle = \mathbf{r}^{-1}|\Psi_{\text{IN}}\rangle \ . \qquad\qquad (8.1.1)$$

Symmetry of the transformation operator $\mathbf{T}$ means it does exactly the same relative thing to any state $|\Psi_{\text{IN}}\rangle$ as it does to the janitor-rotated state $|\Psi_{\text{IN} (r^{-1})}\rangle$, that is

$$|\Psi_{\text{OUT}}\rangle = \mathbf{T}\,|\Psi_{\text{IN}}\rangle \qquad\qquad \text{implies:} \qquad |\Psi_{\text{OUT} (r^{-1})}\rangle = \mathbf{T}\,|\Psi_{\text{IN} (r^{-1})}\rangle \qquad (8.1.2\text{a})$$

or

$$\mathbf{r}^{-1}|\Psi_{\text{OUT}}\rangle = \mathbf{T}\,\mathbf{r}^{-1}|\Psi_{\text{IN}}\rangle \qquad\qquad\qquad (8.1.2\text{b})$$

$$|\Psi_{\text{OUT}}\rangle = \mathbf{r}\,\mathbf{T}\,\mathbf{r}^{-1}|\Psi_{\text{IN}}\rangle \qquad\qquad\qquad (8.1.2\text{c})$$

If this is true for all input states $|\Psi_{\text{IN}}\rangle$ then it follows that effect of analyzer operator $\mathbf{T}$ in (8.1.2a) and in (8.1.2c) are indistinguishable, or $\mathbf{T}$ is *invariant* to $\mathbf{r}$

$$\mathbf{T} = \mathbf{r}\,\mathbf{T}\,\mathbf{r}^{-1} \quad \text{or:} \ \ \mathbf{r}^{-1}\mathbf{T}\,\mathbf{r} = \mathbf{T} \qquad\qquad\qquad (8.1.2\text{d})$$

or, that $\mathbf{r}$ *commutes* with $\mathbf{T}$; the latter being the most common way to say that $\mathbf{T}$ *has* $\mathbf{r}$-*symmetry*.

$$\mathbf{T}\,\mathbf{r} = \mathbf{r}\,\mathbf{T} \qquad\qquad\qquad (8.1.2\text{e})$$

All the above parts of equation (8.1.2) are really the same requirement for $\mathbf{r}$-*symmetry of* $\mathbf{T}$.

Note: This is <u>not</u> the same as just multiplying both sides of $|\Psi_{OUT}\rangle = \mathbf{T}\,|\Psi_{IN}\rangle$ by $\mathbf{r}$ or $\mathbf{r}^{-1}$ which just gives a whole-Earth/lab rotation, that is, operate with $\mathbf{r}^{-1}$ and insert the identity ($\mathbf{r}\,\mathbf{r}^{-1} = \mathbf{1}$) to get

$$\mathbf{r}^{-1}\,|\Psi_{OUT}\rangle = \mathbf{r}^{-1}\,\mathbf{T}\,|\Psi_{IN}\rangle = \mathbf{r}^{-1}\,\mathbf{T}\,\mathbf{r}\,\mathbf{r}^{-1}\,|\Psi_{IN}\rangle\,. \tag{8.1.3a}$$

This reduces to an expression *similar* to the original $|\Psi_{OUT}\rangle = \mathbf{T}\,|\Psi_{IN}\rangle$

$$|\Psi_{OUT\,(r^{-1})}\rangle = \mathbf{r}^{-1}\,\mathbf{T}\,|\Psi_{IN}\rangle = \mathbf{r}^{-1}\,\mathbf{T}\,\mathbf{r}\,|\Psi_{IN\,(r^{-1})}\rangle = \mathbf{T}_{(r^{-1})}\,|\Psi_{IN\,(r^{-1})}\rangle \tag{8.1.3b}$$

where $\mathbf{T}_{(r^{-1})}$ is a *similarity transformation* $\mathbf{r}^{-1}\mathbf{T}\,\mathbf{r}$ of $\mathbf{T}$. (This is an <u>active</u> transformation; <u>devices</u> move.)

$$\mathbf{T}_{(r^{-1})} = \mathbf{r}^{-1}\,\mathbf{T}\,\mathbf{r} \tag{8.1.3c}$$

These relations hold true for any analyzer operator $\mathbf{T}$ whether it has symmetry or not.

For $\mathbf{T}$ to have $\mathbf{r}$-symmetry it is necessary that the similarity transformation leaves $\mathbf{T}$ unchanged or invariant ($\mathbf{T}_{(r^{-1})} = \mathbf{T}$), as in (8.1.2d).To recap

An analyzer has $\mathbf{r}$-symmetry if and only if its operator $\mathbf{T}$ commutes with $\mathbf{r}$, that is ($\mathbf{T}\,\mathbf{r} = \mathbf{r}\,\mathbf{T}$).

(b) C_N Symmetry groups and representations

Now, the janitor, having fooled the physicists once, does it again the next night, by rotating by $\mathbf{r}$ one more time giving the same positions as if $\mathbf{r}^2$ had been done the first night. Then a combination of $\mathbf{r}^2$ and $\mathbf{r}^3$ is tried. (This just gives $\mathbf{r}^{-1} = \mathbf{r}^5$ the inverse of which was tried on the first night.) All of these products are symmetries if the factors are. (So the physicists end up getting fooled night after night for almost a week of different positions! Saturday, they have to take off since they read right-to-left.)

If operators $\mathbf{a}$ and $\mathbf{b}$ commute with an analyzer $\mathbf{T}$-matrix then so do all their products

$$\text{If: } \mathbf{aT} = \mathbf{Ta} \quad \text{and} \quad \mathbf{bT} = \mathbf{T}\,\mathbf{b} \quad \text{then} \quad \mathbf{abT} = \mathbf{Tab} \quad \text{and} \quad \mathbf{baT} = \mathbf{T}\,\mathbf{ba} \tag{8.1.4a}$$

and inverses. $\text{If: } \mathbf{aT} = \mathbf{Ta} \qquad\qquad\qquad \text{then} \quad \mathbf{a}^{-1}\mathbf{T} = \mathbf{Ta}^{-1} \tag{8.1.4b}$

This shows that the set of unitary operators that commute with a particular $\mathbf{T}$-operator must satisfy the group axioms (1-4) stated in Sec. 2.2. This set is called a *symmetry group $G=\{\,\mathbf{a}\,,\,\mathbf{b}\,,\,\mathbf{c}\,,...,\,\mathbf{g}\,,...\}$* of the operator $\mathbf{T}$. We are supposing that the analyzer matrix $\mathbf{T}$ associated with the experiment in Fig. 8.1.1 has an *N*-cyclic symmetry group $C_6 = \{\,\mathbf{1}\,,\,\mathbf{r}\,,\,\mathbf{r}^2\,,\,\mathbf{r}^3,\,\mathbf{r}^4,\,\mathbf{r}^5\}$ of six (*N*=6) operators that have the following *group multiplication table*. We put the <u>inverses</u> of the first column in the top row so $\mathbf{1}$ is on the diagonal.

C_6	$\mathbf{1}$	r^5	r^4	r^3	r^2	r
$\mathbf{1}$	$\mathbf{1}$	r^5	r^4	r^3	r^2	r
r	r	$\mathbf{1}$	r^5	r^4	r^3	r^2
r^2	r^2	r	$\mathbf{1}$	r^5	r^4	r^3
r^3	r^3	r^2	r	$\mathbf{1}$	r^5	r^4
r^4	r^4	r^3	r^2	r	$\mathbf{1}$	r^5
r^5	r^5	r^4	r^3	r^2	r	$\mathbf{1}$

(8.1.5a)

$$\mathbf{1} = \begin{pmatrix} 1 & \cdot & \cdot & \cdot & \cdot & \cdot \\ \cdot & 1 & \cdot & \cdot & \cdot & \cdot \\ \cdot & \cdot & 1 & \cdot & \cdot & \cdot \\ \cdot & \cdot & \cdot & 1 & \cdot & \cdot \\ \cdot & \cdot & \cdot & \cdot & 1 & \cdot \\ \cdot & \cdot & \cdot & \cdot & \cdot & 1 \end{pmatrix} \tag{8.1.5b}$$

Think of the table as a matrix in a basis $\{|0\rangle|1\rangle|2\rangle|3\rangle|4\rangle|5\rangle\}$ defined by operators $\{\mathbf{1},\mathbf{r},\mathbf{r}^2,\mathbf{r}^3,\mathbf{r}^4,\mathbf{r}^5\}$.

This makes a matrix representation for each operator using the channel states as a basis by simply replacing each operator's table entry by a "1" in that position of its matrix and "0" or "dot" ($\cdot$) elsewhere.

$$|0\rangle|1\rangle|2\rangle|3\rangle|4\rangle|5\rangle \qquad |0\rangle|1\rangle|2\rangle|3\rangle|4\rangle|5\rangle \qquad |0\rangle|1\rangle|2\rangle|3\rangle|4\rangle|5\rangle \qquad |0\rangle|1\rangle|2\rangle|3\rangle|4\rangle|5\rangle \qquad |0\rangle|1\rangle|2\rangle|3\rangle|4\rangle|5\rangle$$

$$\mathbf{r}=\begin{pmatrix} . & . & . & . & . & 1 \\ 1 & . & . & . & . & . \\ . & 1 & . & . & . & . \\ . & . & 1 & . & . & . \\ . & . & . & 1 & . & . \\ . & . & . & . & 1 & . \end{pmatrix}, \mathbf{r}^2=\begin{pmatrix} . & . & . & . & 1 & . \\ . & . & . & . & . & 1 \\ 1 & . & . & . & . & . \\ . & 1 & . & . & . & . \\ . & . & 1 & . & . & . \\ . & . & . & 1 & . & . \end{pmatrix}, \mathbf{r}^3=\begin{pmatrix} . & . & . & 1 & . & . \\ . & . & . & . & 1 & . \\ . & . & . & . & . & 1 \\ 1 & . & . & . & . & . \\ . & 1 & . & . & . & . \\ . & . & 1 & . & . & . \end{pmatrix}, \mathbf{r}^4=\begin{pmatrix} . & . & 1 & . & . & . \\ . & . & . & 1 & . & . \\ . & . & . & . & 1 & . \\ . & . & . & . & . & 1 \\ 1 & . & . & . & . & . \\ . & 1 & . & . & . & . \end{pmatrix}, \mathbf{r}^5=\begin{pmatrix} . & 1 & . & . & . & . \\ . & . & 1 & . & . & . \\ . & . & . & 1 & . & . \\ . & . & . & . & 1 & . \\ . & . & . & . & . & 1 \\ 1 & . & . & . & . & . \end{pmatrix}$$

$$(8.1.5c)$$

These are sometimes called the *regular permutation representations* because they permute each of the p-position states. The first column of matrix $\mathbf{r}^{p-1}$ represents the basic ket definition $|p\rangle = \mathbf{r}^{p-1}|1\rangle$ as follows.

$$|0\rangle = \mathbf{1}|0\rangle \;,\; |1\rangle = \mathbf{r}|0\rangle \;,\; |2\rangle = \mathbf{r}^2|0\rangle \;,\; |3\rangle = \mathbf{r}^3|0\rangle \;,\; |4\rangle = \mathbf{r}^4|0\rangle \;,\; |5\rangle = \mathbf{r}^5|0\rangle \qquad (8.1.6a)$$

The $\mathbf{r}$-transform is unitary $\mathbf{r}^\dagger = \mathbf{r}^{-1}$. The Hermitian conjugate of these relations is the basic bra definition.

$$\langle 0| = \langle 0|\mathbf{1} \;,\; \langle 1| = \langle 0|\mathbf{r}^{-1} \;,\; \langle 2| = \langle 0|\mathbf{r}^{-2} \;,\; \langle 3| = \langle 0|\mathbf{r}^{-3} \;,\; \langle 4| = \langle 0|\mathbf{r}^{-4} \;,\; \langle 5| = \langle 0|\mathbf{r}^{-5} \quad (8.1.6b)$$

These defintions may be summed up by defining a *representation matrix* $\mathbf{R}(\mathbf{g})$ with components $R_{pq}(\mathbf{g})$.

$$R_{pq}(\mathbf{g}) = \langle p|\mathbf{g}|q\rangle \qquad\qquad (8.1.6c)$$

(c) So what's a group representation?

To use a more "kosher" mathematical language we should say that the representation matrices in (8.1.5b-c) are functions $\mathbf{R}(\mathbf{g})$ of the group $G=\{\mathbf{1},\mathbf{g_1},\mathbf{g_2},\ldots\}=C_6=\{\mathbf{1},\mathbf{r},\mathbf{r}^2,\mathbf{r}^3,\mathbf{r}^4,\mathbf{r}^5\}$. That is, every group operator gets mapped onto a matrix so that the matrix $\mathbf{R}(\mathbf{g_1g_2})$ of a group product $\mathbf{g_1g_2}$ is the matrix product $\mathbf{R}(\mathbf{g_1})\cdot \mathbf{R}(\mathbf{g_2})$ of the factors.

$$\mathbf{R}(\mathbf{g_1})\cdot \mathbf{R}(\mathbf{g_2}) = \mathbf{R}(\mathbf{g_1}\cdot\mathbf{g_2}) \qquad\qquad (8.1.7a)$$

Stated simply, "*The product of representations must equal the representation of the product.*" The matrices in (8.1.5b-c) must obey the group multiplication table (8.1.5a)! It is easy to see that the first matrix (8.1.5b) satisfies this requirement trivially.

$$\mathbf{R}(\mathbf{1})\cdot \mathbf{R}(\mathbf{1}) = \mathbf{R}(\mathbf{1}\cdot\mathbf{1}) = \mathbf{R}(\mathbf{1}) \qquad\qquad (8.1.7b)$$

The remainder have to satisfy it because of definition (8.1.6) involve bras and kets which obey Axioms 1-4, that is, $\mathbf{R}(\mathbf{g})$ is a *unitary representation*. The conjugation axiom $(\langle p|q\rangle^* = \langle q|p\rangle)$ implies that the $\dagger$-conugate $(R^\dagger{}_{pq} = R^*{}_{qp})$ of a representation must be the representation of the group inverse $\mathbf{r}^\dagger = \mathbf{r}^{-1}$.

$$R_{pq}(\mathbf{g}^\dagger) = \langle p|\mathbf{g}^\dagger|q\rangle = (\langle q|\mathbf{g}|p\rangle)^* = (R_{qp}(\mathbf{g}))^* \qquad\qquad (8.1.8a)$$

Stated more simply this is simply demanding operator unitarity from its representations.

$$\mathbf{R}^\dagger(\mathbf{g}) = \mathbf{R}(\mathbf{g}^\dagger) = \mathbf{R}(\mathbf{g}^{-1}) = \mathbf{R}^{-1}(\mathbf{g}) \qquad\qquad (8.1.8b)$$

All of the above are properties that are invariant to a change-of-basis transformation $U^\dagger U = 1$. Given $\mathbf{R}^U(\mathbf{g}) = U\,\mathbf{R}(\mathbf{g})U^\dagger$, it follows that the new $\mathbf{R}^U$ matrices also satisfy (8.1.7) thru (8.1.8). For example,

$$\mathbf{R}^U(\mathbf{g_1})\mathbf{R}^U(\mathbf{g_1}) = U\,\mathbf{R}(\mathbf{g_1})U^\dagger U\,\mathbf{R}(\mathbf{g_2})U^\dagger = U\,\mathbf{R}(\mathbf{g_1})\mathbf{R}(\mathbf{g_2})U^\dagger = \mathbf{R}^U(\mathbf{g_1g_2}) \quad (8.1.9)$$

Now we discuss finding and applying the diagonalizong transformation or *d-tran* of $\mathbf{R}(\mathbf{g})$.

8.2 C_N Spectral Decomposition: Solving a C_6 transfer matrix

The main analyzer of Fig. 8.1.1 is supposed to have C_6 symmetry. However, it is also supposed to do some things that we haven't let single analyzers do to an incoming base state $|\Psi_{IN}\rangle=|p\rangle$, and that is, *mix it up*! No longer will a base state $|1\rangle$ or $|2\rangle$ just fly on through with nothing more than an extra phase attached, so it just comes out $e^{i\Omega_1}|1\rangle$ or $e^{i\Omega_2}|2\rangle$. From now on, each base state $|p\rangle$ is going to get treated to a full-blown transformation matrix T that is not necessarily diagonal. A general base state $|\Psi_{IN}\rangle$ will be output as $|\Psi_{OUT}\rangle$, as follows,

$$\begin{pmatrix} \langle 0|\Psi_{OUT}\rangle \\ \langle 1|\Psi_{OUT}\rangle \\ \langle 2|\Psi_{OUT}\rangle \\ \langle 3|\Psi_{OUT}\rangle \\ \langle 4|\Psi_{OUT}\rangle \\ \langle 5|\Psi_{OUT}\rangle \end{pmatrix} = \begin{pmatrix} T_{00} & T_{01} & T_{02} & T_{03} & T_{04} & T_{05} \\ T_{10} & T_{11} & T_{12} & T_{13} & T_{14} & T_{15} \\ T_{20} & T_{21} & T_{22} & T_{23} & T_{24} & T_{25} \\ T_{30} & T_{31} & T_{32} & T_{33} & T_{34} & T_{35} \\ T_{40} & T_{41} & T_{42} & T_{43} & T_{44} & T_{45} \\ T_{50} & T_{51} & T_{52} & T_{53} & T_{54} & T_{55} \end{pmatrix} \bullet \begin{pmatrix} \langle 0|\Psi_{IN}\rangle \\ \langle 1|\Psi_{IN}\rangle \\ \langle 2|\Psi_{IN}\rangle \\ \langle 3|\Psi_{IN}\rangle \\ \langle 4|\Psi_{IN}\rangle \\ \langle 5|\Psi_{IN}\rangle \end{pmatrix} \quad (8.2.1a)$$

where off-diagonal *(p≠q)* matrix elements

$$T_{pq} = \langle p|\mathrm{T}|q\rangle \qquad (8.2.1b)$$

of **T** are not all zero if $|p\rangle$ and $|q\rangle$ do not belong to **T**'s "own" eigenbasis. (Bilingual redundancy, again.)

So, are we ready to diagonalize a general six-by-six matrix? No way, Jose'! But, here is where symmetry analysis rides to the rescue. If we can diagonalize the **r**-matrix in (8.1.5) then, barring appearance of nilpotents or other obnoxious gremlins, we may be able to also diagonalize the **T**-matrix (8.2.1). This is because (8.2.1) isn't just any old six-by-six matrix; it has C_6 symmetry and must therefore commute with each of its symmetry operators like **r**. Recall **T r = r T** in (8.1.2). This means that **T** and **r** share projectors $\mathbf{P}_k$ as shown in (3.1.37). Diagonalize **r** and you may have diagonalized **T** as well!

(a) Spectral decomposition of symmetry operators r^p

The problem of analyzing (8.2.1) is then reduced to diagonalizing **r** in (8.1.5a), another six-by-six matrix, albeit a simpler one. But wait! No matrix need bother us. The minimal equation for **r** is simply

$$\mathbf{r}^N = \mathbf{1} \ (N=6, \text{ here.}) \qquad (8.2.2)$$

and all its eigenvalues are the roots of unity given before by (7.3.5) and displayed in Fig. 7.3.3.

$$\chi_m = \left(r_N\right)^m = \left(e^{-i2\pi/N}\right)^m = e^{-i2\pi m/N} \quad \text{where: } m = 0,1,2,...,N-1 \qquad (8.2.3)$$

(Again, *N=6*). The spectral projectors of **r** follow easily. To help understand this recall that a spectral decomposition of any matrix **M** come with beautiful and powerful consequential relations. First, **M**'s *eigen-projector* $\mathbf{P}_k$ satisfies: $\mathbf{M}\mathbf{P}_k = \varepsilon_k \mathbf{P}_k$ and *orthonormality* $\mathbf{P}_j\mathbf{P}_k = \delta_{jk} \mathbf{P}_k$. Then there is *completeness*

$$\mathbf{1} = \mathbf{P}_1 + \mathbf{P}_2 + ...+ \mathbf{P}_n . \qquad (3.1.15d)_{repeated}$$

and *spectral decomposition of operator* **M**, and *functional spectral decomposition of an operator* **M** .

$$\mathbf{M} = \varepsilon_1 \mathbf{P}_1 + \varepsilon_2 \mathbf{P}_2 + ...+ \varepsilon_n \mathbf{P}_n \qquad (3.1.15e)_{repeated}$$

$$f(\mathbf{M}) = f(\varepsilon_1) \mathbf{P}_1 + f(\varepsilon_2) \mathbf{P}_2 + ...+ f(\varepsilon_n) \mathbf{P}_n \qquad (3.1.17)_{repeated}$$

Applying the spectral relations using the eigenvalues (roots) in (8.2.3) gives a functional (power) spectral decomposition *(3.1.17)repeated* of all powers $\mathbf{r}^p$ of rotation operator $\mathbf{r}$ by putting $(\chi_m)^p$ before each $\mathbf{P}^m$.

$$
\begin{aligned}
\mathbf{1} &= \mathbf{P}^0 + \mathbf{P}^1 + \mathbf{P}^2 + \mathbf{P}^3 + \mathbf{P}^4 + \mathbf{P}^5 \\
\mathbf{r} &= \mathbf{P}^0 + \chi_1\mathbf{P}^1 + \chi_2\mathbf{P}^2 + \chi_3\mathbf{P}^3 + \chi_4\mathbf{P}^4 + \chi_5\mathbf{P}^5 \\
\mathbf{r}^2 &= \mathbf{P}^0 + \chi_1^2\mathbf{P}^1 + \chi_2^2\mathbf{P}^2 + \chi_3^2\mathbf{P}^3 + \chi_4^2\mathbf{P}^4 + \chi_5^2\mathbf{P}^5 \\
\mathbf{r}^3 &= \mathbf{P}^0 + \chi_1^3\mathbf{P}^1 + \chi_2^3\mathbf{P}^2 + \chi_3^3\mathbf{P}^3 + \chi_4^3\mathbf{P}^4 + \chi_5^3\mathbf{P}^5 \\
\mathbf{r}^4 &= \mathbf{P}^0 + \chi_1^4\mathbf{P}^1 + \chi_2^4\mathbf{P}^2 + \chi_3^4\mathbf{P}^3 + \chi_4^4\mathbf{P}^4 + \chi_5^4\mathbf{P}^5 \\
\mathbf{r}^5 &= \mathbf{P}^0 + \chi_1^5\mathbf{P}^1 + \chi_2^5\mathbf{P}^2 + \chi_3^5\mathbf{P}^3 + \chi_4^5\mathbf{P}^4 + \chi_5^5\mathbf{P}^5
\end{aligned}
$$

where: $\chi_m^p = \left(\chi_m\right)^p = e^{-i2\pi(mp)/N}$ (8.2.4a)

Apart from the normalization, the $\mathbf{P}^m$-to-$\mathbf{r}^p$ relation above is a unitary linear combination having the same Fourier transformation coefficients $\langle k_m | x_p \rangle$ as (7.3.10a). The inverse $\mathbf{r}^p$-to-$\mathbf{P}^m$ relation is obtained by transpose conjugating the coefficients χ_m^p above to give coefficients just like $\langle x_p | k_m \rangle$ in (7.3.10b).

$$(\chi_m^p)^* = \sqrt{N} \langle k_m | x_p \rangle^* = \sqrt{N} \langle x_p | k_m \rangle = e^{i2\pi(mp)/N} = \rho_p{}^m \tag{8.2.4b}$$

Then divide all by the norm $N=6$ to make the following idempotent projectors.

$$
\begin{aligned}
\mathbf{P}^0 &= \left(\mathbf{1} + \mathbf{r} + \mathbf{r}^2 + \mathbf{r}^3 + \mathbf{r}^4 + \mathbf{r}^5\right)/6 \\
\mathbf{P}^1 &= \left(\mathbf{1} + \rho_1\mathbf{r} + \rho_2\mathbf{r}^2 + \rho_3\mathbf{r}^3 + \rho_4\mathbf{r}^4 + \rho_5\mathbf{r}^5\right)/6 \\
\mathbf{P}^2 &= \left(\mathbf{1} + \rho_1^2\mathbf{r} + \rho_2^2\mathbf{r}^2 + \rho_3^2\mathbf{r}^3 + \rho_4^2\mathbf{r}^4 + \rho_5^2\mathbf{r}^5\right)/6 \\
\mathbf{P}^3 &= \left(\mathbf{1} + \rho_1^3\mathbf{r} + \rho_2^3\mathbf{r}^2 + \rho_3^3\mathbf{r}^3 + \rho_4^3\mathbf{r}^4 + \rho_5^3\mathbf{r}^5\right)/6 \\
\mathbf{P}^4 &= \left(\mathbf{1} + \rho_1^4\mathbf{r} + \rho_2^4\mathbf{r}^2 + \rho_3^4\mathbf{r}^3 + \rho_4^4\mathbf{r}^4 + \rho_5^4\mathbf{r}^5\right)/6 \\
\mathbf{P}^5 &= \left(\mathbf{1} + \rho_1^5\mathbf{r} + \rho_2^5\mathbf{r}^2 + \rho_3^5\mathbf{r}^3 + \rho_4^5\mathbf{r}^4 + \rho_5^5\mathbf{r}^5\right)/6
\end{aligned}
$$

where: $\rho_p^m = \chi_m^p = e^{i2\pi(pm)/N}$ (8.2.4c)

Operating on the first position state with these projectors gives the desired eigenstates of the $\mathbf{T}$-matrix. The norm is $\langle 1 | \mathbf{P}^m | 1 \rangle = 1/N$. (Recall $(3.1.13)_{\text{example}}$) Its root $1/\sqrt{N}$ results to give normalized eigenkets.

$$\left| k_m \right\rangle = \mathbf{P}^m \left| 0 \right\rangle \sqrt{N} = \sum_{p=0}^{N-1} \rho_p^m \mathbf{r}^p \left| 0 \right\rangle \sqrt{N} / N = \sum_{p=0}^{N-1} e^{i2\pi(pm)/N} \left| p \right\rangle / \sqrt{N} \tag{8.2.5a}$$

The inverse ket relations give position states $|x_p\rangle = |p\rangle$ in terms of wave $|k_m\rangle$ eigenkets.

$$\left| p \right\rangle = \mathbf{r}^p \left| 0 \right\rangle = \sum_{p=0}^{N-1} \chi_p^p \mathbf{P}^m \left| 0 \right\rangle \sqrt{N} = \sum_{p=0}^{N-1} e^{-i2\pi(mp)/N} \left| k_m \right\rangle / \sqrt{N} \tag{8.2.5b}$$

The preceding ket relations (8.2.5) and their operator equivalents (8.2.4) are the discrete-N Fourier transformations whose N-by-N transformation matrices are pictured for $N=1, 2, 3, 4, 5,$ and 6 in Fig. 7.3.3 and for $N=24$ in Fig. 7.3.5. The physical transformation is between N "quantum-dot" position point $|p\rangle$-states $(|x_p\rangle = |p\rangle)$ and their N quantum momentum Fourier-wave $|k_m\rangle$-states. Much of the above is mathematical "legalese" which gets short-circuited in the calculations that are described next.

(b) Writing transfer operator T in terms of symmetry operators rᵖ

In order for main analyzer **T**-matrix (8.2.1) to have C_N symmetry, it must commute with all the rotation operator **r**-matrices in (2.7.5). **T** does this by being a linear combination of $\mathbf{r}^p$ as follows.

$$\mathbf{T} = A\,\mathbf{1} + B\,\mathbf{r} + C\,\mathbf{r}^2 + D\,\mathbf{r}^3 + C'\,\mathbf{r}^4 + B'\,\mathbf{r}^5, \qquad (8.2.6)$$

The $\mathbf{r}^p$-matrices in (2.7.5) are thus combined to give the general C_6 -symmetric **T**-matrix relation (8.2.1).

$$
\begin{pmatrix}
\langle 0|\Psi_{\text{OUT}}\rangle \\
\langle 1|\Psi_{\text{OUT}}\rangle \\
\langle 2|\Psi_{\text{OUT}}\rangle \\
\langle 3|\Psi_{\text{OUT}}\rangle \\
\langle 4|\Psi_{\text{OUT}}\rangle \\
\langle 5|\Psi_{\text{OUT}}\rangle
\end{pmatrix}
=
\begin{pmatrix}
A & B' & C' & D & C & B \\
B & A & B' & C' & D & C \\
C & B & A & B' & C' & D \\
D & C & B & A & B' & C' \\
C' & D & C & B & A & B' \\
B' & C' & D & C & B & A
\end{pmatrix}
\cdot
\begin{pmatrix}
\langle 0|\Psi_{\text{IN}}\rangle \\
\langle 1|\Psi_{\text{IN}}\rangle \\
\langle 2|\Psi_{\text{IN}}\rangle \\
\langle 3|\Psi_{\text{IN}}\rangle \\
\langle 4|\Psi_{\text{IN}}\rangle \\
\langle 5|\Psi_{\text{IN}}\rangle
\end{pmatrix}
\qquad (8.2.7)
$$

The undetermined coefficients A, B, C, D, C', and B' correspond to all the *transition amplitudes* that state $|0\rangle$ could possibly have to other states $|0\rangle, |1\rangle, |2\rangle, |3\rangle, |4\rangle,$ and $|5\rangle$ as indicated by arrows in Fig. 8.2.1a.
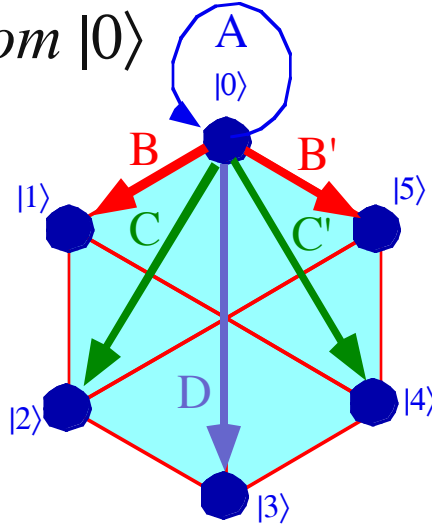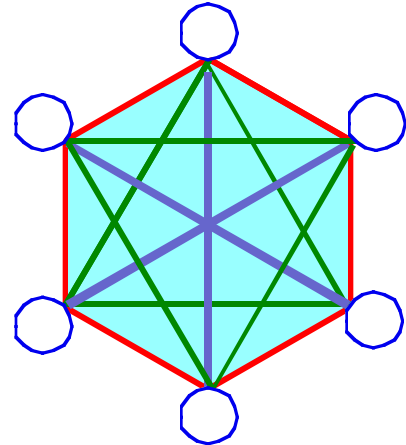
Fig. 8.2.1 Generic 6-channel (C_6) beam transitions (a) Amplitudes (b) Paths

In order that the system really have C_6 symmetry, the next state $|1\rangle$ must make the same amplitudes to the states $|1\rangle, |2\rangle, |3\rangle, |4\rangle, |5\rangle,$ and $|6\rangle$, respectively, and so on for $|2\rangle, |3\rangle, |4\rangle,$ and $|5\rangle$. All the equivalent paths are indicated in Fig. 8.2.1b.

The expression of a quantum operator, such as the analyzer transfer matrix **T**, in terms of its symmetry operators, such as the $\mathbf{r}^p$, is a deep and important idea which will be used a lot in the rest of this text. It is useful if, as the case is here, the $\mathbf{r}^p$ and **T** have the same set of eigenstates or projectors so that a (presumably!) easy spectral decomposition of the former also solves the latter. Also, it is useful to label by symmetry operators both the system coordinate base states, as in (8.1.6), and the transfer or transition amplitudes or *paths* between the base states, as in Fig. 8.2.1.

(c) Spectral decomposition of transfer operator T

Now a C_6-symmetric **T** operator equation with these *A, B, C,.. amplitudes* must be diagonalized if represented in the symmetry projected $|k_m\rangle$ basis (8.2.5).

$$
\begin{pmatrix} \langle k_0|\Psi_{OUT}\rangle \\ \langle k_1|\Psi_{OUT}\rangle \\ \langle k_2|\Psi_{OUT}\rangle \\ \langle k_3|\Psi_{OUT}\rangle \\ \langle k_4|\Psi_{OUT}\rangle \\ \langle k_5|\Psi_{OUT}\rangle \end{pmatrix} = \begin{pmatrix} \varepsilon(k_0) & 0 & 0 & 0 & 0 & 0 \\ 0 & \varepsilon(k_1) & 0 & 0 & 0 & 0 \\ 0 & 0 & \varepsilon(k_2) & B & 0 & 0 \\ 0 & 0 & 0 & \varepsilon(k_3) & 0 & 0 \\ 0 & 0 & 0 & 0 & \varepsilon(k_4) & 0 \\ 0 & 0 & 0 & 0 & 0 & \varepsilon(k_5) \end{pmatrix} \bullet \begin{pmatrix} \langle k_0|\Psi_{IN}\rangle \\ \langle k_1|\Psi_{IN}\rangle \\ \langle k_2|\Psi_{IN}\rangle \\ \langle k_3|\Psi_{IN}\rangle \\ \langle k_4|\Psi_{IN}\rangle \\ \langle k_5|\Psi_{IN}\rangle \end{pmatrix} \quad (8.2.8)
$$

This is because **T** in (8.2.6) is a combination of symmetry operators (2.7.5) and all the symmetry operators have $|k_m\rangle$ as eigenvectors with eigenvalues (8.2.3).

$$\mathbf{r}^p\,|k_m\rangle = \mathbf{r}^p\,\mathbf{P}^{\,m}|1\rangle = e^{-i2\pi\,mp/N}\,\mathbf{P}^{\,m}|1\rangle = e^{-i2\pi\,mp/6}\,|k_m\rangle \qquad (8.2.9)$$

Eigensolutions for **r**-operators are examples of elementary *Bloch symmetry conditions*.

$$\mathbf{r}\,|k_m\rangle = e^{-ik_m\,a}\,|k_m\rangle = e^{-i2\pi\,m/6}\,|k_m\rangle \text{ where: } k_m = \frac{2\pi}{Na}m \qquad (8.2.10)$$

It says that a translation by distance *a* (*60°* rotation **r** along analyzer circumference) sees each phase timer advance <u>forward</u> by $k_m a$ consistent with pictures Fig. 7.3.3 of Bloch $(m)_N$ waves. (Remember: phasor clocks turn <u>clockwise</u> with time, a <u>negative</u> angle.) Bloch symmetry is based upon the **r** -eigenoperator relation $\mathbf{r}\,\mathbf{P}^{\,m} = \chi_m\,\mathbf{P}^{\,m}$ with (m)-th-root-of-unity eigenvalues $\chi_m = e^{-i2\pi\,m/N}$ of **r** from (8.2.3).

An eigenvalue formula for all possible C_6 symmetric T-matrices

To compute the **T**-eigenvalues we just have to substitute the **r**-values of (8.2.9) into (8.2.6)!

$$\langle k_m|\mathbf{T}|k_m\rangle = A\,\langle k_m|\mathbf{1}|k_m\rangle + B\,\langle k_m|\mathbf{r}|k_m\rangle + C\,\langle k_m|\mathbf{r}^2|k_m\rangle + D\,\langle k_m|\mathbf{r}^3|k_m\rangle + C'\,\langle k_m|\mathbf{r}^4|k_m\rangle + B'\,\langle k_m|\mathbf{r}^5|k_m\rangle$$

$$= A + B\,e^{-ik_m\,a} + C\,e^{-i2k_m\,a} + D\,e^{-i3k_m\,a} + C'\,e^{i2k_m\,a} + B'\,e^{ik_m\,a} \qquad (8.2.11a)$$

(Note: $e^{-i4k_m\,a} = e^{i2k_m\,a}$ since *-4 mod 6 = 2 mod 6*. Also, $e^{-i5k_m\,a} = e^{ik_m\,a}$ since *-5 mod 6 = 1 mod 6*) Another way to derive eigenvalues is to put $|k_m\rangle$ into a matrix eigenequation (8.2.7) for **T**.

$$
\begin{pmatrix} A & B' & C' & D & C & B \\ B & A & B' & C' & D & C \\ C & B & A & B' & C' & D \\ D & C & B & A & B' & C' \\ C' & D & C & B & A & B' \\ B' & C' & D & C & B & A \end{pmatrix} \bullet \begin{pmatrix} 1 \\ e^{ik_m a} \\ e^{i2k_m a} \\ e^{i3k_m a} \\ e^{-i2k_m a} \\ e^{-ik_m a} \end{pmatrix} = \varepsilon(k_m)\begin{pmatrix} 1 \\ e^{ik_m a} \\ e^{i2k_m a} \\ e^{i3k_m a} \\ e^{-i2k_m a} \\ e^{-ik_m a} \end{pmatrix} \qquad (8.2.11b)
$$

The first row multiplication shows gives the same eigenvalue.

$$\varepsilon(k_m) = A + B\,e^{-ik_m\,a} + C\,e^{-i2k_m\,a} + D\,e^{-i3k_m\,a} + C'\,e^{i2k_m\,a} + B'\,e^{ik_m\,a} \qquad (8.2.11c)$$

It is important to understand what has been accomplished. A general eigenvalue and eigenvector formula has been derived *for all possible matrices* **T** *that have the symmetry C_6* of this particular "thought-experimental" problem. That is pretty neat, and it is just the beginning of a powerful set of symmetry tools!

What do the k_m- eigensolutions mean?

The physical interpretation of C_N eigensolutions is well known to electrical engineers. The ket in (8.2.11b) is a 6-phase generalization of the voltage in 3-phase wires commonly used to transport 220V power. A C_3 example shown in Fig. 8.2.2 resembles the $2_3=-1_3$-row of the C_3 table in Fig.7.3.3 with a time-phase of $t=5\pi/6$. (The $2_3=-1_3$-bra (row) is the †-conjugate of a $1_3=-2_3$-ket (column) eigenvector.) The result is a *(k=1)*-wave moving left to right in Fig. 8.2.2a or clockwise in Fig. 8.2.2b. (Recall: phasor-ahead feeds into phasor-behind. Imaginary ImΨ precedes the real ReΨ in time since phasors turn like clocks.)
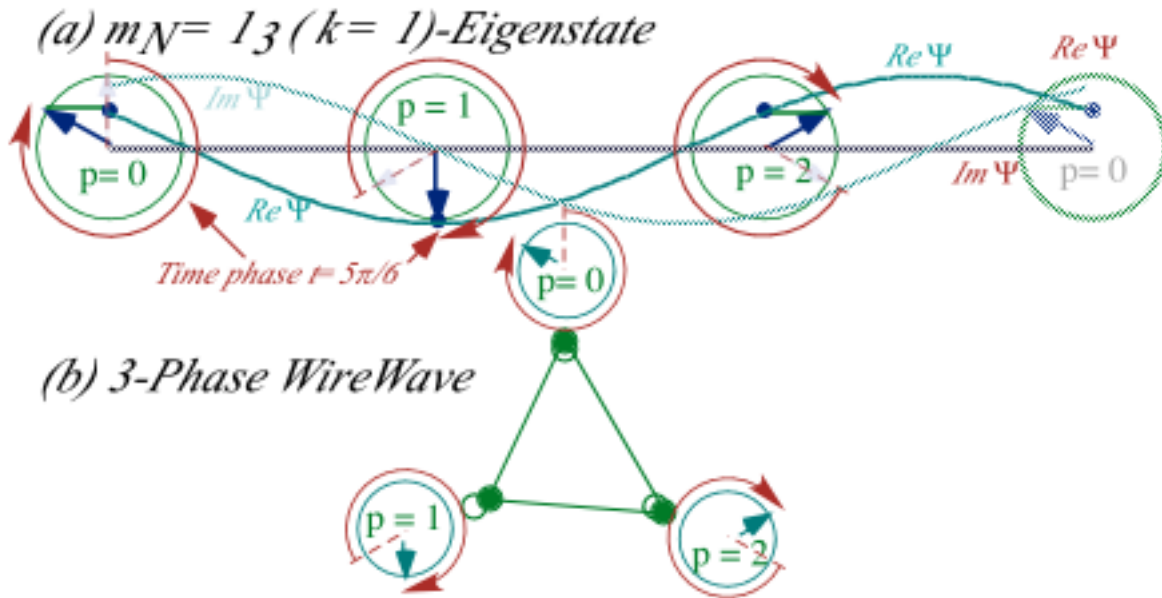
Fig. 8.2.2 (k=1) 3-channel (C_3) wave eigenstate (a) Real and imaginary waves (b) Phasors

A beam with all amplitudes equally dephased from their next neighbor is a $|k_m\rangle$-state that is not changed by a cyclically wired device that has C_N symmetry such as the C_6 analyzer sketched in Fig. 8.2.1. Also, if the **T**-matrix is *unitary* ($\mathbf{T}^\dagger = \mathbf{T}^{-1}$), $|k_m\rangle$-state eigenvalues $\varepsilon(k_m)$ must be unitary, too.

$$\varepsilon(k_m)^* = 1/\varepsilon(k_m) \qquad \text{or:} \ \ \varepsilon(k_m) = e^{i\phi_m} \qquad (8.2.12)$$

So the effect of the analyzer on an *eigenchannel* $|k_m\rangle$-state can only be to add an overall phase ϕ_m to it.

$$\mathbf{T}\,|k_m\rangle = e^{i\phi_m}\,|k_m\rangle \qquad (8.2.13)$$

The phase ϕ_m is sometimes called an *eigenchannel phase-shift* or *eigenphase* ϕ_m. Below we write the *eigenchannel basis representation* of the $\mathbf{T}\,|k_m\rangle$-equation for a general input state $|\Psi_{IN}\rangle$ with arbitrary values for its N-*eigenchannel-amplitudes* $\langle k_m|\Psi_{IN}\rangle$ of (8.2.7). (This means the N-*channel-amplitudes* $\langle p|\Psi_{IN}\rangle$ in the original representation (8.2.6) are arbitrary, too.) Below is for general $|\Psi_{IN}\rangle$.

$$
\begin{pmatrix} \langle k_0|\Psi_{OUT}\rangle \\ \langle k_1|\Psi_{OUT}\rangle \\ \langle k_2|\Psi_{OUT}\rangle \\ \langle k_3|\Psi_{OUT}\rangle \\ \langle k_4|\Psi_{OUT}\rangle \\ \langle k_5|\Psi_{OUT}\rangle \end{pmatrix}
=
\begin{pmatrix}
e^{i\phi_0} & 0 & 0 & 0 & 0 & 0 \\
0 & e^{i\phi_1} & 0 & 0 & 0 & 0 \\
0 & 0 & e^{i\phi_2} & 0 & 0 & 0 \\
0 & 0 & 0 & e^{i\phi_3} & 0 & 0 \\
0 & 0 & 0 & 0 & e^{i\phi_4} & 0 \\
0 & 0 & 0 & 0 & 0 & e^{i\phi_5}
\end{pmatrix}
\bullet
\begin{pmatrix} \langle k_0|\Psi_{IN}\rangle \\ \langle k_1|\Psi_{IN}\rangle \\ \langle k_2|\Psi_{IN}\rangle \\ \langle k_3|\Psi_{IN}\rangle \\ \langle k_4|\Psi_{IN}\rangle \\ \langle k_5|\Psi_{IN}\rangle \end{pmatrix}
\qquad (8.2.14)
$$

(d) OK, where <u>did</u> those e^{ikx} wavefunctions come from?

Every student of differential equations is told early on to try the exponential solutions e^{At} or e^{iat} in independent variable t with little reason given except, "It works!...sometimes." Now we can see why and when such solutions work. The key to our exponential eigenfunctions $\psi_{k_m}(x_p) = e^{ik_m x_p}/\sqrt{N}$ was C_N symmetry which demanded in (2.7.5) that we use roots of unity, that is, the roots of the minimal equation $\mathbf{r}^N=\mathbf{1}$ for symmetry operator $\mathbf{r}$.

If we let N approach infinity ($N \to \infty$) the symmetry approaches continuous translation symmetry C_∞, and the eigenfunctions $\psi_{k_m}(x_p)$ approach plane waves $\psi_k(x) = e^{ikx}/\sqrt{2\pi}$ such as given by (2.6.20b) in Sec. 2.6b. Symmetry demands independence or invariance to translation of the independent variable x. In other words, you should get the same differential equation no matter whether you let the origin be at $x=0$ or at $x=2,517$ in Timbuktu. For example, the differential equation

$$\frac{d^2\psi}{dx^2} + 2\gamma\frac{d\psi}{dx} + k^2\psi = 0 \qquad\qquad (8.2.15)$$

does have C_∞ symmetry so e^{ikx} will work, but an equation like

$$\frac{d^2\psi}{dx^2} + 2\gamma x\frac{d\psi}{dx} + k^2 x^2\psi = 0 \qquad\qquad (8.2.16)$$

does not have C_∞ symmetry because of the x-dependence; it's not the same equation in Timbuktu. An example of a C_N-symmetric differential equation is Matieu's equation for waves in a periodic solid.

$$\frac{d^2\psi}{dx^2} + k^2\cos(Nx)\psi = 0$$

All that we have said applies as well when the independent variable is time t. For example, the differential equation

$$\frac{d^2\psi}{dt^2} + 2\Gamma\frac{d\psi}{dt} + \omega^2\psi = 0$$

does have C_∞ symmetry so $e^{i\omega t}$ will work. An example of a C_N-symmetric time differential equation is Mathieu's equation for a periodic force. Later we use C_N-symmetry to help solve this type of equation.

$$\frac{d^2\psi}{dt^2} + k^2\cos(Nt)\psi = 0$$

8.3 Related Symmetry Analysis Examples

The homo-cyclic two-dot C_2 and three-dot C_3 sytems are sketched below in the way the C_6 system was sketched in Fig. 8.2.1. The transfer matrix equations (8.3.1) have eigenket tables (8.3.2).

$$\begin{pmatrix} \langle 0|\Psi_{OUT}\rangle \\ \langle 1|\Psi_{OUT}\rangle \end{pmatrix} = \begin{pmatrix} A & B \\ B & A \end{pmatrix}\begin{pmatrix} \langle 0|\Psi_{IN}\rangle \\ \langle 1|\Psi_{IN}\rangle \end{pmatrix} \quad (8.3.1a)$$

$$\begin{pmatrix} \langle 0|\Psi_{OUT}\rangle \\ \langle 1|\Psi_{OUT}\rangle \\ \langle 2|\Psi_{OUT}\rangle \end{pmatrix} = \begin{pmatrix} A & B' & B \\ B & A & B' \\ B' & B & A \end{pmatrix}\begin{pmatrix} \langle 0|\Psi_{IN}\rangle \\ \langle 1|\Psi_{IN}\rangle \\ \langle 2|\Psi_{IN}\rangle \end{pmatrix} (8.3.1b)$$

(a) C_2 System   (b) C_3 System
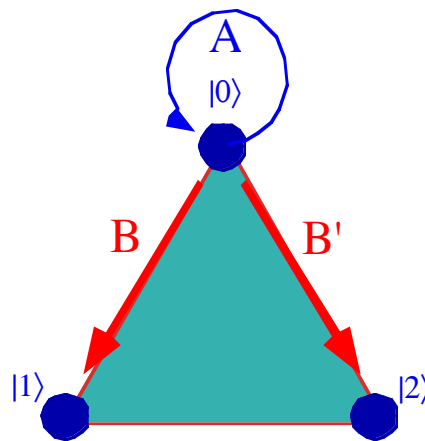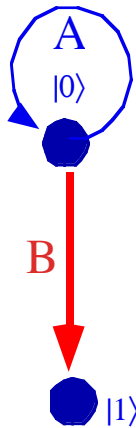
Fig. 8.3.1 Generic N-channel (C_N) quantum dot systems. (a)N=2 (b) N=3

(8.3.2a)   (8.3.2b)

C_2	$\|x_0\rangle = \mathbf{R}^0\|0\rangle$	$\|x_1\rangle = \mathbf{R}^1\|0\rangle$	
$\|(0)_2\rangle$	1	1	$/\sqrt{2}$
$\|(1)_2\rangle$	1	−1	$/\sqrt{2}$

C_3	$\|x_0\rangle = \mathbf{r}^0\|0\rangle$	$\|x_1\rangle = \mathbf{r}^1\|0\rangle$	$\|x_2\rangle = \mathbf{r}^2\|0\rangle$	
$\|(0)_3\rangle$	1	1	1	$/\sqrt{3}$
$\|(1)_3\rangle$	1	$e^{2\pi i/3}$	$e^{-2\pi i/3}$	$/\sqrt{3}$
$\|(2)_3\rangle$	1	$e^{-2\pi i/3}$	$e^{2\pi i/3}$	$/\sqrt{3}$

The eigenket tables are from Fig. 7.3.3. Each phasor in the $\langle$bra$|$ table for C_3 in Fig. 7.3.3 is replaced by its complex conjugate to make kets. A preceding Fig. 8.2.2 shows a $|(1)_3\rangle$ wave with eigen-phase shift of $-5\pi/6$. The corresponding transfer matrix eigenvalues $\langle m_N|\mathbf{T}|m_N\rangle$ in terms of parameters $A,B,..$ are left as exercises.

Besides such cyclic C_N systems there are an enormous number of ways to connect N-dots in ways that have more or less symmetry. A few of these are considered below and in problems. Most of the interesting (Also, read "doable!") quantum problems have an underlying symmetry.

(a) Dihedral symmetry D₂

Two 4-dot symmetries are shown in Fig. 8.3.2 below with transfer matrix relations.

$$\begin{pmatrix} \langle 0|\Psi_{OUT}\rangle \\ \langle 1|\Psi_{OUT}\rangle \\ \langle 2|\Psi_{OUT}\rangle \\ \langle 3|\Psi_{OUT}\rangle \end{pmatrix} = \begin{pmatrix} A & B & C & C \\ B & A & C & C \\ C & C & A' & B' \\ C & C & B' & A' \end{pmatrix} \begin{pmatrix} \langle 0|\Psi_{IN}\rangle \\ \langle 1|\Psi_{IN}\rangle \\ \langle 2|\Psi_{IN}\rangle \\ \langle 3|\Psi_{IN}\rangle \end{pmatrix}$$

(8.3.3a)

$$\begin{pmatrix} \langle 0|\Psi_{OUT}\rangle \\ \langle 1|\Psi_{OUT}\rangle \\ \langle 2|\Psi_{OUT}\rangle \\ \langle 3|\Psi_{OUT}\rangle \end{pmatrix} = \begin{pmatrix} A & B & B' & C \\ B & A & C & B' \\ B' & C & A & B \\ C & B' & B & A \end{pmatrix} \begin{pmatrix} \langle 0|\Psi_{IN}\rangle \\ \langle 1|\Psi_{IN}\rangle \\ \langle 2|\Psi_{IN}\rangle \\ \langle 3|\Psi_{IN}\rangle \end{pmatrix}$$

(8.3.3b)
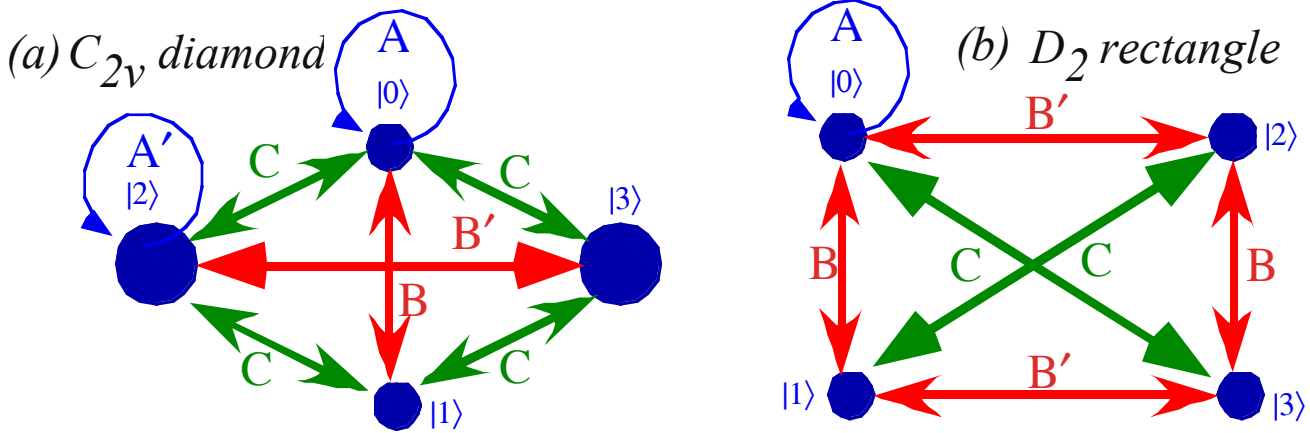
Fig. 8.3.2 Generic 4-channel (D₂) quantum dot systems. (a)Diamond C₂ᵥ (b) Rectangular D₂.

Consider the rectangular D_2 system. Its transfer matrix may be written in terms of four operators.

$$\mathbf{T} = A\,\mathbf{1} + B\,\mathbf{R}_x + B'\,\mathbf{R}_y + C\,\mathbf{R}_z$$

$$\begin{pmatrix} A & B & B' & C \\ B & A & C & B' \\ B' & C & A & B \\ C & B' & B & A \end{pmatrix} = A\begin{pmatrix} 1&0&0&0 \\ 0&1&0&0 \\ 0&0&1&0 \\ 0&0&0&1 \end{pmatrix} + B\begin{pmatrix} 0&1&0&0 \\ 1&0&0&0 \\ 0&0&0&1 \\ 0&0&1&0 \end{pmatrix} + B'\begin{pmatrix} 0&0&1&0 \\ 0&0&0&1 \\ 1&0&0&0 \\ 0&1&0&0 \end{pmatrix} + C\begin{pmatrix} 0&0&0&1 \\ 0&0&1&0 \\ 0&1&0&0 \\ 1&0&0&0 \end{pmatrix}$$

(8.3.4)

Each of the operators $\mathbf{R}_x$, $\mathbf{R}_y$, or $\mathbf{R}_z$, corresponds to *180°*-rotations around *x*, *y*, or *z* axes, respectively, the effect of which is indicated in Fig. 8.3.1b by transfer path arrows labeled *B*, *B′*, and *C*, respectively. A transfer path *B′* along the *x*-direction is done by a *y*-rotation $\mathbf{R}_y$, while *B* along *y* is done by $\mathbf{R}_x$.

D₂ group structure

The multiplication table for the *Verrgrupe* (4-group) is quite famous and relevant to quantum theory.

1	R_x	R_y	R_z
R_x	1	R_z	R_y
R_y	R_z	1	R_x
R_z	R_y	R_x	1

(8.3.5a)

Its structure reduces to a few simple products. The first is *(xyz)*-cyclic: It holds for *(zxy)* and *(yzx)*, too.

$$\mathbf{R_x R_y = R_y R_x = R_z}, \quad (8.3.5b) \qquad\qquad \mathbf{R_x}^2 = \mathbf{R_y}^2 = \mathbf{R_z}^2 = \mathbf{1}. \quad (8.3.5c)$$

D_2 spectral decomposition: The old "1=1•1 trick" again

The latter (8.3.5c) are of immediate interest to a quantum algebraist because they give minimal equations.

$$\mathbf{R_x}^2 - \mathbf{1} = \mathbf{0}, \quad (8.3.5d) \qquad\qquad \mathbf{R_y}^2 - \mathbf{1} = \mathbf{0}. \quad (8.3.5e)$$

From the roots (± 1) of each minimal equation is constructed a spectral decomposition of $\mathbf{R_x}$ and $\mathbf{R_y}$. This is the simplest application of the Chapter 3 projector formula (3.1.15a) you will probably ever see.

$$P_x^+ = \frac{1 + R_x}{2}$$
$$P_x^- = \frac{1 - R_x}{2} \qquad (8.3.6a)$$

$$P_y^+ = \frac{1 + R_y}{2}$$
$$P_y^- = \frac{1 - R_y}{2} \qquad (8.3.6b)$$

This spectrally decomposes $\mathbf{R_x}$ and $\mathbf{R_y}$ separately. We can do $\mathbf{R_z}$, too, but all three must be done *together*.

$$\mathbf{1} = P_x^+ + P_x^-$$
$$R_x = P_x^+ - P_x^- \qquad (8.3.7a)$$

$$\mathbf{1} = P_y^+ + P_y^-$$
$$R_y = P_y^+ - P_y^- \qquad (8.3.7b)$$

To make projectors for the whole D_2 symmetry together we use the old "**1=1•1** trick" from (3.1.36).

$$\mathbf{1} = \mathbf{1 \cdot 1} = \left(P_x^+ + P_x^-\right) \cdot \left(P_y^+ + P_y^-\right) = P_x^+ \cdot P_y^+ + P_x^- \cdot P_y^+ + P_x^+ \cdot P_y^- + P_x^- \cdot P_y^- \qquad (8.3.8)$$

The result are *irreducible* projectors $\mathbf{P}^{(i)}$ for the whole D_2 symmetry. Irreducible means $\mathsf{TraceR}(\mathbf{P}^{(i)}) = 1$.

$$\mathbf{P}^{++} \equiv P_x^+ \cdot P_y^+ = \frac{\left(1 + R_x\right) \cdot \left(1 + R_y\right)}{2 \cdot 2} = \frac{1}{4}\left(1 + R_x + R_y + R_z\right)$$

$$\mathbf{P}^{-+} \equiv P_x^- \cdot P_y^+ = \frac{\left(1 - R_x\right) \cdot \left(1 + R_y\right)}{2 \cdot 2} = \frac{1}{4}\left(1 - R_x + R_y - R_z\right)$$

$$\qquad\qquad (8.3.9a)$$

$$\mathbf{P}^{+-} \equiv P_x^+ \cdot P_y^- = \frac{\left(1 + R_x\right) \cdot \left(1 - R_y\right)}{2 \cdot 2} = \frac{1}{4}\left(1 + R_x - R_y - R_z\right)$$

$$\mathbf{P}^{--} \equiv P_x^- \cdot P_y^- = \frac{\left(1 - R_x\right) \cdot \left(1 - R_y\right)}{2 \cdot 2} = \frac{1}{4}\left(1 - R_x - R_y + R_z\right)$$

Each $\mathbf{P}$ is multiplied by its own eigenvalue (± 1) of $\mathbf{1}$, $\mathbf{R_x}$, $\mathbf{R_y}$, and $\mathbf{R_z}$ in the D_2 spectral decomposition.

$$\mathbf{1} \;= (+1)\mathbf{P}^{++} + (+1)\mathbf{P}^{-+} + (+1)\mathbf{P}^{+-} + (+1)\mathbf{P}^{--} \quad (completeness)$$

$$\mathbf{R}_x = (+1)\mathbf{P}^{++} + (-1)\mathbf{P}^{-+} + (+1)\mathbf{P}^{+-} + (-1)\mathbf{P}^{--}$$

$$\qquad\qquad (8.3.9b)$$

$$\mathbf{R}_y = (+1)\mathbf{P}^{++} + (+1)\mathbf{P}^{-+} + (-1)\mathbf{P}^{+-} + (-1)\mathbf{P}^{--}$$

$$\mathbf{R}_z = (+1)\mathbf{P}^{++} + (-1)\mathbf{P}^{-+} + (-1)\mathbf{P}^{+-} + (+1)\mathbf{P}^{--}$$

Spectral decomposition of D_2 transfer matrices

Spectral decomposition applies to transfer matrix (8.3.4) and yields its eigenvalue spectrum.

$$\langle + + |\mathbf{T}| + + \rangle = \varepsilon^{++} = A\langle \mathbf{1} \rangle + B\langle \mathbf{R}_x \rangle + B'\langle \mathbf{R}_y \rangle + C\langle \mathbf{R}_z \rangle = A + B + B' + C$$

$$\langle - + |\mathbf{T}| - + \rangle = \varepsilon^{-+} = A\langle \mathbf{1} \rangle + B\langle \mathbf{R}_x \rangle + B'\langle \mathbf{R}_y \rangle + C\langle \mathbf{R}_z \rangle = A - B + B' - C$$

$$\langle + - |\mathbf{T}| + - \rangle = \varepsilon^{+-} = A\langle \mathbf{1} \rangle + B\langle \mathbf{R}_x \rangle + B'\langle \mathbf{R}_y \rangle + C\langle \mathbf{R}_z \rangle = A + B - B' - C$$

$$\qquad\qquad (8.3.10)$$

$$\langle - - |\mathbf{T}| - - \rangle = \varepsilon^{--} = A\langle \mathbf{1} \rangle + B\langle \mathbf{R}_x \rangle + B'\langle \mathbf{R}_y \rangle + C\langle \mathbf{R}_z \rangle = A - B - B' + C$$

Again, this is a formula for *all possible D_2*-symmetric operators in this device space of Fig. 8.3.2b. Higher symmetry, such as "square" or *tetragonal D_4*–symmetry is obtained if parameters B and B' are equal. Then the

eigenvalues ε^{+-} and ε^{-+} become equal or *degenerate*. Such a symmetry is non-commutative or *non-Abelian* and requires further theory which will be taken up in a later chapter.

(b) Outer product structure: Double qubit registers

One of the things that makes group algebra powerful is the concept of an *outer (×) product* of two groups. You may have noticed that the D_2 group multiplication table was divided up so that the C_2 subgroup $\{\mathbf{1}, \mathbf{R_x}\}$ was isolated from the rest. The outer product is appropriate when two isolated "factors" correspond to orthogonal or independent systems such as two separate particles or two dimensions or two qubits.

D_2 is product $C_2 \times C_2$

An outer product of the eigenvalue tables in (8.3.2a) yields the D_2 eigenvalue table. This is basically what was happening in the algebraic maneuver of (8.3.8) based upon the old "$\mathbf{1}=\mathbf{1} \cdot \mathbf{1}$" trick.

C_2^x	$\mathbf{1}$	$\mathbf{R}_x$
$+$	1	1
$-$	1	-1

$\times$

C_2^y	$\mathbf{1}$	$\mathbf{R}_y$
$+$	1	1
$-$	1	-1

$=$

$C_2^x \times C_2^y$	$\mathbf{1} \cdot \mathbf{1}$	$\mathbf{R}_x \cdot \mathbf{1}$	$\mathbf{1} \cdot \mathbf{R}_y$	$\mathbf{R}_x \cdot \mathbf{R}_y$
$+ \cdot +$	$1 \cdot 1$	$1 \cdot 1$	$1 \cdot 1$	$1 \cdot 1$
$- \cdot +$	$1 \cdot 1$	$-1 \cdot 1$	$1 \cdot 1$	$-1 \cdot 1$
$+ \cdot -$	$1 \cdot 1$	$1 \cdot 1$	$1 \cdot (-1)$	$1 \cdot (-1)$
$- \cdot -$	$1 \cdot 1$	$-1 \cdot 1$	$1 \cdot (-1)$	$-1 \cdot (-1)$

(8.3.11a)

$=$

D_2	$\mathbf{1}$	$\mathbf{R}_x$	$\mathbf{R}_y$	$\mathbf{R}_z$
$++$	1	1	1	1
$-+$	1	-1	1	-1
$+-$	1	1	-1	-1
$--$	1	-1	-1	1

(8.3.11b)

Note that the numbers in (8.3.11b) are exactly the coefficients of *A, B, B′*, and *C* in the eigenvalue formulas for ε^{++}, $\varepsilon^{-+}, \varepsilon^{+-}$, and ε^{--} in (8.3.10). So the ×-product makes this calculation very easy indeed.

The outer product requires every operator in D_2 to be *uniquely* a product of one element in C_2^x and one element in C_2^y. The elements in C_2^x must commute with all those in C_2^y so each product is unique.

$$C_2^x \times C_2^y = \{\mathbf{1}, \mathbf{R}_x\} \times \{\mathbf{1}, \mathbf{R}_y\} =$$

$C_2^x \times C_2^y$	$\mathbf{1}$	$\mathbf{R}_y$
$\mathbf{1}$	$\mathbf{1} \cdot \mathbf{1}$	$\mathbf{1} \cdot \mathbf{R}_y$
$\mathbf{R}_x$	$\mathbf{R}_x \cdot \mathbf{1}$	$\mathbf{R}_x \cdot \mathbf{R}_y$

(8.3.11c)

$$= \{\mathbf{1}, \mathbf{R}_x, \mathbf{R}_y, \mathbf{R}_z\} = D_2$$

If a group *G* has *g* operators and a group *H* has *h* members, then *G×H* must have exactly *gh* members. It can be a great help to find a symmetry group is an outer product of its parts.

Multiple outer products are possible. The $D_2 = C_2 \times C_2$ system is like a double-binary or 4-bit register. A $C_2 \times C_2 \times C_2$ system is a triple-binary or 8-bit register known as *1-byte*. A double-binary D_2 register differs from a quadrary *(C_4)* register as a 1-byte binary systemis not a single octal *(C_8)* system.

Big-endian versus Little-endian

Computer scientists differ on whether the right ending bit should be the most significant bit (and least rapidly changing) or least significant bit and most often changing. (The former is called the Big-Endian

convention while the latter is called the Little-Endian convention after a perjorative folk-song.) The sequence *(00, 01, 10, 11)* is Little-Endian and more like our decimal numbering system. The sequence *(00, 10, 01, 11)* or in (8.3.11) (++, -+, +-, --) is Big-Endian and what we are using here.

C_6 is product $C_3 \times C_2$ (but C_4 is NOT $C_2 \times C_2$)

Our first example, the cyclic group C_6, is a composite $C_3 \times C_2$ of two of its subgroups C_2 and C_3 as shown below. Here the eigenvalue table (8.3.2a) of C_2 is crossed with the C_3 table (8.3.2b).

$C_3 \times C_2$	1	r	r^2	$1 \cdot R$	$r \cdot R$	$r^2 \cdot R$
$(0)_3 \cdot (0)_2$	$1 \cdot 1$	$1 \cdot 1$	$1 \cdot 1$	$1 \cdot 1$	$1 \cdot 1$	$1 \cdot 1$
$(1)_3 \cdot (0)_2$	$1 \cdot 1$	$e^{2\pi i/3} \cdot 1$	$e^{-2\pi i/3} \cdot 1$	$1 \cdot 1$	$e^{2\pi i/3} \cdot 1$	$e^{-2\pi i/3} \cdot 1$
$(2)_3 \cdot (0)_2$	$1 \cdot 1$	$e^{-2\pi i/3} \cdot 1$	$e^{2\pi i/3} \cdot 1$	$1 \cdot 1$	$e^{-2\pi i/3} \cdot 1$	$e^{2\pi i/3} \cdot 1$
$(0)_3 \cdot (1)_2$	$1 \cdot 1$	$1 \cdot 1$	$1 \cdot 1$	$1 \cdot (-1)$	$1 \cdot (-1)$	$1 \cdot (-1)$
$(1)_3 \cdot (1)_2$	$1 \cdot 1$	$1 \cdot 1$	$e^{-2\pi i/3} \cdot 1$	$1 \cdot (-1)$	$e^{2\pi i/3} \cdot (-1)$	$e^{-2\pi i/3} \cdot (-1)$
$(2)_3 \cdot (1)_2$	$1 \cdot 1$	$e^{-2\pi i/3} \cdot 1$	$1 \cdot 1$	$1 \cdot (-1)$	$e^{-2\pi i/3} \cdot (-1)$	$e^{2\pi i/3} \cdot (-1)$

C_3	1	r	r^2
$(0)_3$	1	1	1
$(1)_3$	1	$e^{2\pi i/3}$	$e^{-2\pi i/3}$
$(2)_3$	1	$e^{-2\pi i/3}$	$e^{2\pi i/3}$

$\times$

C_2	1	R
$(0)_2$	1	1
$(1)_2$	1	-1

$=$

$C_3 \times C_2 = C_6$	1	$r = h^2$	$r^2 = h^4$	$R = h^3$	$r \cdot R = h$	$r^2 \cdot R = h^5$
$(0)_3 \cdot (0)_2 = (0)_6$	1	1	1	1	1	1
$(1)_3 \cdot (0)_2 = (2)_6$	1	$e^{2\pi i/3}$	$e^{-2\pi i/3}$	1	$e^{2\pi i/3}$	$e^{-2\pi i/3}$
$(2)_3 \cdot (0)_2 = (4)_6$	1	$e^{-2\pi i/3}$	$e^{2\pi i/3}$	1	$e^{-2\pi i/3}$	$e^{2\pi i/3}$
$(0)_3 \cdot (1)_2 = (3)_6$	1	1	1	-1	-1	-1
$(1)_3 \cdot (1)_2 = (5)_6$	1	$e^{2\pi i/3}$	$e^{-2\pi i/3}$	-1	$-e^{2\pi i/3}$	$-e^{-2\pi i/3}$
$(2)_3 \cdot (1)_2 = (1)_6$	1	$e^{-2\pi i/3}$	$e^{2\pi i/3}$	-1	$-e^{-2\pi i/3}$	$-e^{2\pi i/3}$

(8.3.12)

The tricky part is to identify the C_6 waves $(k)_6$ that belong to a each product $(m)_3.(n)_2$. That is,

$$e^{i(k)_6 x} = e^{i(m)_3 x} e^{i(n)_2 x} = e^{i\left(m\frac{2\pi}{3} + n\frac{2\pi}{2}\right)x} = e^{i(2m+3n)\frac{2\pi}{6}x}.$$ (8.3.13a)

The desired k-value is: $k = (2m + 3n)$ mod 6   (8.3.13b)

For, example, the last row of (8.3.12) belongs to C_6 wave $k=(2.2+3.1)$ mod 6 = 7 mod 6 = 1 or $(1)_6$. The result is a reordered C_6 table, but otherwise it is the same as the one first drawn in Fig. 7.3.3. Verify!

Symmetry Catalog

Cataloging the number of symmetry groups of a given order N is a difficult problem with a long history. But, for commutative or Abelian groups considered so far, it reduces to finding all the distinct outer products $C_p \times C_q \times C_r \times C_s \times C_t \ldots$ of cyclic groups such that $N=pqrst\ldots$ is a product of primes. Product $C_p \times C_q$ is the same as C_{pq} if p and q share no factor in common so we don't include C_{pq} in the catalog if p and q are prime since then $C_{pq} = C_p \times C_q$ as in the case of $C_6 = C_2 \times C_3$ above. But we do include both $C_p \times C_p$ and C_{pp} which are distinct as were $C_2 \times C_2$ and C_4 above. If $N=p^P$ is a power of a prime such as $N=8=2^3$, then a distinct group exists for each *partition* of the power P. For example, $P=3 = 1+2 = 1+1+1$ has three distinct prime base-$(p=2)$ groups: C_8 and $C_4 \times C_2$ and $C_2 \times C_2 \times C_2$ are all distinct symmetries.

Problems for Chapter 8.

Subgroup soup

8.1.1 (a) The C_6 symmetry group has subgroups. List all of them except C_6 itself.

(b) Do the same for the symmetry groups C_3, C_4, and C_5. What is special about groups C_N of prime order N?

Ttrace'o **g**

8.1.2 (a) By group axioms (Sec. 2.2) show each row and column of a group table has an operator **g** only once.

(b) Use (a) to show that the regular representation trace *TraceR(**g**)* is zero for all but "do-nothing" unit operator **g=1**.

Turn-about's fair play

8.2.1 Suppose we are given the eigenvalues $\{\tau_0, \tau_1, \tau_2, \tau_3, \tau_4, \tau_5\}$ of a unitary C_6 transfer matrix **T** in (8.2.1).

(a) Can the $\{\tau_0, \tau_1, \tau_2, \tau_3, \tau_4, \tau_5\}$ be any old complex numbers? What restrictions, if any, apply?

(b) Can one give a formula for all 36 components T_{pq} of **T** in terms of $\{\tau_0, \tau_1, \tau_2, \tau_3, \tau_4, \tau_5\}$? If so do it. If not expalin why not and under what conditions you may be able to do it.

A Hex on pairing

8.2.2 Suppose the C_6 transfer matrix **T** is the form of the *Pairing operato*r, that is all components equal $T_{pq} = T$.

(a) Derive the resulting eigenvalue spectrum.

(b) What, if any, limitations need to be placed on parameter T?

(c) Discuss which waves belong to which eigenvalues

Phase o'Hex

8.2.3 (a) Could the hexagonal C_6 analyzer be wired so input $|even\ sites\rangle=(1,0,1,0,1,0)$ comes out $e^{i\phi}$ $|even\rangle$?

What k_m-eigenstates make up $|even\ sites\rangle$? Does your "rewiring" maintain C_6 symmetry?

(b) Could the C_6 analyzer be wired so input $|even\ sites\rangle$ comes out $e^{i\phi}$ $|odd\ sites\rangle=(0,1,0,1,0,1)$?

What k_m-eigenstates make up $|odd\ sites\rangle$? Does your "rewiring" maintain C_6 symmetry?

(c) Could the C_6 analyzer be wired so input $|odd\ symm\rangle=(1,-1,1,-1,1,-1)$ comes out $e^{i\phi}$ $|odd\ symm\rangle$?

What k_m-eigenstates make up $|odd\ symm\rangle$? Does your "rewiring" maintain C_6 symmetry?

 (d) Could the C_6 analyzer be wired so input $|\ odd\ symm\rangle$ comes out $e^{i\phi}$ $|even\ symm\rangle=(1,1,1,1,1,1)$?

What k_m-eigenstates make up $|\ even\ symm\rangle$? Does your "rewiring" maintain C_6 symmetry?

Little diamond

8.3.1. The symmetry eigensolution analysis of the C_{2v} diamond quantum dot device in Fig. 8.3.2(a) is a little different than its D_2 cousin in Fig. 8.3.2(b). Symmerty multiplication table and spectral decomposition is essentially the same but the transfer **T**-operator is not such a simple linear combination of symmetry operators. Represent the symmetry and give a decomposition of symmetry and **T**-matrix. (Note that x and y-plane mirror reflections are symmetry operators, too. There was no distinction between rotations and reflections in the D_2 problem.)

Double Crossed

8.3.2. Complete a symmetry catalog of commutative (Abelian) groups in terms of distinct $C_p{\times}C_q{\times}...$ cross products.

(a) for order N=8. (b) N=9. (c) N=10. (d) N=11. (e) N=12. (f) N=16.
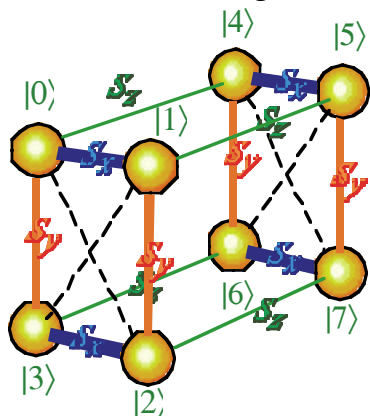
Problem 8.3.3 "Big box"　　　　　　　　　　　*Problem 8.3.4 "Big diamond"*
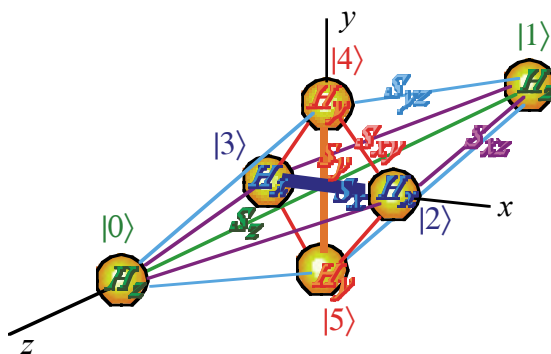
Big box

8.3.3. Give a complete symmetry eigensolution analysis of the D_{2h} device pictured here. First show that the full symmetry with horizontal reflection group $C_h = \{1, \sigma_{xy}(\text{thru } z\text{-axis})\}$ is $C_2 \times C_2 \times C_h = C_2 \times C_2 \times C_2$ which is called D_{2h}.

Derive character table of D_{2h} using the cross product trick of (8.3.11).

Big diamond

8.3.4. Give a complete symmetry eigensolution analysis of the D_{2h} device pictured above.

Ttrace'o **P**

8.3.5. Before (8.3.9a) it is noted that *TraceR(P)=1* means projector **P** is irreducible, that is, not a sum **P= P₁+ P₂** of other "smaller" projectors. Explain this and verify by constructing the representation of the **P^{++}** ,… in (8.3.9).
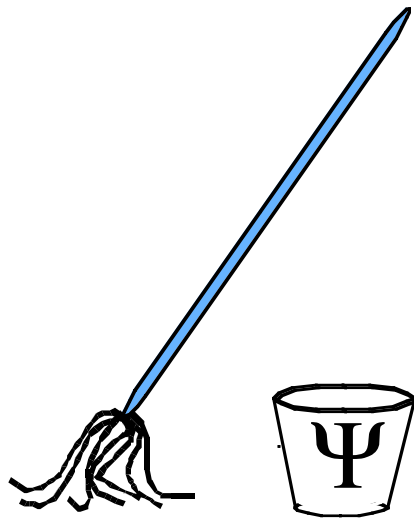
QM
for
Ψ AMOP

Chapter 9

Time Evolution
and
Fourier Dynamics

W. G. Harter

Now we consider the transfer operator from Hell, the time evolution operator U. This "grim-reaper" of the quantum world determines everything that happens in a non-relativistic (Schrodinger) system. Nothing escapes U-action including you! So learn U well, and pay particular attention to U's generator H which is called the Hamiltonian. The expression e^{-iHt} (for constant H) is an icon of modern quantum theory. Quantum dot systems from Chapters 7 and 8 will be used as examples and provide our first introduction to quantum periodic band theory and quantum "revival" beats. (Yes, some waves can survive the grim reaper by reviving repeatedly while doing arithmetic, too!)

Chapter 9. Time Evolution and Fourier Dynamics

9.1 Time Evolution Operator

It is often said that nothing that is more demanding than the test of time. All the analyzer experiments considered so far have required time to do, lots and lots of time. Never forget that all our fancy theory of analyzers and wave mechanics is just giving us probabilities; not too different from odds posted at the racetrack. Millions of counts need to be registered before those fancy predictions are seen in a laboratory, and all that counting takes time.

Now we consider a very demanding kind of analyzer, good old Father Time, in the form of *the time evolution operator* $\mathbf{U}(t_{FINAL}, ; t_{INITIAL})$. This "grim reaper" is supposed to be able to take any state at an initial time and transform it into what the state will be at a later time.

$$|\Psi(t_{FINAL,})\,\rangle = \mathbf{U}(t_{FINAL}\,;\,t_{INITIAL})\ |\Psi(t_{INITIAL})\,\rangle \qquad (9.1.1)$$

The main task of this section will be to begin theory and derivation of $\mathbf{U}$ operators. This is the main problem of quantum theory, so we won't finish the job here. In fact, we won't be done with $\mathbf{U}$ operators until the twelfth hour of never!

Let's first suppose *time translation symmetry* is present. By that I mean there is no one (such as perfidious janitors) "messing" with our analyzers. So, the experiments run the same day and night. Then we can often simplify the evolution operator equation by just having one time variable as follows

$$|\Psi(t)\,\rangle = \mathbf{U}(t\,;\,0)\ |\Psi(0)\,\rangle\,, \qquad (9.1.2)$$

so you may pick a "time origin" ($t{=}0$) arbitrarily.

(a) Planck's oscillation hypothesis

At first, the time evolution problem looks formidable, even for a little six-state beam analyzer problem that was studied in Chapter 8. Its evolution equation (9.1.2) looks like the following at any point z in the beam and varies with z. We will put off discussing z-dependence until a later chapter.

$$
\begin{pmatrix}
\langle 1|\Psi(t)\rangle \\
\langle 2|\Psi(t)\rangle \\
\langle 3|\Psi(t)\rangle \\
\langle 4|\Psi(t)\rangle \\
\langle 5|\Psi(t)\rangle \\
\langle 6|\Psi(t)\rangle
\end{pmatrix}
=
\begin{pmatrix}
U_{11} & U_{12} & U_{13} & U_{14} & U_{15} & U_{16} \\
U_{21} & U_{22} & U_{23} & U_{24} & U_{25} & U_{26} \\
U_{31} & U_{32} & U_{33} & U_{34} & U_{35} & U_{36} \\
U_{41} & U_{42} & U_{43} & U_{44} & U_{45} & U_{46} \\
U_{51} & U_{52} & U_{53} & U_{54} & U_{55} & U_{56} \\
U_{61} & U_{62} & U_{63} & U_{64} & U_{65} & U_{66}
\end{pmatrix}
\bullet
\begin{pmatrix}
\langle 1|\Psi(0)\rangle \\
\langle 2|\Psi(0)\rangle \\
\langle 3|\Psi(0)\rangle \\
\langle 4|\Psi(0)\rangle \\
\langle 5|\Psi(0)\rangle \\
\langle 6|\Psi(0)\rangle
\end{pmatrix}
\qquad (9.1.3a)
$$

Here the matrix elements are

$$U_{pq} = \langle p|\mathbf{U}(t\,;\,0)|q\rangle \qquad (9.1.3b)$$

How in the world can one derive all those $N^2{=}36$ time functions U_{pq} ? Woe is us!

But wait! The $\mathbf{U}$-operator and any matrix representing it should have the C_N symmetry of the analyzer system shown in Fig. 9.1.1. And, like the analyzer $\mathbf{T}$-operator, it should be reduced by the Fourier C_N -symmetry

$|k_m\rangle$ basis to a diagonal matrix made of phase factors $e^{i\phi_m}$ as in (9.1.17b). Furthermore, the Planck hypothesis indicates that the phase factors should have the time phasor "clock" form $e^{-i\omega_m t}$ that is conventional clockwise phasor rotation. Then the **U**-operator in (9.1.3) can be made to have a much simpler form if the basis is changed to its eigenbasis $|k_m\rangle$ as shown below.

$$\begin{pmatrix} \langle k_0|\Psi(t)\rangle \\ \langle k_1|\Psi(t)\rangle \\ \langle k_2|\Psi(t)\rangle \\ \langle k_3|\Psi(t)\rangle \\ \langle k_4|\Psi(t)\rangle \\ \langle k_5|\Psi(t)\rangle \end{pmatrix} = \begin{pmatrix} e^{-i\omega_0 t} & 0 & 0 & 0 & 0 & 0 \\ 0 & e^{-i\omega_1 t} & 0 & 0 & 0 & 0 \\ 0 & 0 & e^{-i\omega_2 t} & 0 & 0 & 0 \\ 0 & 0 & 0 & e^{-i\omega_3 t} & 0 & 0 \\ 0 & 0 & 0 & 0 & e^{-i\omega_4 t} & 0 \\ 0 & 0 & 0 & 0 & 0 & e^{-i\omega_5 t} \end{pmatrix} \cdot \begin{pmatrix} \langle k_0|\Psi(0)\rangle \\ \langle k_1|\Psi(0)\rangle \\ \langle k_2|\Psi(0)\rangle \\ \langle k_3|\Psi(0)\rangle \\ \langle k_4|\Psi(0)\rangle \\ \langle k_5|\Psi(0)\rangle \end{pmatrix} \quad (9.1.4)$$

Now, instead of $N^2=36$ unknown U_{pq} functions we have only $N=6$ frequency values ω_m to derive.

This is quite a simplification, if true. It is also a reasonable one since the evolution operators need to form a group called the *time evolution group* that multiplies as follows. (Recall (1.4.12d).)

$$\mathbf{U}(t_3 ; t_1) = \mathbf{U}(t_3 ; t_2) \cdot \mathbf{U}(t_2 ; t_1) \quad (9.1.5a)$$

Also, axioms 1-4 require $\mathbf{U}(t_2 ; t_1)$ to be unitary operators. (Recall (1.5.5b).)

$$\mathbf{U}^\dagger(t_2 ; t_1) = \mathbf{U}^{-1}(t_2 ; t_1) = \mathbf{U}(t_1 ; t_2) \quad (9.1.5b)$$

These requirements are satisfied by the Planck phasor forms in the diagonal matrix (9.1.4) or as follows,

$$\mathbf{U}(t_2 ; t_1) = \mathrm{diag}\{ e^{-i\omega_0(t_2 - t_1)} , e^{-i\omega_1(t_2 - t_1)} , .. \, e^{-i\omega_m(t_2 - t_1)} , ... \} \quad (9.1.6a)$$

since

$$e^{-i\omega_m(t_3 - t_1)} = e^{-i\omega_m(t_3 - t_2)} \, e^{-i\omega_m(t_2 - t_1)}, \text{ and } (e^{-i\omega_m(t_2 - t_1)})^* = e^{-i\omega_m(t_1 - t_2)} \quad (9.1.6b)$$

which depends only on relative time <u>difference</u> $(t_1 - t_2)$: $\mathbf{U}(t_1 ; t_2) = \mathbf{U}(t_1 - t_2 ; 0) = \mathbf{U}(0; t_2 - t_1)$

Indeed, we shall demand that a **U**-eigenbasis $\{ |\omega_0\rangle, |\omega_1\rangle, ...|\omega_m\rangle, \}$ shall exist even for asymmetric evolution operators for which a convenient symmetry basis $\{ |k_0\rangle, |k_1\rangle, ...|k_m\rangle, \}$ is not available to give "instant" diagonalization. We shall describe how to generally find eigenkets $|\omega_m\rangle$ so that

$$\mathbf{U}(t_2 ; t_1) |\omega_m\rangle = e^{-i\omega_m(t_2 - t_1)} |\omega_m\rangle \quad (9.1.7)$$

This is always possible in principle since we know that all unitary operators are diagonalizable. (Recall exercises in Ch. 3.) However, in practice the problem of diagonalization can be a bit of a chore for large systems consisting of millions, billions, or more states! We will need all the help that symmetry analysis can give us.

9.2 Schrodinger Time Equations

Time evolution operators and the states they evolve satisfy time differential equations known as *Schrodinger equations*. This is a common way to restate Planck's oscillation axiom in differential form.

(a) Schrodinger's time equations. Hamiltonian time generators

If time evolution equation (9.1.4) can predict the quantum state future far in advance, then it should certainly give the *rate* of evolution correctly. The time derivative of (9.1.4) is the following.

$$\frac{\partial}{\partial t}\begin{pmatrix} \langle k_0|\Psi(t)\rangle \\ \langle k_1|\Psi(t)\rangle \\ \langle k_2|\Psi(t)\rangle \\ \langle k_3|\Psi(t)\rangle \\ \langle k_4|\Psi(t)\rangle \\ \langle k_5|\Psi(t)\rangle \end{pmatrix} = -i \begin{pmatrix} \omega_0 e^{-i\omega_0 t} & 0 & 0 & 0 & 0 & 0 \\ 0 & \omega_1 e^{-i\omega_1 t} & 0 & 0 & 0 & 0 \\ 0 & 0 & \omega_2 e^{-i\omega_2 t} & 0 & 0 & 0 \\ 0 & 0 & 0 & \omega_3 e^{-i\omega_3 t} & 0 & 0 \\ 0 & 0 & 0 & 0 & \omega_4 e^{-i\omega_4 t} & 0 \\ 0 & 0 & 0 & 0 & 0 & \omega_5 e^{-i\omega_5 t} \end{pmatrix} \cdot \begin{pmatrix} \langle k_0|\Psi(0)\rangle \\ \langle k_1|\Psi(0)\rangle \\ \langle k_2|\Psi(0)\rangle \\ \langle k_3|\Psi(0)\rangle \\ \langle k_4|\Psi(0)\rangle \\ \langle k_5|\Psi(0)\rangle \end{pmatrix}$$

Simplifying the notation and factoring gives   (9.2.1)

$$\frac{\partial}{\partial t}\begin{pmatrix} \Psi_{k_0}(t) \\ \Psi_{k_1}(t) \\ \Psi_{k_2}(t) \\ \Psi_{k_3}(t) \\ \Psi_{k_4}(t) \\ \Psi_{k_5}(t) \end{pmatrix} = -i \begin{pmatrix} \omega_0 & 0 & 0 & 0 & 0 & 0 \\ 0 & \omega_1 & 0 & 0 & 0 & 0 \\ 0 & 0 & \omega_2 & 0 & 0 & 0 \\ 0 & 0 & 0 & \omega_3 & 0 & 0 \\ 0 & 0 & 0 & 0 & \omega_4 & 0 \\ 0 & 0 & 0 & 0 & 0 & \omega_5 \end{pmatrix} \cdot \begin{pmatrix} e^{-i\omega_0 t}\Psi_{k_0}(0) \\ e^{-i\omega_1 t}\Psi_{k_1}(0) \\ e^{-i\omega_2 t}\Psi_{k_2}(0) \\ e^{-i\omega_3 t}\Psi_{k_3}(0) \\ e^{-i\omega_4 t}\Psi_{k_4}(0) \\ e^{-i\omega_5 t}\Psi_{k_5}(0) \end{pmatrix}$$

(9.2.2)

Here we lose the Dirac notation briefly with

$$\Psi_{km}(t) = \langle k_m|\Psi(t)\rangle = e^{-i\omega_m t}\langle k_m|\Psi(0)\rangle = e^{-i\omega_m t}\Psi_{km}(0) . \tag{9.2.3}$$

Multiplying by $i\hbar$ and then putting back the Dirac notation gives the following.

$$i\hbar\frac{\partial}{\partial t}\begin{pmatrix} \Psi_{k_0}(t) \\ \Psi_{k_1}(t) \\ \Psi_{k_2}(t) \\ \Psi_{k_3}(t) \\ \Psi_{k_4}(t) \\ \Psi_{k_5}(t) \end{pmatrix} = \begin{pmatrix} \hbar\omega_0 & 0 & 0 & 0 & 0 & 0 \\ 0 & \hbar\omega_1 & 0 & 0 & 0 & 0 \\ 0 & 0 & \hbar\omega_2 & 0 & 0 & 0 \\ 0 & 0 & 0 & \hbar\omega_3 & 0 & 0 \\ 0 & 0 & 0 & 0 & \hbar\omega_4 & 0 \\ 0 & 0 & 0 & 0 & 0 & \hbar\omega_5 \end{pmatrix} \cdot \begin{pmatrix} \Psi_{k_0}(t) \\ \Psi_{k_1}(t) \\ \Psi_{k_2}(t) \\ \Psi_{k_3}(t) \\ \Psi_{k_4}(t) \\ \Psi_{k_5}(t) \end{pmatrix} ,$$

(9.2.4a)

$$
i\hbar\frac{\partial}{\partial t}
\begin{pmatrix}
\langle k_0|\Psi(t)\rangle \\
\langle k_1|\Psi(t)\rangle \\
\langle k_2|\Psi(t)\rangle \\
\langle k_3|\Psi(t)\rangle \\
\langle k_4|\Psi(t)\rangle \\
\langle k_5|\Psi(t)\rangle
\end{pmatrix}
=
\begin{pmatrix}
\hbar\omega_0 & 0 & 0 & 0 & 0 & 0 \\
0 & \hbar\omega_1 & 0 & 0 & 0 & 0 \\
0 & 0 & \hbar\omega_2 & 0 & 0 & 0 \\
0 & 0 & 0 & \hbar\omega_3 & 0 & 0 \\
0 & 0 & 0 & 0 & \hbar\omega_4 & 0 \\
0 & 0 & 0 & 0 & 0 & \hbar\omega_5
\end{pmatrix}
\bullet
\begin{pmatrix}
\langle k_0|\Psi(t)\rangle \\
\langle k_1|\Psi(t)\rangle \\
\langle k_2|\Psi(t)\rangle \\
\langle k_3|\Psi(t)\rangle \\
\langle k_4|\Psi(t)\rangle \\
\langle k_5|\Psi(t)\rangle
\end{pmatrix},
\qquad (9.2.4b)
$$

which is called *Schrodinger's time equation*. Its abstract Dirac form is the following

$$
i\hbar\frac{\partial}{\partial t}|\Psi(t)\rangle = \mathbf{H}|\Psi(t)\rangle \qquad (9.2.5a)
$$

where the *Hamiltonian energy operator* **H** is related to $i\hbar$ times the time evolution operator derivative by

$$
i\hbar\frac{\partial}{\partial t}\mathbf{U}(t,0) = \mathbf{H}\,\mathbf{U}(t,0) \qquad (9.2.5b)
$$

and is **H** also called the *generator of time translation*. An exponential solution to (9.1.5b) is

$$
\mathbf{U}(t,0) = e^{-i\mathbf{H}t/\hbar}\,\mathbf{U}(0,0) = e^{-i\mathbf{H}t/\hbar} \quad \text{where: } \mathbf{U}(0,0) = \mathbf{1} \qquad (9.2.5c)
$$

if **H** is an *N-by-N* constant matrix operator as it is in (9.1.4a-b). (It must be constant if there is time translation symmetry. Remember, it is time translation symmetry that permits exponential solutions.)

All of the above "derivations" of Schrodinger's equations (9.2.5) are really only Planck's frequency and energy axiom, starting with (9.1.4) and restated in many fancy ways for an *N*-state system for *N=6*.

(b) Schrodinger's matrix equations

The thing that makes a Hamiltonian **H** powerful is that it may be easily derived it in some other basis like the original channel basis {|*1*⟩, |*2*⟩, ...|*N*⟩ } and then diagonalized using symmetry techniques or numerical methods to find its eigenvectors { |ω_0⟩, |ω_1⟩, ...|ω_{N-1}⟩} known as *energy eigenstates* and eigenvalues { $\hbar\omega_0$, $\hbar\omega_1$, ...$\hbar\omega_{N-1}$} known as *energy or frequency spectra* $\varepsilon_m = \hbar\omega_m$. This time, the word *spectra* is used as it was intended by the pioneering spectroscopists who first saw atomic spectral lines in laboratory and in astrophysical observations. (Mathematicians co-opt the term *spectra* other ways.)

Rewriting Schrodinger's time equation (9.2.5a)

$$
i\hbar\frac{\partial}{\partial t}|\Psi(t)\rangle = \mathbf{H}|\Psi(t)\rangle \qquad (9.2.6a)
$$

in an arbitrary basis gives

$$
i\hbar\frac{\partial}{\partial t}
\begin{pmatrix}
\langle 0|\Psi(t)\rangle \\
\langle 1|\Psi(t)\rangle \\
\langle 2|\Psi(t)\rangle \\
\langle 3|\Psi(t)\rangle \\
\langle 4|\Psi(t)\rangle \\
\langle 5|\Psi(t)\rangle
\end{pmatrix}
=
\begin{pmatrix}
H_{00} & H_{01} & H_{02} & H_{03} & H_{04} & H_{05} \\
H_{10} & H_{11} & H_{12} & H_{13} & H_{14} & H_{15} \\
H_{20} & H_{21} & H_{22} & H_{23} & H_{24} & H_{25} \\
H_{30} & H_{31} & H_{32} & H_{33} & H_{34} & H_{35} \\
H_{40} & H_{41} & H_{42} & H_{43} & H_{44} & H_{45} \\
H_{50} & H_{51} & H_{52} & H_{53} & H_{54} & H_{55}
\end{pmatrix}
\bullet
\begin{pmatrix}
\langle 0|\Psi(t)\rangle \\
\langle 1|\Psi(t)\rangle \\
\langle 2|\Psi(t)\rangle \\
\langle 3|\Psi(t)\rangle \\
\langle 4|\Psi(t)\rangle \\
\langle 5|\Psi(t)\rangle
\end{pmatrix},
\qquad (9.2.6b)
$$

where the matrix elements

$$H_{pq} = \langle p | \mathbf{H} | q \rangle \tag{9.2.6c}$$

are generally non-diagonal except in $\mathbf{H}$'s or $\mathbf{U}$'s own (eigen) basis $|k_m\rangle$ as in (9.2.4).

(c) Writing Hamiltonian H in terms of symmetry operators $\mathbf{r^p}$

If analyzer $\mathbf{H}$-matrix (8.2.1) has C_6 symmetry, it commutes with all the rotation operator $\mathbf{r}$-matrices in (2.7.5) and is a linear combination of $\mathbf{r^p}$ as follows.

$$\mathbf{H} = H\,\mathbf{1} + S\,\mathbf{r} + T\,\mathbf{r}^2 + U\,\mathbf{r}^3 + T^*\,\mathbf{r}^4 + S^*\,\mathbf{r}^5, \tag{9.2.6}$$

The $\mathbf{r^p}$-matrices in (2.7.5) combine to give a C_6-symmetric $\mathbf{H}$-matrix Schrodinger equation (9.2.7) in analogy to the $\mathbf{T}$-matrix transfer equation (8.2.7), and label its *tunneling paths* from point-to-point.

$$i\hbar \frac{\partial}{\partial t}
\begin{pmatrix}
\langle 0 | \Psi(t) \rangle \\
\langle 1 | \Psi(t) \rangle \\
\langle 2 | \Psi(t) \rangle \\
\langle 3 | \Psi(t) \rangle \\
\langle 4 | \Psi(t) \rangle \\
\langle 5 | \Psi(t) \rangle
\end{pmatrix}
=
\begin{pmatrix}
H & S^* & T^* & U & T & S \\
S & H & S^* & T^* & U & T \\
T & S & H & S^* & T^* & U \\
U & T & S & H & S^* & T^* \\
T^* & U & T & S & H & S^* \\
S^* & T^* & U & T & S & H
\end{pmatrix}
\bullet
\begin{pmatrix}
\langle 0 | \Psi(t) \rangle \\
\langle 1 | \Psi(t) \rangle \\
\langle 2 | \Psi(t) \rangle \\
\langle 3 | \Psi(t) \rangle \\
\langle 4 | \Psi(t) \rangle \\
\langle 5 | \Psi(t) \rangle
\end{pmatrix}, \tag{9.2.7}$$

The undetermined coefficients $H, S, T, U, T^*,$ and S^* correspond to all the *tunneling amplitudes* that state $|0\rangle$ could possibly have to other states $|0\rangle, |1\rangle, |2\rangle, |3\rangle, |4\rangle,$ and $|5\rangle$ as indicated by arrows in Fig. 9.2.1 which are analogous to the transfer amplitude paths for the $\mathbf{T}$–matrix (or of a $\mathbf{U}$-matrix) in Fig. 8.2.1.

(a) Tunneling Amplitudes from $|0\rangle$

$H = \langle 0|\mathbf{H}|0\rangle = H^*$
$S = \langle 1|\mathbf{H}|0\rangle$
$T = \langle 2|\mathbf{H}|0\rangle$
$U = \langle 3|\mathbf{H}|0\rangle = U^*$
$T^* = \langle 4|\mathbf{H}|0\rangle$
$S^* = \langle 5|\mathbf{H}|0\rangle$
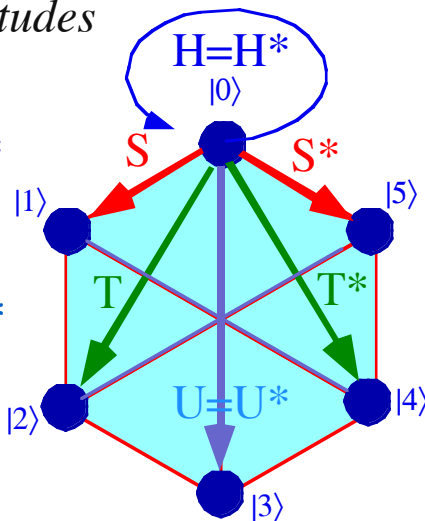
(b) All C_6 Tunneling Paths
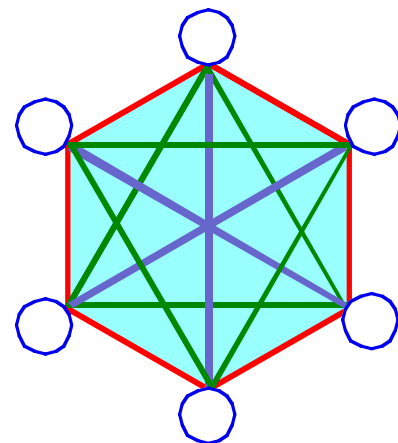
Fig. 9.2.1 Generic 6-channel (C_6)Hamiltonian tunneling (a) Amplitudes (b) Paths

But, there is one important difference. Hamiltonian matrices must be *Hermitian* (self-conjugate: $\mathbf{H}^\dagger = \mathbf{H}$).

$$H_{pq} = \langle p | \mathbf{H} | q \rangle = \langle p | \mathbf{H}^\dagger | q \rangle = H_{qp}{}^* \tag{9.2.8a}$$

Unitary $\mathbf{U}$ implies Hermitian $\mathbf{H}$

Hamiltonian $\mathbf{H}$ is Hermitian because the time evolution operator is unitary by definition (9.2.5).

$$\mathbf{U}(t,0)^{\dagger} = \left(e^{-i\mathbf{H}t/\hbar}\right)^{\dagger} = e^{i\mathbf{H}^{\dagger}t/\hbar} = \mathbf{U}(t,0)^{-1} = \mathbf{U}(-t,0) = e^{i\mathbf{H}t/\hbar} \qquad (9.2.8b)$$

So, an inverse tunneling amplitude such as S^* is the complex conjugate of the forward one S. Also, diagonal components of a Hamiltonian matrix are thus always real.

$$H_{pp} = H_{pp}{}^* \qquad (9.2.8c)$$

This means the eigenvalues are also real since relations (9.2.8) are true in any basis including the **H** operator's own basis or eigenbasis where **H** is diagonal.

Note that a diametric tunneling amplitude such as $U=U^*$ also is real because its operator $\mathbf{r}^3$ is its own inverse $(\mathbf{r}^3 = \mathbf{r}^{3\dagger} = \mathbf{r}^{-3})$. Conjugation reverses direction of rotation for all C_6 operators except **1** and $\mathbf{r}^3$. $\dagger$-conjugation is time reversal for Schrodinger equation (9.2.6). Axiom-2 says bra-clocks run backwards.

9.3 Schrodinger Eigen-Equations

Time evolution is simple for eigenstates $|\omega_m\rangle$ because only a single eigenfrequency ω_m is present. Energy or frequency eigenstates and eigenvalues satisfy *Schrodinger's eigenvalue equation*, also called the *Schrodinger time-independent equation*.

$$\mathbf{H}\,|\omega_m\rangle = \hbar\omega_m\,|\omega_m\rangle = \varepsilon_m\,|\omega_m\rangle \qquad (9.3.1a)$$

In a "quantum-dot" basis this is a matrix eigenvalue problem such as the following for $N=6$.

$$\begin{pmatrix} H_{00} & H_{01} & H_{02} & H_{03} & H_{04} & H_{05} \\ H_{10} & H_{11} & H_{12} & H_{13} & H_{14} & H_{15} \\ H_{20} & H_{21} & H_{22} & H_{23} & H_{24} & H_{25} \\ H_{30} & H_{31} & H_{32} & H_{33} & H_{34} & H_{35} \\ H_{40} & H_{41} & H_{42} & H_{43} & H_{44} & H_{45} \\ H_{50} & H_{51} & H_{52} & H_{53} & H_{54} & H_{55} \end{pmatrix} \cdot \begin{pmatrix} \langle 0|\omega_m\rangle \\ \langle 1|\omega_m\rangle \\ \langle 2|\omega_m\rangle \\ \langle 3|\omega_m\rangle \\ \langle 4|\omega_m\rangle \\ \langle 5|\omega_m\rangle \end{pmatrix} = \hbar\omega_m \begin{pmatrix} \langle 0|\omega_m\rangle \\ \langle 1|\omega_m\rangle \\ \langle 2|\omega_m\rangle \\ \langle 3|\omega_m\rangle \\ \langle 4|\omega_m\rangle \\ \langle 5|\omega_m\rangle \end{pmatrix}, \qquad (9.3.1b)$$

The Schrodinger time equation (9.2.6b) is a simple 1-dimensional relation for each amplitude.

$$i\hbar\frac{\partial}{\partial t}\langle p|\omega_m\rangle = \langle p|\mathbf{H}|\omega_m\rangle = \hbar\omega_m\langle p|\omega_m\rangle \qquad (9.3.2)$$

Its solution has each amplitude $\langle p|\omega_m\rangle$ spinning its clock at the same rate ω_m at constant size $|\langle p|\omega_m\rangle|^2$.

$$\langle p|\omega_m(t)\rangle = \langle p|\omega_m(0)\rangle e^{-i\omega_m t} \qquad (9.3.3)$$

$$\left|\langle p|\omega_m(t)\rangle\right|^2 = \left|\langle p|\omega_m(0)\rangle\right|^2 = const. \qquad (9.3.4)$$

Such is the fate of an eigenstate or stationary state. Its observable probability distribution is forever fixed.

But, how does one find just the right $\langle p|\omega_m\rangle$ amplitudes to solve (9.3.1)? Aren't we back in hot water again with $N^2=36$ unknown constants H_{pq} and a big diagonalization job facing us? Woe is us, again! But, fortunately, there are all kinds of techniques and approximation tricks to find the Hamiltonian matrix elements and then find the energy spectrum. That is what most of the rest of the book is about!

Chief among the eigensolution techniques is symmetry analysis. The time evolution matrix **U** and the Hamiltonian matrix **H** for the C_6-analyzer in Fig. 8.1.1 can be treated to the same techniques that worked for the analyzer **T**-matrix. Again, all possible C_6–symmetric Hamiltonian matrices are given with a single complete set

of eigensolutions. Then all possible motions are obtained from combinations of eigensolutions, which, by their completeness are able to produce an arbitrary initial condition.

After that, the motion is just the interference beating between all the eigenfrequencies that participate in producing a given initial state. Remember, it takes two to tango! At least two eigenstates with different eigenfrequencies need to be up and spinning to have observable motion. Otherwise, nothin's happening!

It turns out that while it takes two to tango, three's a crowd! Two state systems are unique in their harmonic simplicity. At the end of this unit we will see how to understand more complicated *3, 4, 5,...*level excitations for some simple systems.

(a) Solving Schrodinger's eigen-equations for C_6 system

H-eigenvalues use **r**-expansion (9.2.6) of **H** and C_6 symmetry $\mathbf{r}^p$-eigenvalues from (8.2.9).

$$\langle k_m|\mathbf{r}^p|k_m\rangle = e^{-ipk_m a} = e^{-ipm2\pi/N} \text{ where: } k_m = m(2\pi/Na)$$

$$\langle k_m|\mathbf{H}|k_m\rangle = H\langle k_m|\mathbf{1}|k_m\rangle + S\langle k_m|\mathbf{r}|k_m\rangle + T\langle k_m|\mathbf{r}^2|k_m\rangle + U\langle k_m|\mathbf{r}^3|k_m\rangle + T^*\langle k_m|\mathbf{r}^4|k_m\rangle + S^*\langle k_m|\mathbf{r}^5|k_m\rangle$$

$$= H + S\,e^{-ik_m a} + T\,e^{-i2k_m a} + U\,e^{-i3k_m a} + T^*\,e^{i2k_m a} + S^*\,e^{ik_m a} \tag{9.3.5a}$$

Again we check that **H** eigenvectors $|\omega_m\rangle$ are the $|k_m\rangle$ in (8.2.11) which solved transfer matrix **T**.

$$
\begin{pmatrix}
H & S^* & T^* & U & T & S \\
S & H & S^* & T^* & U & T \\
T & S & H & S^* & T^* & U \\
U & T & S & H & S^* & T^* \\
T^* & U & T & S & H & S^* \\
S^* & T^* & U & T & S & H
\end{pmatrix}
\cdot
\begin{pmatrix}
1 \\ e^{ik_m a} \\ e^{i2k_m a} \\ e^{i3k_m a} \\ e^{-i2k_m a} \\ e^{-ik_m a}
\end{pmatrix}
= \hbar\omega_m
\begin{pmatrix}
1 \\ e^{ik_m a} \\ e^{i2k_m a} \\ e^{i3k_m a} \\ e^{-i2k_m a} \\ e^{-ik_m a}
\end{pmatrix}
\tag{9.3.5b}
$$

Because of Hermiticity ($\mathbf{H}^\dagger = \mathbf{H}$) eigenvalues ω_m or ε_m will be real eigenfrequency and energy spectra.

$$\hbar\omega_m = \varepsilon_m = H + S\,e^{-ik_m a} + T\,e^{-i2k_m a} + U\,e^{-i3k_m a} + T^*\,e^{i2k_m a} + S^*\,e^{ik_m a} \tag{9.3.5c}$$

$$\hbar\omega_m = \varepsilon_m = H + 2|S|\cos(k_m a - \sigma) + 2|T|\cos(2k_m a - \tau) - U(-1)^m \tag{9.3.5d}$$

Here we note: $e^{-i3k_m a} = e^{-i3\pi m} = (-1)^m$ for $N=6$. Also, let the complex parameters be in polar form.

$$S = |S|\,e^{i\sigma}, \qquad T = |T|\,e^{i\tau} \tag{9.3.5e}$$

Their phase angles σ and τ correspond to what is sometimes called a *gauge symmetry breaking* or *Zeeman splitting* parameters. To begin the discussion, we shall let the phase angles be zero or pi.

A little physical intuition helps to make some sense of the energy eigenvalues. The parameters *S, T,* and *U* are called *tunneling amplitudes* because they are "sneak factors" that tell how rapidly (and with what phase σ, $\tilde{\tau}$) an evanescent wave in one channel can sneak or tunnel over to one of its neighbors as indicated in Fig. 9.2.1. The *S, T, U* give *rates* at which the *A, B, C* amplitudes of a **T** or **U** matrix grow.

(b) Energy spectrum and tunneling rates

We saw how the evanescent waves in (6.3.10a) of Sec. 6.3c(3) decay exponentially and die off with distance. Channel waves are like this, a channel wave state $|0\rangle$ will be exponentially more likely to tunnel to its nearest neighbor channels $|1\rangle$ or $|5\rangle$ than to more distant channels $|2\rangle, |3\rangle,$ or $|4\rangle$ in Fig. 9.2.1. So, the distant tunneling amplitudes *U* and *T* might be approximated by zero in (9.3.5d) to give

$$\hbar\omega_m = \varepsilon_m = H + 2|S|\cos(k_m a - \sigma). \tag{9.3.5f}$$

This is an elementary *Bloch dispersion relation*. If wavevector k_m were a continuous variable k the dispersion function $\omega(k)$ would trace a cosine as shown in Fig. 9.3.1 where the gauge phase is set to pi ($\sigma=\pi$) to make the k_0 state lowest. Now the spectra correspond to hexagonal projections of $e^{i2\pi m/6}$.

$$\hbar\omega_m = \varepsilon_m = H - 2|S|\cos(k_m a). \qquad (\sigma=\pi) \tag{9.3.5g}$$

Note that while the eigenvalues ($\hbar\omega_m = \varepsilon_m$) vary with parameters *H, S, T,* or *U*, the eigen*vectors* $|\omega_m\rangle$ or eigen*functions* $\psi_m(x_p)$ are the <u>same</u> for all values of parameters due to C_N-symmetry.
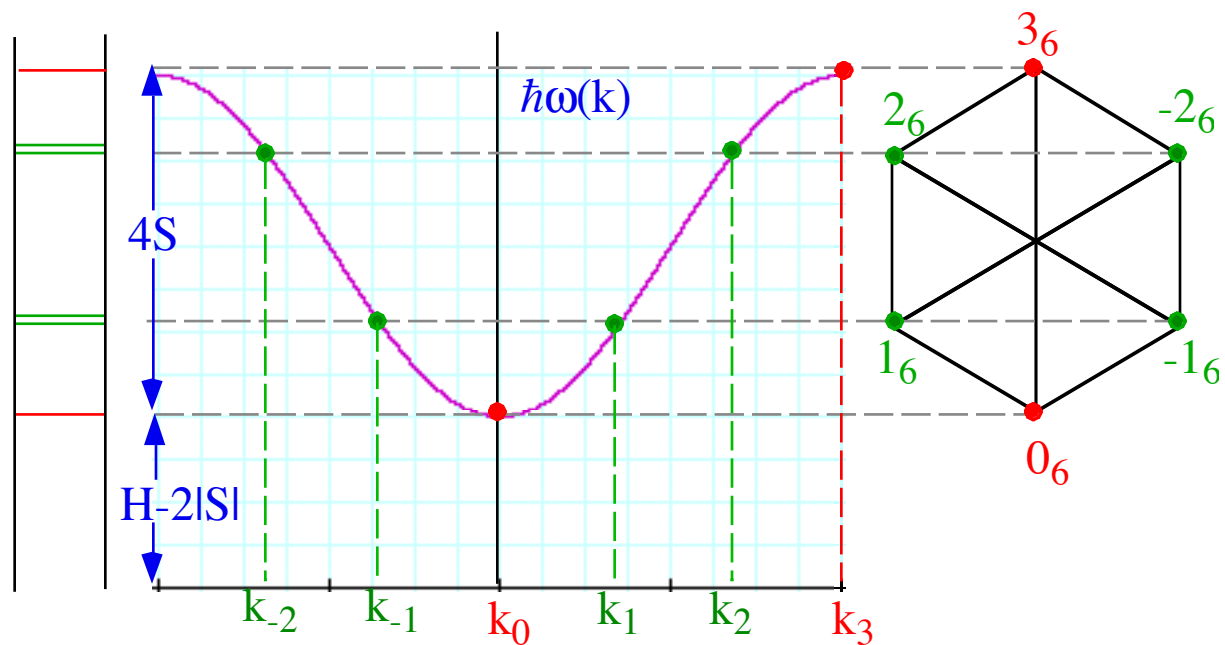
Fig. 9.3.1 Generic 6-channel (C₆) tunneling spectra and Bloch dispersion.

If the tunneling phase σ increases by $\pi/12$ it shifts the dispersion relation to the right by $\pi/12$ in k-space. It rotates the hexagonal spectral diagram by $\pi/12$ or *15°* as shown in Fig. 9.3.2. The resulting spectra shifts and splits the degenerate doublets $\pm1_6$ and $\pm2_6$.
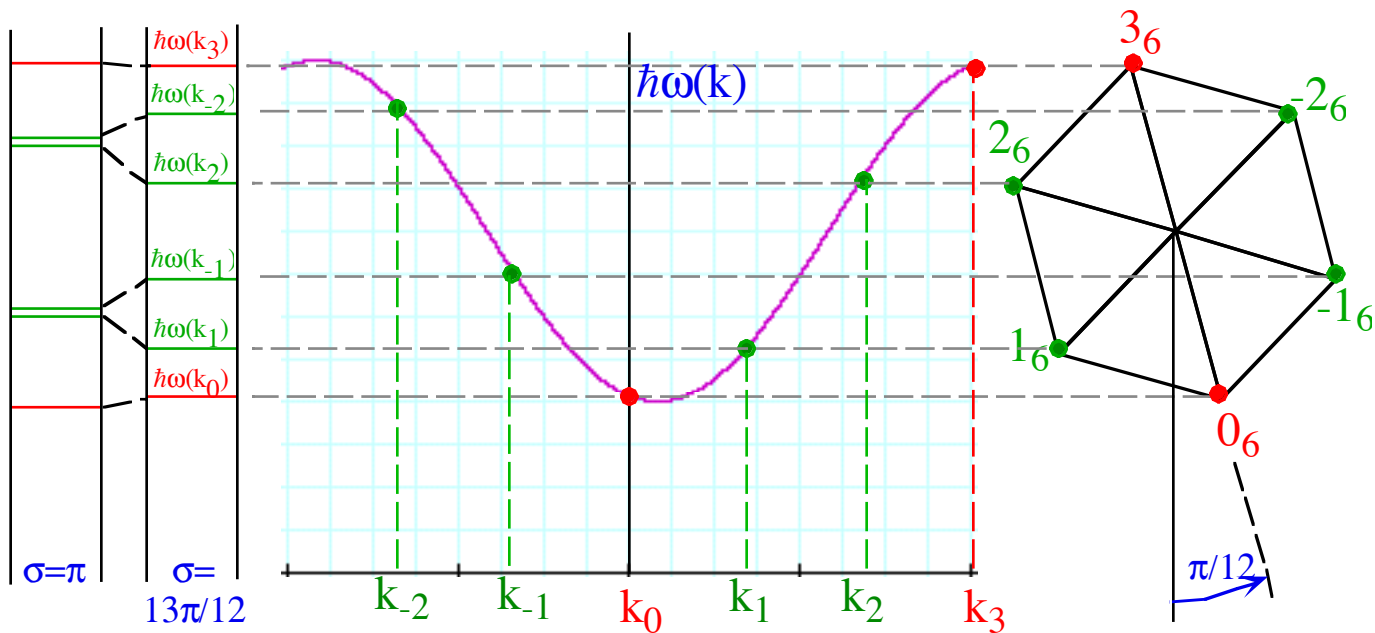
Fig.9.3.2 Same 6-channel (C₆) tunneling spectra with broken symmetry and doublet splitting

This is equivalent to rotating the analyzer disk in Fig. 8.1.1 at a constant negative or clockwise velocity so negatively moving waves increase in energy while the positively moving ones have less energy.

Such a tunneling phase or gauge factor causes a *right-left symmetry breaking* so right-handed and left-handed waves are no longer degenerate in energy. It is analogous to the Doppler shift that is observed by an observer moving through a monochromatic standing wave and sees red-shifted and blue-shifted frequencies while the stationary observer sees equal frequencies. (Recall Sec. 4.2.)

A similar effect occurs if a magnetic field is applied perpendicular to the plane of the analyzer along a beam of charged particles. Then the splitting of doublets is called *Zeeman splitting* which is a very well known atomic spectral effect that will be studied later.

Bloch's waves vs. Bohr's

One should compare the discrete Bloch spectra and dispersion in Fig. 9.3.1 here to the simple Bohr spectra in Fig. 7.1.1. The orbital wavefunctions for both have a plane-wave form of "Bohr's ghost" waves.

$$\psi_m(x) = e^{ik_m x} \tag{9.3.6a}$$

However, Bloch waves for C_6 are discretized into $N=6$ phasors at discrete points x_p. ($p=1, 2, ..., 6$)

$$\psi_m(x_p) = e^{ik_m x_p} = e^{i2\pi mp/N} \tag{9.3.6b}$$

Each Bloch quantum number $m=0, 1, 2, ..., 5$, is a number *m-modulo-6* as in (7.3.7) and in Fig. 7.3.3.

Bloch eigenvalues, however, differ from Bohr's. Bohr orbital dispersion or energy is a simple parabola (7.1.16) as follows using momentum quantization $p_m = \hbar k_m = \hbar 2\pi m/L$ with: $m=0, \pm 1, \pm 2, \ldots$

$$E_m = (\hbar k_m)^2/2M = m^2 \, [h^2/2ML^2] \tag{9.3.7}$$

This parabola is a low-energy approximation to the relativistic hyperbola in Fig. 5.2.1. In contrast, the Bloch curve is a flipped cosine function (9.3.5g) as plotted in Fig.9.3.3 and superimposed upon the Bohr parabola. For larger N (Fig. 9.3.3 it is $N=24$) and small m the cosine curve is approximated by a Bloch-like parabola given by a Taylor expansion at the origin ($k=0=k_0$) in k-space.

$$\hbar\omega_m = E_m = H - 2|S| \, cos(k_m a) = H - 2|S| + |S|(k_m a)^2 +.. \tag{9.3.8}$$

In this limit the Bloch dispersion is approximated by the simple Bohr parabola.

In the limit of large number N of "quantum dot" coordinates x_p. ($p=1, 2, 3, 4, ...,N$) the continuum coordinate x of the Bohr orbitals is approached. As long as the waves considered have low k_m, that is, are long compared to the lattice interval $a=L/N$ that divides up the Bohr coordinate range L, then Bohr and Bloch waves have nearly the same dispersion $\omega_m(k_m)$ and will behave the same.

(c) Brillouin's boundary

For larger wavevector k_m the wavelength becomes shorter until its waves begin to "fall through the cracks" in the lattice. Recall the difficulty in following the "Bohr's ghost" wave through the C_6 phasors in Fig. 7.3.3 for the higher waves $(m)_N = (4)_6$ or $(5)_6$, or even $(2)_6$. A break occurs when a <u>half</u>-wave length matches the lattice spacing a. This is when $(m)_N = (N/2)_N = (3)_6$, a "half-way point" known as the *first Brillouin zone boundary (BZB-1)*. It is at k_{12} or $(m)_N = (12)_{24}$ in Fig. 9.3.3 ($N=24$).

$$(m)_{BZB-1} = (N/2) \quad or: \; k_{BZB-1} = \pi/a \quad or: \; \lambda_{BZB-1} = 2a \tag{9.3.9a}$$
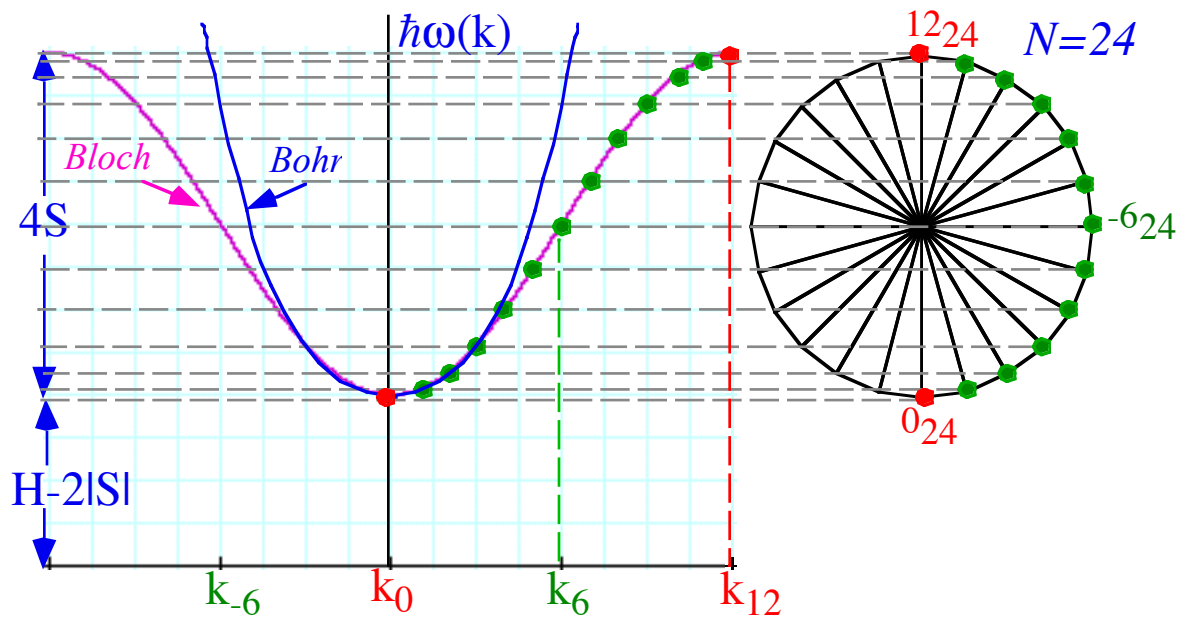
Fig.9.3.3 Generic 24-channel (C_{24}) tunneling spectra and Bohr vs. Bloch dispersion.

At this *m*-number or *k*-value the wave amplitudes are alternating ± 1 at the lattice points x_p.

$$\psi_{N/2}(x_p) = e^{ik_{N/2}x_p} = e^{i2\pi(N/2)p/N} = e^{i\pi p} = (-1)^p \tag{9.3.9b}$$

Phases that are in or π-out of phase make a <u>standing</u> wave with zero group velocity as in Fig. 9.3.4.
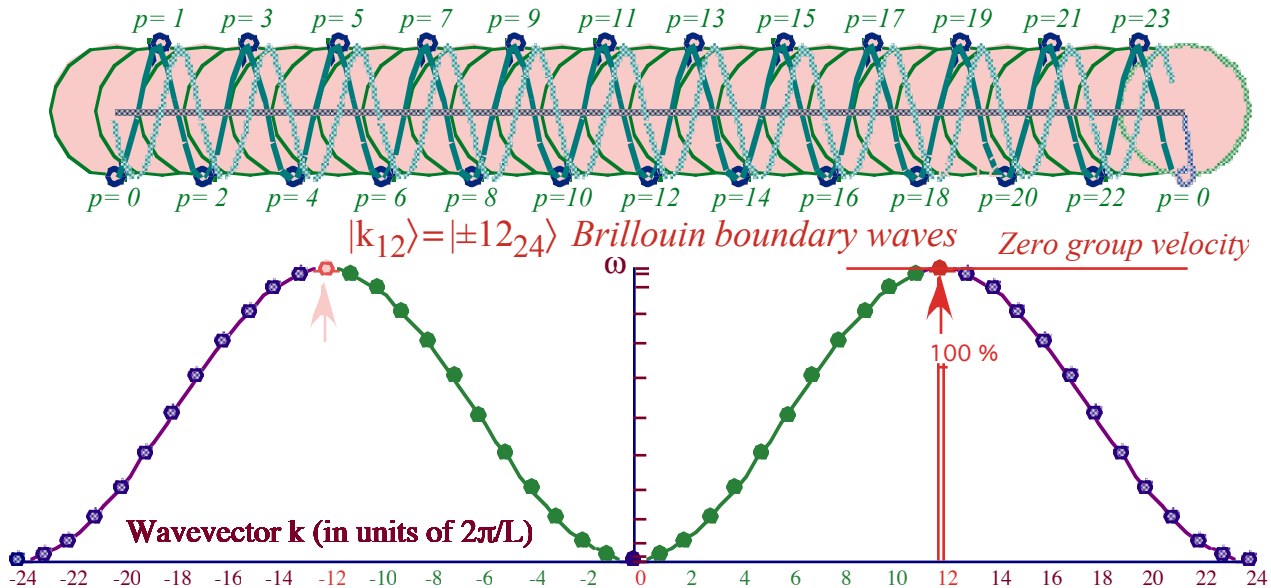
Fig.9.3.4 (C_{24}) Brillouin boundary wave must be standing. (No group velocity)

    Postive or negative ($k=\pm 12$) waves have the same effect on the 24 lattice points; both give standing wave motion with no transmission one way or the other. In C_{24} symmetry $+12\ mod\ 24 = -12\ mod\ 24$.

    The wave group velocity is the velocity V_{group} associated with classical particle or "message" velocity. (Recall discussions in Sec. 4.4 (b-c).) From (9.3.8) the V_{group} for Bloch (or for low-k Bohr) is

$$V_{group} = \frac{d\omega_m}{dk_m} = 2\frac{|S|}{\hbar}a\sin(k_m a) \quad \left(\cong 2\frac{|S|}{\hbar}k_m a^2 \text{ , for: } k_m << \pi/a \right) \qquad (9.3.10)$$

The group velocity goes to zero at the origin ($k_m=0$) and at the Brillouin zone boundary ($k_m=k_{BZB}$). This is consistent with our picture Fig. 9.3.4 of a standing wave. It just goes nowhere but up and down.

Effective mass: Another quantum view of inertia

Low velocity *(u<<c)* particle momentum is mass times particle velocity: $Mu=MV_{group}$. DeBroglie relation (5.2.5c) gives momentum as $\hbar k_m$. For low-k_m-Bloch waves (Bohr waves), (9.3.10) gives V_{group} proportional to the tunneling amplitude S implying an *effective mass M_{eff}* inversely proportional to S.

$$M_{eff}(0) = \hbar^2/(2|S| a^2) \qquad (9.3.11a)$$

This is consistent with a comparison of Bohr energy values $\varepsilon_m = {}^1/_2(\hbar k_m)^2/M$ and the low-k_m Bloch energy eigenvalues (9.3.8). Recall the quantum effective mass introduced in (5.3.13) and repeated here.

$$M_{eff} = \frac{F}{a} = \frac{\hbar\dot{k}}{\left(\dfrac{dV_{group}}{dt}\right)} = \frac{\hbar\dot{k}}{\left(\dfrac{dV_{group}}{dk}\dfrac{dk}{dt}\right)} = \frac{\hbar}{\left(\dfrac{d^2\omega}{dk^2}\right)} \quad \text{where: } V_{group} = \frac{d\omega}{dk} \qquad (9.3.11b)$$

Effective mass is inversely proportional to the <u>curvature</u> of the dispersion relation. As k_m increases in Fig. 9.3.3 the effective mass starts out at $k=0$ with the $M_{eff}(0)$ value (9.3.11a). Then it increases until it goes to infinity at $k_m = k_{N/4} = k_6$. Then it comes back from negative infinity losing much of its negativity to end up at ($M_{eff}(k_{12})=-M_{eff}(0)$) on the Brillouin zone boundary $k_m = k_{N/2} = k_{12}$. There $\omega_{Bloch}(k)$ is a downward curving dispersion like Dirac negative-energy anti-particle band in the lower half of Fig. 5.4.1. But, $\omega_{Bloch}(k)$ in Fig. 9.3.3 differs from a continuum relativistic dispersion relation (5.2.8)

$$E = \hbar\omega_{relativistic} = \pm\sqrt{\left(Mc^2\right)^2 + \left(c\hbar k\right)^2} \qquad (5.2.8)_{repeated}$$

For $\omega_{rela.}(k)$ effective mass approaches infinity only as the momentum or k becomes large. For a vacuum , a constant applied electric field would cause k to increase uniformly. But, for a C_N lattice k-space is periodic so a field causes a charged particle to just oscillate back and forth each time k passes through another Brillouin zone. Based on this, relativistic symmetry appears quite different from that of a Bloch lattice. But then, have we really looked closely enough at that vacuum continuum? It may take some pretty high k-values to do so!

The final sections of this unit are devoted to dynamics of Bohr waves shown in space-time plots of the following Fig. 9.3.5-6. Recall also Fig. 5.5.5-6. The interference anti-nodes that spring up and then vanish are called *revivals*, a term coined by Joe Eberly to describe atom-laser simulations he noticed around 1976. Much of the intricate structure are called *fractional revivals* first noticed in molecular rotor simulations around 1980. Much of the first analyses of fractional revivals, done during the 1990's, involves particle-in-a-box and atomic Rydberg states. However, Bohr orbitals provide the clearest understanding of revivals because of their underlying C_N symmetry.

(Next pages: Figs. 9.3.5a-c)

1/1

10/11
9/10
8/9
7/8
6/7
5/6
9/11
4/5
7/9
3/4
5/7
7/10
2/3
3/8
3/5
4/7
5/9
6/11
1/2
3/11
4/9
3/7
2/5
3/8
4/11
1/3
3/10
2/7
3/11
1/4
2/9
1/5
2/11
1/6
1/7
1/8
1/9
1/10
1/11
0/1

$\Delta m = 9$

-15　-10　-5　　0　　5　　10　　15　　= m

$2\Delta r = 4\%$

1/1

7/8
6/7
5/6
4/5

3/4

5/7

2/3

5/8
3/5
4/7

$\Delta m = 3$

-2 -1 0 1 2 3 4   = m

1/2

3/7
2/5
3/8

1/3

2/7

1/4

1/5

1/6
1/7
1/8

$2\Delta x = 12\%$

0/1

1/1

3/4

$\Delta m = 1.5$

-2 -1 0 1 2 = m

1/2

1/4

$2\Delta x = 24\%$

0/1
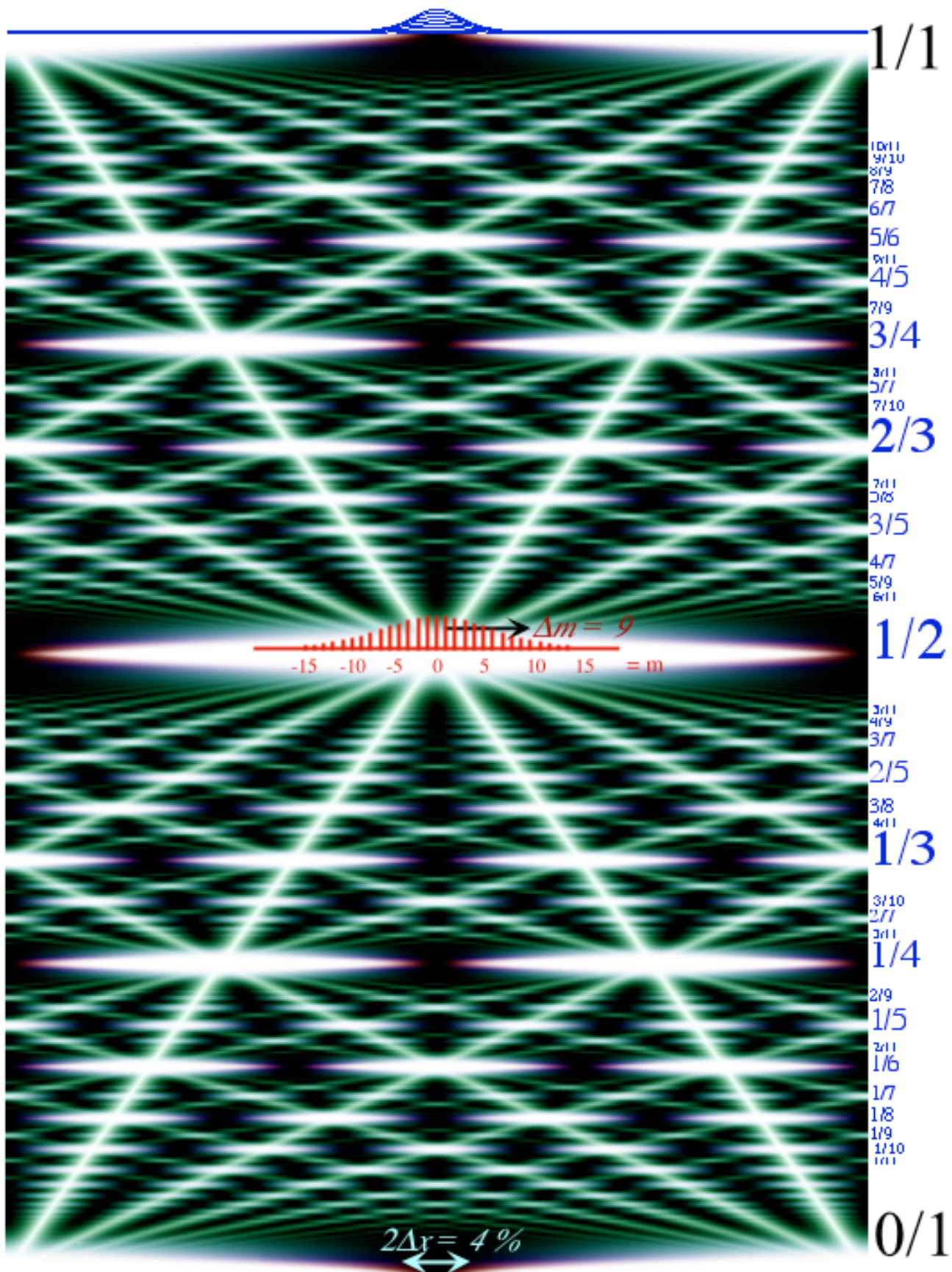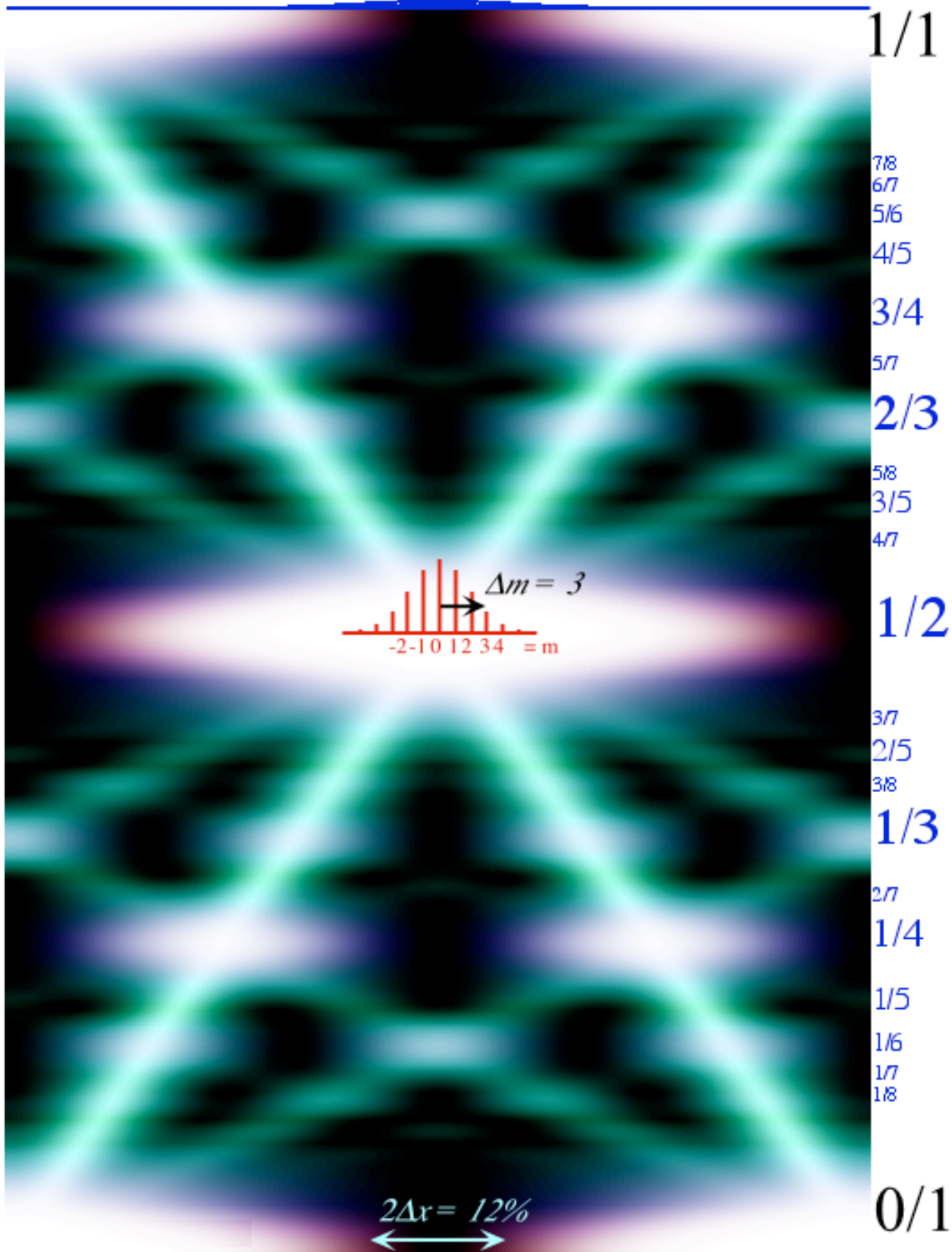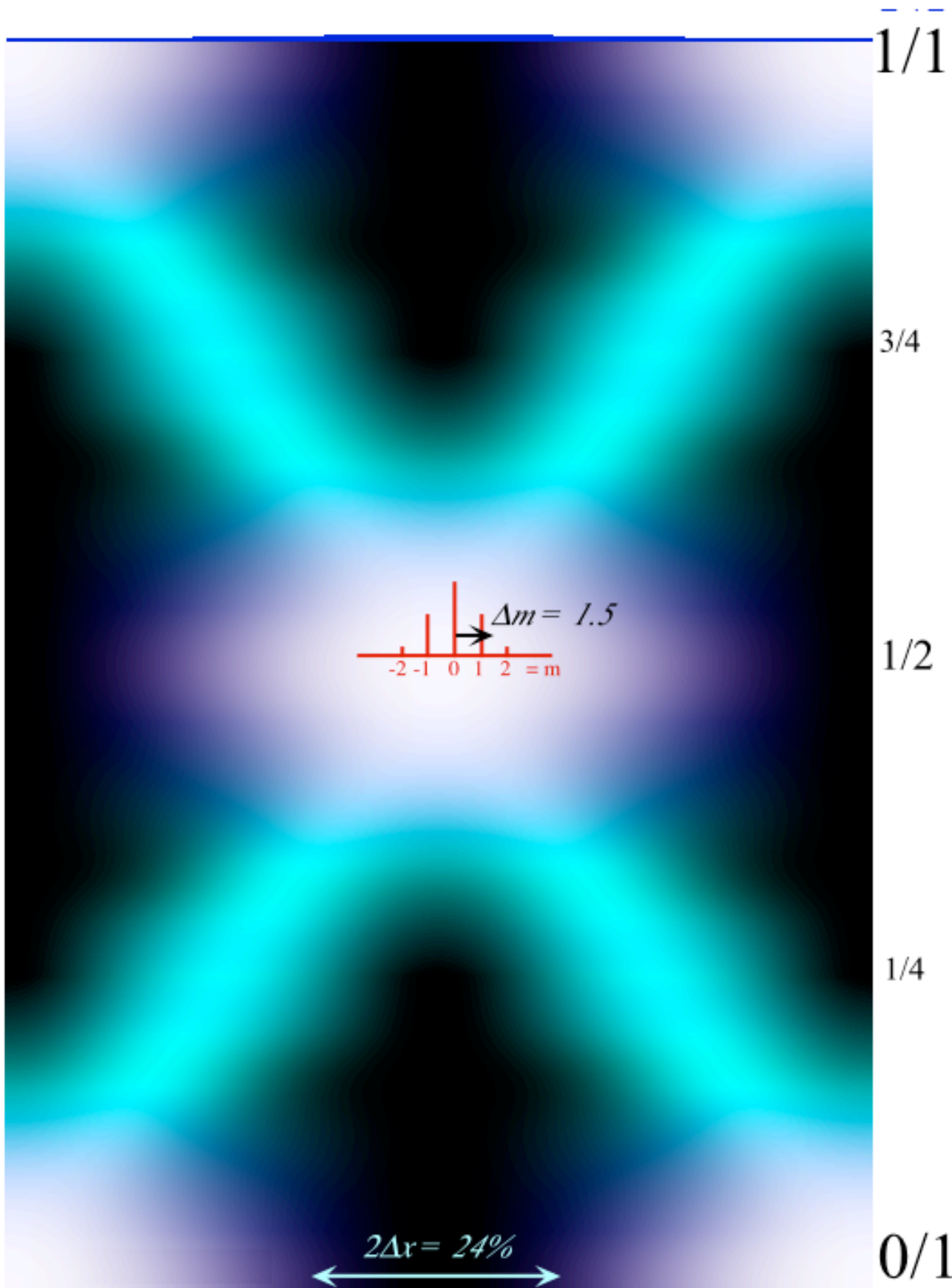
(Preceding pages: Figs. 9.3.5a-c Bohr wavepact revivals in space-time)

(d) Bohr wavepacket dynamics: Uncertainty and revival

We now study Bohr waves that are a Gaussian combination of momentum-*m* plane waves.

$$\Psi(\phi,0) = \langle\phi,0|\Psi\rangle = \frac{1}{2\pi}\sum_{m=-\infty}^{\infty} e^{-m^2/\Delta m^2}\, e^{im\phi} \qquad (9.3.12a)$$

Here, *m=0, ±1, ±2, ±3,...*are momentum quantum numbers in Bohr energy formula (9.3.7).

$$E_m = (\hbar k_m)^2/2M = m^2\,[h^2/2ML^2] = m^2 h\upsilon_1 = m^2\hbar\omega_1 \qquad (9.3.12b))$$

The *fundamental Bohr frequency* $\omega_1 = 2\pi\upsilon_1$ is the lowest *transition (beat) frequency* $\upsilon_1 = (E_1-E_0)/h$.
Completing the square of the exponent provides a simpler ϕ-angle wavefunction.

$$\Psi(\phi,0) = \frac{1}{2\pi}\sum_{m=-\infty}^{\infty} e^{-\left(\frac{m}{\Delta m}-i\frac{\Delta m}{2}\phi\right)^2-\left(\frac{\Delta m}{2}\phi\right)^2} = \frac{A(\Delta m,\phi)}{2\pi}e^{-\left(\frac{\Delta m}{2}\phi\right)^2} \qquad (9.3.13a)$$

Only the lower-*m* terms with *m<Δm* in the sum *A(Δm,φ)* have significant $e^{-(m/\Delta m)^2}$ values, but for larger *Δm* the number of significant terms grows until sum *A* approaches a Gaussian integral independent of ϕ .

$$A(\Delta m,\phi) = \sum_{m=-\infty}^{\infty} e^{-\left(\frac{m}{\Delta m}-i\frac{\Delta m}{2}\phi\right)^2} \xrightarrow[\Delta m\gg 1]{} \int_{-\infty}^{\infty} dk\, e^{-\left(\frac{k}{\Delta m}\right)^2} = \sqrt{\pi}\Delta m \qquad (9.3.13b)$$

The variable factor $e^{-(\Delta m\,\phi/2)^2}$ is a Gaussian function of angle ϕ or position *x*. It is remarkable that the Fourier transform of a Gaussian $e^{-(m/\Delta m)^2}$ momentum distribution is a Gaussian $e^{-(\phi/\Delta\phi)^2}$ in coordinate ϕ.

$$\langle m|\Psi\rangle = e^{-(m/\Delta m)^2} \quad \text{implies:} \qquad \langle\phi|\Psi\rangle = e^{-(\phi/\Delta\phi)^2} \qquad (9.3.14)$$

The relation between *momentum uncertainty* Δm and *coordinate uncertainty* $\Delta\phi$ is a *Heisenberg relation*.

$$\Delta m/2 = 1/\Delta\phi \text{ ,or:} \qquad \Delta m\,\Delta\phi = 2 \qquad (9.3.15)$$

A Gaussian is an eigenvector of the Fourier C_n transformation matrix. (More about this later.)

Three space-time plots are given in Fig. 9.3.5a, b, and c, respectively, with decreasing momentum half-width $\Delta m=9, 3,$ and *1.5* and courser spatial resolution $\Delta\phi/2\pi=2\%, 6\%,$ and *12%* . Each is plotted for a full time period $\tau_1 = 1/\upsilon_1 = 2\pi/\omega_1$ after which it repeats. The first Fig. 9.3.5a uses fine spatial resolution $\Delta x \cdot =0.02$ which requires 9-quantum excitation *(Δm=9)*. It shows a labyrinth of increasingly fine self-similar X-patterns of wave *revivals*. In the second and third figures (9.3.5b and c), of lower excitation (*Δm=3,* and *1.5*, respectively), the finer X-patterns begin to disappear leaving one big X over Fig. 9.3.5c.

Semi-classical Theory: Farey Sums and Quantum Speed Limits

Fig. 9.3.5c provides a clue to the theory of revivals. Its X is like a zero crossing in the Lorentz grid in Fig. 4.2.9, but with momentum values restricted by $\Delta m=1.5$ to the first two levels *m=0* , *±1*, leaving two group (or phase) velocities $V_{\pm 1} = \pm L/\tau_1$ by (4.2.20), that is, a Bohr length *L* per Bohr time unit τ_1.

$$V_{group}^{Bohr}(m\leftrightarrow n) = \frac{\omega_m-\omega_n}{k_m-k_n} = \frac{(m^2-n^2)h\upsilon_1}{(m-n)h/L} = (m+n)\frac{L}{\tau_1} = (m+n)V_1 \qquad (9.3.16)$$

The X in Fig. 9.3.5c has two zeros doing one lap in opposite directions around the Bohr ring in a Bohr period τ_1. The packet anti-nodes or "particles" do laps, too, but their paths are not as contiguous.

Fig. 4

1/1

1/2

3/7

2/5
3/8

1/3

2/7

1/4

1/5

1/6

1/7

1/8

0/1

Zeros start here   *Wave packet starts here*   *Zeros start here*
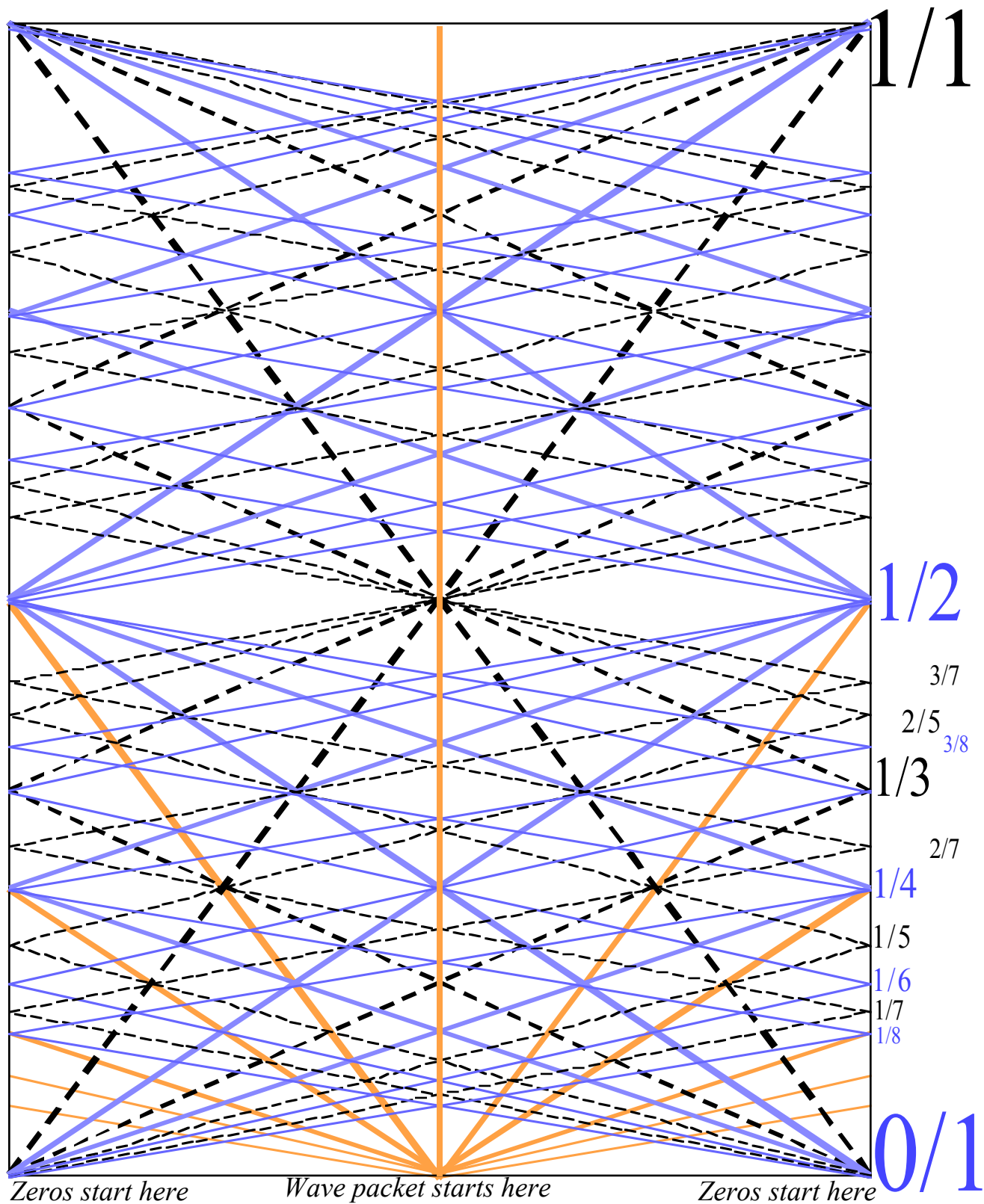
Fig. 9.3.6 Intersecting wave space-time X-path trajectories of nodes and anti-nodes.

(Anti-nodal revival peaks and phases are discussed later.) |Ψ|-nodes, being virtually dead, have an indestructibility not had by zeros of *Re*Ψ that annihilate and re-create as they gallop through Fig. 4.2.9.

Relaxing the momentum uncertainty Δm allows more *m*-values and wave velocities: $\pm V_1, \pm 2V_1, \pm 3V_1,...$ ranging up to $2\Delta m V_1$. By (9.3.16) the maximum lap rate or *quantum speed limit* is $2\Delta m$, *i.e.*, twice the maximum |*m*|. Each velocity gives a fractional lap time of *1/1, 1/2, 1/3, ..., 1/(2Δm)* of the Bohr period. Such fractions are written in the margin of Fig. 9.3.5 at the point where a lap trajectory passes the point $\phi = \pm\pi$ opposite the origin $\phi = 0$ of the wave packet. An *n-th* multiple *n/D* of an allowed fraction *1/D* corresponds to the *n-th* lap of a wave node ("zero") if *D* is odd or the *n-th* lap of a wave anti-node ("particle") if *D* is even.

The *n/D* fractional lines in Fig. 9.3.6 highlight the wave paths in Fig. 9.3.5a. As excitation Δm increases, even-*D* "particle" paths show up as dark shadows in between the odd-*D* "zero" paths in Fig. 9.3.5a. Also seen in a high-Δm plot (Fig. 9.3.5a) are "particle" paths with odd *and* even fractional slopes emanating from the origin $\phi = 0$ of the wave packet. This is indicated in Fig. 9.3.6, too.

The geometry of generic group velocity rays is sketched in Fig. 9.3.7 using two rays to form an asymmetric X around an intersection. (A symmetric X has equal group speeds d_1 and d_2.) Fig. 9.3.5a is a patchwork of self-similar X patterns of nodal *(odd-d_k)* or anti-nodal *(even-d_k)* rays. The equations for the two lines in Fig. 9.3.6 are

$$\phi = -d_1 t + n_1 + 1/2 \qquad\qquad \phi = d_2 t - n_2 + 1/2 \qquad\qquad (9.3.17)$$

Subtracting the first ϕ equation from the second gives the intersection time for the center of the X.

$$t_{12-intersection} = \frac{n_2 + n_1}{d_2 + d_1} = \frac{n_2}{d_2} \oplus_F \frac{n_1}{d_1} \qquad\qquad (9.3.18)$$

The resulting combination is called a *Farey Sum* $\oplus_F$ of the rational fractions n_1/d_1 and n_2/d_2 after John Farey, an 1800's geologist.

Fig. 9.3.7 Farey-sum geometry and algebra of intersecting wave space-time trajectories.

The Farey sum has been used to analyze classically "chaotic" or "fractal" structures , but its use in organizing quantum resonance structure is new. It begins with a fundamental Farey sum relating the beginning fraction *(0/1)* and ending fraction *(1/1)* of the *(0↔1)*-quantum beat or fundamental revival.

$$\frac{0}{1} \oplus_F \frac{1}{1} = \frac{1}{2} \tag{9.3.19}$$

This is the instant $t/\tau_1 = 1/2$ for a half-time revival and the zero at the center of the fundamental X in Fig. 9.3.5c. The fundamental sum makes up the second row of a *Farey Tree* of such sums shown in (9.3.20). The sums in the *D-th* row of a Farey tree are an ordered set of all reduced fractions with denominator equal to *D or less*. The tree need not go beyond $D>2\Delta m$ where denominator *D* exceeds the wave quantum speed limit $2\Delta m$ of (9.3.16). Finer revivals will be unresolvable. More energy is needed to see finer X's.

	0/1	1/8	1/7	1/6	1/5	1/4	2/7	1/3	3/8	2/5	3/7	1/2	4/7	3/5	5/8	2/3	5/7	3/4	4/5	5/6	6/7	7/8	1/1
$D \le 1$	0/1																						1/1
$D \le 2$	0/1											1/2											1/1
$D \le 3$	0/1							1/3				1/2				2/3							1/1
$D \le 4$	0/1					1/4		1/3				1/2				2/3		3/4					1/1
$D \le 5$	0/1				1/5	1/4		1/3		2/5		1/2		3/5		2/3		3/4	4/5				1/1
$D \le 6$	0/1			1/6	1/5	1/4		1/3		2/5		1/2		3/5		2/3		3/4	4/5	5/6			1/1
$D \le 7$	0/1		1/7	1/6	1/5	1/4	2/7	1/3		2/5	3/7	1/2	4/7	3/5		2/3	5/7	3/4	4/5	5/6	6/7		1/1
$D \le 8$	0/1	1/8	1/7	1/6	1/5	1/4	2/7	1/3	3/8	2/5	3/7	1/2	4/7	3/5	5/8	2/3	5/7	3/4	4/5	5/6	6/7	7/8	1/1

(9.3.20)

The tracking of crests or wave peaks yields information about classical particle-like or group-wave motion. It is comforting to see familiar classical paths in what is often bewildering quantum cacophony but, the clearest X-paths in Fig. 9.3.5a are *zeros* emanating from the point $\phi = \pm\pi$ where the particle packet originally was *not*. Quantum wave dynamics differs from classical dynamics is that multiple Fourier components easily interfere much of a wave to death. Most path phases lead to *non*-existence except near (rare) stationary-phase paths that may be familiar classical ones. This is what is responsible for particle localization that allows us to enjoy a Newtonian world and largely conceals its quantum wave nature from us. Where the wave is *not* provides important quantum clues. One recalls Sherlock Holmes' revelation that it is the "dog that did *not* bark" which solved a mystery.

9.4 Homo-cyclic Cn Revivals

Wave phase is key to the C_N dynamics beginning with the "beats" of two-state C_2 system. As we have said, "It takes two to tango." First we review the two-state-system dynamics with analogies to optical polarization from Chapter 1 and coupled pendulum dynamics. (Later chapters will use this analogy.) C_2 holds the first key to analyzing the revivals introduced in the preceding section.

We have also said, "Three's a crowd." The dynamics associated with C_3 systems is discussed after that of C_2 and then that of C_4, C_5, C_6, and C_{15} systems. Each is part of the revival milieu of Fig. 9.3.5.

(a) Two–state *C₂* systems: Beats

Motion of anti-nodal revivals for a 2-level excitation such as Fig. 9.3.5c are like beats of coupled pendulums. Fig. 9.4.1a shows *phasor* pictures of 2-cyclic *(C₂)* eigenstates. Phasor "clocks" are phase-space plots of $Re\Psi$ vs. $Im\Psi$ for wavefunction $\Psi(p)$ at each spatial point $p=0,1$. $Re\Psi$ is up, $Im\Psi$ is to the left, and the area $\pi|\Psi|^2$ of the phasor is proportional to probability $|\Psi|^2$ at point p.

Each eigenstate phasor rotates <u>clockwise</u> at its Bohr eigenfrequency $\omega_m = m^2\omega_1$, that is, $\Psi(t)=e^{-i\omega_m t}\Psi(0)$. The C_2 eigenstates are labeled *even (0₂)=(+)* or *odd (1₂)=(–)* as usual.

$$|+\rangle =|0_2\rangle=(|x\rangle+|y\rangle)/\sqrt{2} \qquad (9.4.1a) \qquad\qquad |-\rangle =|1_2\rangle=(|x\rangle-|y\rangle)/\sqrt{2} \qquad (9.4.1b)$$

$$\textit{Bohr eigenfrequency: } \omega_0 = 0 \qquad (9.4.2a) \qquad\qquad \textit{Bohr eigenfrequency: } \omega_1 \qquad (9.4.2b)$$

$|m_2\rangle$ eigenfrequencies ω_m are $\omega_0 = 0$ and $\omega_1 = h/(2ML^2)$ by (9.3.12b). States $|m_2\rangle$ are + or − combinations of a local oscillator base state labeled $|x\rangle=|r^0\rangle$ (localized at spatial point $p=0$ or $\phi=0$) and a "flipped" base state $|y\rangle=\mathbf{r}|x\rangle$ $=|r^1\rangle$ (localized at point $p=1$ or $\phi=\pi$). States $|+\rangle$ and $|-\rangle$ are also eigenstates of C_2 "flip" operator $\mathbf{r}$ defined by $\mathbf{r}|x\rangle$ $=|y\rangle$ and $\mathbf{r}|y\rangle=|x\rangle$, that is, $\mathbf{r}|+\rangle=+|+\rangle$, and $\mathbf{r}|-\rangle=-|-\rangle$. State $|+\rangle$ is analogous to $+45°$ polarization which is the "slow" eigenstate. State $|-\rangle$ is analogous to the "fast" $-45°$ optical axis.

An initial *50-50* combination of the $|+\rangle$ and $|-\rangle$ eigenstates briefly recovers the $|x\rangle=|r^0\rangle$ local base

$$|x\rangle =(|+\rangle+|-\rangle)/\sqrt{2} =(|0_2\rangle+|1_2\rangle)/\sqrt{2}, \qquad\qquad \textit{(Time t=0)}$$

lying between $|+\rangle$ and $|-\rangle$ in Fig. 9.4.1b. The $|1_2\rangle$-eigenstate is faster than the $|0_2\rangle$-eigenstate (which does not move at all by (9.4.2a)) The $|x\rangle$-state is always a sum of 0_2 and 1_2 phasors. (Left and right 0_2 phasors are at 12 PM in Fig. a while the left 1_2 phasor starts at 12 PM and the right 1_2 phasor at 6 PM.) After 12 PM the 1_2 phasors "tick" but 0_2 phasors are stuck at 12PM. Their sum $|x\rangle$ varies with time.

By *1/4* of beat period τ_1, the fast $|1_2\rangle$ clocks are $90°$ ahead of the stuck $|0_2\rangle$. (Clockwise is $-i$.)

$$|L\rangle =(|+\rangle-i|-\rangle)/\sqrt{2} =(|0_2\rangle-i |1_2\rangle)/\sqrt{2}. \qquad\qquad \textit{(Time t=(1/4)}\tau_1)$$

The left and right hand 1_2 clocks move to 3 PM and 9 PM, respectively, but 0_2 clocks are stuck at 12 PM. On the left: 12 PM plus 3 PM is half-size clock at 2:30 PM. On the right: 12 PM plus 9PM is a half-size clock at 10:30 PM. Note two half-phasors at $-45°$ (2:30 PM) and $+45°$ (10:30 PM) at *1/4*-period. The *1/4* period situation is analogous to optical *1/4*-wave plates that change $|x\rangle$-polarization to left-circular $|L\rangle$.

By $\tau_1/2$ the fast 1_2 -clocks go *180°* ahead to give the "flipped" local base state of *y*-polarization.

$$|y\rangle =(|+\rangle-|-\rangle)/\sqrt{2} =(|0_2\rangle-|1_2\rangle)/\sqrt{2} \qquad\qquad \textit{(Time t=(1/2)}\tau_1)$$

(a)

$\mathbf{r}^0\ (\phi=0)$ $\mathbf{r}^1\ (\phi=\pi)$ *Coupled Pendula*   *Optical E(t)*

even   +45°

0_2 0°   0° $|+\rangle$

C_2

parity states   *odd*   -45°

1_2 0°   180° $|-\rangle$

(b)

localized   x

t = 0   0° $\dfrac{|+\rangle + |-\rangle}{\sqrt{2}}$

1/4   45°   -45° $\dfrac{|+\rangle - i|-\rangle}{\sqrt{2}}$ L

revivals or beats

0°

1/2 $\dfrac{|+\rangle - |-\rangle}{\sqrt{2}}$ *flipped*   y

3/4   -45°   45° $\dfrac{|+\rangle + i|-\rangle}{\sqrt{2}}$ R
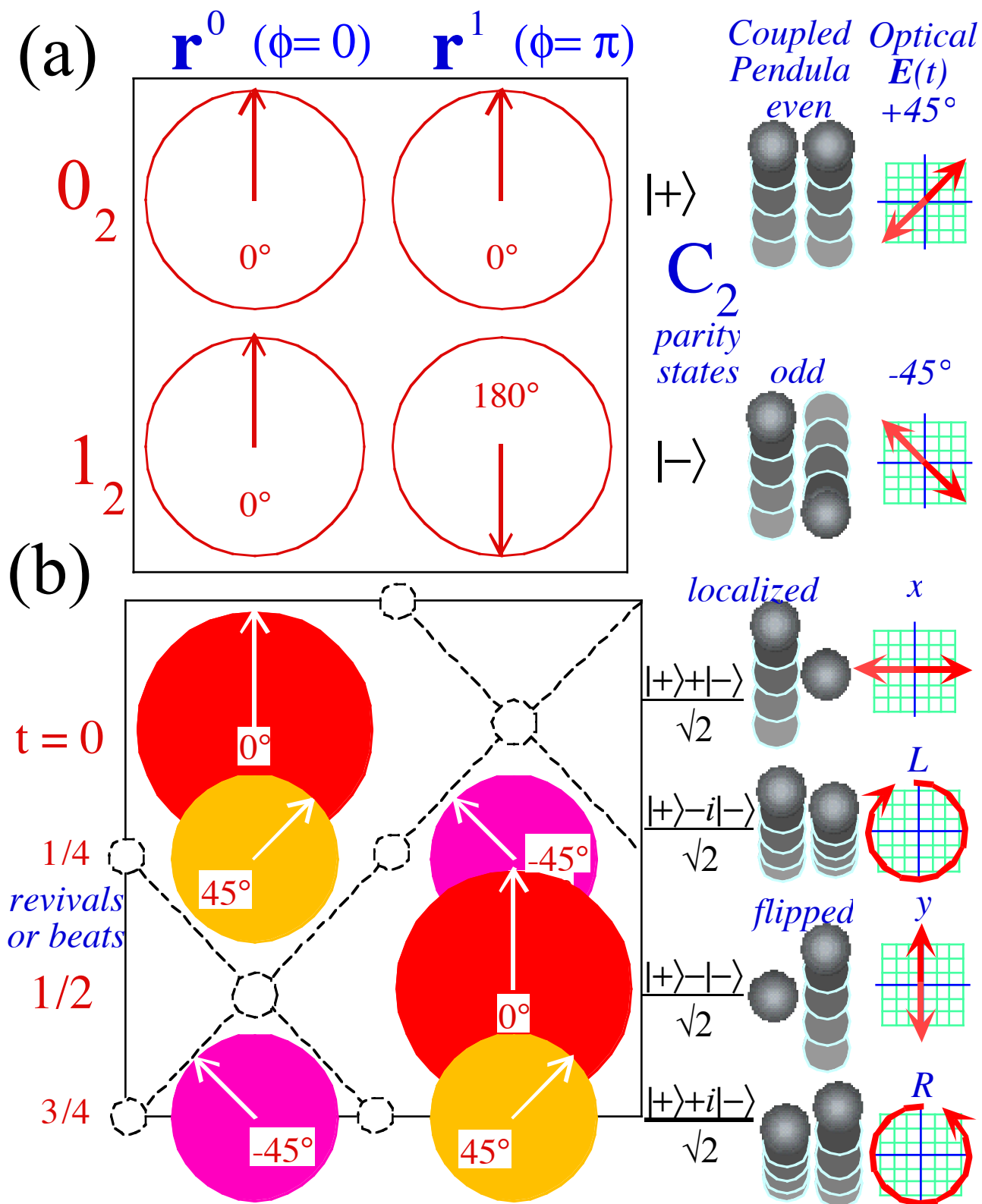
Fig. 9.4.1 (a) C_2 eigenstate phasors. (b) 50% combination states de localizing and reviving.

At $\tau_1/2$, the left 1_2 clock is at 6 PM the right one at 12 PM, but both 0_2 clocks still read 12PM . On the left: 12 PM plus 6 PM is zero (a node). On the right: 12 PM plus 12PM is *big* 12 PM. All the wave flips to the $|y\rangle$-state. The *1/2*-period situation is like *1/2*-wave plate changing $|x\rangle$-polarization to $|y\rangle$.

Still later at $(3\tau_1/4)$ the initial $|x\rangle$-state has become a right circular state. (Fig. 9.4.1b bottom)

$$|R\rangle = (\,|+\rangle + i\,|-\rangle\,)/\sqrt{2} = (\,|0_2\rangle + i\,|1_2\rangle\,)/\sqrt{2} \qquad\qquad \text{(Time } t=(3/4)\,\tau_1\text{)}$$

Finally, at full-time $(1/1)\tau_1$ the initial $|x\rangle$ state (top of Fig. 9.4.1b) is once again back to being $|x\rangle$ and would reappear beneath Fig. 9.4.1b to begin repeating the revival sequence.

In Fig. 9.4.1b, dotted lines making an X are drawn around the phasors to connect places where wave amplitude is low like the X-pattern in Fig. 9.3.5c. Low *m*-uncertainty $(\Delta m=1.5)$ means the revival wave is mostly a combination of the first <u>two</u> Bohr eigenlevels $m=0$ and $|m|=1$ having just two group (or phase) velocities $+V_1$ and $-V_1$. In other words, Fig. 9.3.5c is essentially just a <u>two</u>-state system, and the major half and full revivals are just binary beat of two coupled symmetric pendulums.

The *1/4* fractional revival corresponds to *transition state* $|L\rangle = (\,|x\rangle - i\,|y\rangle\,)/\sqrt{2}$ (analogous to left circular polarization) between the major revivals. In $|L\rangle$ the left hand position phasor is *90°* ahead of the right hand one being resonantly pumped up. The roles of the two phasors are reversed at $3\tau_1/4$.

(b) C_n group structure: n=3, 4,...6 Eigenstates

To understand finer X-zero patterns and fractional revivals between zeros in Fig. 9.3.5 a-b we go beyond the binary $\{|0_2\rangle|1_2\rangle\}$ basis to, at least, the base-3 basis $\{|0_3\rangle|1_3\rangle|2_3\rangle\}$ of C_3 The bra state vectors $\{\langle 0_3|\langle 1_3|\langle 2_3|\}$ were defined in Fig. 2.6.4 and are re-drawn in Fig. 9.4.2a. The C_3 wave states have quantized momentum *m=0, 1, and 2 modulo 3* . Each *m* labels a row of three phasors in Fig. 9.4.2a which are a discrete sampling of the waves in the first three Bohr levels *m=0,1,* and *2.*

In Fig. 9.4.2b are *4-nary C_4* base states of *m=0, 1, 2 and 3 modulo 4* quanta and Fig. 9.4.3a reintroduces *5-nary C_5* bases of *m=0, 1, 2,3, and 4 modulo 5* quanta, and similarly in Fig. 9.4.3b for C_6. These systems are like counters; a binary C_2 system can count only to two, that is, *0* to *1*, but each of the C_N systems are capable of counting to *N*, that is, *0, 1, 2,3,..,N-1*.

Physically the C_N waves are bases of a finite and discrete Fourier analysis. Each C_N *character table* in Fig. 9.4.2a-b or 9.4.3a-b (if all divided by $\sqrt{N}$) is the *N-by-N* unitary *(U(n))* transformation matrix $\langle p|m\rangle$ of *discrete Fourier transformation coefficients*. (Recall Fig. 7.3.3 and discussion.)

$$\left\langle p\,\middle|(m)_N\right\rangle = e^{i\,p\,m/2\pi N}\,/\sqrt{N} = \left\langle (m)_N\,\middle|p\right\rangle^{*} \quad (p,m=0,1,2,...,N\text{ - }1) \qquad (9.4.3a)$$

Each phasor in Fig. 9.4.2-12 sits at one of *N* equally spaced lattice points *p=0, 1, ...,N-1*. Each phasor gives for a particular angular point *p=0, 1, 2,3,..,N-1* the complex wave amplitude (7.3.10a)

$$\psi_{\pm m}(2\pi p/N) = \langle p|(m)_N\rangle = \langle (m)_N|p\rangle^{*}$$

of a continuous running wave that is one of Bohr-Schrodinger eigenfunctions $\psi_{\pm m}(\phi)$.

A real (cosine) part of the eigenfunction is drawn for each eigenstate $|(m)_N\rangle$ in Fig. 9.4.2-3 to help connect it to the latter. The state notation $(m)_N$ labels these waves and should be read *m-modulo-N* (or *m%N* in C) meaning

that waves having $m \pm nN$ wavelengths or quanta will give a physically and mathematically identical state $(m)_N$. (They are Fourier *aliases* $(m)_N = (m \pm nN)_N$, states differing only by reciprocal lattice vectors $K = \pm nN$.)

In Fig. 9.4.2-12 each one of N equally spaced lattice points $p=0, 1, 2, 3,...,N-1$, is labeled by a *p-th* power $\mathbf{r}^p$ of a fundamental C_N group rotation $\mathbf{r}$ by angle $2\pi/N$, that is, by $\mathbf{r}^0=1$, $\mathbf{r}^1$, $\mathbf{r}^2$, $\mathbf{r}^3$ ... , $\mathbf{r}^{N-1}$, $\mathbf{r}^N=1$ respectively. This labeling notation simply lists the operator elements of the cyclic C_N symmetry group as was done in equations (8.1.5a). The entries $e^{-ipm/2\pi N}$ are *m-th* eigenvalues of $\mathbf{r}^0, \mathbf{r}^1, \mathbf{r}^2 ..., \mathbf{r}^p$.

The phasors are graphical representations of the complex eigenvalues or *characters* of the various cyclic groups. It should be noted that the binary C_2 phasor table (Fig. 9.4.1a) is embedded as a subset in the C_4 table since C_2 is a subgroup of C_4. C_2 is also seen in the C_6 table (Fig. 9.4.3b) or any C_N table of even-N since C_2 is a subgroup of all C_{2n}. The C_6 table also has the C_3 table (Fig. 9.4.2a) embedded. Symmetry embedding is of utmost importance for analyzing group algebra, their representations, and their physical applications. Here it is what gives the revival structure down to the finest observable details of revival wave phase or amplitude shown in Fig. 9.3.5 a.

The same numbers (without the $\sqrt{N}$) serve triple or quadruple duty in algebraic group theory. Besides Fourier transforms they are *irreducible representations $D^m(\mathbf{r}^p)$ of C_N*

$$D^{(m)}{}_N \left(\mathbf{r}^p \right) = e^{-i\frac{pm}{2\pi N}} \qquad (9.4.3b)$$

such that

$$D^m(\mathbf{a})\, D^m(\mathbf{b}) = D^m(\mathbf{ab}) \,.$$

This goes along with the $D^m(\mathbf{c})$ being eigen*values* of the group operators $\mathbf{c}=\mathbf{r}^p$. (Note $(\mathbf{r}^p)^\dagger = \mathbf{r}^{-p}$.)

$$\mathbf{r}^p \left| (m)_N \right\rangle = D^{(m)}{}_N \left(\mathbf{r}^p \right) \left| (m)_N \right\rangle = e^{-i\frac{pm}{2\pi N}} \left| (m)_N \right\rangle \qquad (9.4.3c)$$

$$\left\langle (m)_N \right| \mathbf{r}^p = D^{(m)}{}_N \left(\mathbf{r}^p \right) \left\langle (m)_N \right| = e^{-i\frac{pm}{2\pi N}} \left\langle (m)_N \right| \qquad (9.4.3d)$$

Also, each row of the character table in Fig. 9.4.2-3 is an eigen-bra-vector wavefunction of discrete points p or powers of $\mathbf{r}^p$. As shown in Sec. 9.2, each bra $\langle (m)_N |$ and ket $|(m)_N\rangle$ must also be an eigenvector of any Hamiltonian operator $\mathbf{H}$ that commutes with C_N, *i.e.*, has C_N symmetry ($\mathbf{H}\mathbf{r}^p=\mathbf{r}^p\mathbf{H}$). So the character tables serve finally as universal energy eigen*vectors* and eigen*states*, too. All the above apply to the generic C_N groups and all their embedded subgroups which include all smaller C_n for which n is *an integral divisor* of N.

(a) C_3 Eigenstate Characters
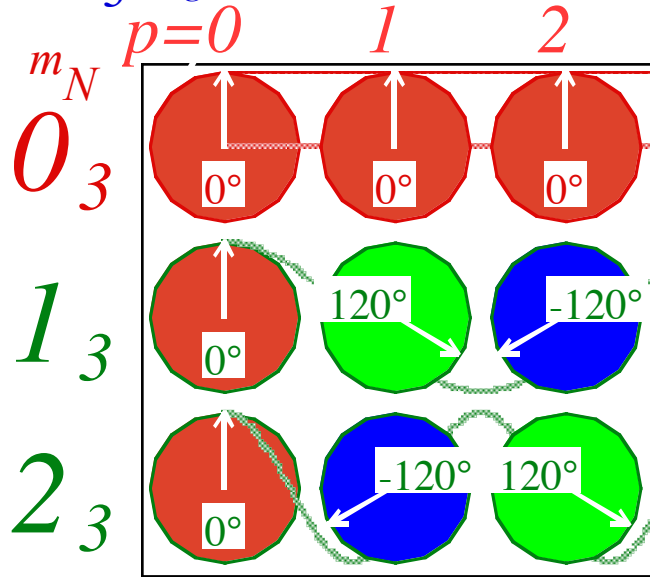
(b) C_4 Eigenstate Characters
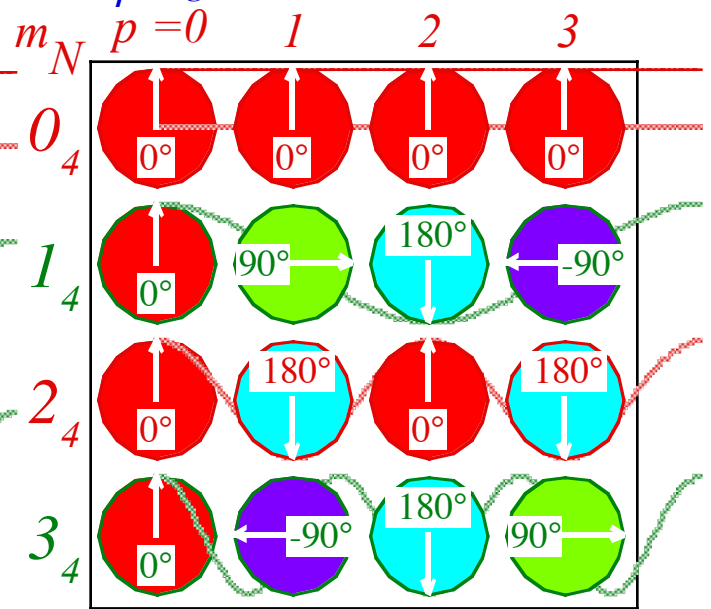
(c) C_3 Revivals
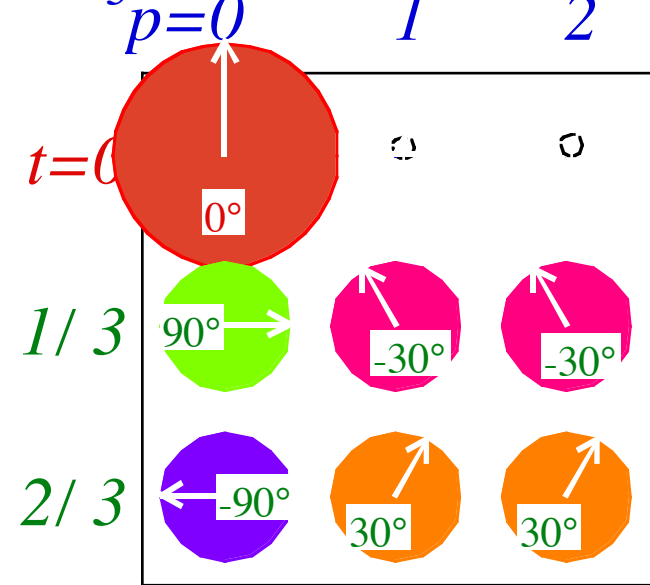
(d) C_4 Revivals
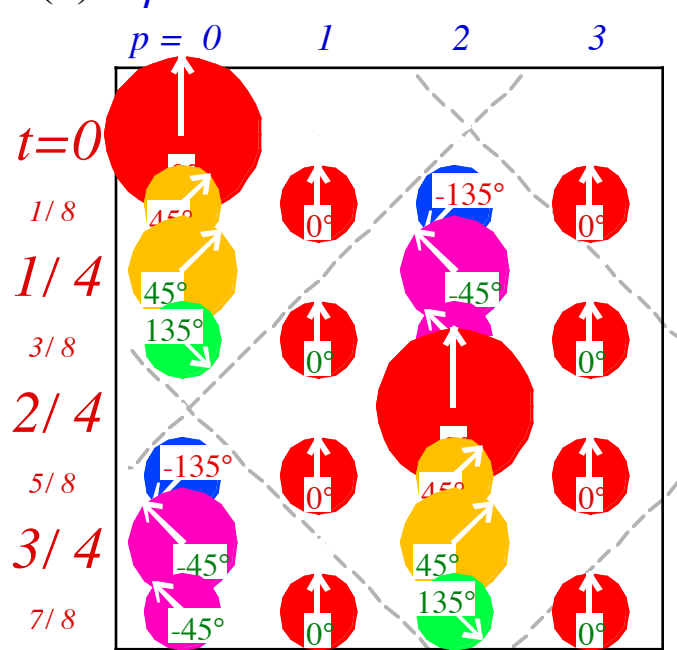
Fig. 9.4.2 C_3 and C_4 eigenstates and revivals.
(a) and (b) C_3 and C_4 eigenstate characters.
(c) and (d) C_3 and C_4 revival space time patterns.

(c) C_n dynamics: n=3, 4,...6 Fractional Revivals

For each subgroup embedding there is a corresponding embedding of the *revival tables* that are shown in Fig. 9.4.2c-d and 9.4.3c-d. Revival tables are obtained, as in Fig. 9.4.1b, by first summing all the rows of phasors in each character table C_3, C_4, C_5, or C_6 of Fig. 9.4.2-3a-b. This localizes the initial wave 100% onto the first phasor position state $|x_0\rangle$. Because $\langle (m)_N| x_0\rangle = 1$ identically, we have

$$|x_0\rangle = \sum_{m=0}^{N-1} |(m)_N\rangle\langle(m)_N|x_0\rangle = \sum_{m=0}^{N-1} |(m)_N\rangle \qquad (9.4.4a)$$

This is called a group *completeness relation* or *resolution of the identity*. All phasors are equivalent due to C_N symmetry, so arbitrarily picking the first column $(r^0=1)$ does not affect the general utility of Fig. 9.4.2-3. Translation by $\mathbf{r}^p$ rephases the sum (9.4.4a) according to (9.4.3c) and translates all waves rigidly.

$$|x_p\rangle = \mathbf{r}^p|x_0\rangle = \sum_{m=0}^{N-1} \mathbf{r}^p|(m)_N\rangle = \sum_{m=0}^{N-1} e^{-i\frac{pm}{2\pi N}}|(m)_N\rangle \qquad (9.4.4b)$$

Then each term $|(m)_N\rangle$ in the sum (9.4.3) is allowed to advance its Bohr phase $e^{-i\omega_m t} = e^{-im^2\omega_1 t}$ in discrete time fractions $1/N$ of τ_1 for *N-odd* or $1/2N$ for *N-even*, that is, through *stroboscopic instants* t_υ.

$$|x_0(t_\upsilon)\rangle = \sum_{m=0}^{N-1} e^{-im^2\omega_1 t_\upsilon}|(m)_N\rangle \qquad t_\upsilon = \begin{cases} \upsilon\dfrac{\tau_1}{N} = \dfrac{2\pi\upsilon}{\omega_1 N} & (\upsilon = 1,2,...,N-1) \ for \ N-odd \\[3mm] \upsilon\dfrac{\tau_1}{2N} = \dfrac{\pi\upsilon}{\omega_1 N} & (\upsilon = 1,2,...,2N-1) \ for \ N-even \end{cases} \qquad (9.4.5)$$

For each stroboscopic instant or row in Fig. 9.4.3 there is an array of equally-sized and equally-spaced phasors, that is, a *kaleidoscopic* phasor array. At each t_υ, phasors are either revived or else zeroed-out.

An even-$N=2p$ revival table, such as $N=4$ and $N=6$ in Fig. Fig. 9.4.3 has embedded the $N=2$ revival or "beat" table in Fig. Fig. 9.4.1b since C_2 is a C_{2p} subgroup. So besides the obvious 1/2-time revival halfway around, there must be *1/4*-time and *3/4*-time revivals for $N=2$ at each of the *1/4*-lattice points, that is for $N=6$, at $t=3/12$ and $t=9/12$, and for $N=4$, at $t=2/8$ and $t=6/8$. Because $N=6$ is also divisible by 3 there will be $N=3$ revivals embedded at $t=4/12=1/3$ and $t=8/12=2/3$. Also, $N=3$ revivals embedded relative to the 1/2-time revival at $t=1/3-1/2=-1/6$ and $t=1/3+1/2=5/6$ and $t=2/3-1/2=1/6$ and at $t=2/3+1/2=7/6$. The phase angle "combinations" for each of the embedded phasors are reproduced perfectly and periodically as in a kind of quantum "odometer" or counter.

An even-N revival table must start all over again at half-time, but from a point half-way around the ring at $\phi=\pi$ if it started at $\phi=0$. This is required by C_N symmetry and by C_2 half-time revival having 100% probability on the antipodal (half-way) point $p=N/2$ if 100% probability starts on the initial $p=0$ point. So the C_4 phasors below the $(p=2, t=2/4=1/2)$ point in Fig. Fig. 9.4.3b, namely, $t=5/8, 3/4,$ and $7/8$, must have positions, amplitudes, and phases relative to the mid-point $p=2$ that are identical to ones at $t=1/8, 1/4,$ and $3/8$, respectively, below the initial $t=0=p$ point. Similar repetition is seen for $N=6$ in Fig. 9.4.3c and for any *even-N* revival table below $t=1/2$.

A prime-N revival table (like $N=3$ in Fig. 9.4.2c or $N=5$ in Fig. 9.4.3c) has no embedded structure because prime C_N has no subgroup but C_1. After the initial localized state each revival has probability distributed equally on all N lattice sites but with distinct phase combinations as in a kind of base-N quantum odometer. In contrast, base-N counters with $N=2^p$, $p!$ or other composite numbers like $N=4$ or 6 in Fig. 9.4.2d or 9.4.3d have the greatest variety of revival amplitudes.
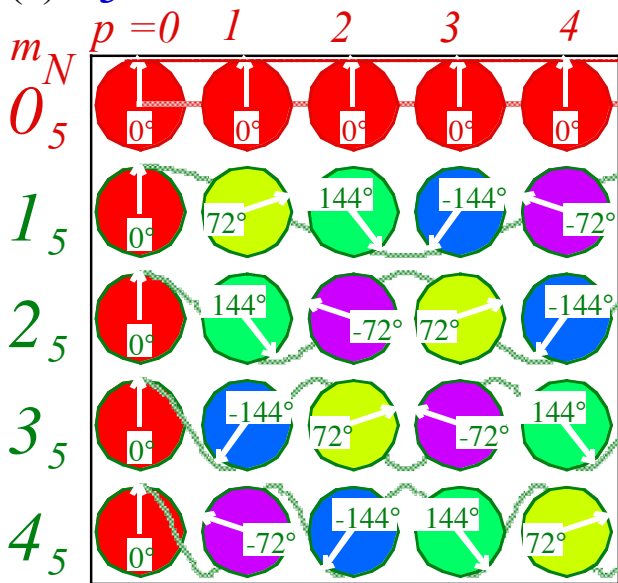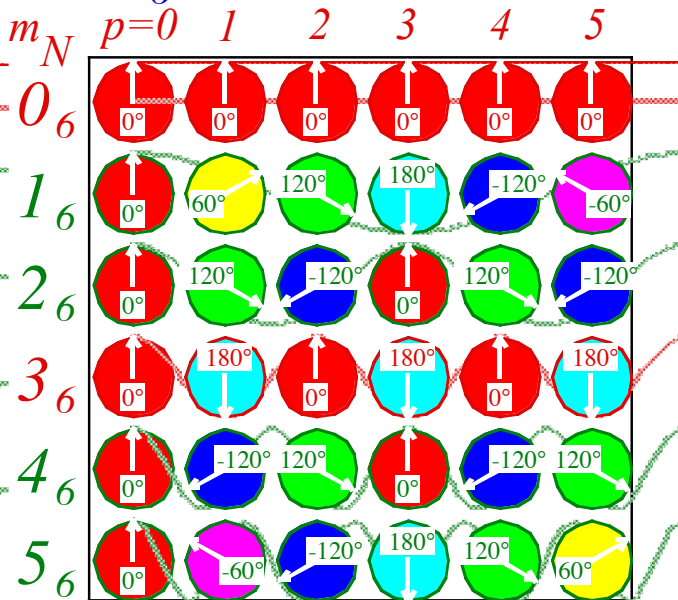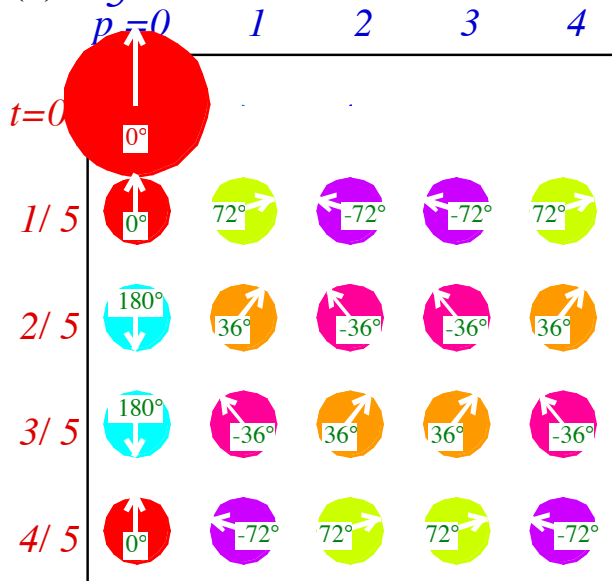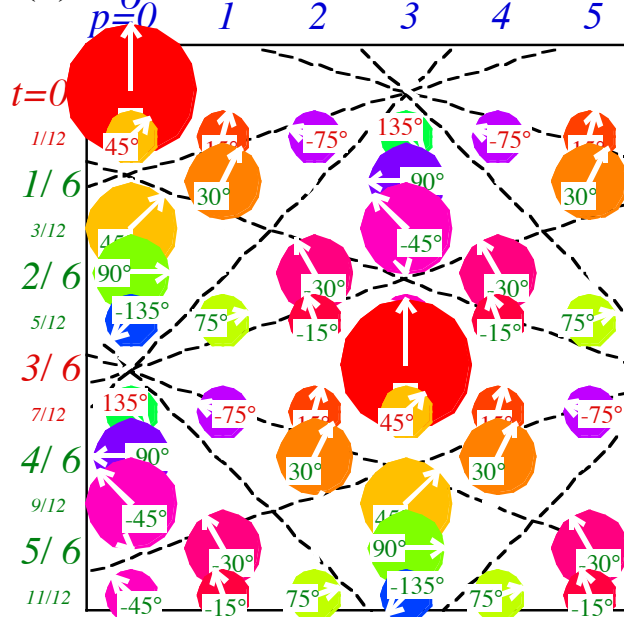
Fig. 9.4.3 C_5 and C_6 eigenstates and revivals.

(a) and (b) C_5 and C_6 eigenstate characters.

(c) and (d) C_5 and C_6 revival space time patterns.

The *N=6* space-time wave patterns of Fig. 9.4.3d match phasor-for-peak with the revival intensity structure of the *1/12ths*, *1/6th*'s, *1/4th*'s, *1/3rd*'s, and *1/2* revivals in Fig. 9.4.5 a or b if Fig. 9.4.3 tables are rescaled to the same size and overlapped with their edges centered in Fig. 9.4.5 a or b. Also, each table gives exactly the correct amplitude *and phase* of each revival peak that belongs to it as well as showing where the zeros reside. Similar character-revival tables of C_5 (Fig. 9.4.3c), *C7, C9,...* will account for finer odd-fractional revivals occurring at stroboscopic odd-time fractions like the *1/5th*'s, *1/7th*'s, *1/9th*'s,...and so on. (Recall *1/8th*'s are

revivals for C_4 shown in Fig. 9.4.2d. They will be copied by a C_8 revival table in between its (new) *1/16th*'s.) The medium resolution wave plot of Fig. 9.4.5b displays *N=2, 3, 4, ...,8* structure more clearly than high-Δm Fig. 9.4.5a by suppressing or defocusing the even finer revivals and prolonging fewer but more robust peaks or zeros of the more fundamental revivals. But, all zero-centered excitations *($\bar{m}$ =0)* for larger-Δm such as shown in Fig. 9.4.5a-b have the same fundamental X of a *(0↔1)* C_2 beat in Fig. 9.4.5c, that is, they show a half-time revival that peaks around the center of the largest X.

Cyclic subgroup hierarchies

$$\cdots C_n \subset C_{pn} \subset C_{p^2 n} \subset C_{p^3 n} \subset \cdots$$

are here being used to organize quantum fractal revival dynamics. Schrodinger's approach to quantum theory, which eschewed the *gruppenpest* in favor of differential equations, is not set up to explain the origins of such discrete fractal structure. This is because each successive integer *N* starts a new hierarchical group family. If the integer is prime the family is entirely new. But, if it is not prime, then older smaller families belonging to each of *N*'s factors are copied and embedded in the new family. In contrast, Schrodinger's wave equation treats every value of its independent variables as just another dumb *x* or *t*, and rational structure is glossed over.

Each new odd integer *N=2m+1* will have *N* new revival peaks at time fractions t/τ=v/N=1/N,...q/N .. but only for fractions *q/N* that are irreducible. Reducible fractions *q/N* that reduce to *q/N = qR/r* (by dividing out a highest common factor *f=N/r=q/qR*) just recreate the "old" *r=N/f*-peak revivals already seen for a lesser or reduced integer N_R =r=N/f. Similarly, for even *N=2m* the only new revivals are at found irreducible time fractions t/τ=v/2N=1/2N,...q/2N ... . All the rest belong to subgroups C_{N_R} (if any) of C_N including C_m and C_2. A formula for new revival phasors based on sum (9.4.5) is given in Appendix 3.A. Now we consider a quasi-classical way to understand revival dynamics.

Odd-*N* revivals clearly display the prime factors and their multiples of the integer *N*. If *N* is a prime number as it is for *N=3* in Fig. 9.4.2c and for *N=5* in Fig. 9.4.3c then all reviving kaleidoscopes except the initial one consist of uniform distributions of *N* phasors of probability *1/N*. However, for a composite odd integer such as *N=15*, the phasor distributions are not uniform as shown in Fig. 9.4.4. There are nodes at the *p=±1* points for all revivals that correspond to factors of the integer *N=15*, namely at the revivals numbered *1, 3, 6, 9, 12,* and *1, 5, 10,* and *15*. The latter are copies of C_3 revivals seen in Fig. 9.4.2c and the former are copies of C_5 revivals seen in Fig. 9.4.3c. Their presence is simply a result of C_3 and C_5 being subgroups of C_{15}.

By definition, *1* is a factor of all *N* and C_1 is a subgroup of all C_N . This is manifest by the first row of each revival table. The only even prime integer is *N=2*. This helps to account for the unique status of the C_2 revival table in Fig. 9.4.1b and the extra significance of the C_2 parity of each integer *N*, that is, the distinction between odd and even integers.
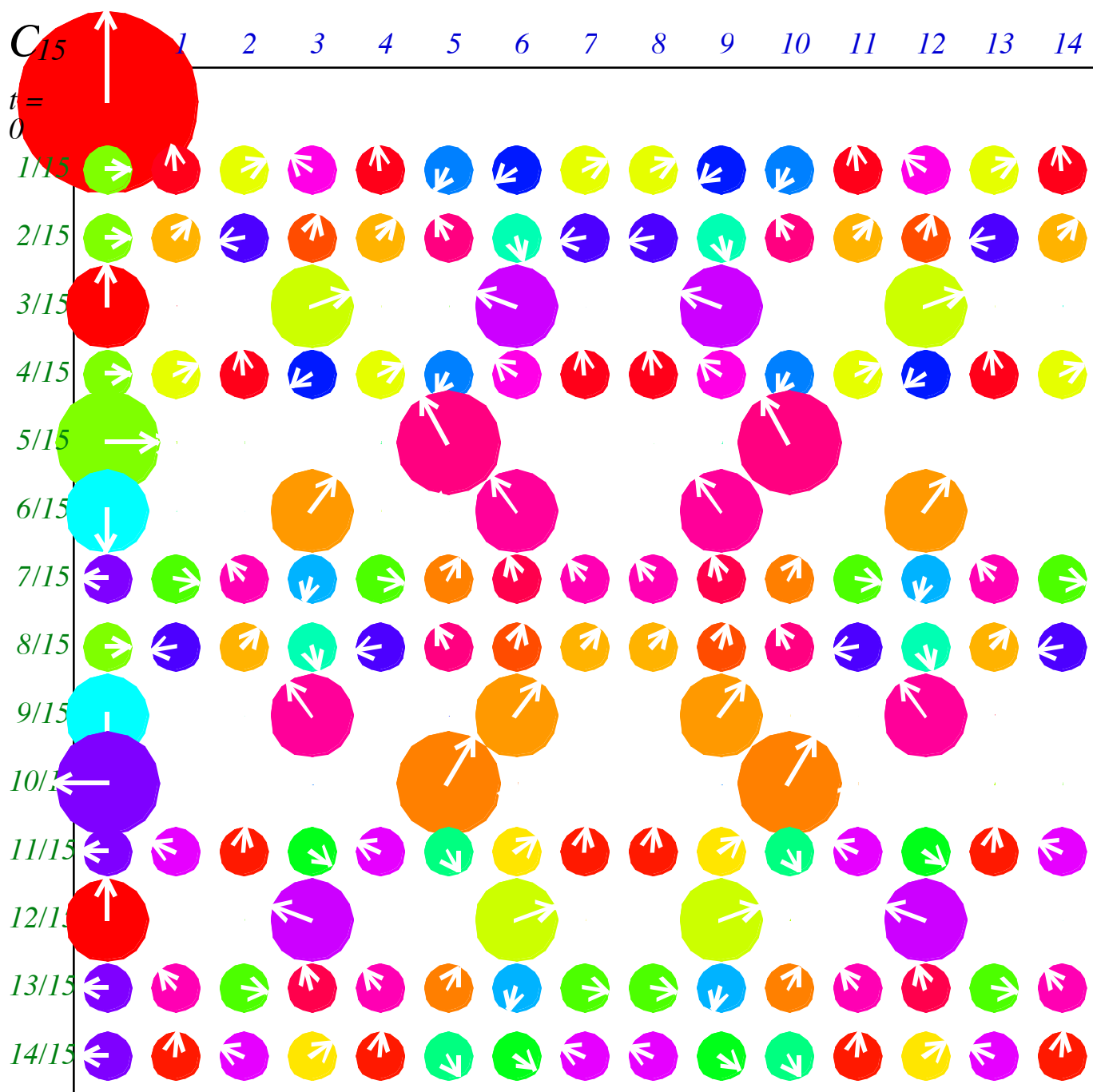
Fig. 9.4.4 Bohr space-time revival pattern for C_{15} Bohr system.

Bohr vs. Bloch dispersion

The value of the C_N models increases when the purely quantum effects, particularly those of a *single C_N*, are to be isolated. One imagines having a discrete Bohr ring like those sketched Fig. 9.4.5 composed of *N* atoms, quantum dots, optical fibers, or Josephson circuits homo-cyclically coupled is such a way that the usual quadratic Bohr dispersion spectrum $\omega_m = m^2\omega_1$ is obtained with a finite number *N* of states per band. As a first approximation, such a ring has a *Bloch* dispersion spectrum $\omega_m = (H_0-2H_1 \cos am)$ where H_1 is the nearest neighbor coupling amplitude. Such a Bloch spectrum only approximates a Bohr spectrum for low *m*-values, and so high-Δm revivals would decay eventually. However, by inserting cross-connecting coupling paths H_2 , H_3 , H_4 , ...$H_{N/2}$, as shown in Fig. 9.4.5, it is possible to achieve any spectrum, including m^2, by adjusting coefficients H_k in a Fourier series.

$$\omega_m = H_0-2S_1 \cos am-2H_2 \cos 2am-2H_3 \cos 3am...-H_{N/2} \cos Nam/2 .$$

A quadratic spectrum *($E_m=h\upsilon m^2$)* is achieved for general *N* by setting Hamiltonian parameters as follows.

$$h\upsilon m^2 = \sum_{p=0}^{N-1} H_p\, e^{-ipm\frac{2\pi}{N}} , \quad \text{where: } H_p = \frac{h\upsilon}{N} \sum_{\{m\}} m^2\, e^{ipm\frac{2\pi}{N}} \qquad (9.4.6)$$

For example, a *4*-level *N=6* quadratic spectrum $\{E_0=0, E_{\pm1}=1^2\ E_{\pm2}=2^2, E_3=3^2.\}$ involves six eigenstates: $|(m)_6\rangle$ $= |(0)_6\rangle, |(\pm1)_6\rangle, |(\pm2)_6\rangle$, and $|(3)_6\rangle$, using the following coupling amplitudes as given in the *N=6* row of Table 9.1.

$$H_0=3.16, H_1=-2.0=H_5*, H_2= 0.67=H_4*, H_3=-0.5 , \qquad (9.4.7)$$

With the adjustments in Table 9.1. of H_k coupling, pure C_N revivals like those in Fig. 9.4.2-3 would repeat at frequency $\upsilon=h^{-1}$ until the coupling is turned off. Such a device would be an *N*-ary counter as implied before. By incorporating the *N*-ring as the crossection of a coaxial *N*-fiber cable, it would be possible for the revival evolution to occur as an *N*-phase wave propagated down the cable. The possibility of storing, processing, and transporting quantum or classical *N*-ary data for *N>>2* using just one kind of basic hardware may yet warm the heart (and portfolio) of a future cyber-entrepreneur.
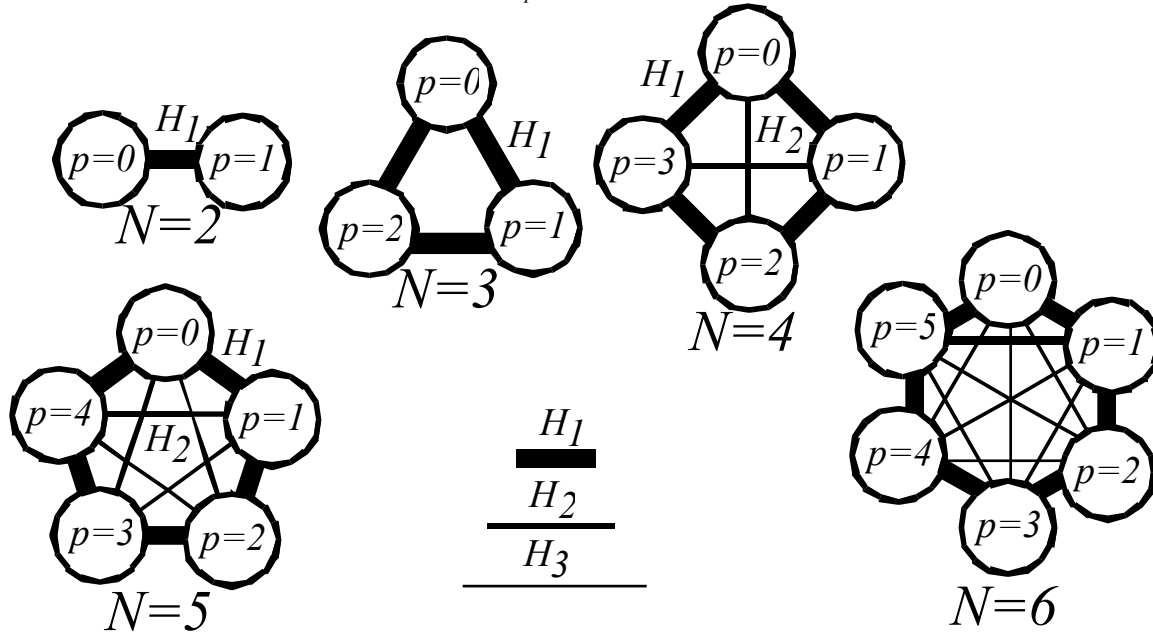
Fig. 9.4.5 Quantum dot or co-axial cable structures with arbitrary dispersion

Table 9.1. N-Discrete m^2-Hamiltonian Coupling Amplitudes. All devices have a unit revival rate: $h\upsilon=1$.

	H_0	H_1	H_2	H_3	H_4	H_5	H_6	H_7	H_8	H_9
N=2	1/2	-1/2								
N=3	2/3	-1/3								
N=4	3/2	-1	1/2							
N=5	2	-1.1708	0.1708							
N=6	19/6	-2	2/3	-1/2						
N=7	4	-2.393	0.51	-0.1171						
N=8	11/2	-3.4142	1	-0.5858	1/2					
N=9	20/3	-4.0165	0.9270	-1/3	0.0895					
N=10	17/2	-5.2361	1.4472	-0.7639	0.5528	-1/2				
N=11	10	-6.0442	1.4391	-0.5733	0.2510	-0.0726				
N=12	73/6	-7.4641	2	-1	2/3	-0.5359	1/2			
N=13	14	-8.4766	2.0500	-0.8511	0.4194	-0.2028	0.06116			
N=14	33/2	-10.098	2.6560	-1.2862	0.8180	-0.6160	0.5260	-1/2		
N=15	57/3	-11.314	2.7611	-1.1708	0.6058	-1/3	0.1708	-0.0528		
N=16	43/2	-13.137	3.4142	-1.6199	1	-0.7232	0.5858	-0.5198	1/2	
N=17	24	-14.557	3.5728	-1.5340	0.81413	-0.4732	0.2781	-0.1479	0.0465	

Problems for Chapter 9.

Evolution   (A 2000 Qualifying exam problem)

9.1.1. A two-state quantum system evolves as follows in 5 sec. (First: Is the evolution unitary?)

$$\text{State } |1\rangle \text{ becomes state } |1'\rangle = -\sqrt{3}/2 \ |1\rangle - i/2 \ |2\rangle$$
$$\text{State } |2\rangle \text{ becomes state } |2'\rangle = \quad -i/2|1\rangle -\sqrt{3}/2|2\rangle$$

(a) Derive a complete set of states as combinations of $|1\rangle$ and $|2\rangle$ so that each combination would stay the same (except for a possible overall phase) at all times.

(b) Compute the energy level splitting $\Delta E=E_2-E_1$ for this system assuming ΔE is the lowest possible to achieve the 5 sec. evolution given in part (a).

(c) Derive an expression for any state at any time t and give $|1(t)\rangle$ and $|2 \ (t)\rangle$ numerically at t=1 sec.

(d) Does this evolution correspond to a Hamiltonian **H**? If so, what **H**?

Revolution

9.1.2. A two-state quantum system evolves as follows in t sec. (First: Is the evolution unitary?)

$$\text{State } |1\rangle \text{ becomes state } |1'\rangle = \cos \omega t \ |1\rangle - \sin \omega t \ |2\rangle$$
$$\text{State } |2\rangle \text{ becomes state } |2'\rangle = \sin \omega t \ |1\rangle + \cos \omega t \ |2\rangle$$

(a) Does this time evolution correspond to a Hamiltonian **H**? If so, what **H**? Is it Hermitian?

_____

Hexapairs

9.3.1 The hexagonal C_6 eigenstates $|0_6\rangle$ and $|3_6\rangle$ are standing waves while $[|+1_6\rangle, |-1_6\rangle]$ and $[|+2_6\rangle, |-2_6\rangle]$ are right and left moving wave pairs.

   (a) Do $[|+3_6\rangle, |-3_6\rangle]$ a moving wave pair make? Explain why or why not?

   (b) Can the $[|+1_6\rangle, |-1_6\rangle]$ pair make a pair of standing waves? If so make them and plot the phasors. If not, explain.

   (c) Can the $[|+2_6\rangle, |-2_6\rangle]$ pair make a pair of standing waves? If so make them and plot the phasors. If not, explain.

   (d) What values, if any, for tunneling parameters $|S|$, σ, $|T|$, τ, and U allow <u>standing</u>-wave-pair <u>eigen</u>states. Must they always be degenerate?

Octapairs

9.3.2 Consider an octagonal C_8 system of 8 quantum dots.

   (a) Write the general form of its Hamiltonian.

   (b) Display its eigenkets and write a formula for its energy eigenvalues.

Back to Roots...again

9.3.3. Eigensolutions of C_2 and C_3 symmetric **H** can be turned into quadratic and cubic root formulas.

(a) Eigenvalues of $\mathbf{H}=\begin{pmatrix} A & B \\ B & A \end{pmatrix}$, namely $\lambda=A\pm B$ give solutions to $\lambda^2-2A\lambda+A^2-B^2=0$ Use this to derive the familiar quadratic formula for roots of $a\lambda^2+b\lambda+c=0$.

(b) Use the above and C_3-derived eigenvalues of $\mathbf{H}=\begin{pmatrix} A & C & B \\ B & A & C \\ C & B & A \end{pmatrix}$ to derive the less familiar formula for roots to general cubic equation $a\lambda^3+b\lambda^2+c\lambda+d=0$. (Hint: First consider $\lambda^3+p\lambda+q=0$.)

Quantum baseball

9.3.3 Suppose the Asumma Tummy Quantum Computer Co. has taken over the world and you are the only one in your country that still knows the difference between an amplitude and a phase. Your assignment is to design, make or experiment with some quantum dot computer elements diagrammed below having charge carrier matter-waves that tunnel along edges and diagonals of squares as indicated below.

(a) Tunneling Paths

$S* = \langle \rho | \mathbf{H} | \rho+1 \rangle$

$S = \langle \rho+1 | \mathbf{H} | \rho \rangle$

(b) C_4 Quantum Dots

$\mathbf{H} = \langle \rho | \mathbf{H} | \rho \rangle = \mathbf{H}*$

(c) Broken symmetry

$\langle 0 | \mathbf{H} | 0 \rangle = H + \Delta H$

$\langle 1 | \mathbf{H} | 0 \rangle = S + \Delta S = \langle 0 | \mathbf{H} | 1 \rangle$

$\langle 0 | \mathbf{H} | 3 \rangle = S + \Delta S = \langle 3 | \mathbf{H} | 0 \rangle$
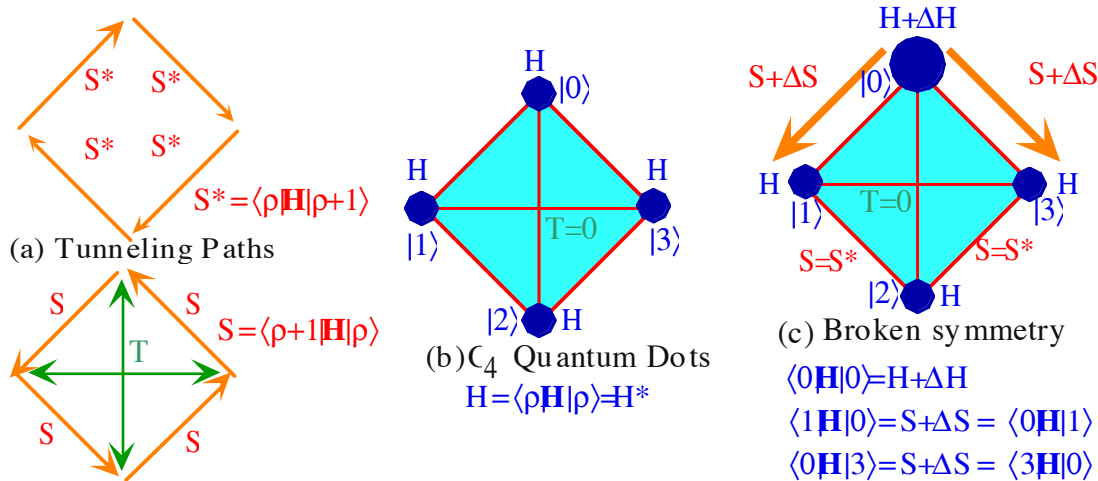
Suppose edge tunneling amplitudes are equal and real ($S = -1.0$) while diagonal tunneling amplitudes are zero ($T=0$) to give C_4 symmetry as shown in Fig. (b). Suppose at time $t=0$ the charge carrier amplitude is 100% on "home" base state $|0\rangle$.($\langle 0 | \Psi(t=0) \rangle = 1$).

(a) Derive eigenlevels and calculate the time dependence of the home-base amplitude $\langle 0 | \Psi(t) \rangle = ?$ Find the period $\tau_{rebound}$ of time it takes home-base to rebound to a maximum again after initially decreasing. Does it rebound to 100% the first time? ever?

(b) Sketch phasors for each of the four bases $|0\rangle$, $|1\rangle$, $|2\rangle$, and $|3\rangle$ at 1/4- $\tau_{rebound}$ time intervals and indicate by arrows between phasors the direction of instantaneous charge flow from one to the other. (Tell how you determine this just by looking at the phasors.) Does first, second, or third base ever hold 100% of the charge?

(c.) Suppose all edge tunneling amplitudes are equal but (possibly) complex ($S = -e^{i\sigma}$) while diagonal tunneling amplitudes are zero ($T=0$).

(a) Adjust the tunneling phase angle σ so as to make four equally spaced energy eigenlevels with quantum numbers $m=(0)_4$, $(-1)_4$, $(1)_4$, and $(2)_4$, in that order.

Is the order $(0)_4$, $(1)_4$, $(2)_4$, and $(3)_4 = (-1)_4$ also possible using this adjustment? If not, can some other kind of adjustment achieve it without changing the form of the eigenstates? Discuss.

Janitor's revenge

9.3.4. Suppose a janitor hits the home-base dot-0 with his broom handle and accidentally resets some $\mathbf{H}$-matrix elements shown in Fig. (c) by small amounts: the first diagonal by $\Delta H = A$ and the first off-diagonal by $\Delta S = \Delta S* = B$. All other matrix elements remain the same as in Problem 9.3.3. Let the new "broken" Hamiltonian be a sum $\mathbf{H'} = \mathbf{H} + \mathbf{V}(A,B)$.

(a) Derive a matrix representation of the janitor's perturbation $\mathbf{V}(A,B)$ in the original $|0\rangle$ to $|3\rangle$ basis, in the *moving-wave* basis $|(0)_4\rangle$, $|(-1)_4\rangle$, $|(1)_4\rangle$, and $|(2)_4\rangle$, and in the *standing-wave cosine and sine* basis $|(0)_4\rangle$, $|(c_1)_4\rangle$, $|(s_1)_4\rangle$, and $|(2)_4\rangle$, where: $|(c_1)_4\rangle = (|(-1)_4\rangle + |(1)_4\rangle)/\sqrt{2}$, and: $|(s_1)_4\rangle = (|(-1)_4\rangle - |(1)_4\rangle)/i\sqrt{2}$.

(b) Use (a) and perturbation theory to estimate (to 2nd order $|A|^2 = |\Delta S|^2$ or $|b|^2 = |\Delta H|$) the effect of the $\mathbf{V}(A=0.1, B=0.2)$ on energy eigenlevels $\varepsilon(0)_4$, $\varepsilon(\pm 1)_4$, and $\varepsilon(2)_4$ as $\varepsilon(m)_4$ turn into eigenlevels of the "broken" Hamiltonian $\mathbf{H'}$. Which representation from (a) should be used and why? Show your work.

(c.) Discuss the effect, if any, on the original eigenstates $|(0)_4\rangle$, $|(-1)_4\rangle$, $|(1)_4\rangle$, and $|(2)_4\rangle$, and sketch their phasor diagrams next to the corresponding eigenlevels. Are moving-wave eigenstates still possible after the janitor does his or her work?
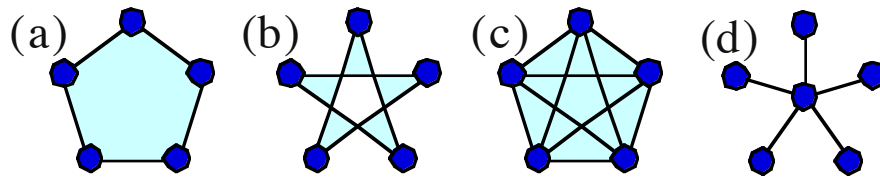
Beware the pentagram

9.3.5. Suppose a *pentagonal* C_5 device in prob. 9.3.3(a).

(a) Could it ever rebound to 100%? Discuss devices (a), (b), and (c).

(b) Discuss the possibility (or impossibility) of constructing such a device that would give a "runner-going-around-the-bases" effect with 100% probability occurring briefly but consecutively on first base, then second base, then third base, and finally home base. If such a device could be made would it also be capable of running in the opposite direction without modifying the H-matrix?

Quantum dot.com

9.3.6 The C_N quantum dots in Fig. 9.4.5 are supposed to belong to an infinite family of structures whose ω_m-spectrum is quadratic in quantum number m_N. This assumes a sequence of tunneling paths or connecting couplers described by (9.4.6). The $N=2$ example seems an exception having only a single $H_1 = S$ connector on each dot. Is this right? Should the

Hamiltonian be $\mathbf{H} = \begin{pmatrix} H & S \\ S & H \end{pmatrix}$ or should it be $\mathbf{H} = \begin{pmatrix} H & 2S \\ 2S & H \end{pmatrix}$ to conform with the rest? Discuss. Compare the $N=2$

case with, say, that of $N=4$.

Quantum dot.com again

9.3.7 The C_N quantum dots in Fig. 9.4.5 might be made to have other spectral band functions such as

(Q) Quadratic spectrum: $\omega(m)=\varepsilon(m)/\hbar = m^2 = 1, 0, 1, 4, 9,...$ for $(m)_N = -1, 0, 1,$ and $\pm2, \pm3,....$

(L) Linear spectrum: $\omega(m)=\varepsilon(m)/\hbar = |m| = 1, 0, 1, 2,3,...$ for $(m)_N = -1, 0, 1, \pm2, \pm3,...$

(SL) Super-linear spectrum: $\omega(m)=\varepsilon(m)/\hbar = m = -1, 0, 1, \pm2, \pm3,...$ for $(m)_N = -1, 0, 1, \pm2, \pm3,...$

      (a) Derive N=8 coupling parameters for each of these spectra.

Review Topics & Formulas for Unit 3

Fourier Series Coefficients   *Fourier Integral Transform*   *Fourier C_N Transformation*

$$\left\langle k_m \middle| \Psi \right\rangle = \int_{-L/2}^{L/2} dx \left\langle k_m \middle| x \right\rangle \left\langle x \middle| \Psi \right\rangle \qquad \left\langle k \middle| \Psi \right\rangle = \int_{-\infty}^{\infty} dx \left\langle k \middle| x \right\rangle \left\langle x \middle| \Psi \right\rangle \qquad \left\langle k_m \middle| \Psi \right\rangle = \sum_{p=0}^{p=N-1} \left\langle k_m \middle| x_p \right\rangle \left\langle x_p \middle| \Psi \right\rangle$$

$$\left\langle k_m \middle| x \right\rangle = \frac{e^{-ik_m x}}{\sqrt{L}} = \left\langle x \middle| k_m \right\rangle^* \qquad Kernal: \left\langle k \middle| x \right\rangle = \frac{e^{-ikx}}{\sqrt{2\pi}} = \left\langle x \middle| k \right\rangle^* \qquad \left\langle k_m \middle| x_p \right\rangle = \frac{e^{-ik_m x_p}}{\sqrt{N}} = \left\langle x_p \middle| k_m \right\rangle^*$$

x-Wavefunction $\Psi(x)=$ *x-Wavefunction $\Psi(x)=$*   *x-Wavefunction $\Psi(x)=$*

$$\left\langle x \middle| \Psi \right\rangle = \sum_{m=-\infty}^{m=\infty} \left\langle x \middle| k_m \right\rangle \left\langle k_m \middle| \Psi \right\rangle \qquad \left\langle x \middle| \Psi \right\rangle = \int_{-\infty}^{\infty} dk \left\langle x \middle| k \right\rangle \left\langle k \middle| \Psi \right\rangle \qquad \left\langle x_p \middle| \Psi \right\rangle = \sum_{m=0}^{m=N-1} \left\langle x_p \middle| k_m \right\rangle \left\langle k_m \middle| \Psi \right\rangle$$

Ortho − Completeness   *Ortho − Completeness*   *Ortho − Completeness*

$$\sum_{m=0}^{m=\infty} \left\langle x \middle| k_m \right\rangle \left\langle k_m \middle| x' \right\rangle = \delta(x-x') \qquad \int_{-\infty}^{\infty} dk \left\langle x \middle| k \right\rangle \left\langle k \middle| x' \right\rangle = \delta(x-x') \qquad \sum_{m=0}^{m=N-1} \left\langle x_p \middle| k_m \right\rangle \left\langle k_m \middle| x_{p'} \right\rangle = \delta_{p,p'}$$

$$\int_{-L/2}^{L/2} dx \left\langle k_m \middle| x \right\rangle \left\langle x \middle| k_{m'} \right\rangle = \delta_{m,m'} \qquad \int_{-\infty}^{\infty} dx \left\langle k \middle| x \right\rangle \left\langle x \middle| k' \right\rangle = \delta(k-k') \qquad \sum_{p=0}^{p=N-1} \left\langle k_m \middle| x_p \right\rangle \left\langle x_p \middle| k_{m'} \right\rangle = \delta_{m,m'}$$

Discrete momentum m   *Continuous momentum k*   *Discrete momentum m*
Continuous position x   *Continuous position x*   *Discrete position x_p*

		U *must be Unitary*

Time Evolution Operator **U**   *Time Evolution Operator* **U** $\mathbf{U}^\dagger(t) = \mathbf{U}^{-1}(t) = \mathbf{U}(-t)$

$$\left| \Psi(t) \right\rangle = \mathbf{U}(t,0) \left| \Psi(0) \right\rangle \qquad \mathbf{U}(t,0) = e^{-itH/\hbar} \qquad \left(e^{-it\mathbf{H}/\hbar} \right)^\dagger = e^{it\mathbf{H}^\dagger/\hbar} = e^{it\mathbf{H}/\hbar}$$

Hamiltonian Generator **H**   *Schrodinger t − Equation*

$$i\hbar \frac{\partial}{\partial t} \mathbf{U}(t,0) = \mathbf{H}\,\mathbf{U}(t,0) \qquad i\hbar \frac{\partial}{\partial t} \left| \Psi(t) \right\rangle = \mathbf{H} \left| \Psi(t) \right\rangle \qquad \text{so } \mathbf{H} \text{ is Hermitiam } \mathbf{H}^\dagger = \mathbf{H}$$

Schrodinger time-independent energy eigen equation.

$$\mathbf{H} \left| \omega_m \right\rangle = \hbar\omega_m \left| \omega_m \right\rangle = \varepsilon_m \left| \omega_m \right\rangle \qquad\qquad (9.3.1a)$$

H-eigenvalues use **r**-expansion (9.2.6) of **H** and C_6 symmetry $\mathbf{r}^p$-eigenvalues from (8.2.9).

$$\left\langle k_m \middle| \mathbf{r}^p \middle| k_m \right\rangle = e^{-ipk_m a} = e^{-ipm2\pi/N} \text{ where: } k_m = m(2\pi/Na)$$

$$\left\langle k_m \middle| \mathbf{H} \middle| k_m \right\rangle = H\left\langle k_m \middle| \mathbf{1} \middle| k_m \right\rangle + S\left\langle k_m \middle| \mathbf{r} \middle| k_m \right\rangle + T\left\langle k_m \middle| \mathbf{r}^2 \middle| k_m \right\rangle + U\left\langle k_m \middle| \mathbf{r}^3 \middle| k_m \right\rangle + T^*\left\langle k_m \middle| \mathbf{r}^4 \middle| k_m \right\rangle + S^*\left\langle k_m \middle| \mathbf{r}^5 \middle| k_m \right\rangle$$

$$= H + S\,e^{-ik_m a} + T\,e^{-i2k_m a} + U\,e^{-i3k_m a} + T^*\,e^{i2k_m a} + S^*\,e^{ik_m a} \qquad (9.3.5a)$$

Bloch dispersion relation. And Bohr limit (k<<π/a) approxiamtion. *Band group velocity V_{group}*.

$$\hbar\omega_m = E_m = H - 2|S| \cos(k_m a) = H - 2|S| + |S|(k_m a)^2 + .. \qquad (9.3.8)$$

$$V_{group} = \frac{d\omega_m}{dk_m} = 2\frac{|S|}{\hbar} a \sin(k_m a) \quad \left(\cong 2\frac{|S|}{\hbar} k_m a^2 \text{, for: } k_m << \pi/a \right) \qquad (9.3.10)$$

Effective mass M_{eff} <u>inversely</u> proportional to S. $M_{eff}(0) = \hbar^2/(2|S|a^2)$ (9.3.11a)

Fourier transform of a Gaussian $e^{-(m/\Delta m)^2}$ momentum distribution is a Gaussian $e^{-(\phi/\Delta\phi)^2}$ in coordinate ϕ.

$$\left\langle m \middle| \Psi \right\rangle = e^{-(m/\Delta m)^2} \text{ implies:} \qquad \left\langle \phi \middle| \Psi \right\rangle = e^{-(\phi/\Delta\phi)^2} \qquad (9.3.14)$$

The relation between *momentum uncertainty* Δm and *coordinate uncertainty* $\Delta\phi$ is a *Heisenberg relation*.

$$\Delta m/2 = 1/\Delta\phi \text{ ,or:} \qquad \Delta m\,\Delta\phi = 2 \qquad (9.3.15)$$

Bohr wave quantum speed limits

$$V_{group}^{Bohr}\left(m \leftrightarrow n\right) = \frac{\omega_m - \omega_n}{k_m - k_n} = \frac{\left(m^2 - n^2\right)h\upsilon_1}{\left(m - n\right)h / L} = (m+n)\frac{L}{\tau_1} = (m+n)V_1 \quad (9.3.16)$$

Predicting fractional revivals: *Farey Sum* $\oplus_F$ of the rational fractions n_1/d_1 and n_2/d_2

$$t_{12-intersection} = \frac{n_2 + n_1}{d_2 + d_1} = \frac{n_2}{d_2} \oplus_F \frac{n_1}{d_1} \quad\quad\quad\quad (9.3.18)$$

Appendix 9.A. Relative phase of peaks in a revival lattice

The first derivation here of revival amplitudes at stroboscopic time fractions $t_\nu = \tau(\nu/N)$ and kaleidescopic angular positions $\phi_\rho = 2\pi(\rho/N)$ assumes N is odd. At times when fraction (ν/N) is reduced, all N revival peak sites hop up with identical magnitude and with particular arrangement of phases that clearly distinguishes each ν/N from all others. First we derive formulas for these phases as a function of site index ρ and revival time index ν. (If time fraction ν/N reduces to ν_R/N_R, then use (ν_R, N_R) in place of (ν, N) to find N_R peak phases of subgroup C_{N_R} revivals.) The first step is to complete the square of exponent in sum.

$$\psi_0\left(\phi_\rho, t_\nu\right) = \frac{1}{N}\sum_{m=0}^{N-1} e^{i\left(m\rho - m^2\nu\right)\frac{2\pi}{N}} = \frac{1}{N}\sum_{m=0}^{N-1} e^{-i\left(m^2\nu - m\rho + \frac{\rho^2}{4\nu}\right)\frac{2\pi}{N}} e^{i\frac{\rho^2}{4\nu}\frac{2\pi}{N}}$$

$$= \frac{1}{N}\sum_{m=0}^{N-1} e^{-i\left(m\nu - \frac{\rho}{2}\right)\left(m - \frac{\rho}{2\nu}\right)\frac{2\pi}{N}} e^{i\frac{\rho^2}{4\nu}\frac{2\pi}{N}} \tag{A.1}$$

$$= \frac{1}{N}\sum_{m=0}^{N-1} e^{-i\left(2m\nu - \rho\right)^2\frac{2\pi}{4\nu N}} e^{i\frac{\rho^2}{4\nu}\frac{2\pi}{N}}$$

The integer square $(2m\nu - \rho)^2$ in the exponent is to be treated as an integer-modulo-$4\nu N$ since the phase factor repeats after that value. However, as summation index m runs through the integers $m = 0, 1, 2, ..., N-1$ it exhausts all the possible values of $(2m\nu-p)^2$-mod-$4\nu N$ for a given ν and ρ, and the values are the same no matter what we take for the range of m. For example, consider tables of phase index $(2m\nu-\rho)^2$-mod-$4\nu N$ for select times of $\nu=1$ and $\nu=2$ for an $N=5$ level excitation.

$(2m\nu - \rho)^2 \bmod 4\nu N$ for $N=5$

$\nu=1$	$m=0$	1	2	3	4	5	6
$\rho=0$	$\overline{0}$	4	16	16	4	0	4
1	1	1	9	$\overline{5}$	9	1	1
2	4	$\overline{0}$	4	16	16	4	0
3	9	1	1	9	$\overline{5}$	9	1
4	16	4	$\overline{0}$	4	16	16	4

(A.2a)

$(2m\nu - \rho)^2_{4\nu N}$ for $N=5$

$\nu=2$	$m=0$	1	2	3	4	5	6	7	8	9	10$\cdots$
$\rho=0$	$\overline{0}$	16	24	24	16	0	16	24	24	16	0
1	1	9	9	1	$\overline{25}$	1	9	9	1	25	1
2	4	4	36	$\overline{20}$	36	4	4	36	20		
3	9	1	$\overline{25}$	1	9	9	1				
4	16	$\overline{0}$	16	24	24	16					

(A.2b)

Note that N consecutive values for m give the same sum no matter whether the sum starts at $m=0$ or at a *sum-shift* value $m=\mu$. The idea is to shift the summation index m to $m-\mu$ so that a $(2m\nu-\rho)^2$-mod-$4\nu N$ binomials in row-ρ can be replaced by a simple square $(2m\nu)^2$-mod-$4\nu N$ monomial found in the $\rho=0$ row. This will reduce the exponent to a term independent of site-index ρ plus a Δ-term independent of summation-index m.

It would be nice if the Δ-term were also independent of ρ but the tables show that is asking too much! So, $\Delta = \Delta(\rho, \nu)$ and, each of the rows $\rho = 1, .., N-1$ differ from the $\rho=0$ row by a single *modular difference* $\Delta(\rho, \nu)$ in phase index which is overlined in the table and is the *single underlined number* in each row. For example, subtracting $\Delta(1,1)=5$-mod-$20 = (5)_{20}$ from the $(\rho=1)$ row of the $(\nu=1)$ table and shifting forward by $\mu_1=2$ gives the $(\rho=0)$ row (mod-20) . The shifts needed to line up rows $\rho=1, 2, 3,$ and 4 are $\mu_1=2$, $\mu_2=4$, $\mu_3=6$, and $\mu_4=8$ respectively, that is $\mu_\rho = \mu_1\rho$. These observations are summarized by a modular equation.

$$\left(2\left(m-\mu_\rho\right)\nu - \rho\right)^2 \bmod 4\nu N \equiv \left(2\left(m-\mu_\rho\right)\nu - \rho\right)^2_{4\nu N} = \left(2m\nu\right)^2_{4\nu N} - \Delta\left(\rho, \nu\right) \tag{A.3a}$$

This is supposedly valid for all values of m so for $m=0$ the equation reads

$$\left(-2\mu_\rho v - \rho\right)^2_{4vN} = 0 - \Delta(\rho, v) \ , \tag{A.3b}$$

where $\qquad\qquad\qquad\qquad \mu_\rho = \mu_1\rho \ . \tag{A.3c}$

Subtracting equation (A.3b) from (A.3a) gives the following, again valid for all m.

$$\left(2\left(m-\mu_\rho\right)v-\rho\right)^2_{4vN} - \left(-2\mu_\rho v - \rho\right)^2_{4vN} = \left(2mv\right)^2_{4vN}$$

$$\left(4mv\left(-2\mu_\rho v - \rho\right)\right)_{4vN} = (0)_{4vN} = \kappa 4vN = 0, \ 4vN, \ 8vN, \ldots, 4vN(N-1)$$

Next, set $m=1$, and solve for the m-sum-shift μ_ρ of row ρ.

$$-8\mu_\rho v^2 - 4v\rho = -\kappa 4vN = 0, \ -4vN, \ -8vN, \ldots, -4vN(N-1)$$

$$2\mu_\rho v + \rho = \kappa N = 0, \ N, \ 2N, \ldots, N(N-1) \text{ or: } \mu_\rho = \frac{\kappa N - \rho}{2v} = (\text{integer})_N \tag{A.4a}$$

A value $\kappa=0,1,2,..,N-1$ is selected so that m-sum-shift μ_ρ is an integer $\mu_\rho=0,1,2,..,N-1$, too. Substituting the resulting μ_ρ value in (A.3a) gives the phase modular difference Δ first defined there and in (A.3b).

$$\Delta(\rho, v) = -\left(2v\mu_\rho + \rho\right)^2_{4vN} = -\left(2v\left(\frac{\kappa N - \rho}{2v}\right) + \rho\right)^2_{4vN} = -\left(\kappa N\right)^2_{4vN} \ , \tag{A.4b}$$

where

$$\kappa = \frac{2v\mu_\rho + \rho}{N} \ . \tag{A.4c}$$

Puttiing (A.3a) into the revival wavefunction sum (A.1) gives

$$\psi_0\left(\phi_\rho, t_v\right) = \frac{1}{N}\Sigma^{N-1}_{m=0} \ e^{-i(2mv-\rho)^2\frac{2\pi}{4vN}} e^{i\frac{\rho^2}{4v}\frac{2\pi}{N}}$$

$$= \frac{1}{N}\Sigma^{N-1}_{m=0} \ e^{-i\left[(2mv)^2 - \Delta(\rho,v)\right]\frac{2\pi}{4vN}} e^{i\frac{\rho^2}{4v}\frac{2\pi}{N}} \qquad \left[\text{using:(A.3a)}\right]$$

$$= \frac{1}{N}\Sigma^{N-1}_{m=0} \ e^{-i\left[(2mv)^2 + (\kappa N)^2 - \rho^2\right]\frac{2\pi}{4vN}} \qquad \left[\text{using:(A.4b)}\right]$$

$$= \frac{1}{N}\Sigma^{N-1}_{m=0} \ e^{-i\left[(2mv)^2 + 4\mu_\rho^2 v^2 + 4\mu_\rho v\rho\right]\frac{2\pi}{4vN}} \qquad \left[\text{using:(A.4c)}\right]$$

$$= P(v)e^{\frac{-i\left[\mu_\rho^2 v + \mu_\rho \rho\right]2\pi}{N}} = P(v)e^{\frac{-i\left[\mu_1^2 v + \mu_1\right]\rho^2 2\pi}{N}} \qquad \left[\text{using:(A.3c)}\right] \quad \text{(A.5a)}$$

The overall phase and amplitude prefactor $P(v)$ is a Gaussian sum discussed in Appendix 9B.

$$P(v) = \frac{1}{N}\Sigma^{N-1}_{m=0} \ e^{-i(2mv)^2\frac{2\pi}{4vN}} = \frac{1}{N}\Sigma^{N-1}_{m=0} \ e^{-ivm^2\frac{2\pi}{N}} \tag{A.5b}$$

Finally, the $(\rho=1)$ m-sum-shift μ_1 is the first fraction $(N-1)/2v$, $(2N-1)/2v$, $(3N-1)/2v$, ..., or $(N^2-1)/2v$, to yield an integer according to (A.4a). Recall that it was assumed that N and v are relatively prime, that is, have no common factors. It seems evident that the integer arithmetic behind base-N counter revivals is not trivial, even for the case of odd-N .To complete this particular $N=5$ example we find the sum-shift μ_1 at each revival time $v=1$- 4.

$$\mu_1 = \frac{\kappa N - 1}{2v} \quad \Bigg| \quad \kappa N - 1 = \quad 4 \quad 9 \quad 14 \quad 19 \quad 24$$

$\mu_1 = \frac{\kappa N - 1}{2v}$	$\kappa N - 1 =$	4	9	14	19	24
$2v = 2$		$\bar{2}$	.	7	.	12
$2v = 4$		$\bar{1}$	.	.	.	6
$2v = 6$		.	.	.	.	$\bar{4}$
$2v = 8$		.	.	.	.	$\bar{3}$

(A.6)

From the discussion of Appendix 9B come the overall prefactors $P(v{=}1)=1/\sqrt{5}$, $P(2)=-1/\sqrt{5}$, $P(3)=-1/\sqrt{5}$, and $P(v{=}1)=1/\sqrt{5}$, which are needed to complete the following $N=5$ revival table using (A.5).

$\psi(\rho, v)$	$\rho = 0$	$\rho = 1$	$\rho = 2$	$\rho = 3$	$\rho = 4$
$v = 0$	1	0	0	0	0
$v = 1$	$1/\sqrt{5}$	e_1^*	e_1	e_1	e_1^*
$v = 2$	$-1/\sqrt{5}$	$-e_2$	$-e_2^*$	$-e_2^*$	$-e_2$
$v = 3$	$-1/\sqrt{5}$	$-e_2^*$	$-e_2$	$-e_2$	$-e_2^*$
$v = 4$	$1/\sqrt{5}$	e_1	e_1^*	e_1^*	e_1

where:

$$e_1 = e^{i2\pi/5} / \sqrt{5}$$

$$e_2 = e^{2i2\pi/5} / \sqrt{5}$$

(A.7)

A phasor gauge plot of the $N=5$ revivals (A.7) is shown in Fig. 9.4.3c.

The summation (A.1) for *even-N* is mostly the same as the above. Time index υ is replaced by $\upsilon/2$.

$$\psi_0\left(\phi_\rho, t_v\right) = \frac{1}{N} \Sigma_{m=0}^{N-1} \, e^{-i(mv-\rho)^2 \frac{2\pi}{2vN}} e^{i\frac{\rho^2}{2v}\frac{2\pi}{N}}, \quad \text{where;} \quad t_v = v\frac{2\pi}{2N}, \quad \text{for } N\text{-even.}$$

$$= P(v)e^{\frac{-i\left[\mu_\rho^2 v + 2\mu_\rho \rho\right]2\pi}{2N}} = P(v)e^{\frac{-i\left[\mu_1^2 v + 2\mu_1\right]\rho^2 2\pi}{2N}}$$

(A.8a)

where

$$\mu_1 = \frac{\kappa N - 1}{v} = \text{first integer in } \frac{N-1}{v}, \frac{2N-1}{v}, \frac{3N-1}{v}, \dots$$

(A.8b)

Again the overall phase and amplitude prefactor $P(v)$ is a Gaussian sum discussed in Appendix B.

$$P(v) = \frac{1}{N} \Sigma_{m=0}^{N-1} \, e^{-i(mv)^2 \frac{2\pi}{2vN}} = \frac{1}{N} \Sigma_{m=0}^{N-1} \, e^{-ivm^2 \frac{2\pi}{2N}}$$

(A.8c)

This works for odd-numerator time fractions $1/2N$, $3/2N$, $5/2N$,...$=\upsilon/2N$. For the even numerator ones, we take advantage of the revival sequence $\upsilon/N = 1/N, 2/N, 3/N, \dots$ for N cut in half and shifted by π. If $N/2$ is odd then (A.5) is used. If $N/2$ is even then (A.8) is used again, but with N cut in half to $N/2$. Note that fractions with singly-even denominators have zeros at $\phi=0$ and peaks at $\phi=\pm\pi$. Fractions with odd denominators have peaks at $\phi=0$ and zeros at $\phi=\pm\pi$. Fractions with doubly-even denominators have zeros at $\phi=0$ <u>and</u> $\phi=\pm\pi$.

Appendix 9.B. Overall phase of peaks in a revival lattice

The evaluation of the *N*-term integral Gaussian sum

$$G(v) = \sum_{m=0}^{N-1} e^{-ivm^2 \frac{2\pi}{N}} = NP(v) \tag{B.1}$$

in the prefactor $P(v)=G(v)/N$ given by (A.5b) is, perhaps, the least trivial part of the revival formulation. The develpment involves complex Gaussian integer analysis, a subject which occupied Gauss for more than the first decade of his most productive years. Here we will be content with giving a list of the results for the first few integer combinations that would be relevant for the revivals shown previously.

$N =$	2	3	4	5	6	7	8	9	10	11	12
$\sum_{m=0}^{N-1} e^{-im^2 \frac{2\pi}{N}} =$	0	$-i\sqrt{3}$	$(1-i)\sqrt{4}$	$\sqrt{5}$	0	$-i\sqrt{7}$	$(1-i)\sqrt{8}$	$\sqrt{9}$	0	$-i\sqrt{11}$	$(1-i)\sqrt{12}$
$\sum_{m=0}^{N-1} e^{-i2m^2 \frac{2\pi}{N}} =$	2	$i\sqrt{3}$	0	$-\sqrt{5}$	$-i\sqrt{12}$	$-i\sqrt{7}$	$(1-i)4$	$\sqrt{9}$	$\sqrt{20}$	$i\sqrt{11}$	0
$\sum_{m=0}^{N-1} e^{-i3m^2 \frac{2\pi}{N}} =$	0	3	$(1+i)\sqrt{4}$	$-\sqrt{5}$	0	$i\sqrt{7}$	$-(1+i)\sqrt{8}$	$-i\sqrt{27}$	0	$-i\sqrt{11}$	$(1-i)6$
$\sum_{m=0}^{N-1} e^{-i4m^2 \frac{2\pi}{N}} =$	2	$-i\sqrt{3}$	4	$\sqrt{5}$	$i\sqrt{12}$	$-i\sqrt{7}$	0	$\sqrt{9}$	$-\sqrt{20}$	$-i\sqrt{11}$	$-i\sqrt{48}$
$\sum_{m=0}^{N-1} e^{-i5m^2 \frac{2\pi}{N}} =$	0	$i\sqrt{3}$	$(1-i)\sqrt{4}$	5	0	$i\sqrt{7}$	$-(1-i)\sqrt{8}$	$\sqrt{9}$	0	$-i\sqrt{11}$	$-(1-i)\sqrt{12}$
$\sum_{m=0}^{N-1} e^{-i6m^2 \frac{2\pi}{N}} =$	2	3	0	$\sqrt{5}$	6	$i\sqrt{7}$	$(1+i)4$	$i\sqrt{27}$	$-\sqrt{20}$	$i\sqrt{11}$	0
$\sum_{m=0}^{N-1} e^{-i7m^2 \frac{2\pi}{N}} =$	0	$-i\sqrt{3}$	$(1+i)\sqrt{4}$	$-\sqrt{5}$	0	7	$(1+i)\sqrt{8}$	$\sqrt{9}$	0	$i\sqrt{11}$	$-(1+i)\sqrt{12}$

$$\tag{B.2}$$

Particuarly simple general results are had for the case of doubly-even integer.

$N = 2n$	$4 = 2 \cdot 2$	$8 = 2 \cdot 4$	$12 = 2 \cdot 6$	$16 = 2 \cdot 8$	$20 = 2 \cdot 10$
$\sum_{m=0}^{N-1} e^{-im^2 \frac{2\pi}{N}} =$	$(1-i)$	$(1-i)\sqrt{2}$	$(1-i)\sqrt{3}$	$(1-i)\sqrt{4}$	$(1-i)\sqrt{5}$

$$\tag{B.3}$$

A complex vector diagram of the first few G(u) sums is shown below in Fig. 9B.1.
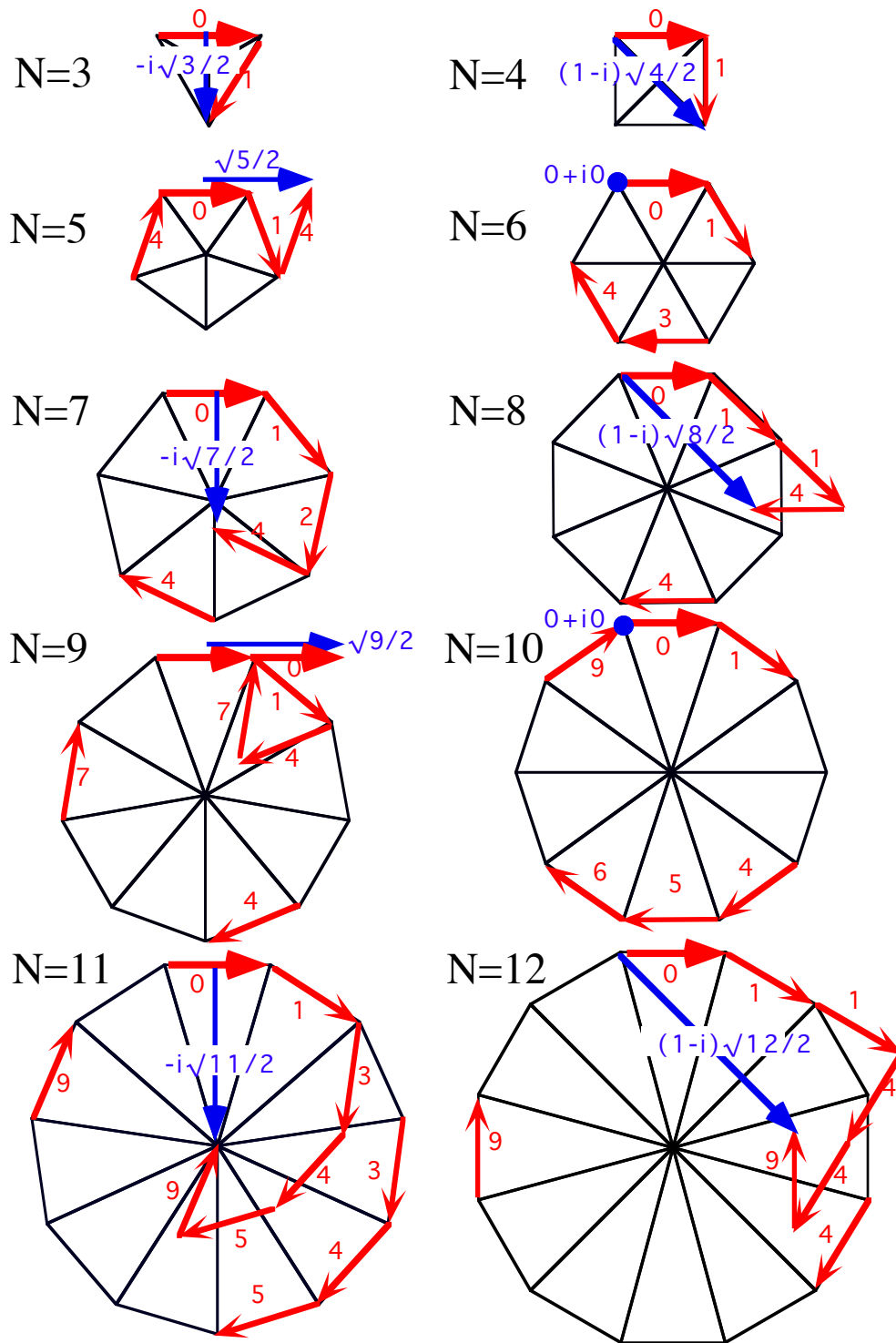
Fig. 9B.1 Sums of modular squares $(m^2)_N = m^2 \bmod N$ (N = 3-12).
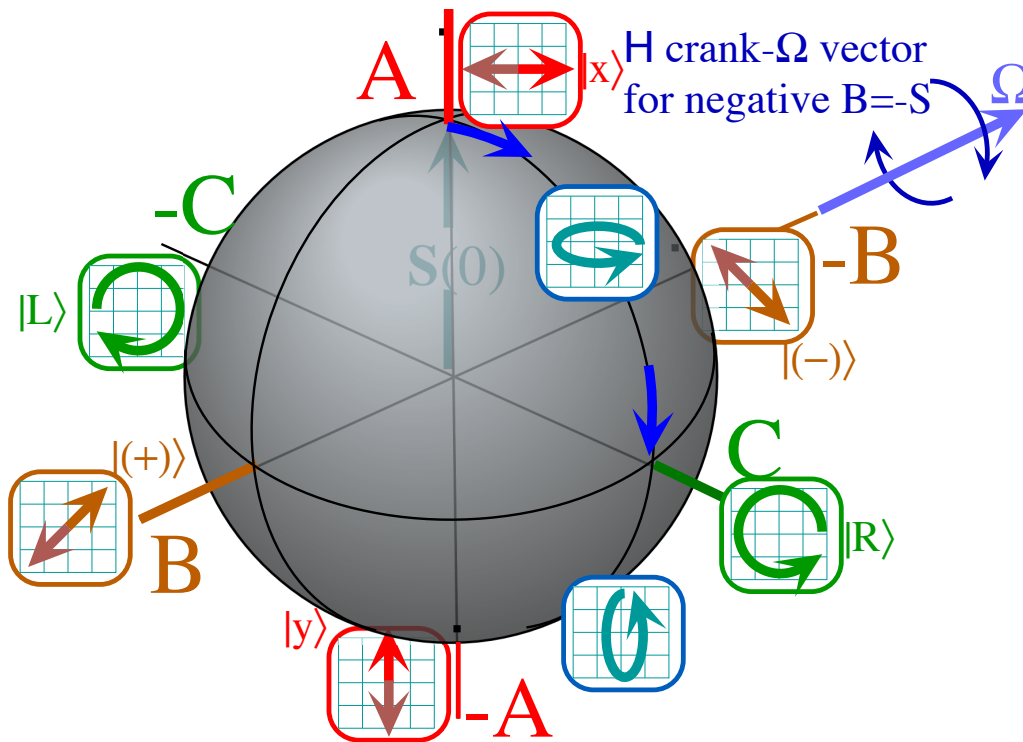
Unit 3 - Chapter 10
Two-State Evolution, Coupled Oscillators, and Spin
W. G. Harter

Schrodinger time evolution is analogous to the motion of coupled oscillators or pendulums. This analogy is valuable for theoretical insight, visualization, and for developing computer simulations. Particularly valuable is the insight into the use of Hamilton-Pauli algebra of reflection-symmetry operators σ_A, σ_B, and σ_C, which are known as *spinor* or *quaternion* operators and generate the U(2) group. Hamiltonians made of the σ_μ apply to many 2-state phenomena including the NH_3 maser, spin resonance, and optical polarization introduced in Chapter 1. We have said that in quantum dynamics, "It takes two to tango." Now we begin to see how the pros do it!

Chapter 10. Two-State Evolution and Analogies

10.1 Mechanical Analogies to Schrodinger Dynamics

The quantum Schrodinger time evolution equations (9.2.5) are similar to the classical Newtonian equations of motion for coupled pendulums. This analogy may help to understand quantum dynamics in this and later chapters. Indeed, for certain constant **H** Hamiltonian operators, the classical and quantum equations are mathematically and dynamically identical. Also, the concept of *spin* will be introduced.

We begin with the simplest non-trivial quantum systems having just two-states (*N=2*) such as optical polarization and electron spin-polarization introduced in Chapter 1. This *U(2)* system is such an experimentally important system that we will devote several units to its technology. This chapter will provide an introduction to *U(2)* systems and their symmetry by using classical mechanical analogies.

The simplest non-trivial quantum system is the *two-level atom* or a spin-1/2 particle. The Schrodinger equation (9.2.5) for these systems has the general form:

$$i\hbar \frac{\partial}{\partial t}\big|\Psi(t)\big\rangle = \mathbf{H}\big|\Psi(t)\big\rangle \tag{10.1.1a}$$

where **H** is a two-by-two Hermitian *(**H**†=**H**)* matrix operator

$$\mathbf{H} = \begin{pmatrix} A & B-iC \\ B+iC & D \end{pmatrix}. \tag{10.1.1b}$$

and ket $\big|\Psi\big\rangle$ is a two-dimensional complex *phasor vector x_j+ip_j*

$$\big|\Psi\big\rangle = \begin{pmatrix} \Psi_1 \\ \Psi_2 \end{pmatrix} = \begin{pmatrix} x_1+ip_1 \\ x_2+ip_2 \end{pmatrix}. \tag{10.1.1c}$$

Separating real x_j and imaginary p_j parts of the amplitudes (10.1.1c) lets us convert the complex Schrodinger equation (10.1.1a) into twice as many real differential equations. The results are as follows.

$$\begin{aligned} \dot{x}_1 &= Ap_1 + Bp_2 - Cx_2 \\ \dot{x}_2 &= Bp_1 + Dp_2 + Cx_1 \end{aligned} \tag{10.1.2a} \qquad \begin{aligned} \dot{p}_1 &= -Ax_1 - Bx_2 - Cp_2 \\ \dot{p}_2 &= -Bx_1 - Dx_2 + Cp_1 \end{aligned} \tag{10.1.2b}$$

The same equations arise from the following <u>classical</u> coupled oscillator Hamiltonian in which x_j and p_j are canonical coordinates and momenta, respectively.

$$H_c = \frac{A}{2}\big(p_1^2 + x_1^2\big) + B\big(x_1x_2 + p_1p_2\big) + C\big(x_1p_2 - x_2p_1\big) + \frac{D}{2}\big(p_2^2 + x_2^2\big) \tag{10.1.3a}$$

Hamilton's classical canonical equations of motion are the following:

$$\begin{aligned} \dot{x}_1 &= \frac{\partial H_c}{\partial p_1} = Ap_1 + Bp_2 - Cx_2 \\ \dot{x}_2 &= \frac{\partial H_c}{\partial p_1} = Bp_1 + Dp_2 + Cx_1 \end{aligned} \tag{10.1.3b} \qquad \begin{aligned} \dot{p}_1 &= -\frac{\partial H_c}{\partial x_1} = -\big(Ax_1 + Bx_2 + Cp_2\big) \\ \dot{p}_2 &= -\frac{\partial H_c}{\partial x_2} = -\big(Bx_1 + Dx_2 - Cp_1\big) \end{aligned} \tag{10.1.3c}$$

Note that these are identical to Schrodinger's equations (10.1.2).

To see a connection with conventional second order coupled oscillator equations, we differentiate the $\dot{x}_j$ equations (10.1.3b) and substitute the $\dot{p}_j$ expressions (10.1.3c). (Note: Canonical momentum here is <u>not</u> the usual $p_j = m\dot{x}_j$. See exercises at the end of the chapter.)

$$\ddot{x}_1 = A\dot{p}_1 + B\dot{p}_2 - C\ddot{x}_2$$

$$= -A\left(Ax_1 + Bx_2 + Cp_2\right) - B\left(Bx_1 + Dx_2 - Cp_1\right) - C\left(Bp_1 + Dp_2 + Cx_1\right)$$

$$= -\left(A^2 + B^2 + C^2\right)x_1 - \left(AB + BD\right)x_2 \qquad -\left(A + D\right)Cp_2 \qquad (10.1.4a)$$

$$\ddot{x}_2 = B\dot{p}_1 + D\dot{p}_2 + C\dot{x}_1$$

$$= -B\left(Ax_1 + Bx_2 + Cp_2\right) - D\left(Bx_1 + Dx_2 - Cp_1\right) + C\left(Ap_1 + Bp_2 - Cx_2\right)$$

$$= -\left(AB + BD\right)x_1 - \left(B^2 + D^2 + C^2\right)x_2 \qquad +\left(A + D\right)Cp_1 \qquad (10.1.4b)$$

If the complex parameter C is zero this reduces to classical coupled oscillator equations

$$-\ddot{x}_1 = K_{11}x_1 + K_{12}x_2 \ , \qquad (10.1.5a) \qquad -\ddot{x}_2 = K_{21}x_1 + K_{22}x_2 , \qquad (10.1.5b)$$

where the force or *acceleration* or *spring matrix K_{ij}* depends on masses and spring constants in Fig. 10.1.1a and is related as follows to the Schrodinger **H** -matrix parameters A, B, and D.

$$m_1 K_{11} = A^2 + B^2 = k_1 + k_{12}, \qquad\qquad m_1 K_{12} = AB + BD = -k_{12}, \qquad (10.1.5c)$$

$$m_2 K_{21} = AB + BD = -k_{12}, \qquad\qquad m_2 K_{22} = B^2 + D^2 = k_2 + k_{12} . \qquad (10.1.5d)$$
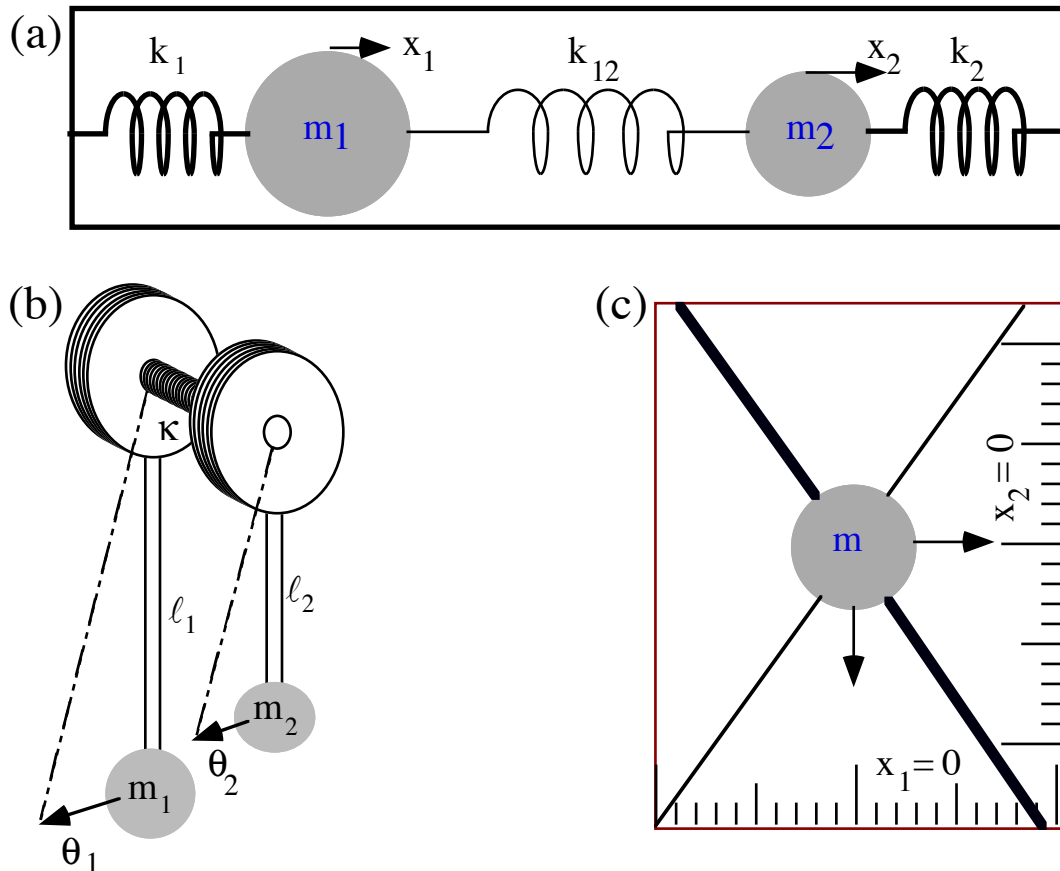
Fig.10.1.1 Classical analogs for spatially asymmetric U(2) quantum system.

Fig. 10.1.1 shows (a) two masses , (b) two pendulums, and (c) a single mass m hung by diagonal springs. Each has an isotropic kinetic energy T (m is divided out) and an anisotropic potential V.

$$T = \frac{1}{2}\dot{x}_1^2 + \frac{1}{2}\dot{x}_2^2 = \frac{1}{2}\dot{\mathbf{x}} \bullet \dot{\mathbf{x}}$$

$$V = \frac{1}{2}K_{11}x_1^2 + \frac{1}{2}(K_{12} + K_{21})x_1x_2 + \frac{1}{2}K_{22}x_2^2 = \frac{1}{2}\mathbf{x} \bullet \mathbf{K} \bullet \mathbf{x}$$

$$(10.1.6a) \qquad\qquad\qquad\qquad\qquad\qquad\qquad (10.1.6b)$$

Constant-V curves (equipotentials) are ellipses as shown in Fig. 10.1.2 below. The parameters A, B, and D in the **K**-matrix (10.1.5) or **H**-matrix (10.1.1b) determine the shape of the ellipses and inclination of their major axes which correspond to different **K**-matrix eigenvalues and eigenvectors, that is, different frequencies and normal modes in the classical models and different energy states in the original quantum *U(2)* model. We now study different cases and see how they correspond to different *symmetries*.
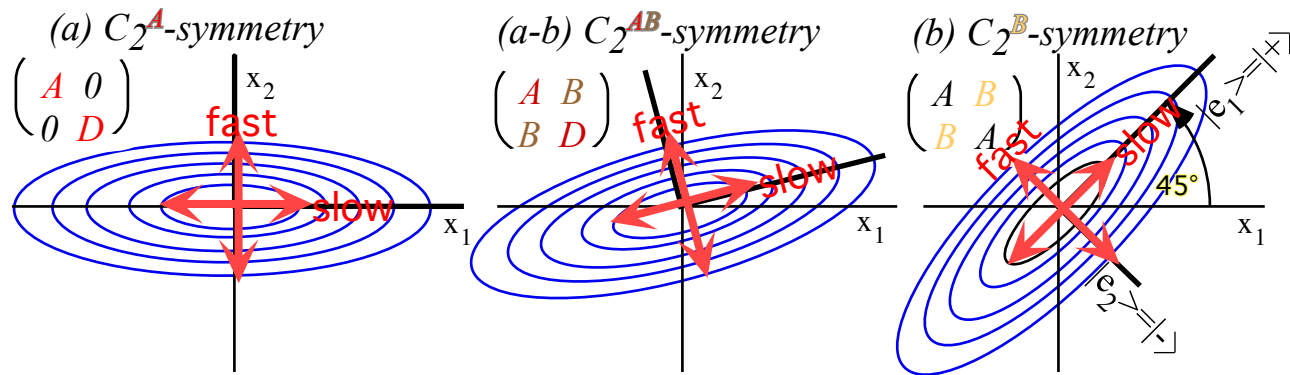
Fig. 10.1.2 Potentials for (a) $C_2{}^A$-asymmetric-diagonal, (ab) $C_2{}^{AB}$-mixed , (b) $C_2{}^B$-bilateral U(2)system.

(a). ABCD Symmetry operator analysis

Following the lead of Chapters 8 and 9, we decompose the Hamiltonian (10.1.1b) into four *ABCD symmetry operators* that are so labeled to provide helpful mnemonics in sections following.

$$\begin{pmatrix} A & B-iC \\ B+iC & D \end{pmatrix} = A\begin{pmatrix} 1 & 0 \\ 0 & 0 \end{pmatrix} + B\begin{pmatrix} 0 & 1 \\ 1 & 0 \end{pmatrix} + C\begin{pmatrix} 0 & -i \\ i & 0 \end{pmatrix} + D\begin{pmatrix} 0 & 0 \\ 0 & 1 \end{pmatrix} = A\mathbf{e}_{11} + B\boldsymbol{\sigma}_B + C\boldsymbol{\sigma}_C + D\mathbf{e}_{22}$$

$$= \frac{A+D}{2}\begin{pmatrix} 1 & 0 \\ 0 & 1 \end{pmatrix} + B\begin{pmatrix} 0 & 1 \\ 1 & 0 \end{pmatrix} + C\begin{pmatrix} 0 & -i \\ i & 0 \end{pmatrix} + \frac{A-D}{2}\begin{pmatrix} 1 & 0 \\ 0 & -1 \end{pmatrix} \quad (10.1.7)$$

$$\mathbf{H} = \frac{A+D}{2}\quad \boldsymbol{\sigma}_1 \;+ B\quad \boldsymbol{\sigma}_B \;+ C\quad \boldsymbol{\sigma}_C \;+ \frac{A-D}{2}\; \boldsymbol{\sigma}_A$$

The $\{\sigma_1, \sigma_A, \sigma_B, \sigma_C\}$ are best known as *Pauli-spin operators* $\{\sigma_1 = \sigma_0, \sigma_B = \sigma_X, \sigma_C = \sigma_Y, \sigma_A = \sigma_Z\}$ but they (or ones quite like them) were discovered almost a century earlier by Hamilton. (He carved them into a bridge in Dublin in 1843.) Hamilton was looking for a consistent generalization of complex numbers to 3-dimensional space. One day he hit upon the idea of a four-dimensional set of operators which he labeled $\{\mathbf{1}, \mathbf{i}, \mathbf{j}, \mathbf{k}\}$. Hamilton's *quaternions* are related as follows to the *ABCD* or *ZXY0* operators.

$$\{\sigma_1 = \mathbf{1} = \sigma_0, \, i\sigma_B = \mathbf{i} = i\sigma_X, \, i\sigma_C = \mathbf{j} = i\sigma_Y, \, i\sigma_A = \mathbf{k} = i\sigma_Z\} \qquad (10.1.8)$$

Note: $\mathbf{i}^2 = \mathbf{j}^2 = \mathbf{k}^2 = -\mathbf{1}$. They square to *negative*-**1** like imaginary number $i^2 = -1$. Pauli's form removes the imaginary i so the σ_μ all square to *positive* **1** ($\sigma_X^2 = \sigma_Y^2 = \sigma_Z^2 = +\mathbf{1}$) and each belongs to a C_2 group. Note that

our first operator σ_A (or Pauli's third σ_Z) is a difference $\sigma_A = e_{11} - e_{22}$ of elementary operators e_{11} and e_{22}. σ_A is a group operator but e_{kk} are not since they are projectors and do not have inverses.

Now each C_2 group $C_2{}^A = \{1, \sigma_A\}$, $C_2{}^B = \{1, \sigma_B\}$, and $C_2{}^C = \{1, \sigma_C\}$ is considered in turn. They are labeled *A (asymmetric-diagonal)*, *B (bilateral balanced beat)*, and *C (circular)* symmetry for reasons that will become clear. Each of them represents a different physical archetype and a different kind of dynamics. Mnemonic alliteration is used for pedagogical enhancement, particularly the *C (circular)* symmetry for which the following *C*-adjectives apply: *complex, circular, chiral, cyclotron, Coriolis, centrifugal, curly, and circulating-current.*

The last symmetry adjective explains its important distinction and the coloring scheme used in formulae and illustrations. The *A* and *B* designations are colored the yellow, orange or red color of traffic signals for **CAUTION**, or **STOP** since these symmetries refer to real-*standing* waves. The green or blue-green **GO** signal color applies to the *C (current-like)* symmetry of imaginary or complex *moving* or *galloping* waves.

10.2 The ABCD's of 2-State Dynamics

Operators σ_A, σ_B, any σ_C within each C_2 group $C_2^A=\{1,\sigma_A\}$, $C_2^B=\{1,\sigma_B\}$, and $C_2^C=\{1,\sigma_C\}$ do not commute with each other. Therefore they are first considered separately as is done in the following sections labeled, appropriately, (a), (b), and (c). Then follows a discussion of how they intermix.

(a) Asymmetric-Diagonal or C₂ᴬ symmetry

The first case involves an **H**-matrix that is *asymmetric-diagonal*, that is ($B=0=C$) and ($A<D$)

$$\mathbf{H} = \begin{pmatrix} A & 0 \\ 0 & D \end{pmatrix}, \quad \text{or:} \quad \mathbf{K} = \begin{pmatrix} A^2 & 0 \\ 0 & D^2 \end{pmatrix}. \qquad (10.2.1a)$$

The **A**-matrix gives *uncoupled* oscillators in (10.1.5) or a single mass in a diagonal potential (10.1.6).

$$V = \frac{1}{2}K_{11}x_1^2 + \frac{1}{2}K_{22}x_2^2 \quad \text{where: } K_{11} = A^2 = \frac{k_1}{m}, \text{ and: } K_{22} = D^2 = \frac{k_2}{m} \qquad (10.2.1b)$$

Such an elliptical potential is plotted in Fig. 10.1.2a. Here cross coupling is zero ($k_{12}=0$), so each mass or pendulum in Fig. 10.1.1a-b is disconnected and independent of the other one. Motion that is purely along one of the Cartesian axes in Fig. 10.1.2a, say purely along the *x* or x_1-axis, or else purely along the *y* or x_2-axis, will be simple harmonic motion whose frequency is a "slow" $A=\sqrt{(k_1/m)}$ or else a "fast" $D=\sqrt{(k_2/m)}$, respectively. This is because the force or gradient for any mass on the *x* -axis is also along the *x* or x_1-axis driving it directly back to the origin. The same holds for the x_2-axis but the force constant k_2 is presumed stronger than k_1 making the x_2-axis gradient steeper so x_2-axial motion is faster than x_1-axial motion.

Arrows in Fig. 10.1.2a indicate elementary normal modes of the uncoupled *x*-and *y*-dimensions. The modes are plotted (using the program *Color U(2)*) as separate functions of time in Fig. 10.2.1a and b.
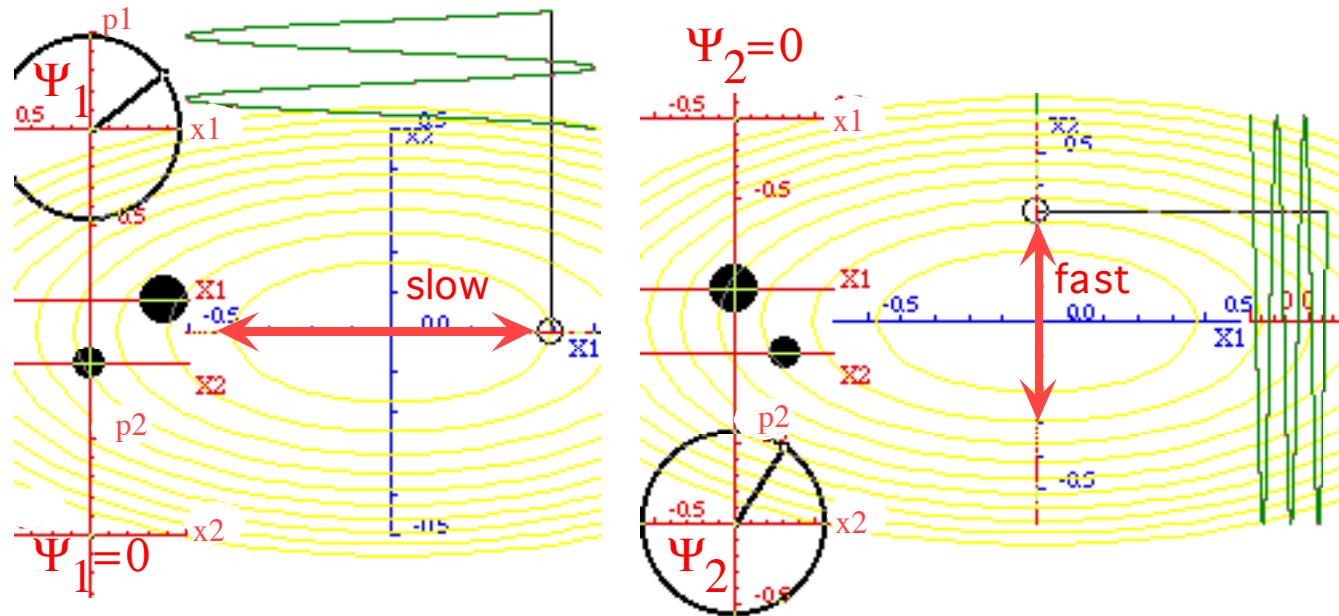
Fig. 10.2.1 Pure normal modes for C_2^A-asymmetric-diagonal potential (a) Slow x-mode (b) Fast y-mode

By setting both the *x*-and-*y*-modes in motion at once we get a plot like the one shown below in Fig. 10.2.2. In this *mixed mode* the two motions go about their business as though the companion oscillator was not even present. Note that the *x* vs. *y* plot of coordinates $x_1=\text{Re}\Psi_1$ and $x_2=\text{Re}\Psi_2$ shows the beginning of a

Lissajous pattern caused by the unequal frequencies of the Ψ_1 and Ψ_2 phasors, but the phasors themselves are each unfazed, so to speak, by the motion of their companion. The *x vs. y* trajectory curves due to the potential gradient whose direction varies continuously for points not following *x* or *y* axes.
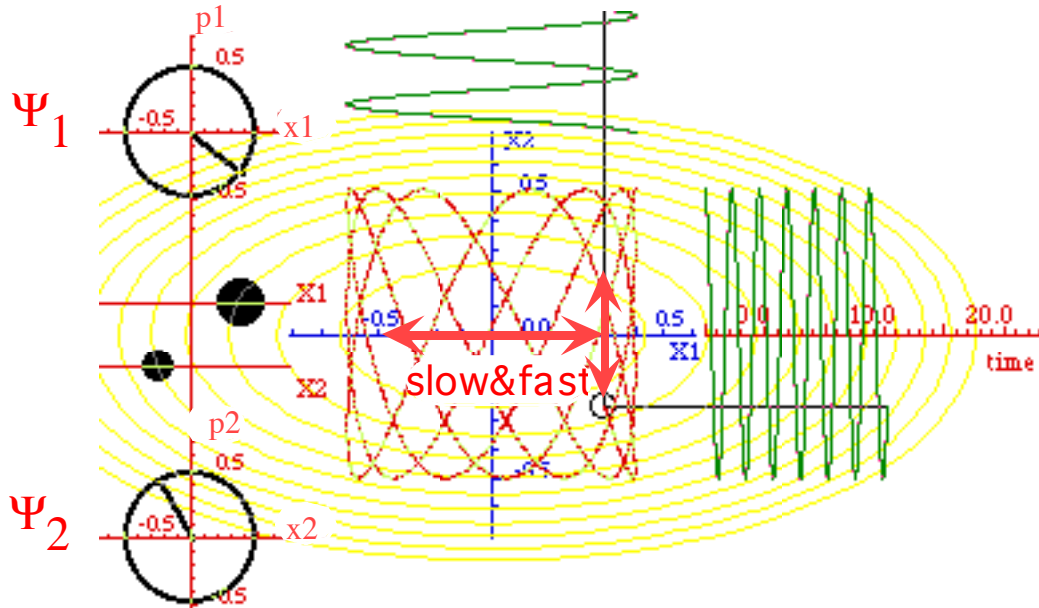
Fig. 10.2.2 Mixed modes for $C_2{}^A$-asymmetric-diagonal potential

　　　　This **H**-matrix Hamiltonian or **K**-matrix potential in Fig. 10.2.2 above has a most elementary example of symmetry, namely *axial-reflection symmetry $C_2{}^A$* or *Cartesian mirror-plane symmetry*. The potential ellipse is invariant to reflecting the *y* or x_2-axis ($x_2 \rightarrow -x_2$). We define an *x*-plane-reflection operator σ_A accordingly to reflect the *y*-base ket $|2\rangle$ but leave the *x*-base ket $|1\rangle$ alone.

$$\sigma_A |1\rangle = |1\rangle \quad , \qquad \sigma_A |2\rangle = -|2\rangle \qquad\qquad (10.2.2a)$$

Operator σ_A and unit operator **1** make the following $C_2{}^A$ group multiplication table and representation.

$$\begin{array}{c|c:c} C_2 & \mathbf{1} & \sigma_A \\ \hline \mathbf{1} & \mathbf{1} & \sigma_A \\ \hdashline \sigma_A & \sigma_A & \mathbf{1} \end{array} \quad \begin{pmatrix} \langle 1|\mathbf{1}|1\rangle & \langle 1|\mathbf{1}|2\rangle \\ \langle 2|\mathbf{1}|1\rangle & \langle 2|\mathbf{1}|2\rangle \end{pmatrix} = \begin{pmatrix} 1 & 0 \\ 0 & 1 \end{pmatrix}, \quad \begin{pmatrix} \langle 1|\sigma_A|1\rangle & \langle 1|\sigma_A|2\rangle \\ \langle 2|\sigma_A|1\rangle & \langle 2|\sigma_A|2\rangle \end{pmatrix} = \begin{pmatrix} 1 & 0 \\ 0 & -1 \end{pmatrix} \quad (10.2.2b)$$

And, as required of symmetry **g**-operators ($\mathbf{H}=\mathbf{gHg}^\dagger$ or $\mathbf{gH}=\mathbf{Hg}$), σ_A must commute with **H** and **K**.

$$\sigma_A \mathbf{H} = \mathbf{H}\sigma_A, \text{ or}: \begin{pmatrix} 1 & 0 \\ 0 & -1 \end{pmatrix}\begin{pmatrix} A & 0 \\ 0 & D \end{pmatrix} = \begin{pmatrix} A & 0 \\ 0 & D \end{pmatrix}\begin{pmatrix} 1 & 0 \\ 0 & -1 \end{pmatrix} \qquad (10.2.2c)$$

So, also, must the negative $-\sigma_A$ operator which is a *y*-plane-reflection operator σ_{-A} defined as follows to reflect the *x*-base ket $|1\rangle$ but leave the *y*-base ket $|2\rangle$ alone.

$$-\sigma_A |1\rangle = -|1\rangle \quad , \qquad -\sigma_A |2\rangle = |2\rangle \qquad\qquad (10.2.2d)$$

Operator $-\sigma_A$ and the unit operator **1** make a similar $C_2{}^A$ group multiplication table and representation.

$$\begin{array}{c|c:c} C_2 & \mathbf{1} & -\sigma_A \\ \hline \mathbf{1} & \mathbf{1} & -\sigma_A \\ \hdashline -\sigma_A & -\sigma_A & \mathbf{1} \end{array} \quad \begin{pmatrix} \langle 1|-\sigma_A|1\rangle & \langle 1|-\sigma_A|2\rangle \\ \langle 2|-\sigma_A|1\rangle & \langle 2|-\sigma_A|2\rangle \end{pmatrix} = \begin{pmatrix} -1 & 0 \\ 0 & 1 \end{pmatrix} \qquad (10.2.2e)$$

Furthermore, the product of the two reflection operators is a symmetry, too, since if two operators commute with **H** then so do their group products. The product $(-\sigma_A)(\sigma_A)$ is a *180° rotation matrix* **R**.

$$-\sigma_A\sigma_A = \begin{pmatrix} 1 & 0 \\ 0 & -1 \end{pmatrix}\begin{pmatrix} -1 & 0 \\ 0 & 1 \end{pmatrix} = \begin{pmatrix} -1 & 0 \\ 0 & -1 \end{pmatrix} = \mathbf{R}\left(180°\right) \qquad (10.2.2f)$$

Together, all four operators $\{\mathbf{1},\sigma_A,-\sigma_A,\mathbf{R}\}$ form a famous group called the *four-group $D^A{}_2$* or $C^A{}_{2v}$ with the group multiplication table shown below. It is like the group D_2 in (8.3.5) and will be used later.

C_{2v}	$\mathbf{1}$	σ_A	$-\sigma_A$	$\mathbf{R}$
$\mathbf{1}$	$\mathbf{1}$	σ_A	$-\sigma_A$	$\mathbf{R}$
σ_A	σ_A	$\mathbf{1}$	$\mathbf{R}$	$-\sigma_A$
$-\sigma_A$	$-\sigma_A$	$\mathbf{R}$	$\mathbf{1}$	σ_A
$\mathbf{R}$	$\mathbf{R}$	$-\sigma_A$	σ_A	$\mathbf{1}$

$$(10.2.2g)$$

Here, σ_A and $\mathbf{1}$ are sufficient to describe the **H**-matrix which, as in Sec. 9.3 (Recall especially (9.3.5).), is a linear combination of its own symmetry operators. This is the *A*-case of expansion (10.1.7).

$$\begin{pmatrix} A & 0 \\ 0 & D \end{pmatrix} = \frac{A+D}{2}\begin{pmatrix} 1 & 0 \\ 0 & 1 \end{pmatrix} + \frac{A-D}{2}\begin{pmatrix} 1 & 0 \\ 0 & -1 \end{pmatrix}, \text{ or}: \mathbf{H} = \frac{A+D}{2}\mathbf{1} + \frac{A-D}{2}\sigma_A \quad (10.2.2h)$$

(b) Bilateral or $C_2{}^B$ symmetry

The next case-*B* involves identical *coupled* oscillators such are shown in Fig. 10.2.3 below. These have a symmetry called *bilateral* or $C_2{}^B$ *symmetry*. We should be very familiar with this symmetry since it is the only one that our human bodies approximate. A *diagonal-reflection* operator σ_B is defined which simply reflects left and right sides of Fig. 10.2.3a-b or trades the x or x_1-axis with the y or x_2-axis.

In terms of base kets we define such a reflection as follows.

$$\sigma_B\,|1\rangle = |2\rangle\ ,\qquad \sigma_B\,|2\rangle = |1\rangle \qquad\qquad (10.2.3a)$$

Operator σ_B and the unit operator $\mathbf{1}$ make a $C_2{}^B$ group multiplication table and representation.

C_2	$\mathbf{1}$	σ_B
$\mathbf{1}$	$\mathbf{1}$	σ_B
σ_B	σ_B	$\mathbf{1}$

$$\begin{pmatrix} \langle1|\mathbf{1}|1\rangle & \langle1|\mathbf{1}|2\rangle \\ \langle2|\mathbf{1}|1\rangle & \langle2|\mathbf{1}|2\rangle \end{pmatrix} = \begin{pmatrix} 1 & 0 \\ 0 & 1 \end{pmatrix},\quad \begin{pmatrix} \langle1|\sigma_B|1\rangle & \langle1|\sigma_B|2\rangle \\ \langle2|\sigma_B|1\rangle & \langle2|\sigma_B|2\rangle \end{pmatrix} = \begin{pmatrix} 0 & 1 \\ 1 & 0 \end{pmatrix} \quad (10.2.3b)$$

The Hamiltonian matrix **H** in (10.1.1b) must be invariant to σ_B operator if **H** is to have $C_2{}^B$ symmetry.

$$\mathbf{H} = \sigma_B\,\mathbf{H}\,\sigma_B{}^\dagger = \sigma_B\,\mathbf{H}\,\sigma_B \qquad\qquad (10.2.4a)$$

Stated another way: **H** must commute with σ_B . $\mathbf{H}\,\sigma_B{}^\dagger = \sigma_B\,\mathbf{H}$

$$\begin{pmatrix} \langle1|\mathbf{H}|1\rangle & \langle1|\mathbf{H}|2\rangle \\ \langle2|\mathbf{H}|1\rangle & \langle2|\mathbf{H}|2\rangle \end{pmatrix}\begin{pmatrix} 0 & 1 \\ 1 & 0 \end{pmatrix} = \begin{pmatrix} 0 & 1 \\ 1 & 0 \end{pmatrix}\begin{pmatrix} \langle1|\mathbf{H}|1\rangle & \langle1|\mathbf{H}|2\rangle \\ \langle2|\mathbf{H}|1\rangle & \langle2|\mathbf{H}|2\rangle \end{pmatrix} \text{ or } \begin{pmatrix} \langle1|\mathbf{H}|2\rangle & \langle1|\mathbf{H}|1\rangle \\ \langle2|\mathbf{H}|2\rangle & \langle2|\mathbf{H}|1\rangle \end{pmatrix} = \begin{pmatrix} \langle2|\mathbf{H}|1\rangle & \langle2|\mathbf{H}|2\rangle \\ \langle1|\mathbf{H}|1\rangle & \langle1|\mathbf{H}|2\rangle \end{pmatrix}$$

The last result demands equality of the following **H**-matrix component pairs.

$$\langle1|\,\mathbf{H}\,|1\rangle = \langle2|\,\mathbf{H}\,|2\rangle \qquad (10.2.4b),\qquad\qquad \langle1|\,\mathbf{H}\,|2\rangle = \langle2|\,\mathbf{H}\,|1\rangle \qquad (10.2.4c)$$

This reduces the number of free parameters in the **H**-matrix (10.1.1) and **A**-matrix components (10.1.5b-c).

$$A = D\ ,\qquad\qquad B - iC = B + iC \qquad\qquad (10.2.4b)$$

$$\begin{pmatrix} \langle 1|\mathbf{H}|1\rangle & \langle 1|\mathbf{H}|2\rangle \\ \langle 2|\mathbf{H}|1\rangle & \langle 2|\mathbf{H}|2\rangle \end{pmatrix} = \begin{pmatrix} A & B \\ B & A \end{pmatrix} \quad \text{or:} \quad \begin{pmatrix} \langle 1|\mathbf{K}|1\rangle & \langle 1|\mathbf{K}|2\rangle \\ \langle 2|\mathbf{K}|1\rangle & \langle 2|\mathbf{K}|2\rangle \end{pmatrix} = \begin{pmatrix} A^2+B^2 & 2AB \\ 2AB & A^2+B^2 \end{pmatrix} \quad (10.2.4c)$$

The complex parameter C must be zero to have $C_2{}^B$ symmetry. (We also needed $C=0$ to get (10.1.5a) but the extra symmetry $A=D$ was not required there. Now we demand $A=D$, as well.)

(b)   (c)
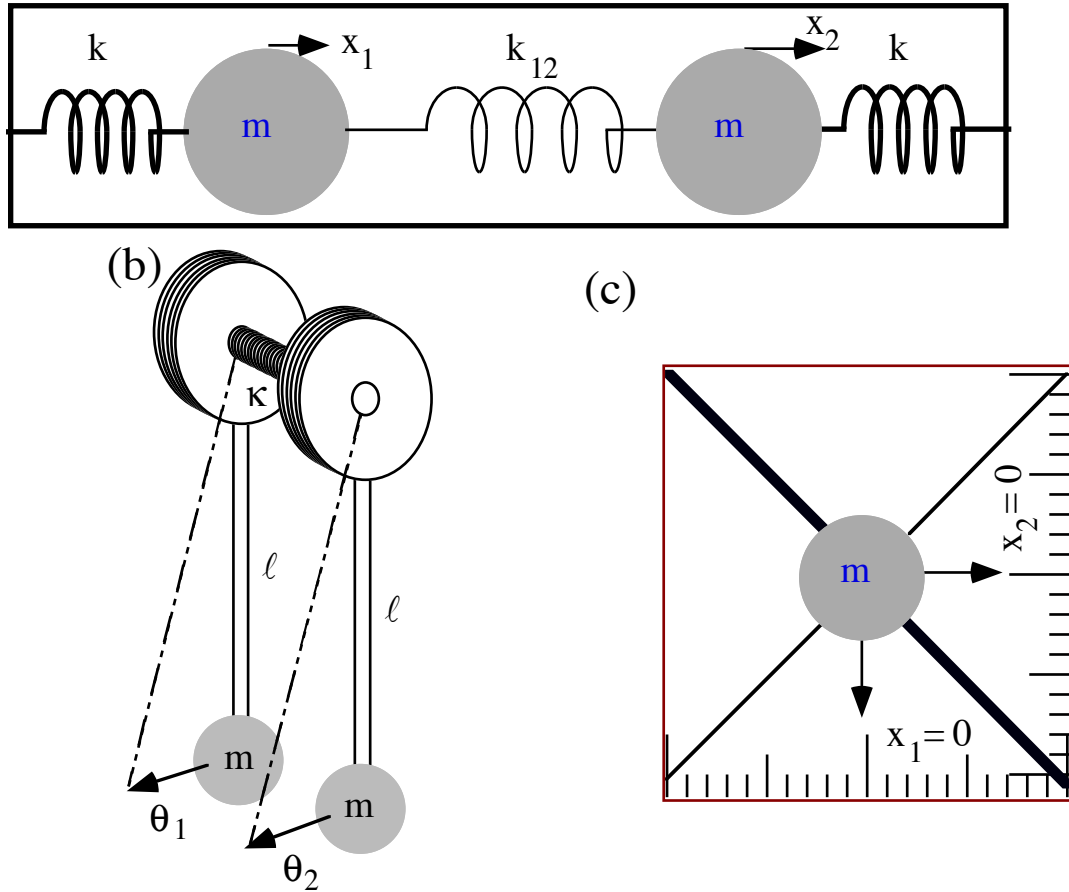
Fig. 10.2.3 Classical analogs for C_2-symmetric U(2) quantum system.

$C_2{}^B$ *projectors and eigenstates: Normal modes*

      The $C_2{}^B$ projectors follow from the minimal equation for $C_2{}^B$ operator σ_B that is simply

$$\sigma_B{}^2 = \mathbf{1} \quad, \text{ or } \quad \sigma_B{}^2 - \mathbf{1} = \mathbf{0} = (\sigma_B - \mathbf{1}) \cdot (\sigma_B + \mathbf{1})$$

We put the roots $\{\varepsilon_+ = 1,\ \varepsilon_- = -1\}$ in the general projection formula (3.1.15a) which is repeated below.

$$\mathbf{P}_k = \frac{\prod\limits_{j \neq k} \left(\mathbf{M} - \varepsilon_j \mathbf{1}\right)}{\prod\limits_{j \neq k} \left(\varepsilon_k - \varepsilon_j\right)} \quad, \qquad\qquad (3.1.15a)_{repeated}$$

With $\mathbf{M} = \sigma_B$ this gives two normalized *symmetric* (+) and *anti-symmetric* (-) projectors

$$\mathbf{P}^{(+)} = (\mathbf{1} + \sigma_B)/2 \ , \quad \mathbf{P}^{(-)} = (\mathbf{1} - \sigma_B)/2 \ , \qquad\qquad (10.2.5)$$

giving two normalized eigenstates of σ_B and the $C_2{}^B$-symmetric **H** and **K** operators in (10.2.4c)

$$|+\rangle = \mathbf{P}^{(+)}|1\rangle \sqrt{2} = (|1\rangle + |2\rangle)/\sqrt{2} \ , \qquad |-\rangle = \mathbf{P}^{(-)}|1\rangle \sqrt{2} = (|1\rangle - |2\rangle)/\sqrt{2} \ , \qquad (10.2.6a)$$

This yields a σ_B- or **H**-diagonalizing transformation (d-tran).

$$\begin{pmatrix} \langle 1|+\rangle & \langle 1|-\rangle \\ \langle 2|+\rangle & \langle 2|-\rangle \end{pmatrix} = \begin{pmatrix} 1/\sqrt{2} & 1/\sqrt{2} \\ 1/\sqrt{2} & -1/\sqrt{2} \end{pmatrix} . \qquad (10.2.6b)$$

This $C_2{}^B$-d-tran is actually a rare example of a d-tran matrix that is Hermitian ($\mathbf{T}^\dagger = \mathbf{T}$) as well as unitary ($\mathbf{T}^\dagger = \mathbf{T}^{-1}$). More about this later. The columns are eigenvectors of any matrix that commutes with $C_2{}^B$-operator σ_B. This includes the **H**-matrix (10.2.4c) that is diagonalized as follows.

$$\begin{pmatrix} \langle +|1\rangle & \langle +|2\rangle \\ \langle -|1\rangle & \langle -|2\rangle \end{pmatrix} \begin{pmatrix} A & B \\ B & A \end{pmatrix} \begin{pmatrix} \langle 1|+\rangle & \langle 1|-\rangle \\ \langle 2|+\rangle & \langle 2|-\rangle \end{pmatrix} = \begin{pmatrix} A+B & 0 \\ 0 & A-B \end{pmatrix} \qquad (10.2.6c)$$

The **H** eigenvalues are

$$\langle +|\mathbf{H}|+\rangle = A+B, \qquad \langle -|\mathbf{H}|-\rangle = A\text{-}B. \qquad (10.2.7a)$$

The **K** eigenvalues are

$$\langle +|\, \mathbf{K}\, |+\rangle = A^2+2AB+A^2 = (A+B)^2, \qquad \langle -|\, \mathbf{K}\, |-\rangle = A^2-2AB+A^2 = (A-B)^2. \qquad (10.2.7b)$$

The physical meaning of eigenvalues is different for quantum mechanics than for the classical analogies. For quantum mechanics, **H** eigenvalues are eigenstate energies or $\hbar$ times eigenfrequencies.

$$\varepsilon^+ = \hbar\omega^+ = A+B, \qquad\qquad \varepsilon^- = \hbar\omega^- = A\text{-}B. \qquad (10.2.8)$$

Classical **K**-eigenvalues are <u>squares</u> of *normal mode frequencies*. (Classical energy is $m\omega^2/2$.)

$$\omega^2{}_{(+)\text{mode}} = (A+B)^2 = k/m, \qquad\qquad \omega^2{}_{(-)\text{mode}} = (A-B)^2 = (k+2k_{12})/m. \quad (10.2.9)$$

Understanding $C_2{}^B$ eigenstates: Tunneling splitting

$C_2{}^B$ eigenstates (10.2.6a) point at $\pm 45°$ angle to the base states $|1\rangle$ and $|2\rangle$ as shown in Fig. 10.1.2c and in Fig. 10.2.4 below. Why exactly $\pm 45°$? It's because the $\pm 45°$ directions are the $\pm\sigma_B$ mirror planes halfway between coordinate axes $|1\rangle$ and $|2\rangle$ that are $C_2{}^B$-equivalent or "indistinguishable."

The $^+45°$ mode $|+\rangle$ corresponds to two masses moving perfectly in phase with each other as in Fig. 10.2.4a. It is the $(0)_2$ "wave" in the C_2 table in Fig. 9.4.1a. The $^-45°$ mode $|-\rangle$ corresponds to two masses moving π out of phase with each other as in Fig. 10.2.4b, or a $(1)_2$ wave in the C_2 table.

The $^-45°$ mode has a higher frequency than the $^+45°$ mode since it stretches the connecting k_{12} spring. The $^+45°$ mode would behave the same if the k_{12} spring was gone. The $|+\rangle$-mode direction is a major or "slow" axes of equipotential ellipses in Fig. 10.1.2c or Fig. 10.2.4; the $|-\rangle$-mode use minor or "fast" axes. The steepest slope is found along the $^-45°$ "fast" mode line, and the gentlest slopes are found along the $^+45°$ "slow" mode line. Along these eigen-axes the motion is simple harmonic oscillation just as it was along x-or y-axes for the uncoupled oscillators in Fig. 10.2.1.

The preceding pictures apply as well to polarization oscillation inside optical analyzers which have "slow" or "fast" optical axes like the X or Y charge axes in the model given in Chapter 1 by Fig. 1.2.2 or the two-spring axes of the single-mass oscillator in Fig. 10.2.1c. Photons initially polarized along a "slow" or "fast" eigenvector direction pass unchanged except for overall phase that undergoes "slow" or "fast" harmonic oscillation, respectively. However, other polarizations are combinations of X and Y, and they undergo multi-harmonic "beating" that changes polarization as will be shown next.
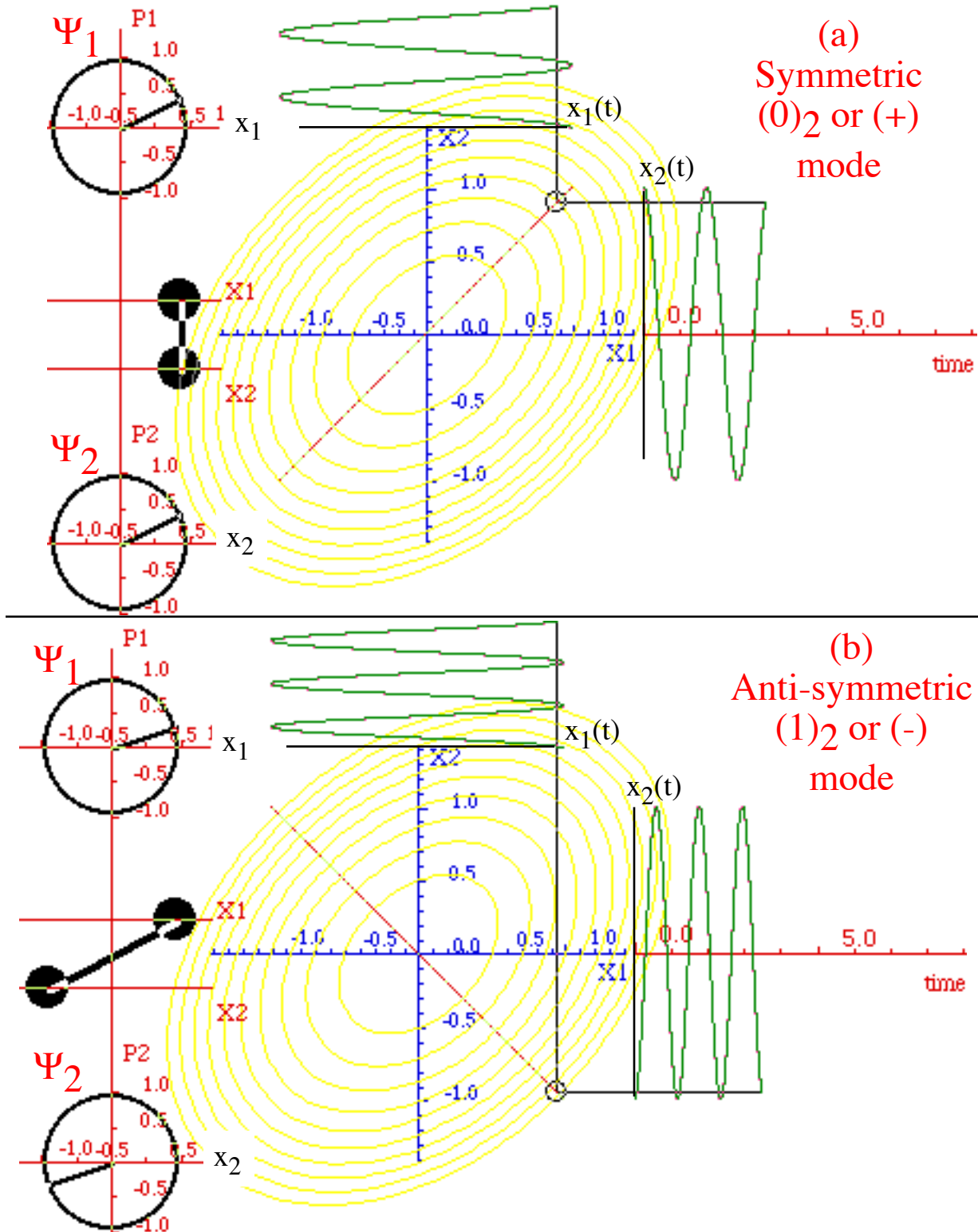
Fig. 10.2.4 Classical analog modes for $C_2{}^B$-symmetric U(2) quantum system. (m=1, k=13, k_{12}=7)

Understanding $C_2{}^B$ dynamics: Beats and transition frequency

We noted that quantum eigenstates are motionless except for their unobservable phase oscillation. Of course, phase oscillation *is* the motion for the classical analog normal modes in Fig. 10.2.4; we can see that easily. But, note that the phasor clocks Ψ_1 or Ψ_2 do not change in size or norm. ($\Psi_m{}^*\Psi_m$ =*const.*) The norm is all we can see in a quantum system. Pure energy states are motionless blobs of probability.

However, *mixed energy states* or combinations of eigenstates will oscillate at a rate equal to the beat frequency or *transition frequency* that is the <u>difference</u> between their eigenfrequencies. (Recall Sec. 4.4.a and Fig. 9.4.1b.) In the example of Fig. 10.2.4 the eigenfrequecies are (from (10.2.9))

$$\omega_{(+)mode} = (A+B) = \sqrt{k} = \sqrt{13} = 3.6 \qquad \omega_{(-)mode} = (A-B) = \sqrt{(k+2k_{12})} = \sqrt{27} = 5.2 \quad (10.2.10)$$

and the transition frequency is the beat frequency $|2B|$ (Actually, B is negative here.)

$$\omega_{(+ -)transition} = \omega_{beat} = |\omega_{(+)mode} - \omega_{(-)mode}| = |2B| = 5.2 - 3.6 = 1.6 \qquad (10.2.11a)$$

which has the beat period shown in Fig. 10.2.5.

$$\tau_{beat} = 2\pi / \omega_{beat} = 3.9 \text{ s} \qquad (10.2.11b)$$
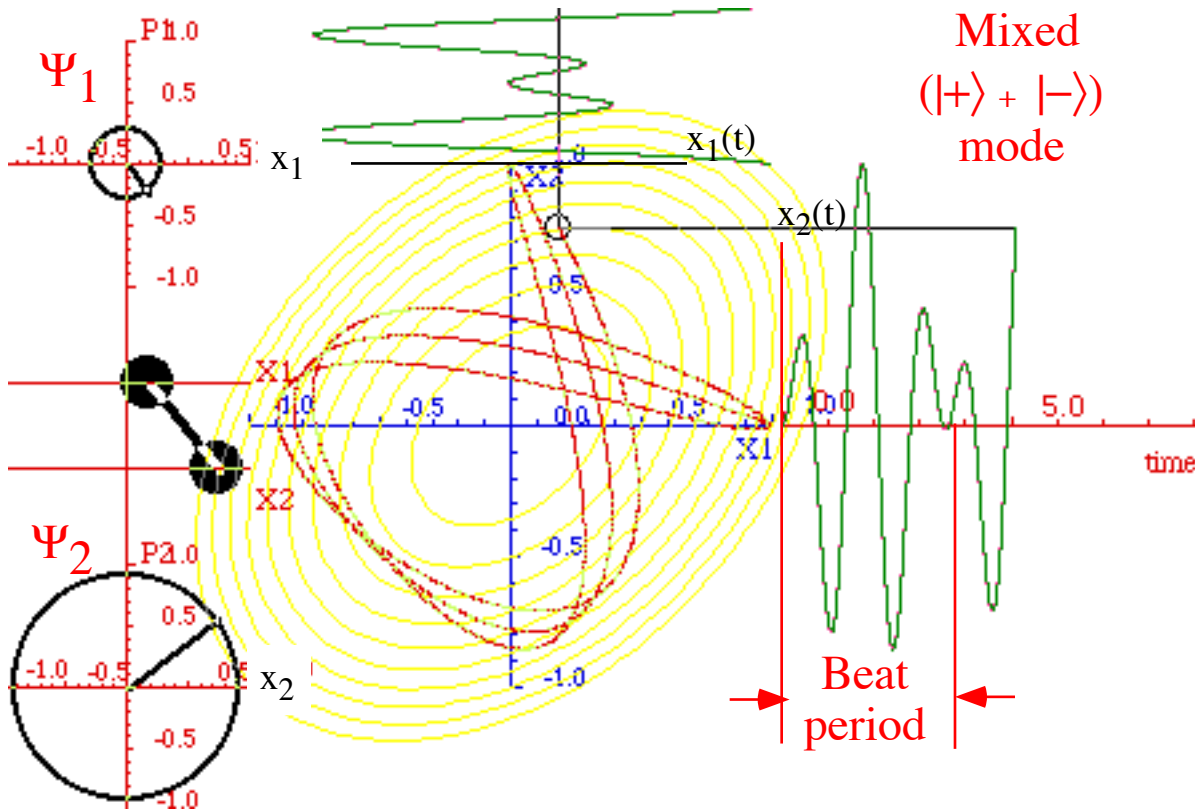
Fig. 10.2.5 Analog mixed modes for $C_2{}^B$-symmetric U(2) quantum system. (m=1, k=13, k$_{12}$=7)

The mixed state in Fig. 10.2.5 was made by initially giving all the amplitude to the first coordinate $(x_1 = \Psi_1(0) = 1)$ but none to the second $(\Psi_2(0) = 0)$. This equivalent to having initial normal coordinates of

$$\langle +|\Psi(0)\rangle = 1/\sqrt{2}, \qquad \langle -|\Psi(0)\rangle = 1/\sqrt{2}. \qquad (10.2.12)$$

The time behavior of the state is then predetermined by the normal modes each oscillating at their eigenfrequencies according to a general diagonal evolution equation, a 2-D case of (9.2.1).

$$\begin{pmatrix} \langle +|\Psi(t)\rangle \\ \langle -|\Psi(t)\rangle \end{pmatrix} = \begin{pmatrix} e^{-i\omega_+ t} & 0 \\ 0 & e^{-i\omega_- t} \end{pmatrix} \begin{pmatrix} \langle +|\Psi(0)\rangle \\ \langle -|\Psi(0)\rangle \end{pmatrix} \qquad (10.2.13a)$$

$$|\Psi(t)\rangle = e^{-i\omega_+ t} |+\rangle\langle +|\Psi(0)\rangle + e^{-i\omega_- t} |-\rangle\langle -|\Psi(0)\rangle \qquad (10.2.13b)$$

This has the following coordinate phasor representation (Replacing abstract kets with representations.)

$$\left| \Psi(t) \right\rangle = e^{-i\omega_+ t} \quad \left| + \right\rangle \ \left\langle + \left| \Psi(0) \right\rangle + e^{-i\omega_- t} \quad \left| - \right\rangle \ \left\langle - \left| \Psi(0) \right\rangle \right.$$

$$\begin{pmatrix} \Psi_1(t) \\ \Psi_2(t) \end{pmatrix} = \begin{pmatrix} \left\langle 1 \middle| \Psi(t) \right\rangle \\ \left\langle 2 \middle| \Psi(t) \right\rangle \end{pmatrix} = e^{-i\omega_+ t} \begin{pmatrix} \left\langle 1 \middle| + \right\rangle \\ \left\langle 2 \middle| + \right\rangle \end{pmatrix} \left\langle + \middle| \Psi(0) \right\rangle + e^{-i\omega_- t} \begin{pmatrix} \left\langle 1 \middle| - \right\rangle \\ \left\langle 2 \middle| - \right\rangle \end{pmatrix} \left\langle - \middle| \Psi(0) \right\rangle \quad (10.2.14a)$$

$$= e^{-i\omega_+ t} \begin{pmatrix} 1/\sqrt{2} \\ 1/\sqrt{2} \end{pmatrix} 1/\sqrt{2} \ + e^{-i\omega_- t} \begin{pmatrix} 1/\sqrt{2} \\ -1/\sqrt{2} \end{pmatrix} 1/\sqrt{2}$$

This reduces to the following. (Recall the use of the expo-sine identity in (4.4.3c).)

$$\begin{pmatrix} \Psi_1(t) \\ \Psi_2(t) \end{pmatrix} = \frac{1}{2} \begin{pmatrix} e^{-i\omega_+ t} + e^{-i\omega_- t} \\ e^{-i\omega_+ t} - e^{-i\omega_- t} \end{pmatrix} = \frac{e^{-i(\omega_+ + \omega_-)t/2}}{2} \begin{pmatrix} e^{-i(\omega_+ - \omega_-)t/2} + e^{i(\omega_+ - \omega_-)t/2} \\ e^{-i(\omega_+ - \omega_-)t/2} - e^{i(\omega_+ - \omega_-)t/2} \end{pmatrix}$$

$$= e^{-i(\omega_+ + \omega_-)t/2} \begin{pmatrix} \cos\left[(\omega_+ - \omega_-)t/2 \right] \\ i\sin\left[(\omega_+ - \omega_-)t/2 \right] \end{pmatrix} \qquad (10.2.14b)$$

According to this, the bottom $\Psi_2(t)$ phasor amplitude grows sinusoidally from zero to its maximum with a rate that is <u>half</u> the beat frequency.

$$\omega_{\text{half-beat}} = \omega_{\text{beat}}/2 = | \ \omega_{(+)\text{mode}} - \omega_{(-)\text{mode}} \ |/2 \qquad (10.2.15)$$

As seen in Fig. 10.2.5, the bottom $\Psi_2(t)$ phasor goes around $90°$ <u>behind</u> the top $\Psi_1(t)$ phasor. That is the *i* factor in the $\Psi_2(t)$ part of (10.2.14b). The overall phase rotates at an <u>average</u> rate

$$\omega_{\text{average}} = (\ \omega_{(+)\text{mode}} + \omega_{(-)\text{mode}} \ )/2. \qquad (10.2.16)$$

Then, just as the bottom $\Psi_2(t)$ phasor passes its maximum, it moves $90°$ <u>ahead</u> of the top $\Psi_1(t)$ phasor that has just gone through zero and starts to grow. The bottom $\Psi_2(t)$ phasor returns to zero amplitude every beat period τ_{beat} given by (10.2.11b) just as the top $\Psi_1(t)$ phasor reaches its maximum amplitude.

The relative phase between the two phasors is important classically as well as in the quantum analog. Whichever phasor is <u>ahead</u> is the one feeding energy to the other that grows while its feeder shrinks. One should recall an important resonance theorem: (Prove this if it's new to you. See exercises.)

Power transfer between two isochronous linearly connected oscillators is proportional to the product of their amplitudes and the sine of their relative phase.

A relative phase of $90°$ gives the best possible work rate. This type of resonance transfer is important in quantum mechanics. A relative phase of $0°$ or $180°$ gives no transfer, as in a classical normal mode or a quantum stationary state; having no <u>net</u> energy gain or loss by individual parts makes them stationary.

Another way to visualize beats is by analogy to optical polarization-wave-plates introduced in Fig. 1.3.6b. One quarter of a beat corresponds to a *quarter wave plate*. The effect is to convert X-polarization into right circular polarization as shown below in Fig. 10.2.6a. A half-beat converts $X=x_1$ to $Y=x_2$ as in Fig. 10.2.6b and corresponds to a *half-wave plate* as shown below in Fig. 10.2.6b. For this example, the coupling constant $2B = \sqrt{k} - \sqrt{(k+2k_{12})}$ is reduced from -1.6 in (10.2.11a) to -0.26 to slow the beat from 3 periods to about 18. Real wave-plate beats take millions of periods so 18 is still <u>way</u> too fast.
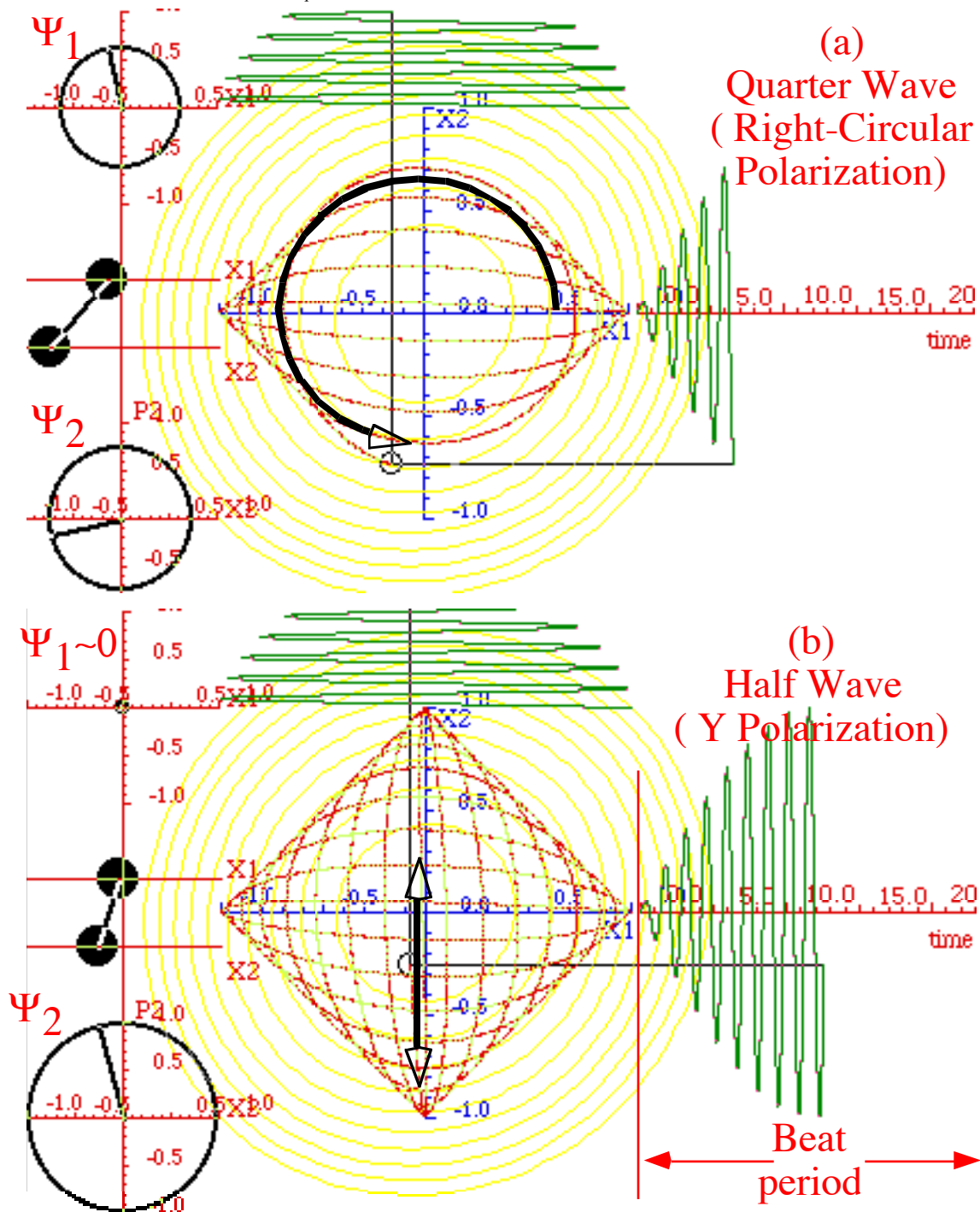
Fig. 10.2.6 Polarization evolution from X to (a) Circular, and (b) Y. (m=1, k=19.1, k_{12}=1.17)

(c) Circular or $C_2{}^C$ symmetry

Now we consider the very different case in which all parameters are zero except *C*. Then a continuous circular rotational C_∞ *symmetry* or *R(2) symmetry* is present. The reflection symmetry associated with the *C*-parameter is called $C_2{}^C$ or $R(2)=C_\infty$. $C_2{}^C$-symmetry states are characterized by circularity and *chirality* or "handedness." Now the circular motion in Fig. 10.2.6a is an eigenstate.

C_∞-symmetry means a two-by-two Hermitian Hamiltonian $\left(\mathbf{H}^\dagger = \mathbf{H}\right)$ matrix operator

$$\mathbf{H} = \begin{pmatrix} \langle 1|\mathbf{H}|1\rangle & \langle 1|\mathbf{H}|2\rangle \\ \langle 2|\mathbf{H}|1\rangle & \langle 2|\mathbf{H}|2\rangle \end{pmatrix} = \begin{pmatrix} A & B-iC \\ B+iC & D \end{pmatrix}. \qquad \text{(10.1.1b)}_{repeated}$$

commutes with <u>any</u> rotation operator $\mathbf{R}(\phi)$ defined as follows. (Recall (2.2.1) in Chapter 2.)

$$\mathbf{R}(\phi)\,|1\rangle = \cos\phi\,|1\rangle + \sin\phi\,|2\rangle \quad, \quad \mathbf{R}(\phi)\,|2\rangle = -\sin\phi\,|1\rangle + \cos\phi\,|2\rangle \text{ (10.2.18a)}$$

Rotation $\mathbf{R}(\phi)$ has the following *R(2)=C$_\infty$* group multiplication rule and C_∞ representation.

$$\mathbf{R}\left(\phi\right)\cdot\mathbf{R}\left(\phi'\right)=\mathbf{R}\left(\phi+\phi'\right)\;, \quad \begin{pmatrix} \langle 1|\mathbf{R}|1\rangle & \langle 1|\mathbf{R}|2\rangle \\ \langle 2|\mathbf{R}|1\rangle & \langle 2|\mathbf{R}|2\rangle \end{pmatrix} = \begin{pmatrix} \cos\phi & -\sin\phi \\ \sin\phi & \cos\phi \end{pmatrix} \qquad \text{(10.2.18b)}$$

Since matrix $\mathbf{H}$ must commute with $\mathbf{R}(\phi)$ for <u>all</u> ϕ, it must also commute with the <u>derivative</u> of $\mathbf{R}(\phi)$ at zero rotation ($\phi=0$ and $\mathbf{R}(0) = \mathbf{1}$). The derivative of a transformation operator near $\mathbf{1}$ is called the *generator* $\mathbf{G}$ of the operator. The generator of the rotation $\mathbf{R}(\phi)$ is as follows.

$$\mathbf{G}=\frac{\partial}{\partial\phi}\mathbf{R}\left(\phi\right)\Big|_{\phi=0} = \begin{pmatrix} -\sin\phi & -\cos\phi \\ \cos\phi & -\sin\phi \end{pmatrix}\Big|_{\phi=0} = \begin{pmatrix} 0 & -1 \\ 1 & 0 \end{pmatrix}, \text{ or: } \mathbf{R}\left(\phi\right)= \mathbf{R}\left(0\right)e^{\phi\mathbf{G}} = e^{\phi\mathbf{G}} \text{ (10.2.18c)}$$

The set *R(2)=C$_\infty$* of all $\mathbf{R}(\phi)$ operators is an example of continuous or *Lie group* symmetry. It is very much like the "empty time" symmetry made of all *time evolution operators* $\mathbf{U}(t)=e^{-i\mathbf{H}\,t}$. The generator of the evolution operators $\mathbf{U}(t)$ is the Hamiltonian $\mathbf{H}$ itself.

Multiplying $\mathbf{R}(\phi)$ generator $\mathbf{G}$ by *i* and gives a third $C_2{}^C$-*Hamilton-Pauli reflection operator* σ_C .

$$\sigma_C = \begin{pmatrix} 0 & -i \\ i & 0 \end{pmatrix} = i\mathbf{G}, \text{ where: } \sigma_C^\dagger\sigma_C = \sigma_C^2 = \mathbf{1} \qquad \text{(10.2.18d)}$$

The *i* makes σ_C Hermitian-unitary like σ_A and σ_B, and gives it a (-1) determinant.$(det|\sigma_C|=-1)$ So σ_C has similar properties to a reflection operator, but it sure doesn't look like one!.

Reflection operator σ_C for circular $C_2{}^C$-symmetry is imaginary unlike σ_A and σ_B that are real. However, the $C_2{}^C$ <u>rotation</u> matrices $\mathbf{R}(\phi)$ are all real, but we will find imaginary rotations associated with $C_2{}^A$-symmetry or $C_2{}^B$-symmetry. Imaginary rotations are Lorentz transformations! More on this later.

The physical idea is that $C_2{}^A$ or $C_2{}^B$-symmetries are associated with "static" or standing wave states that have a <u>real</u> (±)-reflection symmetry about their nodes or anti-nodes. For the classical analogies the nodes corresponded to normal modes or polarization planes. The nodes, modes, or planes sit in different places depending on whether it is $C_2{}^A$, $C_2{}^{AB}$, or $C_2{}^B$-symmetry, but they must sit <u>still</u>.

In contrast, states having $C_2{}^C$-symmetry are <u>moving</u> waves that have no fixed nodes or anti-nodes. Instead, they are characterized by a <u>real</u> (±)-direction of motion and a *chirality* of left or right handed motion.

This is why $C_2{}^C$-rotation operators are real while it is the <u>reflection</u> operators that are real for $C_2{}^A$, $C_2{}^{AB}$, or $C_2{}^B$-symmetries. The former has a constant momentum, the latter a constant position.

Commutation with reflection σ_C or generator **G** yields $C_2{}^C$-symmetry restrictions on **H**-matrices.

$$\mathbf{H} \cdot \mathbf{G} \quad = \quad \mathbf{G} \cdot \mathbf{H}$$

$$\begin{pmatrix} \langle 1|\mathbf{H}|1\rangle & \langle 1|\mathbf{H}|2\rangle \\ \langle 2|\mathbf{H}|1\rangle & \langle 2|\mathbf{H}|2\rangle \end{pmatrix} \begin{pmatrix} 0 & -1 \\ 1 & 0 \end{pmatrix} = \begin{pmatrix} 0 & -1 \\ 1 & 0 \end{pmatrix} \begin{pmatrix} \langle 1|\mathbf{H}|1\rangle & \langle 1|\mathbf{H}|2\rangle \\ \langle 2|\mathbf{H}|1\rangle & \langle 2|\mathbf{H}|2\rangle \end{pmatrix} \tag{10.2.19a}$$

$$\begin{pmatrix} \langle 1|\mathbf{H}|2\rangle & -\langle 1|\mathbf{H}|1\rangle \\ \langle 2|\mathbf{H}|2\rangle & -\langle 2|\mathbf{H}|1\rangle \end{pmatrix} = \begin{pmatrix} -\langle 2|\mathbf{H}|1\rangle & -\langle 2|\mathbf{H}|2\rangle \\ \langle 1|\mathbf{H}|1\rangle & \langle 1|\mathbf{H}|2\rangle \end{pmatrix}$$

Thus, $R(2)=C_\infty$ or $C_2{}^C$-symmetry demands the following for **H** matrix components.

$$\langle 1|\ \mathbf{H}\ |1\rangle = \langle 2|\ \mathbf{H}\ |2\rangle \ , \qquad \langle 1|\ \mathbf{H}\ |2\rangle = -\langle 2|\ \mathbf{H}\ |1\rangle \tag{10.2.19b}$$

For the **H** example (10.1.1b) we have

$$A = D \ , \qquad\qquad B - iC = -(B + iC) \tag{10.2.19c}$$

so only two free parameters remain.

$$\begin{pmatrix} \langle 1|\mathbf{H}|1\rangle & \langle 1|\mathbf{H}|2\rangle \\ \langle 2|\mathbf{H}|1\rangle & \langle 2|\mathbf{H}|2\rangle \end{pmatrix} = \begin{pmatrix} A & -iC \\ iC & A \end{pmatrix} \tag{10.2.19d}$$

This **H** matrix is easy to diagonalize, but let's use symmetry projection just to get some more practice.

$R(2)=C_\infty$ projectors and $C_2{}^C$ eigenstates

The $R(2)=C_\infty$ projectors follow from the secular equation for $R(2)=C_\infty$ operator $\mathbf{R}(\phi)$ which is

$$\varepsilon^2 - (trace\ \mathbf{R}(\phi))\ \varepsilon + (det\ \mathbf{R}(\phi)) = 0 = \varepsilon^2 - (2\cos\phi)\ \varepsilon + 1 \tag{10.2.20}$$

The $\pm$eigenvalues are labeled L and R for "Left" and "Right" for reasons that we'll see below.

$$\varepsilon_L = \cos\phi + \sqrt{\cos\phi^2 - 1} = \cos\phi + i\sin\phi = e^{i\phi} \tag{10.2.21a}$$

$$\varepsilon_R = \cos\phi - \sqrt{\cos\phi^2 - 1} = \cos\phi - i\sin\phi = e^{-i\phi} \tag{10.2.21b}$$

Substituting the roots $\{\varepsilon_L=e^{i\phi},\ \varepsilon_R=e^{-i\phi}\}$ of $\mathbf{M}=\mathbf{R}(\phi)$ in the projection formula ((3.1.15) repeated below)

$$\mathbf{P}_k = \frac{\prod\limits_{j\neq k}\left(\mathbf{M} - \varepsilon_j\mathbf{1}\right)}{\prod\limits_{j\neq k}\left(\varepsilon_k - \varepsilon_j\right)} \ , \tag{3.1.15a}_{repeated}$$

gives two normalized projectors

$$\mathbf{P}^{(L)} = \frac{\begin{pmatrix} \cos\phi - e^{-i\phi} & -\sin\phi \\ \sin\phi & \cos\phi - e^{-i\phi} \end{pmatrix}}{e^{i\phi} - e^{-i\phi}} \ , \qquad \mathbf{P}^{(R)} = \frac{\begin{pmatrix} \cos\phi - e^{i\phi} & -\sin\phi \\ \sin\phi & \cos\phi - e^{i\phi} \end{pmatrix}}{e^{-i\phi} - e^{i\phi}} \ , \tag{10.2.22}$$

$$= \frac{\begin{pmatrix} i\sin\phi & -\sin\phi \\ \sin\phi & i\sin\phi \end{pmatrix}}{2i\sin\phi} = \frac{\begin{pmatrix} 1 & i \\ -i & 1 \end{pmatrix}}{2} \ , \qquad = \frac{\begin{pmatrix} i\sin\phi & -\sin\phi \\ \sin\phi & i\sin\phi \end{pmatrix}}{-2i\sin\phi} = \frac{\begin{pmatrix} 1 & -i \\ i & 1 \end{pmatrix}}{2}$$

which in turn, give two normalized eigenstates of the $R(2)$ -symmetric **H** operator in (10.2.19d)

$$|L\rangle = \mathbf{P}^{(L)}|1\rangle\ \sqrt{2} = (|1\rangle - i|2\rangle)/\sqrt{2} \ , \qquad |R\rangle = \mathbf{P}^{(R)}|1\rangle\ \sqrt{2} = (|1\rangle + i|2\rangle)/\sqrt{2} \ , \tag{10.2.23a}$$

and a diagonalizing transformation

$$\left(\begin{array}{cc} \langle 1|L \rangle & \langle 1|R \rangle \\ \langle 2|L \rangle & \langle 2|R \rangle \end{array} \right) = \left(\begin{array}{cc} 1/\sqrt{2} & 1/\sqrt{2} \\ -i/\sqrt{2} & i/\sqrt{2} \end{array} \right) . \tag{10.2.23b}$$

The columns are eigenvectors of any matrix that commutes with $R(2)=C_\infty$ operator $\mathbf{R}(\phi)$. This includes the **H**-matrix (10.2.19d) that is diagonalized as follows.

$$\left(\begin{array}{cc} \langle L|1 \rangle & \langle L|2 \rangle \\ \langle R|1 \rangle & \langle R|2 \rangle \end{array} \right) \left(\begin{array}{cc} A & -iC \\ iC & A \end{array} \right) \left(\begin{array}{cc} \langle 1|L \rangle & \langle 1|R \rangle \\ \langle 2|L \rangle & \langle 2|R \rangle \end{array} \right) = \left(\begin{array}{cc} A-C & 0 \\ 0 & A+C \end{array} \right) \tag{10.2.23c}$$

The **H** eigenvalues are (for $\hbar=1$) eigenfrequencies that determine the time evolution dynamics.

$$\varepsilon_L = \langle L|\mathbf{H}|L \rangle = A-C = \hbar\omega_L , \qquad \varepsilon_R = \langle R|\mathbf{H}|R \rangle = A+C = \hbar\omega_R , \tag{10.2.24}$$

Understanding $C_2{}^C$ eigenstates: Zeeman-like splitting and coriolis or cyclotron motion

The eigenstate evolution is given below and represented in the original xy or $\{|1\rangle, |2\rangle\}$ basis.

$$|L(t)\rangle = |L\rangle e^{-i\omega_L t} = \left(\begin{array}{c} \langle 1|L \rangle \\ \langle 2|L \rangle \end{array} \right) e^{-i\omega_L t}, \qquad |R(t)\rangle = |R\rangle e^{-i\omega_R t} = \left(\begin{array}{c} \langle 1|R \rangle \\ \langle 2|R \rangle \end{array} \right) e^{-i\omega_R t} \tag{10.2.25}$$

To help visualize the $R(2)$ base states $\{|L\rangle, |R\rangle\}$ we plot their real parts in the center parts of Fig. 10.2.7.

$$\mathrm{Re}\left(\begin{array}{c} \langle 1|L(t) \rangle \\ \langle 2|L(t) \rangle \end{array} \right) = \mathrm{Re}\left(\begin{array}{c} e^{-i\omega_L t}/\sqrt{2} \\ -ie^{-i\omega_R t}/\sqrt{2} \end{array} \right) = \left(\begin{array}{c} \cos\omega_L t \\ -\sin\omega_L t \end{array} \right), \qquad \mathrm{Re}\left(\begin{array}{c} \langle 1|R(t) \rangle \\ \langle 2|R(t) \rangle \end{array} \right) = \mathrm{Re}\left(\begin{array}{c} e^{-i\omega_R t}/\sqrt{2} \\ ie^{-i\omega_R t}/\sqrt{2} \end{array} \right) = \left(\begin{array}{c} \cos\omega_R t \\ \sin\omega_R t \end{array} \right)$$

$$\tag{10.2.26}$$
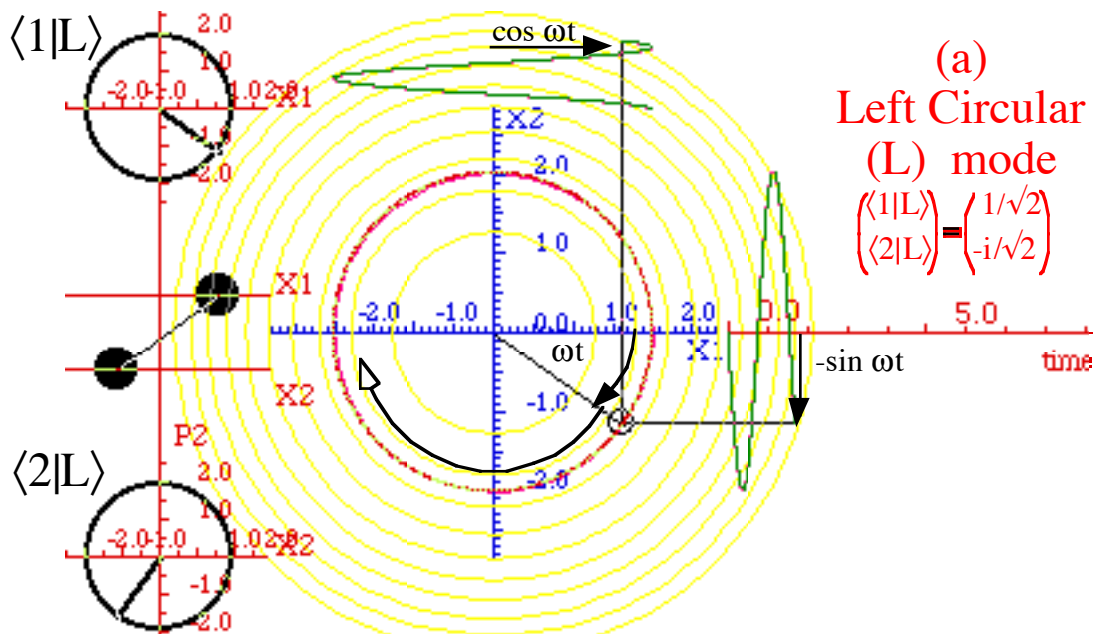
Fig. 10.2.7 R(2)=C$_\infty$ symmetry eigenstates (a) Left circular

From the Figures 10.2.7 a and b it seen how $|L\rangle$ and $|R\rangle$ stand for left and right handed *circular polarization* states. Previously, we have seen how to briefly achieve right circular polarization using a 1/4-beat of mixed C_2-mode or a quarter wave plate in Fig. 10.2.6a. Here it's a pure $R(2)$ mode. Circular orbits are also known as *cyclotron modes*. They are the orbits that a positively charged particle in an isotropic 2-D oscillator

potential could have in the presence of a magnetic field normal to the orbit plane. They are also called *Coriolis modes* or *Foucault orbits* if the oscillator is on a rotating table.
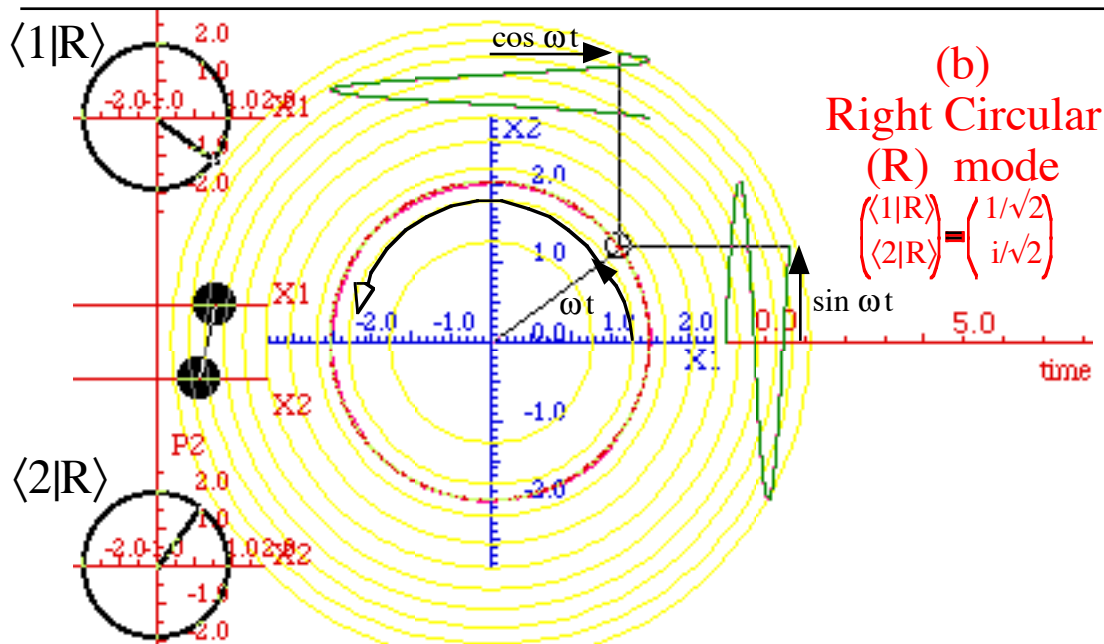
Fig. 10.2.7 R(2)=C∞ symmetry eigenstates (a) Left circular (b) Right circular polarization

    With no magnetic field or rotation the particle orbits either way with the same orbit frequency as shown on the left-hand side of Fig. 10.2.8. It is only necessary that the centrifugal force $m\omega^2 r$ balance the attractive "spring" force $-kr$ of the oscillator. But, a magnetic field **B** or rotation Ω will either help to attract or else repel the particle depending on the particles direction of orbit. For left handed $|L\rangle$-orbits the magnetic **F**=q**v**x**B** force (or Coriolis force **F**=m**v**xΩ) teams up with the attractive **F** = -k**r** of the oscillator. So, the centrifugal force must increase to balance these two and keep the particle at the same radius. That means faster orbit frequency ω as shown in the upper right hand side of Fig. 10.2.8. For right hand $|R\rangle$-rotation the magnetic q**v**x**B** force or Coriolis m**v**xΩ teams up with the centrifugal force $m\omega^2 r$ against the attractive $-kr$, so $m\omega^2 r$ must be reduced to maintain a given orbit radius, hence reduced orbit frequency ω.

    This mechanics is also analogous to our prevailing weather phenomena. The Earth's counter clockwise rotation tends to create counterclockwise cyclones in the Northern hemisphere and the opposite ω in the Southern latitudes. Anti-cyclones are not impossible, just energetically disfavored.

    The classical analogs for the rotational *R(2)*-symmetric (Zeeman-like) quantum splitting are quite different from the corresponding analogs for bilateral *AB*-symmetric (Stark-like) splitting described later. The frequency equation resulting from cyclotron orbits in Fig. 10.2.8 is a force balance equation.

$$F_{centrifugal} + F_{B-field} + F_{oscillator} = 0 = mr\omega^2 + qBr\omega - kr \qquad (10.2.27a)$$

It has quadratic solutions that are plotted in Fig. 10.2.9.

$$\omega = \frac{-qB \pm \sqrt{(qB)^2 + 4mk}}{2m} = \frac{-qB}{2m} \pm \sqrt{\left(\frac{qB}{2m}\right)^2 + \frac{k}{m}} = \frac{\omega_C}{2} \pm \sqrt{\left(\frac{\omega_C}{2}\right)^2 + (\omega_O)^2} \quad (10.2.27b)$$

The vacuum *cyclotron frequency* ω_C and zero-B-field *harmonic oscillator frequency* ω_O are labeled.

$$\omega_C = \frac{-qB}{m} \,, \qquad \omega_O = \sqrt{\frac{k}{m}} \qquad\qquad (10.2.27c)$$
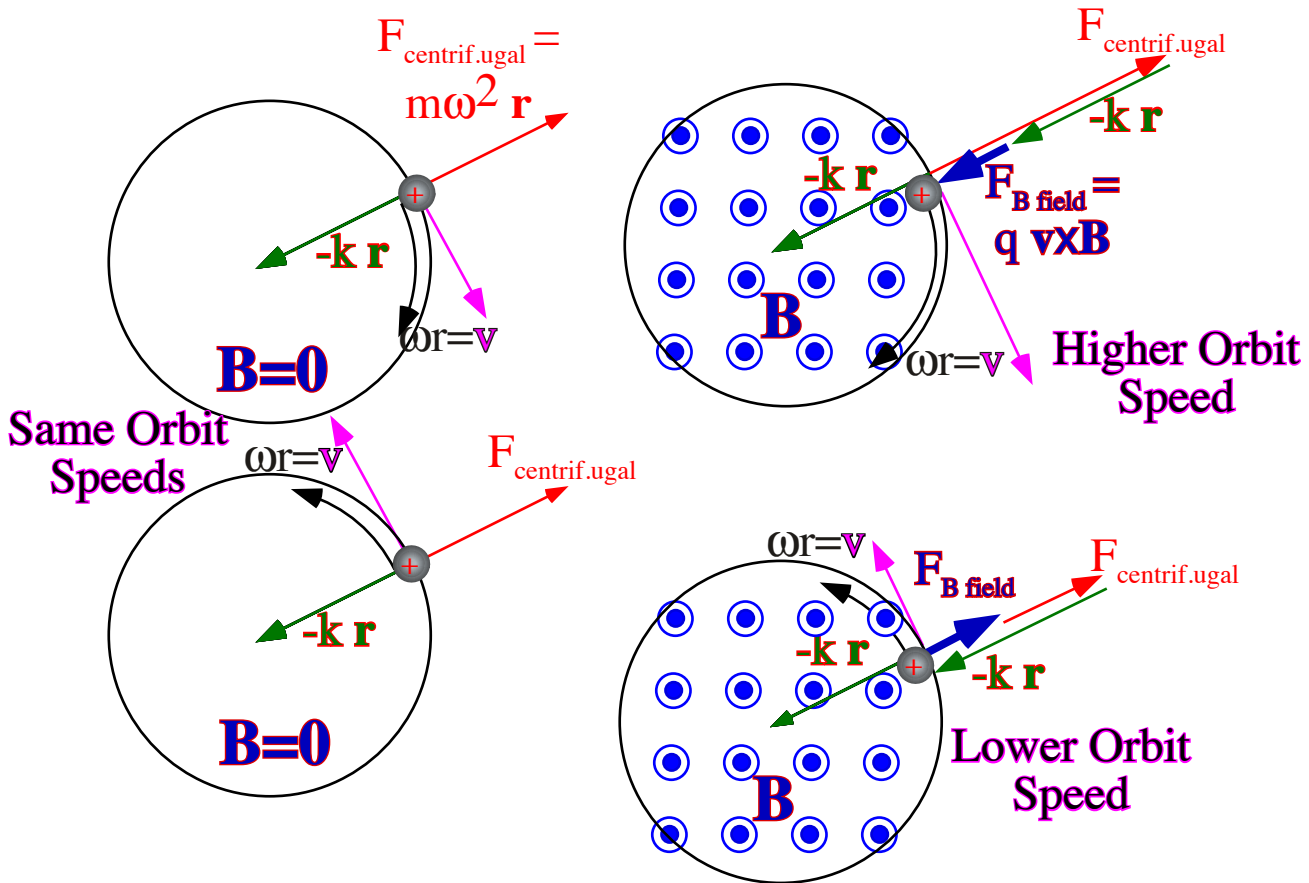
*Fig. 10.2.8 Cyclotron or Coriolis orbit degeneracy lifted by **B***-field or rotation.*

Note: the cyclotron frequency ω_C is <u>minus</u> the field parameter qB while ω_O is a positive (+)-root of parameter k/m. While ω_O is positive, orbit frequency or angular velocity ω or ω_C can each be positive or negative. In the vacuum case ($k=0$), positive qB means <u>negative</u> $\omega=\omega_C$ and clockwise or left L orbits only, as shown on the extreme upper right hand side of Fig. 10.2.9. Negative qB means positive $\omega=\omega_C$ and counter clockwise or R orbits only, as shown on the extreme upper left hand side of Fig. 10.2.9. The negative (-)-root in (10.2.10b) gives a zero frequency mode, that is, no motion at all, as indicated by dashed circles in Fig. 10.2.9. (A B-field does not affect effect a stationary charge.)

The plot in Fig. 10.2.9 is one of orbital <u>speed</u> $|\omega|$ which is quantum phasor velocity or energy $\hbar|\omega|$ rather than classical orbital velocity ω. An orbital <u>velocity</u> ω-plot would flip the ascending curve about the *x*-axis so it was below the axis and descending parallel to the other descending one. Classical kinetic energy is simply $^1/_2 mr^2|\omega|^2$ and resembles Fig. 10.2.9, too.
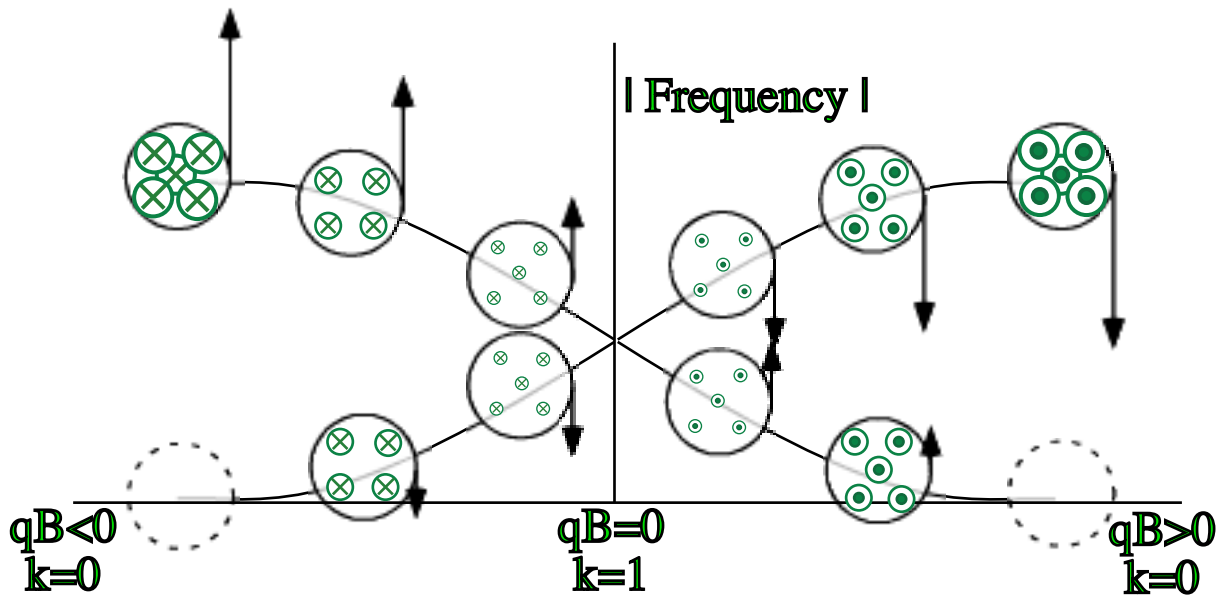
*Fig. 10.2.9 Cyclotron orbital speed for varying **B**-field (qB=x) and oscillator spring constant k=|1-x|.*

Consider the limiting cases. For weak oscillator potential (ω_O<<|ω_C|) or strong qB-field, the approximate frequencies shift <u>quadratically</u> in ω_O.

$$\omega = \frac{-qB}{2m} \pm \sqrt{\left(\frac{qB}{2m}\right)^2 + \frac{k}{m}} = \frac{\omega_C}{2} \pm \sqrt{\left(\frac{\omega_C}{2}\right)^2 + \left(\omega_O\right)^2} \approx \frac{\omega_C}{2} \pm \left(\frac{\omega_C}{2} + \frac{\left(\omega_O\right)^2}{\omega_C} \cdots\right) = \begin{cases} \omega_C + \dfrac{\left(\omega_O\right)^2}{\omega_C} \\[3mm] -\dfrac{\left(\omega_O\right)^2}{\omega_C} \end{cases}$$

(10.2.28a)

For strong potential (ω_O>>|ω_C|) or weak qB-field, the approximate frequencies split <u>linearly</u> in ω_C .

$$\omega = \frac{-qB}{2m} \pm \sqrt{\left(\frac{qB}{2m}\right)^2 + \frac{k}{m}} = \frac{\omega_C}{2} \pm \sqrt{\left(\omega_O\right)^2 + \left(\frac{\omega_C}{2}\right)^2} \approx \frac{\omega_C}{2} \pm \left(\omega_O + \frac{\omega_C^2}{8\omega_O} \cdots\right) = \begin{cases} \omega_O + \dfrac{\omega_C}{2} + \dfrac{\omega_C^2}{8\omega_O} \\[3mm] -\omega_O + \dfrac{\omega_C}{2} - \dfrac{\omega_C^2}{8\omega_O} \end{cases}$$

(10.2.28b)

Compare this to <u>phasor</u> frequencies (10.2.24) that, unlike the <u>orbital</u> velocities, are positive.

$$\hbar\omega_L = A\text{-}C \approx \hbar(\omega_O - \omega_C /2) , \qquad \hbar\omega_R = A+C \approx \hbar(\omega_O + \omega_C /2) . \qquad (10.2.29)$$

This connects the ω_C to the off-diagonal C-parameter in (10.2.19d) and ω_O to A, but only for weak qB.

Understanding $C_2{}^C$ *dynamics: Faraday rotation*

The effect of mixing R and L modes in Fig. 10.2.7a-b is quite dramatic as shown in Fig. 10.2.10 where a 50-50 mixture gives perfect beats as were seen in Fig. 10.2.6 when x-polarization evolved into elliptic then circular then y-polarization. However, in Fig. 10.2.10 there is a rotation or precession of the plane of polarization directly from x to y. In the classical analogy this is a famous effect called *Foucault precession*

demonstrated in many science museums which trace the daily motion of a great pendulum due to Earth rotation. In optics, this is known as *Faraday rotation* of the plane of polarization.

       A 50-50 mixture of *R* and *L* modes with the same frequency would just be plain old (or plane old) x-polarization. However, if, as in Fig. 10.2.10, *R* is a little faster in its counter-clockwise orbit than *L* is in going the other way then they will meet further and further to the right each period. The result is a nearly planar polarization ellipse that is slowly rotating to the right as shown in Fig. 10.2.10 where a half beat rotates x-into-y-polarization. Note that a <u>whole</u> beat will only be <u>half</u> a rotation, that is, x-polarization will only been rotated into <u>minus</u>-x-polarization. Later, we will see this is related to the spin-1/2 half-angle conundrum we encountered in Chapter 1. There in (1.2.12) a "whole" rotation by $\beta=2\pi$ of a spin vector only rotates spin-up $|{\uparrow}\rangle$ by $\beta/2=\pi$ and into <u>minus</u> spin-up ($-|{\uparrow}\rangle$). Same math, different physics!
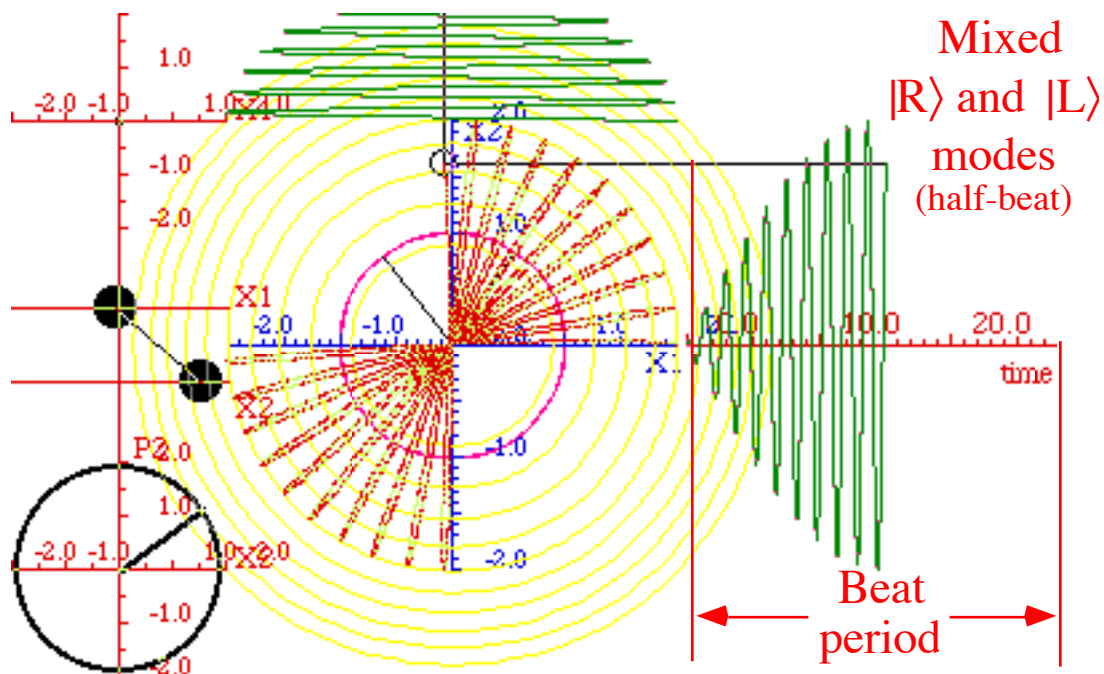
Fig. 10.2.10 Faraday rotation from X to Y. (A=4.1=D, C=0.1, B=0)

       The picture changes radically if right handed rotation is much faster than the left handed orbit which would be zero in a purely negative q**B**-field cyclotron indicated on the left of Fig. 10.2.9. This sort of motion is shown in Fig. 10.2.11 where left-handed orbit is nearly zero and a cyclotron orbit circle is seen precessing around a circle of nearly the same radius.
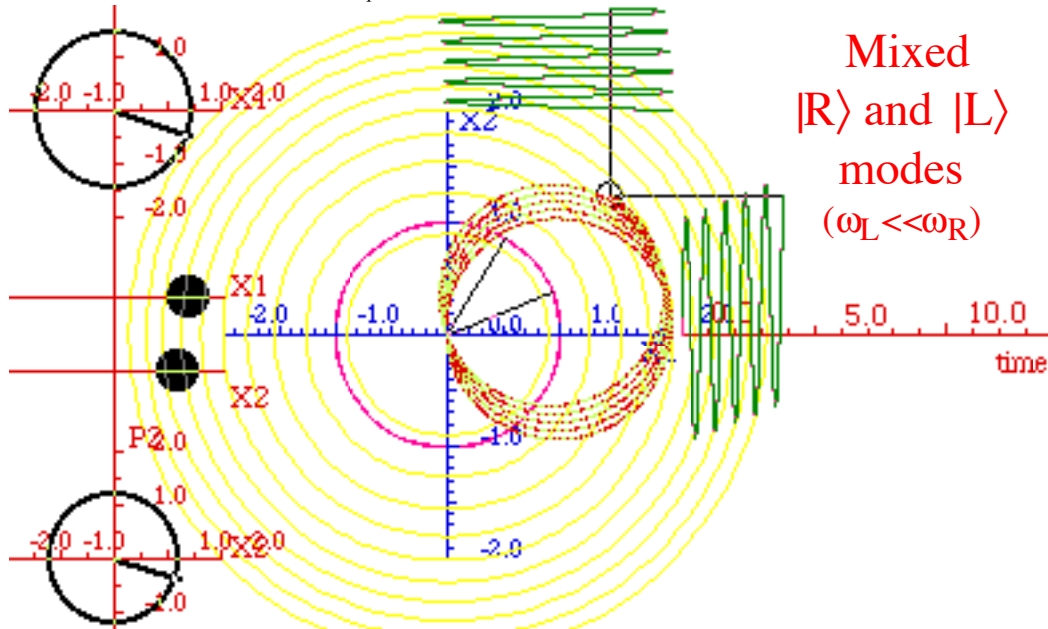
Fig. 10.2.11 Hyper-Faraday rotation. (A=4.1=D, C=4.2, B=0)

The analogy between Foucault precession and magnetic cyclotron orbiting, and Faraday rotation are profound and deep ones. The Foucault precession is due to an underlying rotation such as that of our Earth. The cyclotron orbit is due to an applied magnetic field as is, in some cases, the Faraday effect. The remarkable similarities of magnetism and rotation of space might lead one to speculate that magnetism *is*, in some sense, a rotation of space. Perhaps, we will have more to say about this later.

The magnetic or Zeeman like splitting seen in Fig. 10.2.9 starts out as a *first order* effect, that is, linear in the field, and then quadratic or *second order* effects show up at higher fields. The **B**-field splitting (*C*-type symmetry) is sketched below in Fig. 10.2.12b and mirrors behavior seen in Fig. 10.2.9.
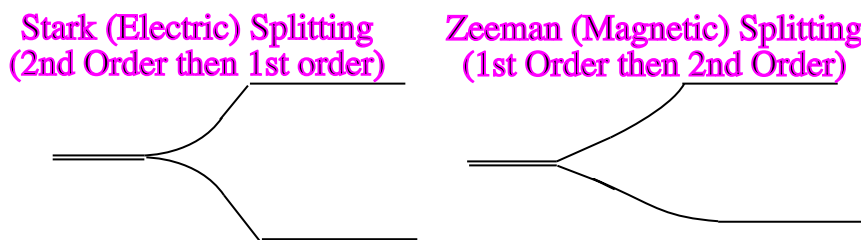
Fig. 10.2.12 Two archetypical splittings (a) Stark-like (1st order) (b) Zeeman-like (2nd order)

The next sections treat electric or Stark-like splitting which is quite the opposite. As sketched in Fig. 10.2.12a below, the electric or Stark-like splitting starts out as a second order effect and then becomes linear at higher **E**-fields. The symmetry differences between electric dipole or Stark effects (*A*-type symmetry) on one hand, and magnetic dipole or Zeeman effects (*C*-type symmetry) on the other, are important ones and are connected with quite different physics. Also, quadratic or 2nd order variation of energy eigenvalues is a first sign that *eigenstates are changing*. Now we study some examples.

10.3 Mixed A and B Symmetry

So far our study of symmetry analysis has concentrated on its "easy" side. We found "easy" eigenvalue formulas that varied linearly with Hamiltonian parameters *H, S, T,* or *A, B, C,* and *D* , but the "easy" eigenstates remained *fixed*. This "easy" situation requires all the relevant symmetry operators commute with each other as do **r**, **r**^{2}, … in Chapter 8 and 9. This is about to change because there is no such commutation between operators σ_A , σ_B , or σ_C. that make up a general *U(2)* Hamiltonian,

$$\mathbf{H} = \frac{A+D}{2}\sigma_1 + B\sigma_B + C\sigma_C + \frac{A-D}{2}\sigma_A \qquad (10.3.1)$$

The following non-commutation relations mean no *two* of σ_A , σ_B , and σ_C can be diagonalized *together*.

$$\sigma_A\sigma_B = -\sigma_B\sigma_A = \sigma_C , \quad \sigma_B\sigma_C = -\sigma_C\sigma_B = \sigma_A , \quad \sigma_C\sigma_A = -\sigma_A\sigma_C = \sigma_B , \qquad (10.3.2)$$

So eigenvalues may vary *non-linearly* with parameters *A, B, C,* and *D* . Most important: *So do the eigenstates*. The study of mixed symmetries is not as "easy" but it's quite interesting!

(a) Asymmetric bilateral C$_2$^{AB} symmetry: Stark-like-splitting

Consider the 2-state Hamiltonian with zero complex constant *C=0* but nonzero *A, B,* and *D*.

$$\mathbf{H} = \begin{pmatrix} A & B \\ B & D \end{pmatrix} = \begin{pmatrix} H-pE & -S \\ -S & H+pE \end{pmatrix} \qquad (10.3.3a)$$

$$\mathbf{H} = (A+D)/2\ \sigma_1 + B\sigma_B + (A-D)/2\sigma_A = H\sigma_1 - 2S\ \sigma_B - pE\ \sigma_A \qquad (10.3.3a)$$

The presence of <u>un</u>equal diagonal energies (*A>D*) spoils bilateral *C$_2$^{B} symmetry* even if the complex constant vanishes (*C=0*). It makes the *C$_2$^{B}* projectors less useful. It appears one has to diagonalize the **H**-matrix *brute force*. (Later, we will see how to elegantly "finesse" this *C$_2$^{AB}* case, too.)

Above it is imagined that a potential energy field *pE=(A-D)/2* is turned on to make the |1⟩ state lower in energy (or higher if *pE* is negative) than the |2⟩ state. The coupling constant *B* has intentionally been set negative (*B=-S*) to match sign of the constant *K$_{12}$* in the coupled pendulum analogy (10.1.5a-c). The *S*-constant is a "sneak rate" or *tunneling amplitude S* like the *S* introduced in Fig. 9.3.5. (That was negative, as well, in (9.3.5g).) A positive field (*pE>0*) corresponds to making the number-1 pendulum lower, slower, and longer than its number-2 neighbor as shown in Fig. 10.1.1b.

Now for the diagonalization. First the secular equation for **H** in (10.3.3a) is (recalling (3.1.5))

$$\varepsilon^2 - (trace\ \mathbf{H})\ \varepsilon + (det\ \mathbf{H}) = 0 = \varepsilon^2 - (2H)\ \varepsilon + (H^2 - (pE)^2 - S^2\ ). \qquad (10.3.4)$$

The eigenvalues are hyperbolic conic sections plotted above a *pE-S* axes in Fig. 10.3.1a-b.

$$\varepsilon_{hi} = H + \sqrt{(pE)^2 + S^2} \qquad (10.3.5a)$$

$$\varepsilon_{lo} = H - \sqrt{(pE)^2 + S^2} \qquad (10.3.5b)$$

The high and low eigenvalues form two halves of an intersecting vertical cone in Fig. 10.3.1a. (Michael Berry calls the cone a diablo after a child's toy top. The intersection is called a *diabolical point* since it's a devilish singularity, as we will see.) The corresponding eigenvector projectors are (using (3.1.15))

$$\mathbf{P}_{hi} = \frac{\begin{pmatrix} H - pE - \varepsilon_{lo} & -S \\ -S & H + pE - \varepsilon_{lo} \end{pmatrix}}{\varepsilon_{hi} - \varepsilon_{lo}} = \frac{\begin{pmatrix} -pE + \sqrt{(pE)^2 + S^2} & -S \\ -S & pE + \sqrt{(pE)^2 + S^2} \end{pmatrix}}{2\sqrt{(pE)^2 + S^2}} \qquad (10.3.5c)$$

$$\mathbf{P}_{lo} = \frac{\begin{pmatrix} H - pE - \varepsilon_{hi} & -S \\ -S & H + pE - \varepsilon_{hi} \end{pmatrix}}{\varepsilon_{lo} - \varepsilon_{hi}} = \frac{\begin{pmatrix} pE + \sqrt{(pE)^2 + S^2} & S \\ S & -pE + \sqrt{(pE)^2 + S^2} \end{pmatrix}}{2\sqrt{(pE)^2 + S^2}} \qquad (10.3.5d)$$

For constant $S>0$ and varying pE the two eigenvalues trace *hyperbolic conic sections* or a *Wigner avoided level crossing* as shown in Fig. 10.3.1. Crossing happens only at one "diabolical" point where tunneling and field both vanish ($S=0=pE$). In Fig. 10.3.1b, relative amplitudes for the "up-field" or $|2\rangle=|y\rangle$ versus "dn-field" or $|1\rangle=|x\rangle$ states vary from *50-50* for $pE=0$ to *99up-1dn* when pE field is up ($pE=+1$) or *1up-99dn* for ($pE=-1$) for the "ground" states on the bottom hyperbola. Meanwhile, the "excited" states on the top curve go *against* the field. For smaller S, polarization shifts near the diabolical point become sharper, finally jumping from *100up-0dn* to *0up-100dn* right at $pE=0$. We now see how this works.

High field splitting: Strong C_2^A or weak C_2^B symmetry

For large $|pE|$ and small tunneling ($|pE|>>S$) the approximate eigenvalues are growing up or down linearly with the applied field energy pE as the energy eigenvalues approach the hyperbolic asymptotes.

$$\varepsilon_{hi} = H + \sqrt{(pE)^2 + S^2} \approx H + pE + \frac{S^2}{2pE} + \cdots \qquad (10.3.6a)$$

$$\varepsilon_{lo} = H - \sqrt{(pE)^2 + S^2} \approx H - pE - \frac{S^2}{2pE} + \cdots \left(\text{for: } pE>>S\right) \qquad (10.3.6b)$$

In this limit, the eigenvectors get their symmetry broken, too. With zero field ($pE=0$) the lowest eigenstate $|+\rangle$ is a perfect 50-50 combination of the "down-field" state $|1\rangle$ and the "up-field" state $|2\rangle$ as in (10.2.6a). With a large field, the lowest state becomes nearly 100% "down-field" state $|1\rangle$ and negligible amplitude in the "up-field" direction of state $|2\rangle$, as seen in the following first column of (10.3.5d).

$$|\varepsilon_{lo}\rangle = \begin{pmatrix} \langle 1|\varepsilon_{lo}\rangle \\ \langle 2|\varepsilon_{lo}\rangle \end{pmatrix} = \frac{1}{\sqrt{norm.}}\begin{pmatrix} pE + \sqrt{(pE)^2 + S^2} \\ S \end{pmatrix}$$

$$\approx \frac{1}{\sqrt{norm.}}\begin{pmatrix} 2pE + S^2/2pE + \cdots \\ S \end{pmatrix} \rightarrow \begin{pmatrix} 1 \\ 0 \end{pmatrix} = |1\rangle \ \left(\text{for: } pE>>S\right) \qquad (10.3.7a)$$

Meanwhile, the highest eigenstate $|-\rangle$, also once a (minus) 50-50 combination, behaves in a contrary fashion and "fights" its way <u>against</u> the field toward almost 100% "up-field" direction of state $|2\rangle$.

$$\left|\varepsilon_{hi}\right\rangle = \begin{pmatrix} \langle 1|\varepsilon_{hi}\rangle \\ \langle 2|\varepsilon_{hi}\rangle \end{pmatrix} = \frac{1}{\sqrt{norm.}} \begin{pmatrix} -S \\ pE + \sqrt{(pE)^2 + S^2} \end{pmatrix}$$

(10.3.7b)

$$\approx \frac{1}{\sqrt{norm.}} \begin{pmatrix} -S \\ 2pE + S^2/2pE + \cdots \end{pmatrix} \rightarrow \begin{pmatrix} 0 \\ 1 \end{pmatrix} = |2\rangle \quad (\text{for: } pE \gg S)$$
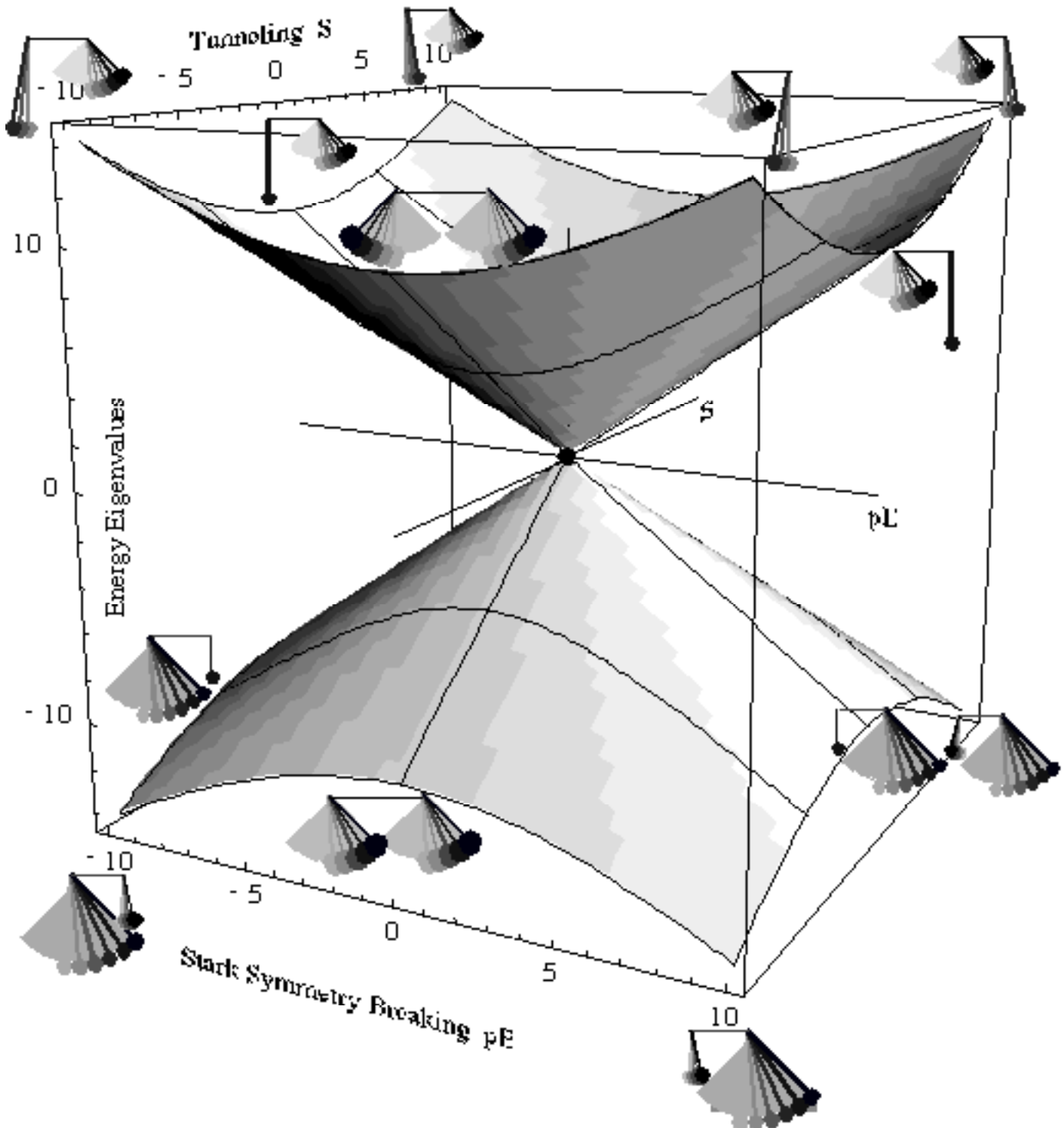
10.3.1 (a) Two state eigenvalue "diablo" surfaces and conical intersection and pendulum eigenstates.

Fig.
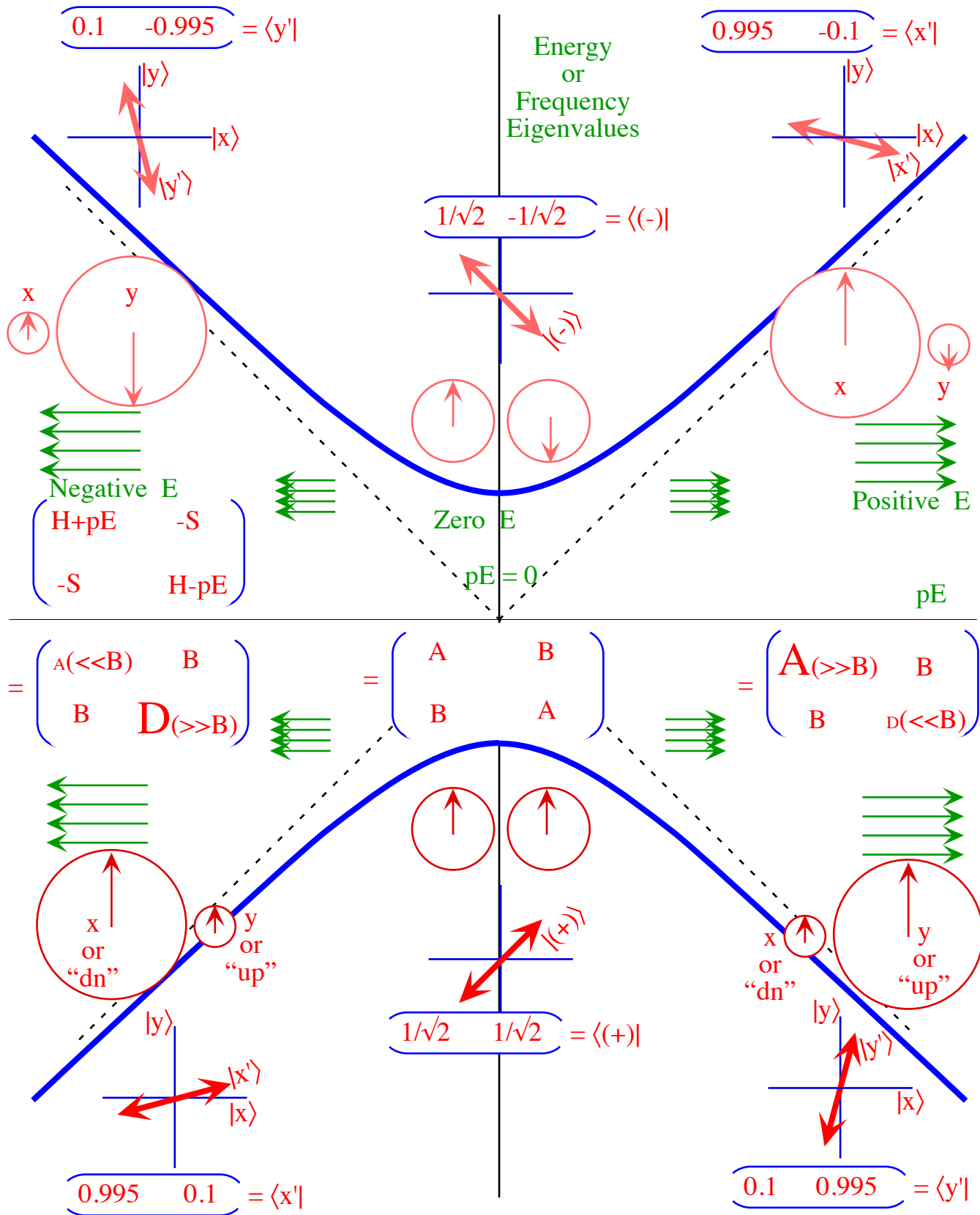
Fig. 10.3.1 (b) Wigner avoided level crossing. (Fixed tunneling S and variable pE field.)

The tendency for a ground state system to acquiesce or "polarize" in the direction of the applied field is quite natural. (Don't you feel like just "giving in" sometimes?) Most systems that we "push" in our classical world are in their ground states and respond accordingly. However, an excited quantum state can be a very different beast and will display a "passive aggressive" behavior, to use an anthropomorphic analogy. (That's right...fight the #%*@ system no matter what it takes!)

The pendulum analogy helps to understand this behavior in terms of resonance, or the lack thereof. If we reduce symmetry by making pendulum-1 longer and slower than pendulum-2 as in Fig. 10.1.1b then we spoil the resonance between them, particularly if the coupling is weak ($|k_{12}|<<|k_2 - k_1|$). The response of faster pendulum-2 to the slower one drops off according to Lorentz's classical formula (Append. 1.B)

response of 2 due to 1$\sim k_{12}/(\omega_2{}^2-\omega_1{}^2)=k_{12}/(k_2 - k_1)$ = -response of 1 due to 2.

So the <u>low</u>-frequency mode is mostly the <u>slow</u> pendulum swinging. The fast pendulum swing is less by a factor ($\sim S/2pE$) in (10.3.7a). But, the <u>high</u> frequency mode is mostly the <u>fast</u> pendulum-2 swinging. The slow pendulum-1 response is down by about $(-S/2pE)$ and <u>π out of phase</u>. (See (-) sign in (10.3.7b).)

For a geometric picture of the effect of reduced symmetry see Fig. 10.1.2(a) and (ab). For lower $S/|pE|$ the mode lines move away from mode axes $|+\rangle$ (low ω) or $|-\rangle$ (high ω) and toward the local axes $|x\rangle=|1\rangle$ (slow) or $|y\rangle=|2\rangle$ (fast) of individual pendulums. That is shown in Fig. 10.3.1b, too.

Low field splitting: Strong $C_2{}^B$ or weak $C_2{}^A$ symmetry and $A{\rightarrow}B$ basis change

For weak fields ($|pE|<<S$) the symmetry breaking and energy splitting is much less severe. The eigenvalue splitting is approximately quadratic or 2nd order in the field pE near the hyperbolic minima.

$$\varepsilon_{hi} = H + \sqrt{\left(pE\right)^2 + S^2} \approx H + S + \frac{\left(pE\right)^2}{2S} + \cdots \qquad (10.3.8a)$$

$$\varepsilon_{lo} = H - \sqrt{\left(pE\right)^2 + S^2} \approx H - S - \frac{\left(pE\right)^2}{2S} + \cdots \left(\text{for: } S>>pE\right) \qquad (10.3.8b)$$

At first, as pE becomes non-zero, there is little change of eigenvalues or eigenvectors. Low pE favors B-symmetry eigenvectors $|+\rangle$ and $|-\rangle$ being the basis. The d-tran (10.2.6c) does the $A{\rightarrow}B$ change of basis.

$$\begin{pmatrix} \langle+|1\rangle & \langle+|2\rangle \\ \langle-|1\rangle & \langle-|2\rangle \end{pmatrix} \begin{pmatrix} \langle1|\mathbf{H}|1\rangle & \langle1|\mathbf{H}|2\rangle \\ \langle2|\mathbf{H}|1\rangle & \langle2|\mathbf{H}|2\rangle \end{pmatrix} \begin{pmatrix} \langle1|+\rangle & \langle1|-\rangle \\ \langle2|+\rangle & \langle2|-\rangle \end{pmatrix} = \begin{pmatrix} \langle+|\mathbf{H}|+\rangle & \langle+|\mathbf{H}|-\rangle \\ \langle-|\mathbf{H}|+\rangle & \langle-|\mathbf{H}|-\rangle \end{pmatrix} \qquad (10.3.9a)$$

$$\begin{pmatrix} 1/\sqrt{2} & 1/\sqrt{2} \\ 1/\sqrt{2} & -1/\sqrt{2} \end{pmatrix} \begin{pmatrix} H - pE & -S \\ -S & H + pE \end{pmatrix} \begin{pmatrix} 1/\sqrt{2} & 1/\sqrt{2} \\ 1/\sqrt{2} & -1/\sqrt{2} \end{pmatrix} = \begin{pmatrix} H - S & -pE \\ -pE & H + S \end{pmatrix} \qquad (10.3.9b)$$

Note that field energy pE and tunneling energy S switch places. Now (10.3.8) are perturbations of $H{\pm}S$ values due to an off-diagonal component $-pE$. In A-bases, tunneling energy $-S$ perturbs $H{\pm}pE$ values.

(b) Ammonia (NH$_3$) maser

If you imagine the ε *vs.* pE hyperbolas in Fig. 10.3.1 are effectively potential energy curves it is possible to understand how the first MASER (Microwave Amplification by Stimulated Excitation of Radiation) was made. To obtain a population of predominately excited ammonia (NH$_3$) molecules, Charles Townes and co-workers put a hot beam of NH$_3$ through a non-uniform electric field that acted as a sorter that distinguished which states belonged to one or the other of the two hyperbolic "potential" energies.
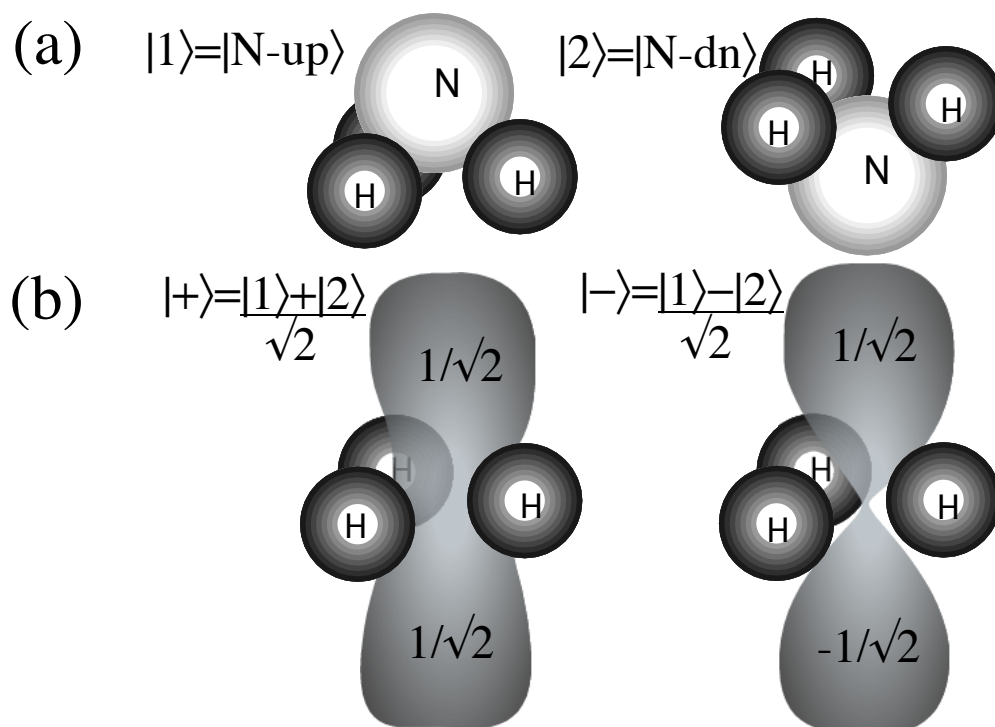
Fig. 10.3.2 Ammonia (NH$_3$) inversion states (a) Base states (b) C$_2$-Eigenstates

The NH$_3$ molecule can be viewed as a $C_2{}^B$-symmetric two-state system in which the N-atom has two possible position base states $|1\rangle = |N\text{-up}\rangle$ and $|2\rangle = |N\text{-dn}\rangle$ wherein the N-atom resides on one or the other side of the H$_3$ plane as shown below in Fig. 10.3.2a. It is assumed that the system has a bilateral $C_2{}^B$-reflection symmetry about the H$_3$ plane.

Ammonia is a peculiar "fluxional" molecule that won't "stick" to one side or another, that is, it has states $|1\rangle = |N\text{-up}\rangle$ and $|2\rangle = |N\text{-dn}\rangle$ are not stationary states. In fact if NH$_3$ were to start out in state $|1\rangle = |N\text{-up}\rangle$ it would "beat" or "tunnel" up and down between state $|1\rangle$ and state $|2\rangle = |N\text{-down}\rangle$ with a beat or transition frequency of 24 GHz. This is analogous to the beat oscillations between $X=x_1$ and $Y=x_2$ in Fig. 10.2.6 and Fig. 9.4.1. It might oscillate like this forever. However, it is a tiny charged dipole coupled to the electromagnetic field as we'll study later. While oscillating its charge, it behaves like a tiny microwave antenna broadcasting at the transition frequency. After billions of cycles it finally must "damp out" to a stationary eigenstate $|\varepsilon_{lo}\rangle = |+\rangle$, that is, it decays to its ground state emitting a 24 GHz photon.

For zero or low E-field the molecules start out in one of two inversion eigenstates $|\varepsilon_{lo}\rangle = |+\rangle$ and $|\varepsilon_{hi}\rangle = |-\rangle$ sketched in Fig. 10.3.2b. The temperature and statistical mechanics determine how many of each. The hotter the beam is, the more nearly the excited $|\varepsilon_{hi}\rangle$ state population will become equal to unexcited ground $|\varepsilon_{lo}\rangle$ state population.

Eigenstates are made of 50-50 (or $1/\sqrt{2}, \pm 1/\sqrt{2}$) combinations of $|1\rangle = |N\text{-up}\rangle$ and $|2\rangle = |N\text{-dn}\rangle$ exactly like the $C_2{}^B$ prototypes in (10.2.6). In other words, the N-atom is "fuzzed-out" so it has the same probability of being found on either side of the H$_3$ plane, and the same or opposite quantum phase. These two states are analogous to the normal modes (+) and (−) in Fig. 10.2.4a and b, respectively.

As the beam of $|\varepsilon_{lo}\rangle=|+\rangle$ and $|\varepsilon_{hi}\rangle=|-\rangle$ molecules enters a non-uniform field the excited $|\varepsilon_{hi}\rangle=|-\rangle$ state molecules fall away from the strong field because they are on the upper branch of the hyperbola in Fig. 10.3.1 and can get to lower energy by heading for the ($pE=0$) point. They become separated from ground state ($|\varepsilon_{lo}\rangle=|+\rangle$)-molecules that gain kinetic energy by "gravitating" toward high field.

This makes it possible to cull out particles in the $|\varepsilon_{hi}\rangle=|-\rangle$ state. The excited output is fed into a cavity tuned to the 24 GHz transition "broadcast" frequency which has a wavelength of 1.25 cm. , and it begins to resonate strongly and coherently. And so, the laser (and kitchen microwave) revolution began!

C_2^{AB} Symmetry : Weyl reflections

The symmetry of a Stark Hamiltonian matrix with $A{\neq}D$ might not be as obvious as the C_2^{B} symmetry of an **H**-matrix with $A{=}D$. However, if you look again at the normal coordinate axes of the C_2^{B} modes in Fig. 10.1.2b you can see they are rotations of the original Cartesian xy-axes in Fig. 10.1.2a by an angle $\phi=45°$. The normal coordinate axes of the "symmetry-broken" modes in Fig. 10.1.2ab are rotations of the original base states in Fig. 10.1.2a by some other angle $\phi=\beta/2$ that is less than $45°$. In fact, each set of axes pictured in Figs. 10.1.2 (a), (ab), and (b) has its own reflection symmetry operator σ_A, σ_{AB}, and σ_B, respectively, and each is related to the other by rotational transformation.

We have used the bilateral reflection σ_B given by (10.2.3b) to switch x-axes with y-axes. The operation σ_B is a reflection through a $45°$ mirror plane lying on major axes of B-potential ellipses. ($V^B{=}const.$) As such, σ_B is a $45°$ rotation of the σ_A mirror reflection through an x-axial plane lying on major axes of A-potential ellipses ($V^A{=}const.$) in Fig. 10.1.2.

$$\sigma_A = \begin{pmatrix} 1 & 0 \\ 0 & -1 \end{pmatrix} \qquad (10.3.9a)$$

$$\sigma_B \quad = \quad R[\tfrac{\pi}{4}] \qquad \sigma_A \qquad R^{\dagger}[\tfrac{\pi}{4}] \quad = \quad R[45°] \qquad \sigma_A \qquad R[-45°]$$

$$\begin{pmatrix} 0 & 1 \\ 1 & 0 \end{pmatrix} = \begin{pmatrix} \cos\tfrac{\pi}{4} & -\sin\tfrac{\pi}{4} \\ \sin\tfrac{\pi}{4} & \cos\tfrac{\pi}{4} \end{pmatrix}\begin{pmatrix} 1 & 0 \\ 0 & -1 \end{pmatrix}\begin{pmatrix} \cos\tfrac{\pi}{4} & \sin\tfrac{\pi}{4} \\ -\sin\tfrac{\pi}{4} & \cos\tfrac{\pi}{4} \end{pmatrix} = \begin{pmatrix} \tfrac{1}{\sqrt{2}} & \tfrac{-1}{\sqrt{2}} \\ \tfrac{1}{\sqrt{2}} & \tfrac{1}{\sqrt{2}} \end{pmatrix}\begin{pmatrix} 1 & 0 \\ 0 & -1 \end{pmatrix}\begin{pmatrix} \tfrac{1}{\sqrt{2}} & \tfrac{1}{\sqrt{2}} \\ \tfrac{-1}{\sqrt{2}} & \tfrac{1}{\sqrt{2}} \end{pmatrix} \qquad (10.3.9b)$$

The matrices σ_A and σ_B are two real *Hamilton-Pauli-Jordan spinor operators*. (The third σ_C operator is the complex one.) The reflections σ_A and σ_B do so-called *Weyl reflections* after the famous theorist Hermann Weyl. Moving the rotations to the left side gives a diagonalization of σ_B and $\mathbf{H}^B$.

$$\begin{pmatrix} \tfrac{1}{\sqrt{2}} & \tfrac{1}{\sqrt{2}} \\ \tfrac{-1}{\sqrt{2}} & \tfrac{1}{\sqrt{2}} \end{pmatrix}\begin{pmatrix} 0 & 1 \\ 1 & 0 \end{pmatrix}\begin{pmatrix} \tfrac{1}{\sqrt{2}} & \tfrac{-1}{\sqrt{2}} \\ \tfrac{1}{\sqrt{2}} & \tfrac{1}{\sqrt{2}} \end{pmatrix} = \begin{pmatrix} 1 & 0 \\ 0 & -1 \end{pmatrix}, \quad \text{and:} \quad \begin{pmatrix} \tfrac{1}{\sqrt{2}} & \tfrac{1}{\sqrt{2}} \\ \tfrac{-1}{\sqrt{2}} & \tfrac{1}{\sqrt{2}} \end{pmatrix}\begin{pmatrix} A & B \\ B & A \end{pmatrix}\begin{pmatrix} \tfrac{1}{\sqrt{2}} & \tfrac{-1}{\sqrt{2}} \\ \tfrac{1}{\sqrt{2}} & \tfrac{1}{\sqrt{2}} \end{pmatrix} = \begin{pmatrix} A+B & 0 \\ 0 & A-B \end{pmatrix}$$

(10.3.9c)

This is like d-tran (10.2.6c) except it is done here by a rotation **R**[-45°] instead of a reflection through the *22.5°* plane that is what we unknowingly wrote down in (10.2.6a). How can this be understood?

To understand this we need a couple of lessons from this elementary introduction of Weyl and Hamilton operations. First, as seen first in (10.1.7), all **H**-matrices are made of "pieces" of their symmetry groups. (It's true whether or not we can easily see it!) Here, $\mathbf{H}^B$ is made of C_2^B "pieces" **1** and σ_B.

$$\mathbf{H}^B = A \cdot \mathbf{1} + B \cdot \sigma_B, \quad \text{or:} \quad \begin{pmatrix} A & B \\ B & A \end{pmatrix} = A \begin{pmatrix} 1 & 0 \\ 0 & 1 \end{pmatrix} + B \begin{pmatrix} 0 & 1 \\ 1 & 0 \end{pmatrix}$$

Rotation $\mathbf{R}[-45°]$ diagonalizes σ_B and $\mathbf{H}^B$. A $\phi=22.5°$ mirror reflection can do it, too, as in Fig. 10.3.3a.
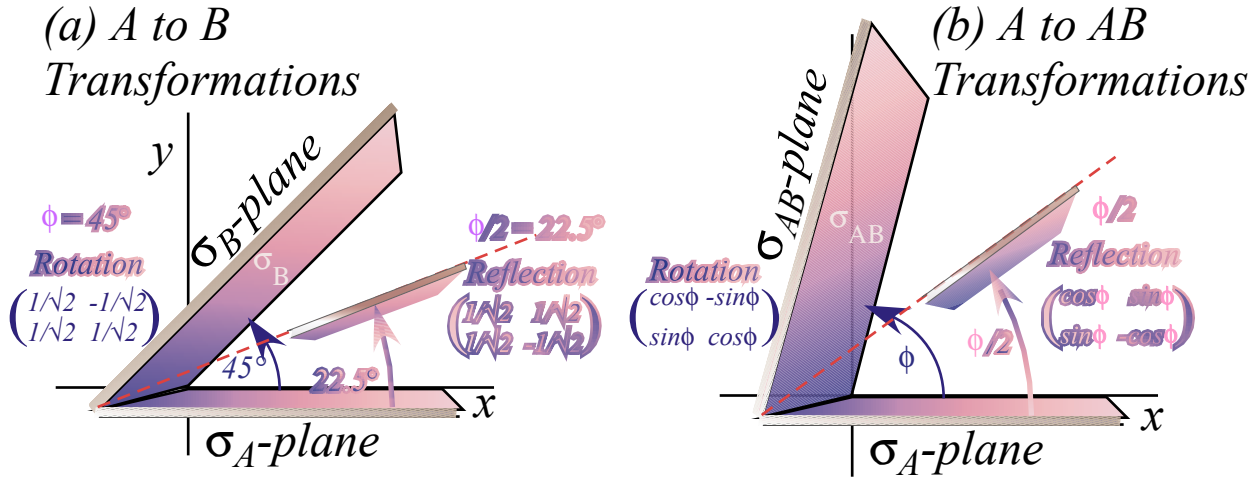
Fig. 10.3.3 Rotations and reflections that convert σ_A into (a) σ_B, (b) σ_{AB}

Generalizing (10.3.9c) for a rotation by angle $\phi=\beta/2$ yields a general ϕ-tipped σ_{AB} plane-reflection.

$$\begin{array}{ccccc} \mathbf{R}[\phi] & \sigma_A & \mathbf{R}^\dagger[\phi] & = & \sigma_{AB} & = \sigma[\phi \; tipped \; plane] \end{array}$$

$$\begin{pmatrix} \cos\phi & -\sin\phi \\ \sin\phi & \cos\phi \end{pmatrix} \begin{pmatrix} 1 & 0 \\ 0 & -1 \end{pmatrix} \begin{pmatrix} \cos\phi & \sin\phi \\ -\sin\phi & \cos\phi \end{pmatrix} = \begin{pmatrix} \cos^2\phi - \sin^2\phi & 2\sin\phi\cos\phi \\ 2\sin\phi\cos\phi & -\cos^2\phi + \sin^2\phi \end{pmatrix} = \begin{pmatrix} \cos2\phi & \sin2\phi \\ \sin2\phi & -\cos2\phi \end{pmatrix} \quad (10.3.10a)$$

This shows we can bring a ϕ-tipped AB-plane parallel to the x-plane in two ways. We can do a rotation $\mathbf{R}[-\phi]$ that "untips" by angle $-\phi=-\beta/2$ or we can perform a reflection through a mirror plane that is tipped by $\phi/2=\beta/4$ half-way between the x-plane and the AB-plane. Here is the latter.

$$\begin{array}{cccc} \sigma[\beta/4 \; tipped \; plane] & \cdot \sigma[\beta/2 \; tipped \; plane] \cdot & \sigma[\beta/4 \; tipped \; plane] & = \sigma_A \end{array}$$

$$\begin{pmatrix} \cos\beta/2 & \sin\beta/2 \\ \sin\beta/2 & -\cos\beta/2 \end{pmatrix} \cdot \begin{pmatrix} \cos\beta & \sin\beta \\ \sin\beta & -\cos\beta \end{pmatrix} \cdot \begin{pmatrix} \cos\beta/2 & \sin\beta/2 \\ \sin\beta/2 & -\cos\beta/2 \end{pmatrix} = \begin{pmatrix} 1 & 0 \\ 0 & -1 \end{pmatrix} \quad (10.3.10b)$$

This transformation then also diagonalizes the general $\mathbf{H}^{AB}$ matrix made of C_2^{AB} "pieces" **1** and σ_{AB}.

$$\mathbf{H}^{AB} = \frac{A+D}{2} \cdot \mathbf{1} + \frac{A-D}{2}\sigma_A + B \cdot \sigma_B, \quad \begin{pmatrix} A & B \\ B & D \end{pmatrix} = \frac{A+D}{2} \begin{pmatrix} 1 & 0 \\ 0 & 1 \end{pmatrix} + \frac{A-D}{2} \begin{pmatrix} 1 & 0 \\ 0 & -1 \end{pmatrix} + B \begin{pmatrix} 0 & 1 \\ 1 & 0 \end{pmatrix} \quad (10.3.11a)$$

$$\mathbf{H}^{AB} = \frac{A+D}{2} \cdot \mathbf{1} + k_{ABD} \cdot \sigma_{AB}, \quad \begin{pmatrix} A & B \\ B & D \end{pmatrix} = \frac{A+D}{2} \begin{pmatrix} 1 & 0 \\ 0 & 1 \end{pmatrix} + k_{ABD} \begin{pmatrix} \cos\beta & 0 \\ 0 & -\cos\beta \end{pmatrix} + k_{ABD} \begin{pmatrix} 0 & \sin\beta \\ \sin\beta & 0 \end{pmatrix}$$

$$k_{ABD}\cos\beta = \frac{A-D}{2}, \quad k_{ABD}\sin\beta = B, \quad \text{or:} \quad \beta = \text{ATAN2}\left(B, \frac{A-D}{2}\right) \quad (10.3.11b)$$

Then tipping angle $\phi=\beta/2$ of the normal coordinate axes is found from the parameters A, B, and D.

This is a shortcut to solving $\mathbf{H}^{AB}$ eigenvalues and eigenvectors. It generalizes to $U(2)$ "spin" in Section 10.5.

Unitary U(2) versus Special Unitary SU(2)

Before continuing, we should elaborate on some fine points and terminology. In Sec. 2.2 (d) and (e) we introduced the *unitary group U(n)* of operators **U** that satisfy *unitarity* (**U**†**U**=**1**) and its subgroup called the *special unitary group SU(n)* which had an additional requirement of *unimodularity*. (*det*|**U**|=*1*)

Note that rotational operators like **R**[-45°] belong to *SU(2)* while reflection operators like σ$_{AB}$ belong to *U(2)* (σ†σ=σσ=**1**) but not *SU(2)* because σ's have (-1) determinants. (*det*|σ|=-1) Mirror reflections change left handed gloves into right handed ones. Since two reflections through the same mirror is an identity operation (σσ=**1**) it follows that reflections are both Hermitian (σ†=σ) and unitary (σ†σ=**1**). In some sense they are the most "perfectly normal" operators.

If you multiply two members of *SU(2)* the product has to be an *SU(2)* member, too. (Closure axiom) So, products of rotations can never yield a reflection. However, the product of two reflections will have a positive unit determinant, in fact, it will be a rotation. This is easily see by an example that multiplies *x*-plane reflection σ$_A$ in (10.2.13a) by an *AB*-plane or ϕ-tipped reflection σ$_{AB}$ in (10.2.14a) .

$$\sigma\big[\phi\ tipped\ plane\big]\ \cdot\ \ \sigma_A\ \ =\ \ \ \ R\big[2\phi\big]\ \ \ \ \ \ ,\ or:\ \ \ \ \sigma_A\ \ \cdot\ \sigma\big[\phi\ tipped\ plane\big]\ =\ \ R\big[-2\phi\big]$$

$$\begin{pmatrix} \cos 2\phi & \sin 2\phi \\ \sin 2\phi & -\cos 2\phi \end{pmatrix}\begin{pmatrix} 1 & 0 \\ 0 & -1 \end{pmatrix} = \begin{pmatrix} \cos 2\phi & -\sin 2\phi \\ \sin 2\phi & \cos 2\phi \end{pmatrix},\ or:\ \begin{pmatrix} 1 & 0 \\ 0 & -1 \end{pmatrix}\begin{pmatrix} \cos 2\phi & \sin 2\phi \\ \sin 2\phi & -\cos 2\phi \end{pmatrix} = \begin{pmatrix} \cos 2\phi & \sin 2\phi \\ -\sin 2\phi & \cos 2\phi \end{pmatrix} \quad (10.3.12)$$

In other words, rotations are composed of reflections, and not vice-versa. The σ's are more fundamental than the **R**'s. In some sense reflections are "square roots" of rotations. One only needs half the angle ϕ=β/2 to do the job that a full angle 2ϕ=β rotation would need. As seen in (10.3.10) a pair of mirror planes separated by angle ϕ=β/2 will perform a rotation by either β or -β , depending on the order of action.

Complete sets of commuting operators

One may turn the discussion of symmetry inside-out by asking what are <u>all</u> the operators **Q** that commute with a given **H**-matrix (or set of commuting **H**-matrices). Spectral decomposition gives the answers to such questions, for if **P**$_k$ are the irreducible projectors of **H** (or set of **H**'s) then the answer is

$$\mathbf{Q} = \Sigma\ \alpha_k\ \mathbf{P}_k\ (= \alpha_1\ \mathbf{P}_1\ + \alpha_2\ \mathbf{P}_2\ ,\ \text{for 2-by-2}\ \mathbf{Q}) \qquad\qquad (10.3.13a)$$

for arbitrary complex numbers α_k . If you further restrict **Q** to be unitary (in *U(n)*) then the answer is

$$\mathbf{Q} = \Sigma\ e^{i\alpha_k}\ \mathbf{P}_k\ (= e^{i\alpha_1}\ \mathbf{P}_1\ + e^{i\alpha_2}\ \mathbf{P}_2\ ,\ \text{for 2-by-2}\ \mathbf{Q}) \qquad (10.3.13b)$$

for arbitrary <u>real</u> numbers α_k . Finally, if you want **Q** to be unimodular (in *SU(n)*), too, then the answer is

$$\mathbf{Q} = \Sigma\ e^{i\alpha_k}\ \mathbf{P}_k\ (= e^{-i\alpha}\mathbf{P}_1\ + e^{i\alpha}\mathbf{P}_2\ \text{for 2-by-2}\ \mathbf{Q}) \qquad\qquad (10.3.13c)$$

where angles in exponents must sum to zero or multiples of 2π. (Σα$_k$ = *2πn*)

For example, the *SU(2)* symmetry operators that commute with **H**^{B} must be of the form

$$\mathbf{Q} = \frac{e^{-i\chi}}{2}\begin{pmatrix} 1 & 1 \\ 1 & 1 \end{pmatrix} + \frac{e^{i\chi}}{2}\begin{pmatrix} 1 & -1 \\ -1 & 1 \end{pmatrix} = \begin{pmatrix} \cos\chi & -i\sin\chi \\ -i\sin\chi & \cos\chi \end{pmatrix} = \mathbf{R}_B(\chi) \qquad\qquad (10.3.14)$$

In other words, the only <u>rotations</u> that commute with **H**^{B} are imaginary or complex. It turns out these are representations of Lorentz transformations that provide a relativistic theory of polarization.

10.4 Mixed **A****B****C****D** *Symmetry: U(2) quantum systems*

With no symmetry restrictions the U(2) modes or eigenstates assume a general nondescript form of *conjugate elliptical polarization*. An example in Fig. 10.4.1 shows results of competition between all three archetypes of the asymmetric (*A*), bilateral (*B*), and circular (*C*) types of symmetry described previously.
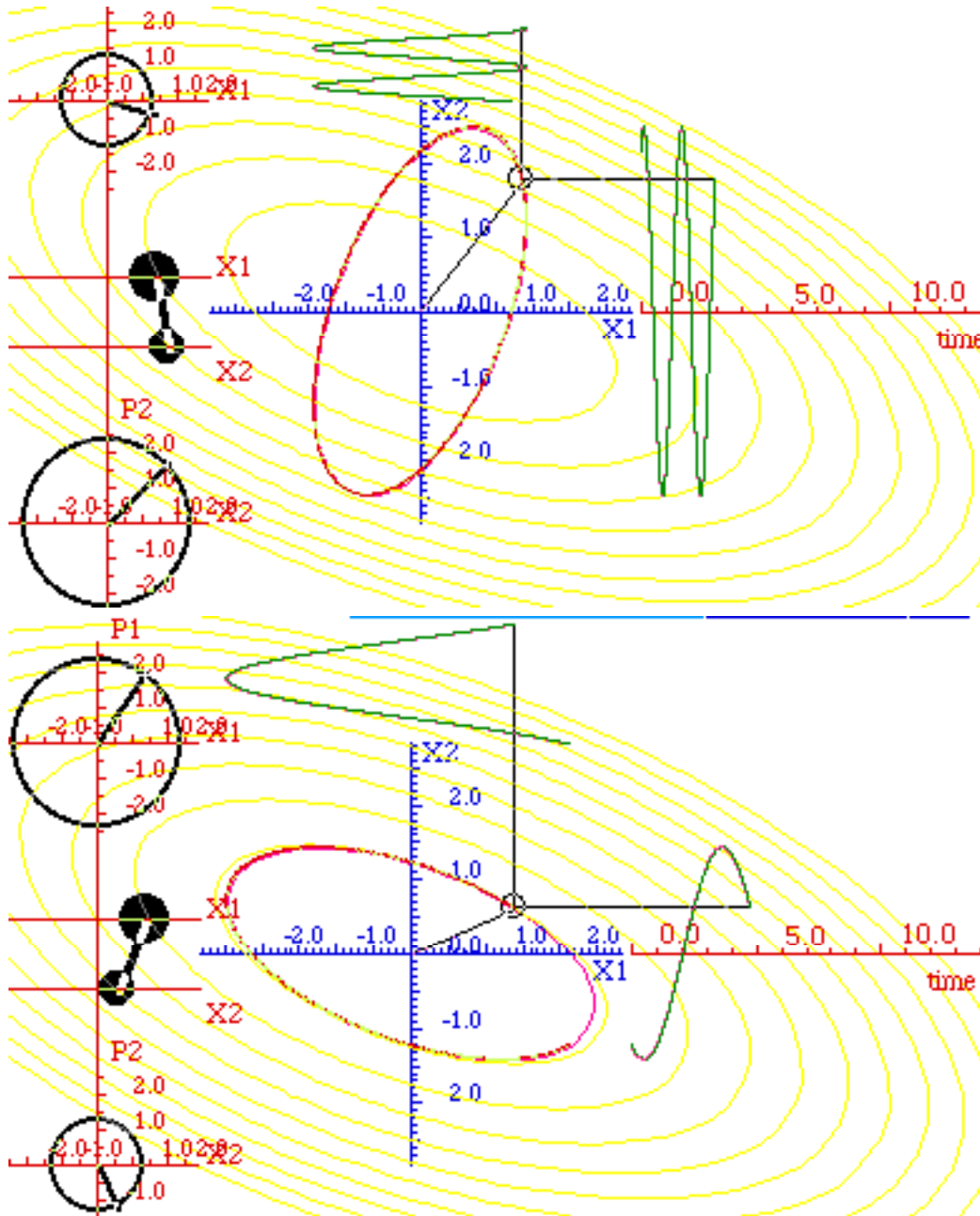
Fig.10.4.1 Typical asymmetric elliptical modes. (A=4.1, B= 0.67, C=1.16, D=3.3)

The types of general 2-state Hamiltonian matrix 10.1.1b discussed so far have involved varying the parameters *A*, *B*, and *D* while parameter *C* is set to zero. If *A=D* then bilateral C_2^B-symmetry is present and parameter *B=-S* determines *tunneling splitting*. If *pE=|A-D|>0* then bilateral C_2^B-symmetry changes to C_2^{AB}-symmetry and *second order Stark splitting* occurs. If *pE* grows so *|A-D|>>B* then parameter *B* becomes

irrelevant and asymmetric-diagonal $C_2{}^A$-symmetry takes effect. The parameter $pE=|A-D|$ for $C_2{}^A$-symmetry determines *first order Stark splitting*. Adding the circular $C_2{}^C$-symmetry makes ellipses.

(a) ABC Symmetry catalog: Standing, moving, or galloping waves

Let us review the archetypes $C_2{}^A$, $C_2{}^B$ and $R(2) \supset C_2{}^C$ symmetry using one-dimensional plane waves or Bohr orbitals (7.1.10) as the base states of a *U(2)* two-state system, and compare that to the coupled-oscillator and optical polarization analogies. Various symmetries are summarized in Fig. 10.4.2.

A, B, and AB-Archetypes are standing waves (Linear polarization)

Asymmetric $C_2{}^A$ systems discussed in 10.2(a) have x-plane $|x_1\rangle$ and y-plane $|x_2\rangle$ modes. These are analogous to a pair of cosine and sine Bohr orbital $|c\rangle$ and $|s\rangle$ *standing waves*. The symmetry operation of reflection σ_A through *x=0* (that is *x→-x*) gives a positive eigenvalue (+1) for symmetric cosine function $\langle x|c\rangle$ and a negative (-1) value for anti symmetric sine wave $\langle x|s\rangle$.

$$\langle x|c\rangle = \cos mx = \cos\text{-}mx =+ \langle -x|c\rangle , \quad \langle x|s\rangle = \sin mx = \text{-}\sin\text{-}mx = -\langle -x|s\rangle \qquad (10.4.1a)$$

Taking (cos ϕ, sin ϕ) combinations of (10.4.1a) gives states of $C_2{}^{AB}$ *systems* discussed in 10.2ab.

$$\langle x|+\rangle = \cos \phi \cos mx + \sin \phi \sin mx \qquad\qquad \langle x|-\rangle = \text{-}\sin \phi \cos mx + \cos \phi \sin mx$$
$$= \cos (mx - \phi) \qquad\qquad\qquad\qquad\qquad = \sin (mx - \phi) \qquad (10.4.1b)$$

These are *standing* waves, too. However, their nodes are shifted by angle ϕ to accommodate a new origin and symmetry plane at *x=ϕ/m*. Weak *D*-field or strong *B*-coupling shifts angle toward $\phi = \pm 45°$ of *bilateral symmetric $C_2{}^B$ system* coupled modes. The *decoupled* system is a $C_2{}^A$ *system* with $|x_1\rangle$, $|x_2\rangle$ bases. Decoupling is encouraged by applying a strong *polar vector field* like a Stark electric *pE* field.

C-Archetypes are moving waves (Circular polarization)

The opposite to the standing-wave systems is the *chiral or circularly symmetric $R^C(2)$ or $C_\infty{}^C$ system* with left handed and right handed modes $|R\rangle$ and $|L\rangle$. For the Bohr orbitals $|R\rangle$ and $|L\rangle$ correspond to positive and negative exponential *moving* waves, respectively. These involve <u>complex</u> combinations.

$$\langle x|R\rangle = e^{+imx} = \cos mx + i \sin mx \qquad\qquad \langle x|L\rangle = e^{-imx} = \cos mx - i \sin mx \qquad (10.4.2)$$

A symmetry reduction of *U(2)* to $R^C(2)$ is caused by an *axial vector field* like a Zeeman magnetic **B** field or a rotational velocity vector axis Ω. It is sometimes called "gauge symmetry" breaking.

....All others are galloping waves (Elliptical polarization)

The general Hamiltonian is labeled as a *C_1 system*, that is, *no symmetry*. It will have eigenstates that are general linear combination of the above, that is, elliptical polarized eigenstates like Fig. 10.4.1.

$$\langle x|\Psi\rangle = a_R \langle x|R\rangle + a_L\langle x|L\rangle = a_R e^{+imx} + a_L e^{-imx} \qquad (10.4.3)$$

In other words, the vast majority of "nondescript" or asymmetric eigenstates are simply the *galloping waves* we introduced Chapter 4. (Fig. 4.2.6) The galloping phase velocity noticed there is related to the polar angle of the elliptic orbit. As the ellipse becomes more eccentric, that is, more like a standing wave states *A*, *B*, or *AB*, the polar angle has to gallop more and more rapidly at the passage of the minor axis. To conserve angular momentum it "gallops" faster at lesser radius and is faster at an orbital perigee than at an apogee. Newton and Kepler were first to note that Coulomb orbits sweep out equal area in equal time, but the same is true of any central force orbit including the isotropic harmonic oscillator which is a full *U(2) symmetric system*. (Recall Fig. 4.2.6b and Fig. 4.2v8.)

Fighting rotational isotropy are the anisotropic (Stark-like) non-central "tensor" $C_2{}^{AB}$-symmetry-breaking forces. The A, B, or AB Hamiltonians do not conserve angular momentum and try to stretch orbits along certain directions and away from their circular $R(2)$ symmetric shape. The compromise is elliptical or galloping eigenstates such as are pictured in Fig. 10.4.1. Rotational $R(2) \supset C_2{}^C$ symmetry is the mortal enemy of "tensor" $C_2{}^{AB}$-symmetries, a yin-and-yang that live together as *subgroups* in the encompassing quantum operator group $U(2)$ of a 2-state system.

With isotropic $U(2)$-symmetry all possible ellipses of any tipping or ratio or handedness are degenerate eigenstates. This is the case listed in the first column on the extreme lefthand side of Fig. 10.4.2. Then and only then do all four operators $\{\sigma_1, \sigma_A, \sigma_B, \sigma_C\}$ or all four quaternions $\{\mathbf{1}, \mathbf{i}, \mathbf{j}, \mathbf{k}\}$ or all four elementary operators $\{\mathbf{e}_{11}, \mathbf{e}_{12}, \mathbf{e}_{21}, \mathbf{e}_{22}\}$ commute with the Hamiltonian which is necessarily reduced to a constant H times a unit-$\mathbf{1}$ matrix. All vectors are eigenstates of such an operator.

$$\mathbf{H}^{U(2)} = H\,\mathbf{1} = H\sigma_1 = H(\mathbf{e}_{11} + \mathbf{e}_{22}) \tag{10.4.4}$$

(b) General H$_{ABCD}$ eigenvalues

The opposite extreme portrayed on the extreme right hand side of Fig. 10.4.2, is a Hamiltonian with no apparent symmetry in which all parameters A, B, C, and D are allowed.

$$\mathbf{H} = \frac{A+D}{2}\begin{pmatrix} 1 & 0 \\ 0 & 1 \end{pmatrix} + B\begin{pmatrix} 0 & 1 \\ 1 & 0 \end{pmatrix} + C\begin{pmatrix} 0 & -i \\ i & 0 \end{pmatrix} + \frac{A-D}{2}\begin{pmatrix} 1 & 0 \\ 0 & -1 \end{pmatrix} \tag{10.4.5a}$$

$$\mathbf{H} = \frac{A+D}{2}\ \ \sigma_1\ \ + B\ \ \sigma_B\ \ + C\ \ \sigma_C\ \ + \frac{A-D}{2}\ \ \sigma_A$$

Being made of all four $\{\sigma_1, \sigma_A, \sigma_B, \sigma_C\}$ guarantees $\mathbf{H}$ will commute only with the unit operator itself. Eigenstates are detemined by values of parameters A, B, C, and D. Any *single* operator of the form (10.4.5a) can be diagonalized and represented in its (own) eigen-basis as follows.

$$\mathbf{H} = \frac{A+D}{2}\begin{pmatrix} 1 & 0 \\ 0 & 1 \end{pmatrix} + H_{ABCD}\begin{pmatrix} 1 & 0 \\ 0 & -1 \end{pmatrix} \tag{10.4.5b}$$

$$\mathbf{H} = \frac{A+D}{2}\ \ \sigma_1\ \ \ + H_{ABCD}\ \ \ \sigma_{ABCD}$$

The constant H_{ABCD} is a Pythagorean sum and σ_{ABCD} is a reflection operator with (± 1)-eigenvalues.

$$\pm H_{ABCD} = \pm\sqrt{\left(\frac{A-D}{2}\right)^2 + B^2 + C^2} \tag{10.4.5c}$$

The combination operator σ_{ABCD} defined as follows

$$\sigma_{ABCD} = \frac{B}{H_{ABCD}}\sigma_B\ \ + \frac{C}{H_{ABCD}}\ \sigma_C\ \ + \frac{A-D}{2H_{ABCD}}\sigma_A \tag{10.4.5d}$$

is a reflection symmetry $(\sigma_{ABCD})^2 = \mathbf{1}$ because of the $\{\sigma_1, \sigma_A, \sigma_B, \sigma_C\}$-multiplication rules.

$$\sigma_A\sigma_B = -\sigma_B\sigma_A = \sigma_C\,, \qquad \sigma_B\sigma_C = -\sigma_C\sigma_B = \sigma_A\,, \quad \sigma_C\sigma_A = -\sigma_A\sigma_C = \sigma_B\,, \qquad \sigma_A{}^2 = \sigma_B{}^2 = \sigma_C{}^2 = \mathbf{1} \tag{10.4.6}$$

A generalization of the AB solution (10.3.11) results. Eigenvectors are discussed in Sec. 10.5.

Catalog of Two - State Hamiltonians

$H = H^\dagger =$	$H_{U(2)} =$ $\begin{pmatrix} A & 0 \\ 0 & A \end{pmatrix}$	$H_{C_2^A} =$ $\begin{pmatrix} A & 0 \\ 0 & D \end{pmatrix}$	$H_{C_2^{AB}} =$ $\begin{pmatrix} A & B \\ B & D \end{pmatrix}$	$H_{C_2^B} =$ $\begin{pmatrix} A & B \\ B & A \end{pmatrix}$	$H_{C_2^C} =$ $\begin{pmatrix} A & -iC \\ iC & A \end{pmatrix}$	$H_{C_1} =$ $\begin{pmatrix} A & B-iC \\ B+iC & D \end{pmatrix}$
Commute with :	$U =$ $\begin{pmatrix} U_{11} & U_{12} \\ U_{21} & U_{22} \end{pmatrix}$	$R(\theta) =$ $\begin{pmatrix} e^{-i\theta} & 0 \\ 0 & e^{i\theta} \end{pmatrix}$	$R(\zeta) =$ $\begin{pmatrix} \cos\zeta & -is\sin\zeta \\ -ic\sin\zeta & \\ & \cos\zeta \\ -is\sin\zeta & +ic\sin\zeta \end{pmatrix}$	$R(\chi) =$ $\begin{pmatrix} \cos\chi & -i\sin\chi \\ -i\sin\chi & \cos\chi \end{pmatrix}$	$R(\varphi) =$ $\begin{pmatrix} \cos\varphi & -\sin\varphi \\ \sin\varphi & \cos\varphi \end{pmatrix}$	$\mathbf{1}(\lambda) =$ $e^{i\lambda}\begin{pmatrix} 1 & 0 \\ 0 & 1 \end{pmatrix}$
Generated by :	$e_{11} = \begin{pmatrix} 1 & 0 \\ 0 & 0 \end{pmatrix}$ $e_{12} = \begin{pmatrix} 0 & 1 \\ 0 & 0 \end{pmatrix}$ $e_{21} = \begin{pmatrix} 0 & 0 \\ 1 & 0 \end{pmatrix}$ $e_{22} = \begin{pmatrix} 0 & 0 \\ 0 & 1 \end{pmatrix}$	$G_A =$ $\left.\dfrac{d R(\theta)}{d\theta}\right|_0 =$ $\begin{pmatrix} -i & 0 \\ 0 & i \end{pmatrix}$	$G_{AB} =$ $\left.\dfrac{d R(\zeta)}{d\zeta}\right|_0 =$ $\begin{pmatrix} -ic & -is \\ -is & ic \end{pmatrix}$	$G_B =$ $\left.\dfrac{d R(\chi)}{d\chi}\right|_0 =$ $\begin{pmatrix} 0 & -i \\ -i & 0 \end{pmatrix}$	$G_C =$ $\left.\dfrac{d R(\varphi)}{d\varphi}\right|_0 =$ $\begin{pmatrix} 0 & -1 \\ 1 & 0 \end{pmatrix}$	$G_1 =$ $\left.\dfrac{d R(\lambda)}{d\lambda}\right|_0 =$ $\begin{pmatrix} 1 & 0 \\ 0 & 1 \end{pmatrix}$
Spin Operator :	*(all)*	$\sigma_A =$ $iG_A =$ $\begin{pmatrix} 1 & 0 \\ 0 & -1 \end{pmatrix}$	$\sigma_{AB} =$ $iG_{AB} =$ $\begin{pmatrix} c & s \\ s & -c \end{pmatrix}$	$\sigma_B =$ $iG_B =$ $\begin{pmatrix} 0 & 1 \\ 1 & 0 \end{pmatrix}$	$\sigma_C =$ $iG_C =$ $\begin{pmatrix} 0 & -i \\ i & 0 \end{pmatrix}$	$\sigma_0 =$ $\begin{pmatrix} 1 & 0 \\ 0 & 1 \end{pmatrix}$
Symmetry :	$U(2)$	$C_2^A \subset R^A(2)$	$C_2^{AB} \subset R^{AB}(2)$	$C_2^B \subset R^B(2)$	$C_\infty^C \subset R^C(2)$	C_1
H Eigenkets	*(Any ket is an eigenvector)*	$\|x\rangle$ $\begin{pmatrix} 1 \\ 0 \end{pmatrix}$, $\|y\rangle$ $\begin{pmatrix} 0 \\ 1 \end{pmatrix}$	$\|x'\rangle$ $\begin{pmatrix} \cos\frac{\beta}{2} \\ \sin\frac{\beta}{2} \end{pmatrix}$, $\|y'\rangle$ $\begin{pmatrix} -\sin\frac{\beta}{2} \\ \cos\frac{\beta}{2} \end{pmatrix}$	$\|(+)\rangle$ $\frac{1}{\sqrt{2}}\begin{pmatrix} 1 \\ 1 \end{pmatrix}$, $\|(-)\rangle$ $\frac{1}{\sqrt{2}}\begin{pmatrix} 1 \\ -1 \end{pmatrix}$	$\|L\rangle$ $\frac{1}{\sqrt{2}}\begin{pmatrix} 1 \\ -i \end{pmatrix}$, $\|R\rangle$ $\frac{1}{\sqrt{2}}\begin{pmatrix} 1 \\ i \end{pmatrix}$	$\|\varepsilon\rangle$ *Depends on* $A,B,C,$ *and* D
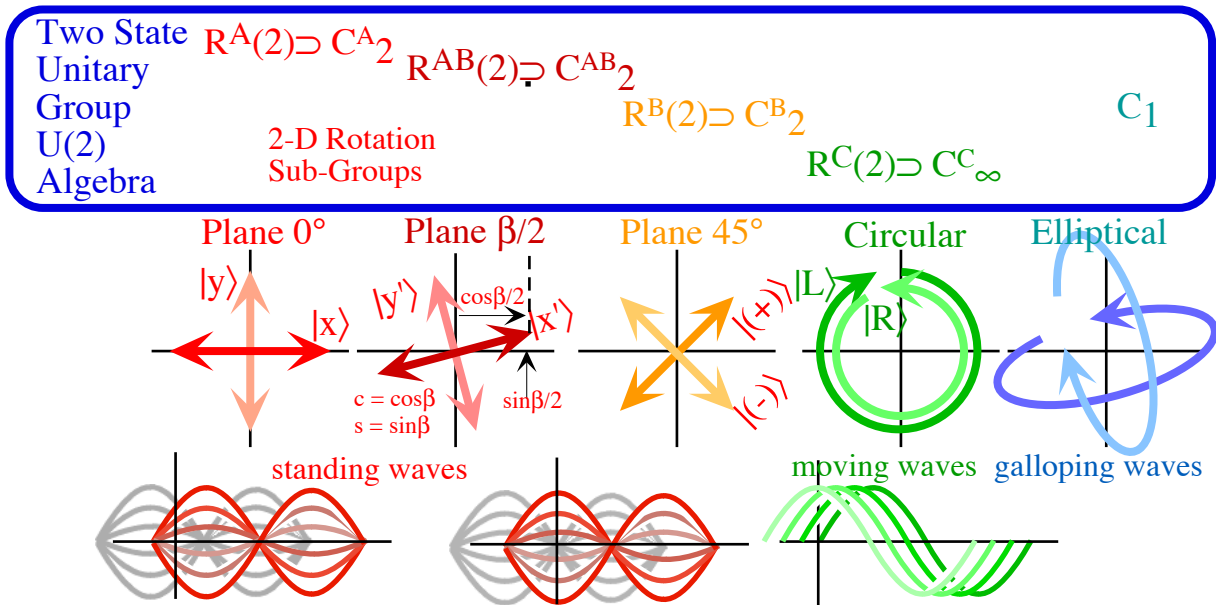
Fig. 10.4.2 Catalog of 2-state Hamiltonians, symmetry groups, eigenstates and analogs

10.5 *Spin-Vector Pictures for Two-State Quantum Systems*

Our most common atomic "particles" are the electron with its 2-component *(up,dn)* spin-$\hbar/2$ and the photon with its two-component *(x,y)* polarization. Then there is the NH_3 inversion states *(UP,DN)* that gave us the laser revolution. These three are summarized in Fig. 10.5.1. Add to these the 2-component Bohr-waves or spins of neutrinos, neutrons, protons, quarks, etc.; it appears that our world is lousy with *U(2)* objects! We need ways to picture them. Here we introduce another way called the *spin-vector*.

(a) Electron Spin-1/2-Polarization

Spin-up
$|1\rangle=|\uparrow\rangle$

Spin-dn
$|2\rangle=|\downarrow\rangle$

$$|\chi\rangle=\begin{pmatrix}\chi\uparrow\\\\\chi\downarrow\end{pmatrix}=\begin{pmatrix}\langle\uparrow|\chi\rangle\\\\\langle\downarrow|\chi\rangle\end{pmatrix}=\begin{pmatrix}\text{circle }p_1=\text{Im }\chi_1,\;x_1=\text{Re }\chi_1\\\\p_2,\;x_2\end{pmatrix}$$

$$=|\uparrow\rangle\langle\uparrow|\Psi\rangle+|\downarrow\rangle\langle\downarrow|\Psi\rangle$$
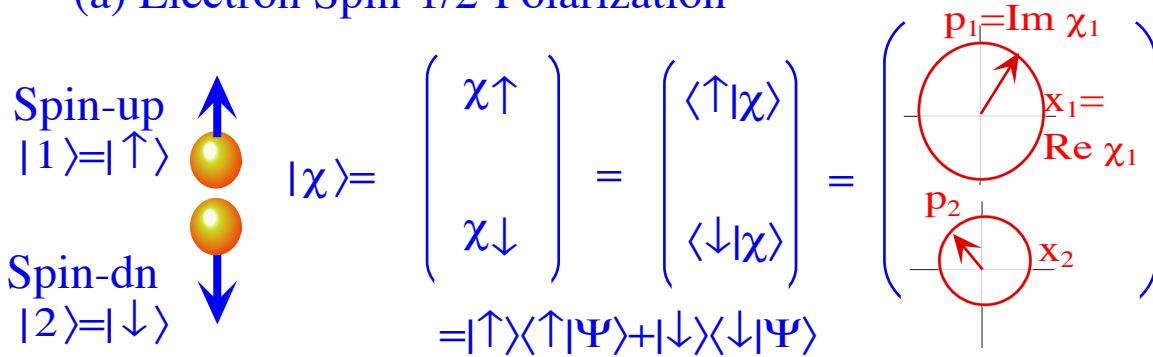
(b) Photon Spin-1-Polarization

Plane-x
$|1\rangle=|x\rangle$

Plane-y
$|2\rangle=|y\rangle$

$$|\psi\rangle=\begin{pmatrix}\psi_x\\\\\psi_y\end{pmatrix}=\begin{pmatrix}\langle x|\psi\rangle\\\\\langle y|\psi\rangle\end{pmatrix}=\begin{pmatrix}p_x,\;x\\\\p_y,\;y\end{pmatrix}$$

$$=|x\rangle\langle x|\psi\rangle+|y\rangle\langle y|\psi\rangle$$

(c) Ammonia (NH_3) Inversion States

N-UP
$|1\rangle=|UP\rangle$

N-DN
$|2\rangle=|DN\rangle$

$$|\nu\rangle=\begin{pmatrix}\nu_{UP}\\\\\nu_{DN}\end{pmatrix}=\begin{pmatrix}\langle UP|\nu\rangle\\\\\langle DN|\nu\rangle\end{pmatrix}=\begin{pmatrix}p_{UP},\;x_{UP}\\\\p_{DN},\;x_{DN}\end{pmatrix}$$

$$=|UP\rangle\langle UP|\nu\rangle+|DN\rangle\langle DN|\nu\rangle$$
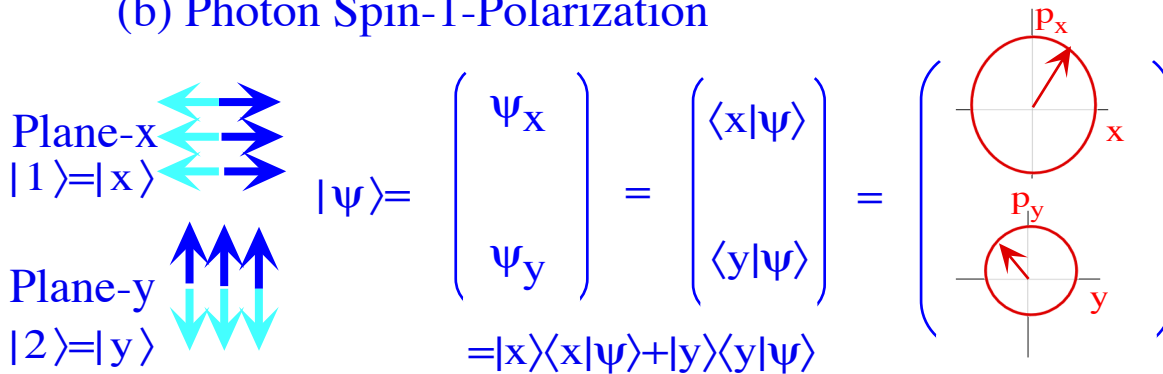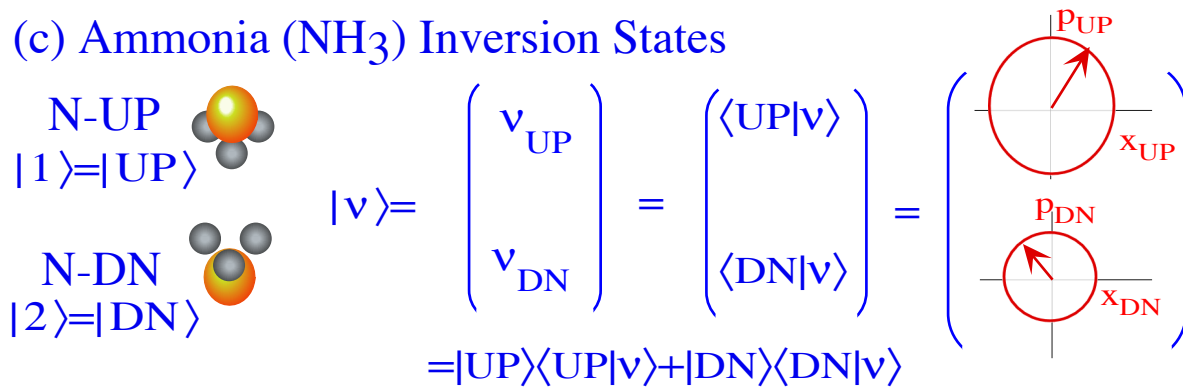
Fig. 10.5.1 Some of the most famous 2-state systems and their two-complex-component coordinates.

Ways to "picture" these *U(2)* worlds begins with the *U(2) 2-phasor* or *spinor* pictures shown in Fig. 10.5.2 (a-b) The full picture (b) is four dimensional but the polarization picture (a) takes only the real parts to make a 2D

orbit path. This was used earlier. If we can ignore overall phase, a three-dimensional *R(3)-SU(2) spin-vector* picture shown in Fig. 10.5.2(c) is sufficient and useful to define a U(2)-state.

(a) Real Spinor Space Picture (2D-Oscillator Orbit)

(b) 2-Phasor U(2) SpinorPicture

(c) 3-Dimensional Real R(3)-SU(2)Vector Picture

$$\Psi_1 = x_1 + ip_1 = |\Psi_1|\,e^{i\phi_1}$$
$$\Psi_2 = x_2 + ip_2 = |\Psi_2|\,e^{i\phi_2}$$

$$S_A = (\Psi_1{}^*\,\Psi_1 - \Psi_2{}^*\,\Psi_2)/2$$
$$S_B = (\Psi_1{}^*\,\Psi_2 + \Psi_2{}^*\,\Psi_1)/2$$
$$S_C = (\Psi_1{}^*\,\Psi_2 - \Psi_2{}^*\,\Psi_1)/2i$$
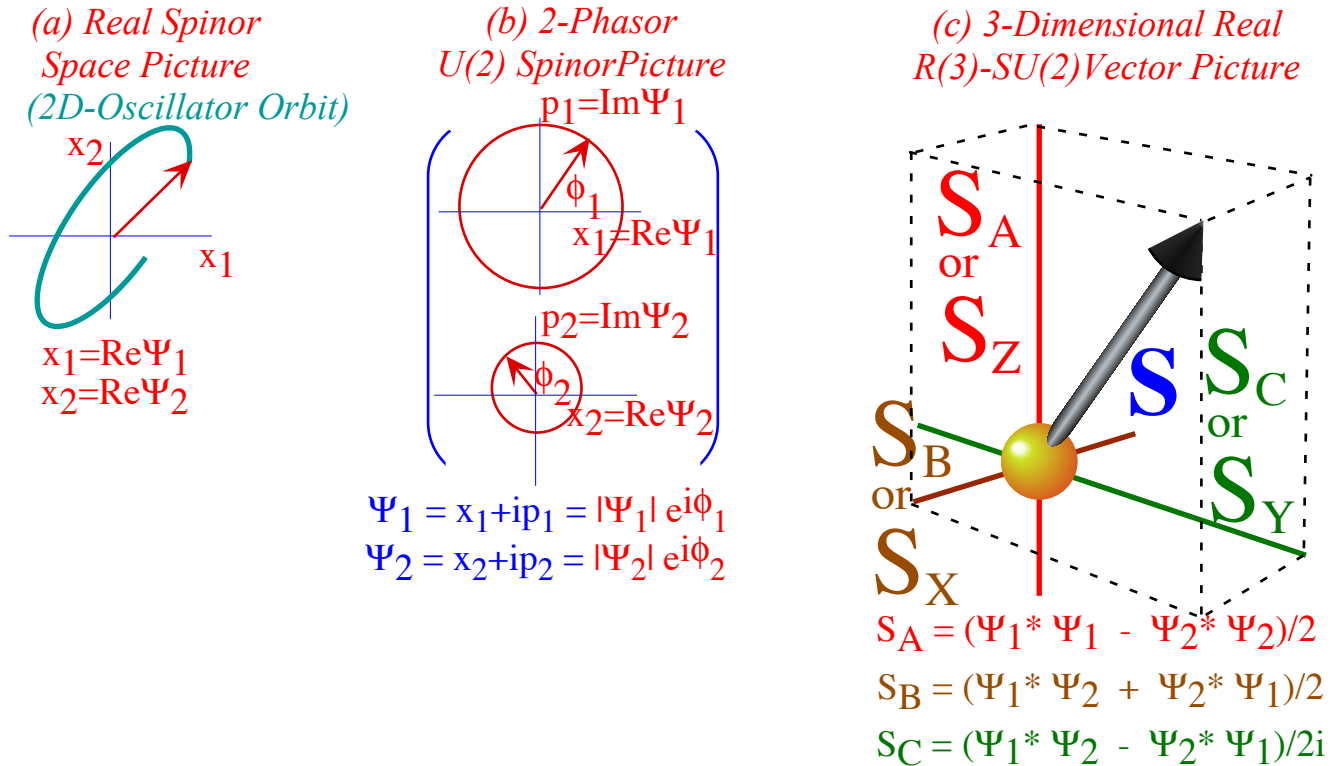
Fig. 10.5.2 Spinor, phasor, and vector descriptions of 2-state systems .

A set of four real coordinates of *U(2)* states from (10.1.1) are listed here with phase angles (ϕ_1,ϕ_2).

$$|\Psi\rangle = \begin{pmatrix} \Psi_1 \\ \Psi_2 \end{pmatrix} = \begin{pmatrix} \langle 1|\Psi\rangle \\ \langle 2|\Psi\rangle \end{pmatrix} = \begin{pmatrix} x_1 + ip_1 \\ x_2 + ip_2 \end{pmatrix} = \begin{pmatrix} |\Psi_1|e^{i\phi_1} \\ |\Psi_2|e^{i\phi_2} \end{pmatrix}, \quad \text{where:} \quad \begin{array}{l} x_1 = \text{Re}\,\Psi_1 \text{ , and: } p_1 = \text{Im}\,\Psi_1 \\ x_2 = \text{Re}\,\Psi_2 \text{ , and: } p_2 = \text{Im}\,\Psi_2 \end{array} \quad (10.5.1a)$$

Overall-phase-independent quantities $\Psi_m{}^*\Psi_n$ define the following three spin-vector coordinates.

$$S_Z = S_A = \frac{1}{2}\left(\Psi_1^*\Psi_1 - \Psi_2^*\Psi_2\right) = \frac{1}{2}\left(|\Psi_1|^2 - |\Psi_2|^2\right)$$

$$S_X = S_B = \frac{1}{2}\left(\Psi_1^*\Psi_2 + \Psi_2^*\Psi_1\right) = \text{Re}\,\Psi_1^*\Psi_2 = |\Psi_1||\Psi_2|\cos(\phi_2 - \phi_1) \qquad (10.5.1b)$$

$$S_Y = S_C = \frac{1}{2i}\left(\Psi_1^*\Psi_2 - \Psi_2^*\Psi_1\right) = \text{Im}\,\Psi_1^*\Psi_2 = |\Psi_1||\Psi_2|\sin(\phi_2 - \phi_1)$$

(a) Density operators and Pauli σ-operators

The $\Psi_m{}^*\Psi_n$ quantities from which a spin-vector is built, are components of a very useful operator called the *density operator* $\rho = |\Psi\rangle\langle\Psi|$, first employed by U. Fano. ρ is defined as an outer (tensor $\otimes$) product of ket-bras as are projection operators in (2.1.19) but it's for a general state $|\Psi\rangle$, not just a base state $|1\rangle$ or $|2\rangle$.

$$\rho = |\Psi\rangle\langle\Psi| = \begin{pmatrix} \Psi_1 \\ \Psi_2 \end{pmatrix} \otimes \begin{pmatrix} \Psi_1^* & \Psi_2^* \end{pmatrix} = \begin{pmatrix} \Psi_1\Psi_1^* & \Psi_1\Psi_2^* \\ \Psi_2\Psi_1^* & \Psi_2\Psi_2^* \end{pmatrix} \qquad (10.5.2)$$

We have three spin-vector components ($S_X = S_B$, $S_Y = S_C$, $S_Z = S_A$) and a fourth quantity, the norm N

$$N = \Psi_1{}^*\Psi_1 + \Psi_2{}^*\Psi_2 \qquad\qquad\qquad (10.5.3)$$

(Norm or total probability must be unity ($N=1$) for base states but may be less than 1 for general states.) the density matrix components can be inverted from (10.5.1) to give

$$\rho_{11} = \Psi_1^*\Psi_1 = \frac{1}{2}N + S_Z , \quad \rho_{12} = \Psi_2^*\Psi_1 = S_X - iS_Y,$$

$$\rho_{21} = \Psi_1^*\Psi_2 = S_X + iS_Y , \quad \rho_{22} = \Psi_2^*\Psi_2 = \frac{1}{2}N - S_Z. \qquad (10.5.4)$$

Density operator $\rho = |\Psi\rangle\langle\Psi|$ becomes the following.

$$\begin{pmatrix} \rho_{11} & \rho_{12} \\ \rho_{21} & \rho_{22} \end{pmatrix} = \begin{pmatrix} \Psi_1^*\Psi_1 & \Psi_2^*\Psi_1 \\ \Psi_1^*\Psi_2 & \Psi_2^*\Psi_2 \end{pmatrix} = \begin{pmatrix} \frac{1}{2}N + S_Z & S_X - iS_Y \\ S_X + iS_Y & \frac{1}{2}N - S_Z \end{pmatrix}$$

$$= \frac{1}{2}N\begin{pmatrix} 1 & 0 \\ 0 & 1 \end{pmatrix} + S_X\begin{pmatrix} 0 & 1 \\ 1 & 0 \end{pmatrix} + S_Y\begin{pmatrix} 0 & -i \\ i & 0 \end{pmatrix} + S_Z\begin{pmatrix} 1 & 0 \\ 0 & -1 \end{pmatrix} \qquad (10.5.5a)$$

$$\rho = \frac{1}{2}N \quad \mathbf{1} \quad + S_X \quad \boldsymbol{\sigma}_X \quad + S_Y \quad \boldsymbol{\sigma}_Y \quad + S_Z \quad \boldsymbol{\sigma}_Z$$

where the σ matrices are known as the *Pauli spin(or) operator matrices*.

$$\mathbf{1} = \begin{pmatrix} 1 & 0 \\ 0 & 1 \end{pmatrix}, \quad \boldsymbol{\sigma}_X = \begin{pmatrix} 0 & 1 \\ 1 & 0 \end{pmatrix}, \quad \boldsymbol{\sigma}_Y = \begin{pmatrix} 0 & -i \\ i & 0 \end{pmatrix}, \quad \boldsymbol{\sigma}_Z = \begin{pmatrix} 1 & 0 \\ 0 & -1 \end{pmatrix}_A \qquad (10.5.5b)$$

These are the spin generators σ_0 , σ_B , σ_C , and σ_A listed in Fig. 10.4.2 catalog of 2-state Hamiltonians and symmetry. This is no accident; these operators are all set up to do an elegant job of completely solving the 2-state Schrodinger problem and quite a bit more. We saw some of this in equation (10.4.5).

Furthermore, the ρ-operator lets us treat *statistical ensembles* of possibly dephased particles that suffer "peeking" or other randomizing effects as in Sec. 1.3b. For *pure-state* beams, each of N particles contributes a spin-*1/2* so the total *expected spin magnitude S* exactly equals half-norm $N/2$ where

$$S = \sqrt{S_X^2 + S_Y^2 + S_Z^2} = \sqrt{S_B^2 + S_C^2 + S_A^2} \qquad (10.5.6)$$

Beams with $S<N/2$ are known as *depolarized* or "dirty" beams, and $S=0$ corresponds to *completely depolarized* (or "filthy"-random) beams. Pure-state ($S=N/2$) beams are also called *100%-polarized*.

Before, beginning ρ-analysis, let us explore some of the possible states in various *U(2)* worlds.   Fig. 10.5.3 below shows the **S**-vectors for our most commonly used base states. Examples 1 and 2 belong to the spin-*up* or *dn* ($|\uparrow\rangle$, $|\downarrow\rangle$), or *x*-or-*y*-polarization ($|x\rangle$, $|y\rangle$), or NH$_3$ base states ($|UP\rangle$, $|DN\rangle$).   Spin vector **S** is,

indeed, up or down, in Example 1 or 2, that is $\pm 180°$, while in real spinor space $|\uparrow\rangle$ and $|\downarrow\rangle$ bases are $90°$ apart. Recall 2:1 ratio between $R(3)$ and $U(2)$ angles first noted in (1.2.13).

Example 1:
   Spin-up

   Plane-x

   N-UP

Example 2: Spin-dn

   Plane-y

   N-DN

Example 3:
   Spin-"north"

   Plane-45°

   N-Ground State
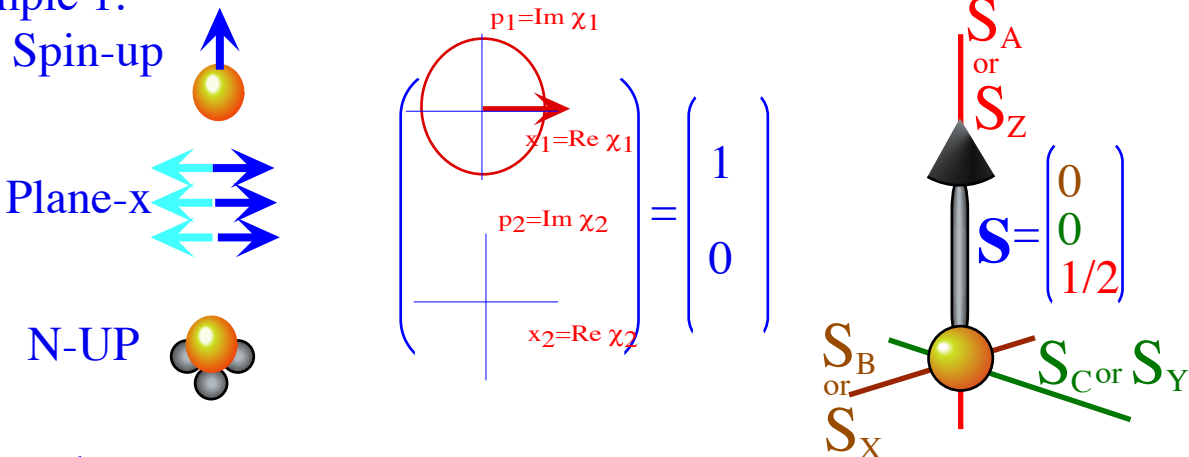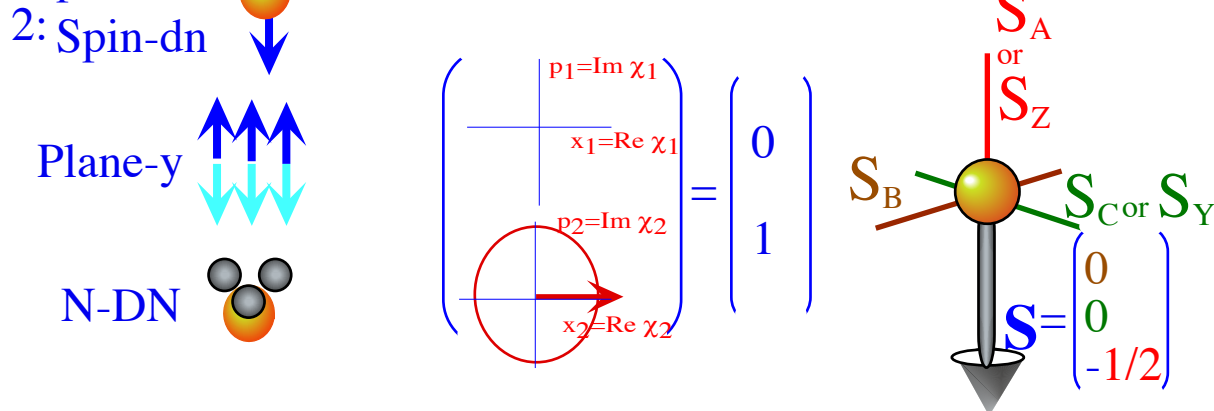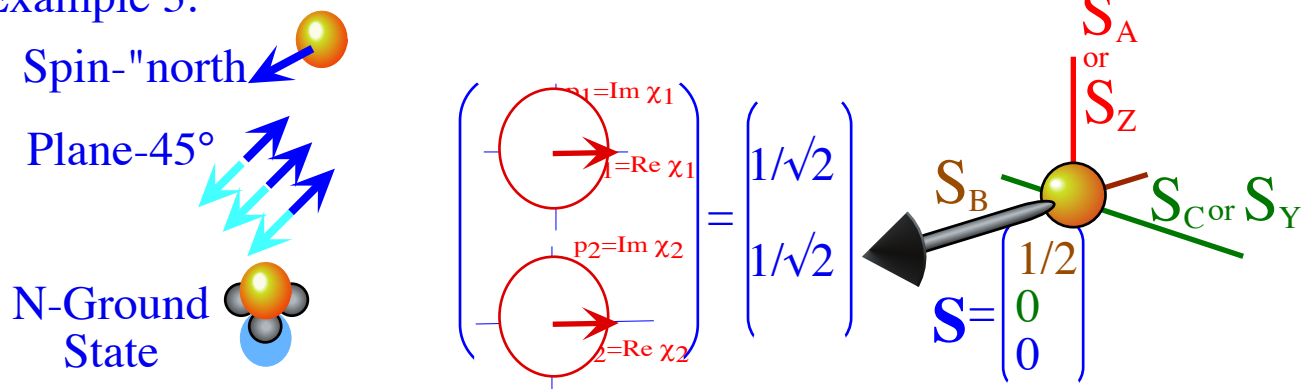
Fig. 10.5.3 Examples of spinor, phasor, and vector base states for electron, photon, or NH$_3$.

Example 3 is an eigenstate of bilateral $C_2{}^B$-symmetric Hamiltonian

$$\mathbf{H}_{C_2^B} = \begin{pmatrix} A & B \\ B & A \end{pmatrix} \qquad (10.2.4a)_{repeated}$$

such as the $\pm 45°$ normal modes $|(+)\rangle$ and $|(-)\rangle$ shown previously in Fig. 10.2.4 or NH$_3$ ground and excited states shown in Fig. 10.3.2b. The $C_2{}^B$-type **S**-eigenvectors lie on the bilateral B-axis.

Spin-West

Right Circular

NH₃-Resonant State

Example 4:

$$\begin{pmatrix} \odot\!\!\rightarrow \\ \odot\!\!\uparrow \end{pmatrix} = \begin{pmatrix} 1/\sqrt{2} \\ i/\sqrt{2} \end{pmatrix}$$

$$\mathbf{S} = \begin{pmatrix} 0 \\ 1/2 \\ 0 \end{pmatrix}$$

Spin-East

Left Circu-lar

NH₃-Resonant State

Example 5:

$$\begin{pmatrix} \odot\!\!\rightarrow \\ \odot\!\!\downarrow \end{pmatrix} = \begin{pmatrix} 1/\sqrt{2} \\ -i/\sqrt{2} \end{pmatrix}$$

$$\mathbf{S} = \begin{pmatrix} 0 \\ -1/2 \\ 0 \end{pmatrix}$$

Spin-somewhere (α,β)

Elliptic Polarization

NH₃ Symmetry Broken & Resonating

Generic Example 6:

$$\begin{pmatrix} \odot\!\!\nearrow \\ \odot\!\!\nearrow \end{pmatrix} = \begin{pmatrix} e^{-i\alpha/2}\cos\beta/2 \\ e^{i\alpha/2}\sin\beta/2 \end{pmatrix} e^{-i\gamma/2}$$

$$\mathbf{S} = 1/2 \begin{pmatrix} \cos\alpha\,\sin\beta \\ \sin\alpha\,\sin\beta \\ \cos\beta \end{pmatrix}$$

S_A $\mathbf{S}$

S_B S_C

Fig. 10.5.4 Other spinor, phasor, and vector base states for electron, photon, or NH₃ .

Examples 4 and 5 shown in Fig. 10.5.4 are eigenstates of circular C_2^C-symmetric Hamiltonians

$$\mathbf{H}_{C_2^C} = \begin{pmatrix} A & -iC \\ iC & A \end{pmatrix} \qquad\qquad (10.2.19d)_{repeated}$$

such as the left and right-circular-polarization eigenstates $|L\rangle$ and $|R\rangle$ shown in Fig. 10.2.7. The **S**-vectors for the circular eigenbasis are "East" and "West" respectively, that is, along the circular C-axis. $|L\rangle$ and $|R\rangle$ are resonant "beat" modes or *transition states* for the NH₃ model. Recall how the beat in Fig. 10.2.6 briefly has two phasors; one "donor" phasor *90°* ahead of a "receiver" phasor to give $|L\rangle$-circular polarization like a 1/4-wave plate. State $|L\rangle$ corresponds to NH₃ actually undergoing an inversion. In example 4, the N-atom probability is moving <u>down</u> (because UP-phasor is ahead of DN), but in Example 5 the N-atom is moving <u>up</u> since the UP-phasor is behind that of DN. Recall phase principle stated after (10.2.16).

Finally, note that Examples 1 and 2 belong to *eigenbasis* of basic C_2^A-symmetric Hamiltonians

$$\mathbf{H}_{C_2^A} = \begin{pmatrix} A & 0 \\ 0 & D \end{pmatrix}$$

(10.2.2h)*repeated*

which have no off-diagonal coupling components of either the bilateral (B) or circular (C) types. Their **S**-vectors must lie "up" and "down" along the A-axis as shown in Fig. 10.5.3. At the other extreme are the vast majority of generic Hamiltonians with generic eigenstates like the one sketched in Example 6 of Fig. 10.5.4. For a generic state it is convenient to introduce *Euler phase-angle coordinates* (α, β, γ) along with a *norm N*.

$$|\Psi\rangle = \begin{pmatrix} \Psi_1 \\ \Psi_2 \end{pmatrix} = \begin{pmatrix} \langle 1|\Psi\rangle \\ \langle 2|\Psi\rangle \end{pmatrix} = \begin{pmatrix} x_1 + ip_1 \\ x_2 + ip_2 \end{pmatrix} = \sqrt{N} \begin{pmatrix} e^{-i\alpha/2}\cos\dfrac{\beta}{2} \\ e^{i\alpha/2}\sin\dfrac{\beta}{2} \end{pmatrix} e^{-i\gamma/2}$$

(10.5.8a)

From (10.5.1) this gives a length-S=N/2 spin **S**-vector with polar angles (α, β) in ABC-space!

$$S_Z = S_A = \frac{1}{2}\left(|\Psi_1|^2 - |\Psi_2|^2\right) = \frac{N}{2}\left(\cos^2\frac{\beta}{2} - \sin^2\frac{\beta}{2}\right) = \frac{N}{2}\cos\beta$$

$$S_X = S_B = \operatorname{Re}\Psi_1^*\Psi_2 \qquad = N\cos\alpha\cos\frac{\beta}{2}\sin\frac{\beta}{2} = \frac{N}{2}\cos\alpha\sin\beta$$

(10.5.8b)

$$S_Y = S_C = \operatorname{Im}\Psi_1^*\Psi_2 \qquad = N\sin\alpha\cos\frac{\beta}{2}\sin\frac{\beta}{2} = \frac{N}{2}\sin\alpha\sin\beta$$

Spin **S**-vector components are *one-half* the Pauli *spinor operator expectation values* $\langle\Psi|\sigma_\mu|\Psi\rangle$.

$$\langle\Psi|\sigma_Z|\Psi\rangle = 2S_A = \begin{pmatrix} \Psi_1^* & \Psi_2^* \end{pmatrix}\begin{pmatrix} 1 & 0 \\ 0 & -1 \end{pmatrix}\begin{pmatrix} \Psi_1 \\ \Psi_2 \end{pmatrix} = N\cos\beta \quad = N\left(p_1^2 + x_1^2 - p_2^2 - x_2^2\right)$$

$$\langle\Psi|\sigma_X|\Psi\rangle = 2S_B = \begin{pmatrix} \Psi_1^* & \Psi_2^* \end{pmatrix}\begin{pmatrix} 0 & 1 \\ 1 & 0 \end{pmatrix}\begin{pmatrix} \Psi_1 \\ \Psi_2 \end{pmatrix} = N\cos\alpha\sin\beta = 2N\left(x_1 x_2 + p_1 p_2\right)$$ (10.5.8c)

$$\langle\Psi|\sigma_Y|\Psi\rangle = 2S_C = \begin{pmatrix} \Psi_1^* & \Psi_2^* \end{pmatrix}\begin{pmatrix} 0 & -i \\ i & 0 \end{pmatrix}\begin{pmatrix} \Psi_1 \\ \Psi_2 \end{pmatrix} = N\sin\alpha\sin\beta = 2N\left(x_1 p_2 - x_2 p_1\right)$$

For 2-state systems, like the electron or photon, which actually carry real-live-spin-angular momentum we need to introduce *Jordan spin operators* $\mathbf{J} = \mathbf{S} = (1/2)\sigma$ that are 1/2 of Pauli's "quasi-spin" σ-operators. Note that the Y-or C-component $J_C = S_C$ is precisely the angular momentum $xp_y - yp_x$ of an orbit in the mechanical analogy involving 2-dimensional oscillators.

$$\langle\Psi|\mathbf{J}_Y|\Psi\rangle = \langle\Psi|\mathbf{J}_C|\Psi\rangle = \langle\Psi|\mathbf{S}_C|\Psi\rangle = 2\langle\Psi|\sigma_C|\Psi\rangle = N(xp_y - yp_x)$$ (10.5.9)

This is analogous to *photon-spin momentum*. Circularly polarized photons hitting make you twist!

(b) Hamiltonian operators and Pauli-Jordan spin operators (J=S)

Symmetry and operator analysis solves the generic asymmetric Hamiltonian (10.1.1). The trick is to expand **H** in terms of the spinor σ-operators as was done for the state density ρ-operator in (10.5.5a). Instead, we use Jordan's $\mathbf{J} = (1/2)\sigma$ operators so as to respect that spin-1/2 factor.

$$\mathbf{J}_B = \mathbf{S}_B = (1/2)\sigma_B = (1/2)\sigma_X , \qquad \mathbf{J}_C = \mathbf{S}_C = (1/2)\sigma_C = (1/2)\sigma_Y , \qquad \mathbf{J}_A = \mathbf{S}_A = (1/2)\sigma_A = (1/2)\sigma_Z$$

The resulting generic **H** Hamiltonian operator expansion is here.

$$\begin{pmatrix} H_{11} & H_{12} \\ H_{21} & H_{22} \end{pmatrix} = \begin{pmatrix} \langle 1|\mathbf{H}|1\rangle & \langle 1|\mathbf{H}|2\rangle \\ \langle 2|\mathbf{H}|1\rangle & \langle 2|\mathbf{H}|2\rangle \end{pmatrix} = \hbar \begin{pmatrix} A & B-iC \\ B+iC & D \end{pmatrix}$$

$$\mathbf{H}/\hbar = \frac{1}{2}(A+D)\begin{pmatrix} 1 & 0 \\ 0 & 1 \end{pmatrix} + 2B\begin{pmatrix} 0 & 1 \\ 1 & 0 \end{pmatrix}\frac{1}{2} + 2C\begin{pmatrix} 0 & -i \\ i & 0 \end{pmatrix}\frac{1}{2} + (A-D)\begin{pmatrix} 1 & 0 \\ 0 & -1 \end{pmatrix}\frac{1}{2} \quad (10.5.10a)$$

$$\mathbf{H}/\hbar = \frac{1}{2}(A+D) \quad \mathbf{1} \quad + 2B \quad \mathbf{S}_X \quad + 2C \quad \mathbf{S}_Y \quad + (A-D) \quad \mathbf{S}_Z$$

$$\mathbf{H}/\hbar = \frac{1}{2}(A+D) \quad \sigma_0 \quad + 2B \quad \mathbf{S}_B \quad + 2C \quad \mathbf{S}_C \quad + (A-D) \quad \mathbf{S}_A$$

The three constants (*2B, 2C, A-D*) multiplying the respective (σ_X, σ_Y, σ_Z) = (σ_B, σ_C, σ_A) operators are components of what is called the *Hamiltonian Ω-cranking vector*

$$\Omega = (\Omega_X, \Omega_Y, \Omega_Z) = (2B, 2C, A\text{-}D) = (\Omega_B, \Omega_C, \Omega_A) \qquad (10.5.10b)$$

while the coefficient *(A+D)/2* of the unit operator σ_0 is just the average overall phase rate or energy $\varepsilon/\hbar$.

$$\Omega_0 = (A+D)/2 \qquad (10.5.10c)$$

The Hamiltonian expression involves an *operator scalar product* $\Omega\bullet\mathbf{S} = \Omega\bullet\sigma/2$.

$$\mathbf{H} = \hbar\Omega_0\mathbf{s}_0 + \hbar\vec{\Omega}\bullet\vec{\mathbf{S}} = \hbar\Omega_0\mathbf{1} + \hbar\vec{\Omega}\bullet\vec{\mathbf{S}} \qquad (10.5.10d)$$

Here Ω is an ordinary 3-vector made of three numerical components Ω_X, Ω_Y, and Ω_Z, but $\mathbf{S}$ is an *operator 3-vector* made of three Jordan-Pauli spin operators $\mathbf{S}_X = (1/2)\sigma_X$, $\mathbf{S}_Y = (1/2)\sigma_Y$, and $\mathbf{S}_Z = (1/2)\sigma_Z$.

Each of the *B*, *C*, or *A* type **H**-matrices (10.5.7 A-C) has its Ω-vector pointing along the *B*, *C*, or *A* axis, respectively, precisely the direction of the **S**-vector for **H**-eigenstates in each case. This lining up of **S** and Ω is particularly useful since it's true for the generic **H**-matrices, too. **S**-vectors of all **H**-<u>eigenstates</u> must lie along (or against) its Hamiltonian Ω-vector.

Bingo! The Hamiltonian Ω-vector completely determines the observable dynamics of <u>all</u> states, not just **H**-eigenstates. The result is a closed-form analytic and pictorial solution of all possible eigenvectors and dynamics, that is, all possible states of all possible *U(2)* Hamiltonians! The first result is frequency

$$|\Omega| = \sqrt{\Omega_X^2 + \Omega_Y^2 + \Omega_Z^2} = \sqrt{(2B)^2 + (2C)^2 + (A-D)^2} \qquad (10.5.10e)$$

which is the beat-transition frequency difference between *ABCD* eigenlevels of (10.4.5). (That factor of 1/2 in defining spin **S** is key to getting the right Ω-cranking rate or *beat frequency* $\Omega = \omega_{hi} - \omega_{lo}$.)

(c) Bloch equations and spin precession

The notion of cranking or precession of a gyroscope is an old classical one. Here it is appearing in a purely quantum mechanical context and applies to all the Schrodinger 2-state dynamics described so far.

Precession arises from the density operator ρ by writing the Schrodinger equation backwards and forwards in time, that is, as a ket equation (forwards) and as a "daggered" bra-equation (backwards).

$$i\hbar|\dot{\Psi}\rangle = \mathbf{H}|\Psi\rangle, \quad \Leftarrow Daggar^\dagger \Rightarrow \quad -i\hbar\langle\dot{\Psi}| = \langle\Psi|\mathbf{H} \qquad (10.5.11)$$

Note: $\mathbf{H}^\dagger = \mathbf{H}$. Combining these gives a time derivative of the density operator $\rho = |\Psi\rangle\langle\Psi|$

$$i\hbar\frac{\partial}{\partial t}\rho = i\hbar\dot{\rho} = i\hbar|\dot{\Psi}\rangle\langle\Psi| + i\hbar|\Psi\rangle\langle\dot{\Psi}| = \mathbf{H}|\Psi\rangle\langle\Psi| - |\Psi\rangle\langle\Psi|\mathbf{H} \qquad (10.5.12a)$$

The result is called a *Bloch equation*. This is the "professional" version of the Schrodinger equation.

$$ i\hbar\frac{\partial}{\partial t}\rho = i\hbar\dot{\rho} = \mathbf{H}\rho - \rho\mathbf{H} = \left[\mathbf{H},\rho\right] \tag{10.5.12b} $$

Then we write ρ and $\mathbf{H}$ in terms spin $\mathbf{S}$-vector and crank Ω-vector by (10.5.5) and (10.5.10), respectively.

$$ \mathbf{H}\rho = \left(\hbar\Omega_0\mathbf{1}+\frac{\hbar}{2}\Omega\bullet\sigma\right)\left(\frac{N}{2}\mathbf{1}+\mathbf{S}\bullet\sigma\right) = \hbar\Omega_0\frac{N}{2}\mathbf{1}+\frac{N}{4}\hbar\Omega\bullet\sigma+\hbar\Omega_0\mathbf{S}\bullet\sigma+\frac{\hbar}{2}(\Omega\bullet\sigma)(\mathbf{S}\bullet\sigma) $$

$$ \rho\mathbf{H} = \left(\frac{N}{2}\mathbf{1}+\mathbf{S}\bullet\sigma\right)\left(\hbar\Omega_0\mathbf{1}+\frac{\hbar}{2}\Omega\bullet\sigma\right) = \hbar\Omega_0\frac{N}{2}\mathbf{1}+\frac{N}{4}\hbar\Omega\bullet\sigma+\hbar\Omega_0\mathbf{S}\bullet\sigma+\frac{\hbar}{2}(\mathbf{S}\bullet\sigma)(\Omega\bullet\sigma) $$

Only the last terms don't cancel, and then only if the spin $\mathbf{S}$ and crank Ω *point in different directions*.

$$ \mathbf{H}\rho - \rho\mathbf{H} = \frac{\hbar}{2}(\Omega\bullet\sigma)(\mathbf{S}\bullet\sigma)-\frac{\hbar}{2}(\mathbf{S}\bullet\sigma)(\Omega\bullet\sigma) $$

To finish this we need to derive the *Pauli-Hamilton identity*. This uses σ-multiplication rules (10.4.6).

$$ (\mathbf{A}\bullet\sigma)(\mathbf{B}\bullet\sigma) = A_\alpha B_\beta\sigma_\alpha\sigma_\beta = A_\alpha B_\beta\left(\delta_{\alpha\beta}+i\varepsilon_{\alpha\beta\gamma}\sigma_\gamma\right) $$
$$ =A_\alpha B_\alpha + i\varepsilon_{\alpha\beta\gamma}A_\alpha B_\beta\sigma_\gamma \tag{10.5.13} $$
$$ =\mathbf{A}\bullet\mathbf{B}+i(\mathbf{A}\times\mathbf{B})\cdot\sigma $$

So finally the time dynamics is reduced to the following.

$$ i\hbar\frac{\partial}{\partial t}\rho = i\hbar\dot{\rho} = \frac{i\hbar}{2}(\Omega\times\mathbf{S})\bullet\sigma - \frac{i\hbar}{2}(\mathbf{S}\times\Omega)\bullet\sigma $$

$$ i\hbar\frac{\partial}{\partial t}\left(\frac{N}{2}\mathbf{1}+\mathbf{S}\bullet\sigma\right) = i\hbar\dot{\mathbf{S}}\bullet\sigma = i\hbar(\Omega\times\mathbf{S})\bullet\sigma $$

Factoring out $\bullet\sigma$ gives a *gyroscopic precession equation*.

$$ \frac{\partial\mathbf{S}}{\partial t} = \dot{\mathbf{S}} = \Omega\times\mathbf{S} \tag{10.5.14} $$

Perhaps, the Fig. 1.2.4 sketch of "helicopter" electrons in Stern-Gerlach analyzers is not so silly after all!

   Magnetic spin precession (ESR, NMR,..)

        Indeed, the classical Hamiltonian for a magnetic moment $\mathbf{m}$ in a magnetic $\mathbf{B}$-field is $H=-\mathbf{m}\bullet\mathbf{B}$. If the particle's magnetic moment is proportional to its spin angular momentum

$$ \mathbf{m} = g\,\mathbf{S} \tag{10.5.15a} $$

where g is called a *gyromagnetic ratio* then the Hamiltonian can be written

$$ H=-\mathbf{m}\bullet\mathbf{B} = -g\,\mathbf{S}\bullet\mathbf{B} = -g\,(B_xS_x + B_yS_y + B_zS_z) \tag{10.5.15b} $$

Replacing each classical spin component S_μ by a spin operator $\hbar\mathbf{S}_\mu$ gives the quantum Hamiltonian.

$$ \mathbf{H}= -g\,\mathbf{S}\bullet\mathbf{B} = -g\,\hbar(B_x\mathbf{S}_x + B_y\mathbf{S}_y + B_z\mathbf{S}_z) \tag{10.5.15c} $$

The matrix representation of this has the $\Omega\bullet\mathbf{S}$ form of the generic *U(2)* Hamiltonian (10.5.10).

$$ \mathbf{H} = -g\hbar\mathbf{B}\bullet\mathbf{S} = \frac{g\hbar}{2}\left[B_x\begin{pmatrix}0 & 1\\1 & 0\end{pmatrix}+B_y\begin{pmatrix}0 & -i\\i & 0\end{pmatrix}+B_z\begin{pmatrix}1 & 0\\0 & -1\end{pmatrix}\right] $$
$$ = \frac{g\hbar}{2}\begin{pmatrix}B_z & B_x-iB_y\\B_x+iB_y & -B_z\end{pmatrix} \tag{10.5.16a} $$

The Ω-crank is the $g\hbar\mathbf{B}/2$-field vector! It will make the spin $\mathbf{S}$-vector precess around Ω at a rate given by the *magnetic resonance frequency* Ω.

$$ \Omega=g|\mathbf{B}|\hbar/2 \tag{10.5.16b} $$

In other words, if you have seen one *U(2)* Hamiltonian, you have seen them all! They are basically all the same no matter whether it describes nuclear magnetic resonance (NMR), electron spin resonance (ESR), muon spin resonance (MSR), and so forth, as long there are just two base states. The difference lies in how we set the parameters B_x, B_y, and, B_z or, for our generic **H** matrix, the parameters *2B, 2C,* and *(A-D)* . Finally (and most important!) we need to understand how parameters may be varied with time to cause a desired resonance.

(d) Visualizing quantum dynamics as S-precession

Perhaps, the greatest advantage of the 3-space spin vector rotational formulation is its power of visualization. Let us return to the earlier 2-state models and analogies to see this. We begin with the bilateral *B*-type Hamiltonian (Sec. 10.2(b)) of NH_3 and our coupled pendulum analogy. This will then be compared with the *C*-type Zeeman-like Hamiltonians of Sec. 10.2(c). Then we see how this changes to the basic *A*-type problem via the "avoided-crossing" Stark-like *AB*-types discussed in Sec. 10.3(a). The *B*-type Hamiltonian

$$\begin{pmatrix} \langle 1|\mathbf{H}|1\rangle & \langle 1|\mathbf{H}|2\rangle \\ \langle 2|\mathbf{H}|1\rangle & \langle 2|\mathbf{H}|2\rangle \end{pmatrix} = \begin{pmatrix} A & B \\ B & A \end{pmatrix} \qquad \text{(10.2.4a)}_{repeated}$$

has a cranking Ω-vector on the *X* or *B*-axis of the spin 3-vector space according to (10.5.10b).

$$\Omega = (\Omega_X, \Omega_Y, \Omega_Z) = (2B, 0, 0) = (\Omega_B, \Omega_C, \Omega_A) \qquad (10.5.17)$$

It has no effect, except for overall phase advance, on the $\pm 45°$ or *B*-eigenvectors $|(+)\rangle$ or $|(-)\rangle$ whose spin vectors lie up and down the *B*-axis as shown in Examples 3 and 4, respectively, of Fig. 10.5.3. However, if the initial state is the first base state $|1\rangle = |x\rangle$ of *x*-polarization whose spin **S**-vector lies on the *A*-axis then it begins to precess at the beat frequency of $\Omega = 2B$. If *2B = -2S* is negative (our choice in (10.3.3)), the precession is clockwise from *A* to the positive *C*-axis and then to -*A* as shown in the Fig. 10.5.5 below. This is a "birds-eye" view of what happened in Fig. 10.2.6.
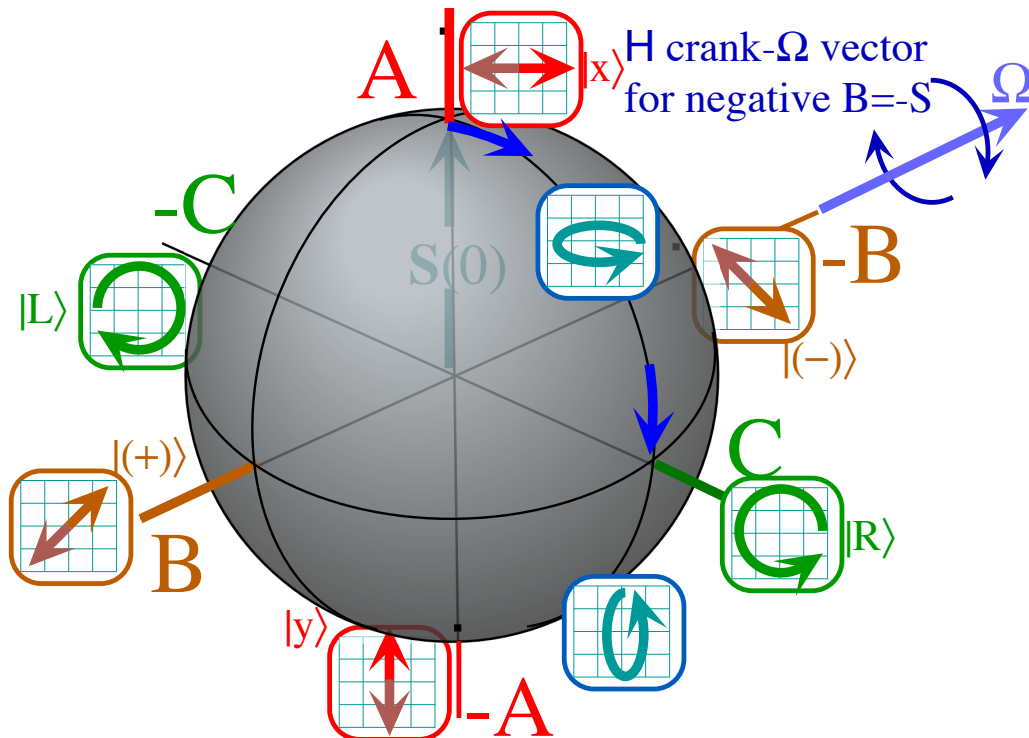

*Fig. 10.5.5 Time evolution of a B-type beat. **S**-vector rotates from A to C to -A to -C and back to A.*

Contrast that to what happened in Fig. 10.2.10 with a circular *C*-type Zeeman-like Hamiltonian.

$$\begin{pmatrix} \langle 1|\mathbf{H}|1\rangle & \langle 1|\mathbf{H}|2\rangle \\ \langle 2|\mathbf{H}|1\rangle & \langle 2|\mathbf{H}|2\rangle \end{pmatrix} = \begin{pmatrix} A & -iC \\ iC & A \end{pmatrix} \qquad \text{(10.2.19d)}_{repeated}$$

Its cranking Ω-vector is aligned with the *C*- or *Y*-axis.

$$\Omega = (\Omega_X, \Omega_Y, \Omega_Z) = (0,\ 2C,\ 0) = (\Omega_B, \Omega_C, \Omega_A) \qquad (10.5.18)$$

The resulting rotation is shown in Fig. 10.5.6. It is a very simple *Faraday Rotation* of the initial x-plane of polarization. However, it is a funny kind of rotation since the plane only rotates at <u>half</u> the angle β of the precessing spin **S**-vector. When the spin is at β=*60°* the plane is only at β/2=*30°*, as seen in the figure. This makes big trouble when the **S**-vector arrives back at *A* after going β=*360°*, all the way around the globe. The polarization is back to being a level *x*-polarization, but it is exactly β/2=*180°* out of phase! That is, the plane has only gone half-way. Once again, there is a 2:1 ratio between what happens to spin *vectors* and spin*ors*.
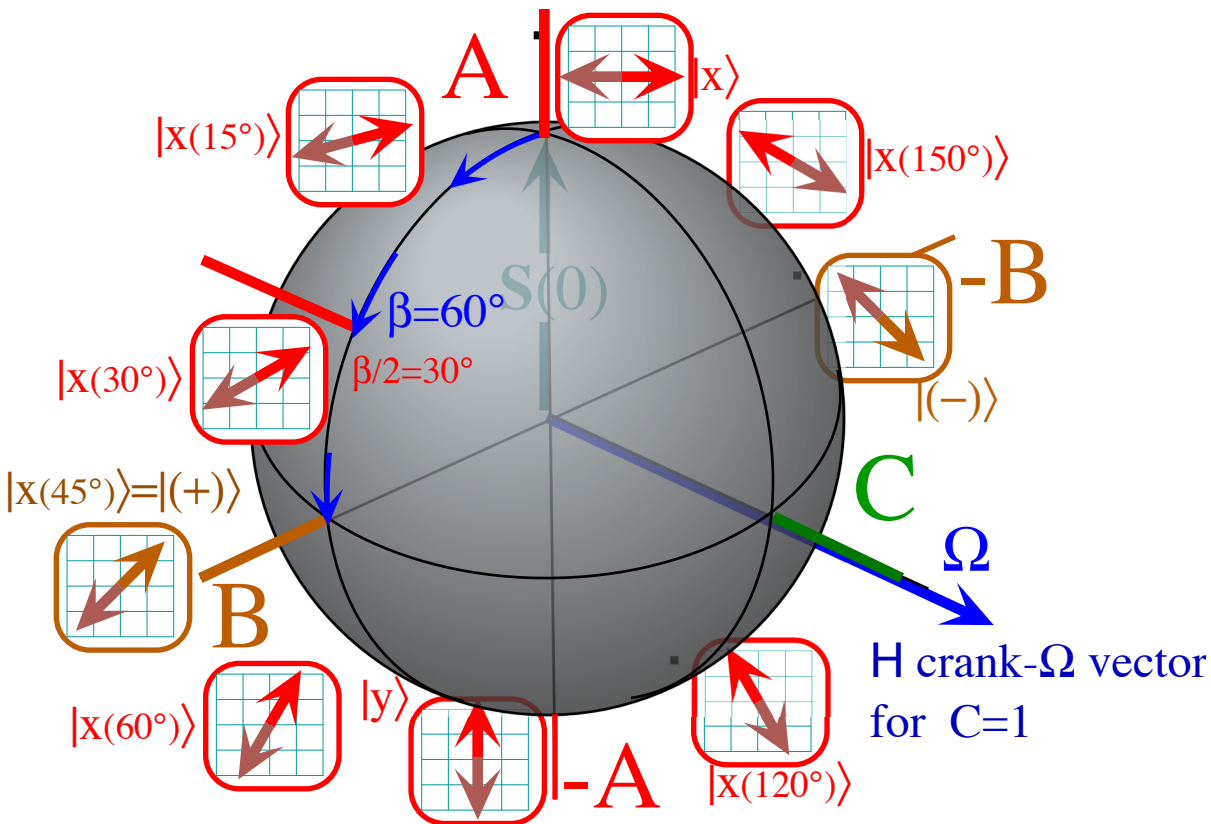
Fig. 10.5.6 Time evolution of a *C*-type beat. **S**-vector rotates from *A* to *B* to -*A* to -*B* and back to *A*.

If you follow carefully the evolution of the beat in the previous Fig. 10.5.5 you find that it, too, acquires a *180°* phase shift upon one "complete" *360°* rotation. So do electrons or any *U(2)* object. It is a fundamental property of rotational space, and a quite mysterious one. This is studied in a later chapter.

By breaking the bilateral *B*-symmetry we make it more difficult for the initial *A*-spin state to resonate or rotate around the *R(3)* globe. This is shown in Fig. 10.5.7 which diagrams the effect of a Stark-like *ABD*-type Hamiltonian

$$\begin{pmatrix} \langle 1|\mathbf{H}|1\rangle & \langle 1|\mathbf{H}|2\rangle \\ \langle 2|\mathbf{H}|1\rangle & \langle 2|\mathbf{H}|2\rangle \end{pmatrix} = \begin{pmatrix} A & B \\ B & D \end{pmatrix} = \begin{pmatrix} H - pE & -S \\ -S & H - pE \end{pmatrix} \qquad (10.3.3a)_{repeated}$$

Its cranking Ω-vector is between the A- or Z-axis and the B- or X-axis..

$$\Omega = (\Omega_X, \Omega_Y, \Omega_Z) = (2B, 0, A\text{-}D) = (\text{-}2S, 0, \text{-}2pE) = (\Omega_B, \Omega_C, \Omega_A) \qquad (10.5.19)$$

The chosen parameters are tunneling $S=1$, and symmetry breaking $pE=\sqrt{3}$. The resulting rotation goes along a much smaller circle that only "throws" the **S**-vector out to $\beta=60°$, twice as far as the polar angle $\vartheta=30°$ of the Ω-vector. Along the way the polarization becomes elliptical briefly with its ellipse always contained in a box which is tipped by exactly the angle $\vartheta/2=15°$. (Prove this!)

Fig. 10.5.7 Time evolution of a AB-type beat. **S**-vector rotates from A to $\beta=60°$ and back to A.

Notice how effectively the symmetry breaking parameter pE quenches resonance when it gets much larger than the coupling or tunneling parameter S. The Ω-vector approaches the A-axis closely. Since the Ω-vector determines the two **S**-vectors that represent eigenstates of **H**, it is seen that the original A-type base states of x and y polarization are recovered quite closely. These are the eigenstates of the A-Hamiltonian that start the ABC classification in Sec. 10.2a.

$$\mathbf{H}_{C_2^A} = \begin{pmatrix} A & 0 \\ 0 & D \end{pmatrix} \qquad (10.2.2h)_{repeated}$$

Crank Ω *polar angles* (φ,ϑ) *versus Spin* **S** *polar angles* (α,β)

   The azimuth-α and polar-β angles of spin **S** of a state $|\psi\rangle$ are set in (10.5.8b). We need azimuth-φ and polar-ϑ angles of crank vectors Ω or $\Theta=\Omega\cdot t$ of a Hamiltonian **H**. These are defined below and in Fig. 10.5.8.

$$S_X =(N/2)\ cos\ \alpha\ sin\ \beta =\mathrm{Re}\psi_1{}^*\psi_2 \qquad\qquad \Omega_X =\Omega\ cos\ \varphi\ sin\ \vartheta =2\mathrm{Re}\ H_{21}=2B \qquad (10.5.20\mathrm{a})$$

$$S_Y =(N/2)\ sin\ \alpha\ sin\ \beta =\mathrm{Im}\psi_1{}^*\psi_2 \qquad\qquad \Omega_Y =\Omega\ sin\ \varphi\ sin\ \vartheta =2\mathrm{Im}\ H_{21}=2C \qquad (10.5.20\mathrm{b})$$

$$S_Z =(N/2)\qquad\ cos\ \beta =(\psi_1{}^*\psi_1-\psi_2{}^*\psi_2)/2 \quad \Omega_Z =\qquad\ \Omega\ cos\ \vartheta =H_{11}-H_{22}=A\text{-}D \qquad (10.5.20\mathrm{c})$$

$$S_0 =(N/2)\qquad\qquad =(\psi_1{}^*\psi_1+\psi_2{}^*\psi_2)/2 \quad \Omega_0 =\qquad\qquad\ =H_{11}+H_{22}=A\text{+}D \qquad (10.5.20\mathrm{d})$$

Since eigenstate **S** aligns to Ω, finding $|\varepsilon_{hi}\rangle$ or $|\varepsilon_{lo}\rangle$ means equating angles: $(\alpha,\beta) = (\varphi,\vartheta)$ or $(\varphi,\vartheta+\pi)$.

This is a very powerful way to analyze and understand eigensolutions of *U(2)* systems. It will be used later.

U(2) World : Complex 2D Spinors
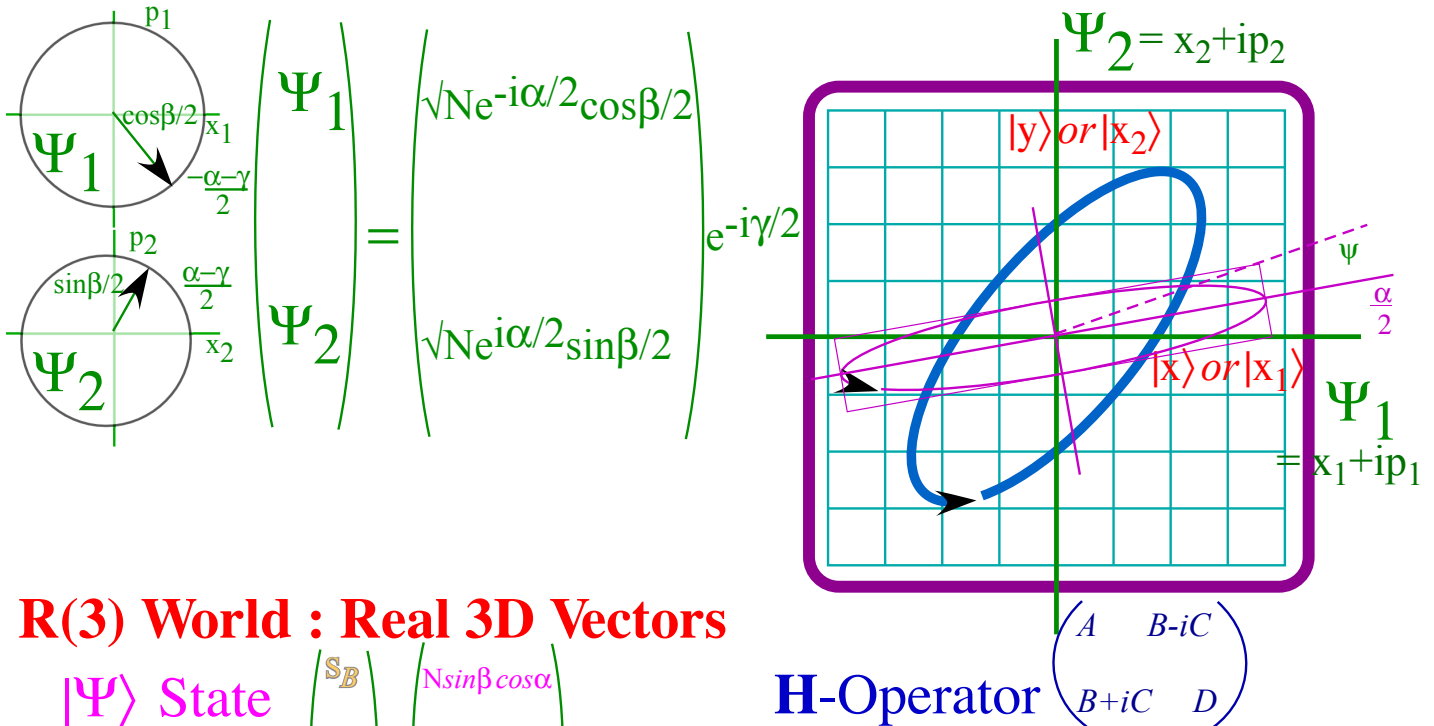
2-State ket $|\Psi\rangle=$

$$\begin{pmatrix} \Psi_1 \\ \Psi_2 \end{pmatrix} = \begin{pmatrix} \sqrt{N}e^{-i\alpha/2}\cos\beta/2 \\ \sqrt{N}e^{i\alpha/2}\sin\beta/2 \end{pmatrix} e^{-i\gamma/2}$$

$\Psi_2 = x_2 + ip_2$

$|y\rangle\, or\, |x_2\rangle$

$|x\rangle\, or\, |x_1\rangle$

$\Psi_1 = x_1 + ip_1$

$\dfrac{\alpha}{2}$

R(3) World : Real 3D Vectors

$|\Psi\rangle$ State
Spin Vector
S

$$\begin{pmatrix} s_B \\ s_C \\ s_A \end{pmatrix} = \begin{pmatrix} N\sin\beta\cos\alpha \\ N\sin\beta\sin\alpha \\ N\cos\beta \end{pmatrix}\frac{1}{2}$$

(for $\alpha=15°$ $\beta=45°$)

H-Operator $\begin{pmatrix} A & B-iC \\ B+iC & D \end{pmatrix}$
Angular velocity

$$\Omega = \begin{pmatrix} \Omega_B \\ \Omega_C \\ \Omega_A \end{pmatrix} = \begin{pmatrix} 2B \\ 2C \\ A-D \end{pmatrix} = \begin{pmatrix} \Omega\sin\vartheta\cos\varphi \\ \Omega\sin\vartheta\sin\varphi \\ \Omega\cos\vartheta \end{pmatrix}$$
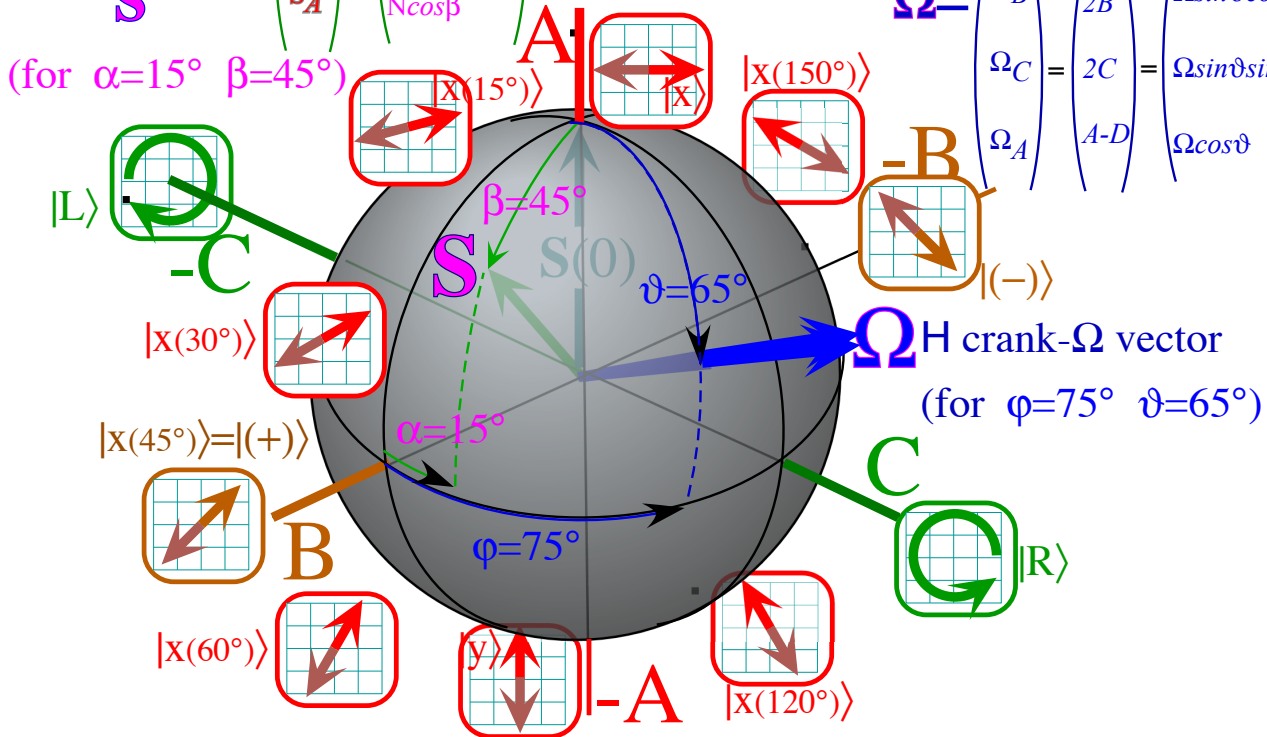
$|L\rangle$

$|x(15°)\rangle$ $|x\rangle$

$|x(150°)\rangle$

$-B$

$|(-)\rangle$

$\beta=45°$

S $S(0)$

$\vartheta=65°$

$|x(30°)\rangle$

Ω H crank-Ω vector

(for $\varphi=75°$ $\vartheta=65°$)

$\alpha=15°$

$|x(45°)\rangle=|(+)\rangle$

C

$|R\rangle$

B

$\varphi=75°$

$|x(60°)\rangle$

$|y\rangle$

$-A$

$|x(120°)\rangle$

Fig. 10.5.8 Comparison of   *(a) Complex U(2) spinor picture in (ψ_1,ψ_2)-space,*
           With   *(b) Real R(3) vector picture in (A,B,C)-space.*

Hamilton's generalization of exp(-iωt)=cosωt-isinωt : exp(-iσ t)=What?

When Hamilton generalized imaginary numbers to quaternions he had also generalized the famous Theorem of DeMoivre ($e^{-i\alpha}=cos\alpha$-$isin\alpha$). Engineers use $e^{i\alpha}$ to rotate phase by α in AC theory, and a 2D Planck time phasor $e^{-i\omega t}=cos\omega t$-$isin\omega t$ of wave theory generalizes to a 3D rotation $e^{-i\Omega\sigma t}$.

An exponential expression for a 2-by-2-polarization rotation matrix was given in (10.2.18).

$$\mathbf{R}(\varphi)=e^{\varphi\mathbf{G}}\ ,\ \ \text{represented by:}\ \ \begin{pmatrix} \cos\varphi & -\sin\varphi \\ \sin\varphi & \cos\varphi \end{pmatrix} = e^{\varphi\begin{pmatrix} 0 & -1 \\ 1 & 0 \end{pmatrix}} = e^{-i\varphi\begin{pmatrix} 0 & -i \\ i & 0 \end{pmatrix}} \quad (10.5.21)$$

This is a *C*- or *Y*-rotation by φ in *(x,y)*-space, and φ is half the angle β=2φ that **S** rotates in 3-space.

$$\mathbf{R_C}(\varphi)=e^{-i\varphi\sigma_\mathbf{C}} \qquad =e^{-i2\varphi\mathbf{S_C}} \qquad\qquad\qquad = \quad \mathbf{1} \quad\ \cos\varphi\ -i \quad\ \sigma_\mathbf{C}\ \ \sin\varphi$$

$$= e^{-i\varphi\begin{pmatrix} 0 & -i \\ i & 0 \end{pmatrix}} = e^{-i2\varphi\begin{pmatrix} 0 & -i \\ i & 0 \end{pmatrix}\frac{1}{2}} = \begin{pmatrix} \cos\varphi & -\sin\varphi \\ \sin\varphi & \cos\varphi \end{pmatrix} = \begin{pmatrix} 1 & 0 \\ 0 & 1 \end{pmatrix}\cos\varphi - i\begin{pmatrix} 0 & -i \\ i & 0 \end{pmatrix}\sin\varphi \quad (10.5.22)$$

The rotation $e^{-i\varphi\sigma_C}$ breaks down to a sum of a unit operator **1** times cos(φ) minus $i\sigma_C$ times sin(φ), a generalization of the DeMoivre exponential: $e^{-i\phi} = cos\ \phi$ -i $sin\ \phi$. These represent enormous milestones in the history of mathematics, but Hamilton's contribution is particularly powerful as we will see. It is hard to imagine quantum theory without either one of these great developments.

The other two types *A* and *B* of rotations are listed in the *U(2)* catalog in Fig. 10.4.2. The *A* or *Z*-type rotation generated by asymmetric-diagonal σ_A is also diagonal but complex.

$$\mathbf{R_A}(\theta)=e^{-i\theta\sigma_\mathbf{A}} \qquad =e^{-i2\theta\mathbf{S_A}} \qquad\qquad\qquad = \quad \mathbf{1} \quad\ \cos\theta\ -\ i \quad\ \sigma_\mathbf{A}\ \ \sin\theta$$

$$= e^{-i\theta\begin{pmatrix} 1 & 0 \\ 0 & -1 \end{pmatrix}} = e^{-i2\theta\begin{pmatrix} 1 & 0 \\ 0 & -1 \end{pmatrix}\frac{1}{2}} = \begin{pmatrix} e^{-i\theta} & 0 \\ 0 & e^{i\theta} \end{pmatrix} = \begin{pmatrix} 1 & 0 \\ 0 & 1 \end{pmatrix}\cos\theta - i\begin{pmatrix} 1 & 0 \\ 0 & -1 \end{pmatrix}\sin\theta \quad (10.5.23)$$

The *B* or *X* type rotation is complex and non-diagonal. (Check it by doing a σ_B spectral decomposition.)

$$\mathbf{R_B}(\chi)=e^{-i\chi\sigma_\mathbf{B}} \qquad =e^{-i2\chi\mathbf{S_B}} \qquad\qquad\qquad = \quad \mathbf{1} \quad\ \cos\chi\ -\ i\ \ \sigma_\mathbf{B}\ \sin\chi$$

$$= e^{-i\chi\begin{pmatrix} 0 & 1 \\ 1 & 0 \end{pmatrix}} = e^{-i2\chi\begin{pmatrix} 0 & 1 \\ 1 & 0 \end{pmatrix}\frac{1}{2}} = \begin{pmatrix} \cos\chi & -i\sin\chi \\ -i\sin\chi & \cos\chi \end{pmatrix} = \begin{pmatrix} 1 & 0 \\ 0 & 1 \end{pmatrix}\cos\chi - i\begin{pmatrix} 0 & 1 \\ 1 & 0 \end{pmatrix}\sin\chi \quad (10.5.24)$$

The key idea here is that $e^{-i\phi\sigma} = cos\ \phi$ -i$\sigma\ sin\ \phi$ works not just for separate $\sigma =\sigma_B$, σ_C, or σ_A *but for any combination-reflection* $\sigma =\sigma_{AB}$ or σ_{ABCD} provided $\sigma^2=1$. Evolution operator **U**= $e^{-i\mathbf{H}t}$ *(ħ=1)* has Hamiltonian **H**=σ•Ω/2=(Ω/2)σ defined by crank vector Ω or *rotation axis vector* Θ=Ω *t* as in (10.5.10).

$$\mathbf{U} = e^{-i\mathbf{H}t} = e^{-i\frac{\Theta}{2}\hat{\Theta}\bullet\sigma} = \mathbf{R}[\Theta]\ =\cos\frac{\Theta}{2}\ \mathbf{1}-i\sin\frac{\Theta}{2}\ \hat{\Theta}\bullet\sigma = e^{-i\frac{1}{2}\Theta\bullet\sigma} = e^{-i\Theta\bullet\mathbf{S}} \qquad (10.5.25a)$$

The rotation axis is given by its *polar coordinates* (φ , ϑ) and *angle of turn* $\Theta = \sqrt{\Theta_X^2 + \Theta_Y^2 + \Theta_Z^2} =\Omega\ t$.

$$\Theta = (\Theta_X, \Theta_Y, \Theta_Z) = |\Theta|\cdot (cos\varphi\ sin\vartheta,\ sin\varphi\ sin\vartheta,\ cos\vartheta)= (\Theta_B, \Theta_C, \Theta_A)$$

Representing $\sigma_X =\sigma_B$, $\sigma_Y =\sigma_C$, and $\sigma_Z =\sigma_A$ by their usual matrices gives a representation of **U**=**R**.

$$\mathbf{R}[\Theta]=\cos\frac{\Theta}{2}\quad \mathbf{1}\quad -\ i\quad \sigma_X\quad \hat{\Theta}_X\sin\frac{\Theta}{2}\ -i\quad \sigma_Y\quad \hat{\Theta}_Y\sin\frac{\Theta}{2}\ -i\quad \sigma_Z\quad \hat{\Theta}_Z\sin\frac{\Theta}{2}$$

$$= \cos\frac{\Theta}{2}\begin{pmatrix} 1 & 0 \\ 0 & 1 \end{pmatrix} -i\begin{pmatrix} 0 & 1 \\ 1 & 0 \end{pmatrix}\hat{\Theta}_X\sin\frac{\Theta}{2}\ -i\begin{pmatrix} 0 & -i \\ i & 0 \end{pmatrix}\hat{\Theta}_Y\sin\frac{\Theta}{2}\ -i\begin{pmatrix} 1 & 0 \\ 0 & -1 \end{pmatrix}\hat{\Theta}_Z\sin\frac{\Theta}{2}$$

Unit rotation axis vector $\hat{\Theta}=\left(\ \hat{\Theta}_X,\ \ \hat{\Theta}_Y,\ \ \hat{\Theta}_Z\ \right)=\left(\ cos\varphi\sin\vartheta\ \ \ sin\varphi\sin\vartheta\ \ \ cos\vartheta\ \right)$ is defined.

$$
\begin{pmatrix} \langle 1|\mathbf{R}[\Theta]|1\rangle & \langle 1|\mathbf{R}[\Theta]|2\rangle \\ \langle 2|\mathbf{R}[\Theta]|1\rangle & \langle 2|\mathbf{R}[\Theta]|2\rangle \end{pmatrix} = \begin{pmatrix} \cos\dfrac{\Theta}{2} - i\hat{\Theta}_Z\sin\dfrac{\Theta}{2} & -i\sin\dfrac{\Theta}{2}\left(\hat{\Theta}_X - i\hat{\Theta}_Y\right) \\[2mm] -i\sin\dfrac{\Theta}{2}\left(\hat{\Theta}_X + i\hat{\Theta}_Y\right) & \cos\dfrac{\Theta}{2} + i\hat{\Theta}_Z\sin\dfrac{\Theta}{2} \end{pmatrix} \tag{10.5.25b}
$$

In terms of polar axis angles $[\varphi,\vartheta,\Theta{=}\Omega{\cdot}t]$ this expands to a general *SU(2) rotation matrix*.

$$
\mathbf{R}[\Theta] = \begin{pmatrix} \cos\dfrac{\Theta}{2} - i\cos\vartheta\sin\dfrac{\Theta}{2} & -i\sin\dfrac{\Theta}{2}\left(\cos\varphi\sin\vartheta - i\sin\varphi\sin\vartheta\right) \\[2mm] -i\sin\dfrac{\Theta}{2}\left(\cos\varphi\sin\vartheta + i\sin\varphi\sin\vartheta\right) & \cos\dfrac{\Theta}{2} + i\cos\vartheta\sin\dfrac{\Theta}{2} \end{pmatrix}
$$

$$
= \mathbf{R}[\varphi\vartheta\Theta] = \begin{pmatrix} \cos\dfrac{\Theta}{2} - i\cos\vartheta\sin\dfrac{\Theta}{2} & -ie^{-i\varphi}\sin\vartheta\sin\dfrac{\Theta}{2} \\[2mm] -ie^{i\varphi}\sin\vartheta\sin\dfrac{\Theta}{2} & \cos\dfrac{\Theta}{2} + i\cos\vartheta\sin\dfrac{\Theta}{2} \end{pmatrix} = e^{-i\mathbf{H}t} = e^{-i\Theta\bullet\mathbf{S}} \tag{10.5.25c}
$$

H eigenstates $|\varepsilon_{hi}(\alpha,\beta)\rangle$ or $|\varepsilon_{lo}(\alpha,\beta)\rangle$ have angles *(α ,β)* in (10.5.8) given by *(φ ,ϑ)* or *(φ ,ϑ+π)*.

Why the 1/2?

        The *1/2* in front of angle Θ is there because $\Theta = \Omega{\cdot}t$ is the angle of rotation in 3D- ABC space in Fig. 10.5.8b. Angle Θ or β is twice the 2D-spinor-space angle φ or β/2 in Fig. 10.5.8a. Why is this?

        One answer is that to transform spinor operator **O** from **O** to **O'=ROR**† by rotation **R** requires *two* **R**'s. For example, **O**= $\sigma_Z = \sigma_A$ transformed by $\mathbf{R}_Y = \mathbf{R}_C$ is the following.

$$
\begin{array}{ccccccccc} \mathbf{R}_Y(\varphi) & & \sigma_Z & & \mathbf{R}_Y(\varphi)^\dagger & & = & \sigma_X & \sin2\varphi + & \sigma_Z & \cos2\varphi \end{array}
$$

$$
\begin{pmatrix} \cos\varphi & -\sin\varphi \\ \sin\varphi & \cos\varphi \end{pmatrix} \begin{pmatrix} 1 & 0 \\ 0 & -1 \end{pmatrix} \begin{pmatrix} \cos\varphi & \sin\varphi \\ -\sin\varphi & \cos\varphi \end{pmatrix} \tag{10.5.26}
$$

$$
= \begin{pmatrix} \cos^2\varphi - \sin^2\varphi & 2\sin\varphi\cos\varphi \\ 2\sin\varphi\cos\varphi & \sin^2\varphi - \cos^2\varphi \end{pmatrix} = \begin{pmatrix} \cos2\varphi & \sin2\varphi \\ \sin2\varphi & -\cos2\varphi \end{pmatrix} = \begin{pmatrix} 0 & 1 \\ 1 & 0 \end{pmatrix}\sin2\varphi + \begin{pmatrix} 1 & 0 \\ 0 & -1 \end{pmatrix}\cos2\varphi
$$

For angle $2\varphi{=}\pi/2$, this relates $\sigma_Z{=}\sigma_A$ to $\sigma_X{=}\sigma_B$ as is done in (10.3.9). A rotation by $2\varphi{=}\Theta{=}\beta$ in ABC-operator 3-space (σ_X, σ_Y, σ_Z) is twice the angle φ used for spinor 2-space. Spinor-1/2 factors double in vector 3-space, and spinors have half-angles $\varphi{=}\beta/2$ so that $\beta{=}\Theta$ is a real 3D-rotation. Also, recall in (10.3.12) that two mirror planes separated by φ yield rotations by *2φ*.

The evolution-rotation-operator **U**= $e^{-i\Theta\bullet\sigma/2} = e^{-i\Theta\bullet\mathbf{S}}$ by 3D-angle Θ may be viewed two ways: A 3D rotation by Θ generated by spin *vector* operator **S**=σ/2, or a 2D rotation by $\Theta/2$ generated by a *spinor* operator σ. The *1/2*-factors have quite deep significance. They are related to electrons having *1/2* quantum of spin **S**=σ/2. They deserve deep consideration. We shall try again later to explain more about the mysterious *1/2*!

Problems for Chapter 10.

ABCDanonical?

10.1.1. The canonical definition of momentum does not always give $p_j=m \, dx_j/dt$. (See "Deep Classical.." Chapter 5.3)
  (a) What is the general definition of p_j in terms of a Lagrangian L? First, what is L in terms of Hamiltonian H?
  (b) Find L and p_j for the classical ABCD Hamiltonian (10.1.3c).
  (c) Is the Schrodinger-to-Classical-Oscillator analogy correct if there is *explicit* time dependence $A(t)$, $B(t)$,..etc.?

All fall down

10.1.2. The fall-line at any point in a 2D potential V(x,y) is determined by ∇V (or $-\nabla V$, which?)
  (a) Relate acceleration-force vector (10.1.5) for the general potential $V=(1/2)\mathbf{x} \cdot \mathbf{A} \cdot \mathbf{x}$ (10.1.6b) to the gradient ∇V.
  (b) Find eigenvectors and eigenvalues of acceleration matrix **A** . Show how eigenvectors relate to V-ellipse axes for:.
       case A: (A=4, D=1, B=0, C=0) , case B: (A=D=4, B=-1, C=0) , case AB: (A=4, D=1, B=1, C=0) .
       Relate each to a classical normal mode frequency.
  (c) Find eigenvectors and eigenvalues of Hamiltonian matrix **H** for:.
       case A: (A=4, D=1, B=0, C=0) , case B: (A=D=4, B=-1, C=0) , case AB: (A=4, D=1, B=1, C=0) .
       Relate each to a quantum energy or eigenfrequency.

Groupie quaternions

10.1.3 Do the quaternions $\{\mathbf{1, i, j, k}\}$ by themselves make a group? How about Pauli $\{\sigma_I, \sigma_A, \sigma_B, \sigma_C\}$?
  (a) How about the set $\{\mathbf{1, i, j, k}, \mathbf{-1, -i, -j, -k}\}$? Construct a 4x4 multiplication table for $\{\mathbf{1, i, j, k}\}$.
  (b) How about the set $\{\sigma_I, \sigma_A, \sigma_B, \sigma_C, -\sigma_I, -\sigma_A, -\sigma_B, -\sigma_C\}$? Construct a 4x4 multiplication table.
  [c] Show that $\sigma_m \cdot \sigma_n = \delta_{mn}\mathbf{1} + ie_{mnp} \, \sigma_p$.

Use the Phase Luke!

10.2.1 Suppose a particle is oscillating at frequency ω according to $x(t) = A \sin (\omega t)$ while experiencing an applied force at the same frequency but ahead in phase angle ϕ according to $F(t) = F \sin (\omega t-\phi)$.
  (a) Does positive ϕ represent a force ahead or behind ?
  (b) Sketch a F versus x (Work-cycle) diagram for $\phi = 0$, $\pi/4$, $\pi/2$, π, and $3\pi/2$.
  (c) Calculate the work F does on x each cycle as a function of ϕ and indicate how it relates to area of F-x plots (b).
  (d) At the moment shown in Fig. 10.2.6, what is the phase angle ϕ between x_1 and x_2. Who's ahead? How does the phase angle vary with time? How does the energy flow (in the classical model) between the two vary with time?

B versus C

10.3.1 The **H**-matrix for the symmetry B, and C was given in the form of the tunneling amplitudes (B=-S) plus magnetic Zeeman (dipole) energy shifts (C) . As the relative magnitudes of these vary the eigenstates, eigenvalues, and symmetry changes, too.
  (a) Write the **H**(H, B, C=0) matrix in a basis that is <u>most appropriate</u> for its (What? B, or C?)-symmetry and use the lowest order perturbation theory to describe the effect of small C-value. Compare your result to that of the exact avoided crossing eigenvalues for (B=1, C=0.2). Describe the set or group of matrix operators that commute with **H**(H, B, C=0) and with **H** (H, B=1, C=0.2) , that is, give both finite "rotation" matrices and their generators.
  Sketch eigenstate phasor and polarization diagrams[†] for each case.
  Sketch ABC Ω and **S** vector diagrams[†] for each case.
  (b) Write the **H**(H, B=0, C) matrix in a basis that is <u>most appropriate</u> for its (What? B, or C?)-symmetry and use the lowest order perturbation theory to describe the effect of small B-value. Compare your result to that of the exact avoided crossing eigenvalues for (B=0.2, C=1). Describe the set or group of matrix operators that commute with **H**(H, B=0, C) and with **H** (H, B=0.2, C=1) , that is, give both finite "rotation" matrices and their generators.
  Sketch eigenstate phasor and polarization diagrams[†] for each case.
  Sketch ABC Ω and **S** vector diagrams[†] for each case.   †*See Sec. 10.5.*

Commute or else!

10.3.2 Use spectral decompositions to <u>derive</u> the form of the general U(2) matrix that commutes...

  (a) ...with $\sigma_A = \begin{pmatrix} 1 & 0 \\ 0 & -1 \end{pmatrix}$ (b) ...with $\sigma_B = \begin{pmatrix} 0 & 1 \\ 1 & 0 \end{pmatrix}$,(c) ...with $\sigma_C = \begin{pmatrix} 0 & -i \\ i & 0 \end{pmatrix}$, (d) ...with $M = \begin{pmatrix} 4 & 1 \\ 3 & 2 \end{pmatrix}$.

  (e to h) <u>Derive</u> the form of the most general SU(2) matrices that commute with each of the above.

Eigenvalues easy as ABCD

10.4.1 The expansion (10.4.5b-c) gives a closed form expression for eigenvalues of a general $\mathbf{H}_{ABCD}$.

    (a) Verify all parts of (10.4.5).

    (b) Show the eigenvalues so obtained agree with a direct diagonalization of $\mathbf{H}_{ABCD}$.

    (c) Show that this is a special case of $\mathbf{H}_{AB}$ eigenvalues in (10.3.11).

Ellipses on ellipses

10.4.2 The elliptical eigenstate orbits of Fig. 10.4.1 are seen to correspond to the elliptical equipotential level curves.

    (a) Do they really? How so?

    (b) Work the eigensolutions for Fig. 10.4.1 and plot their ellipses.

    (c) Are the ellipse major axes of orthogonal eigenvectors themselves orthogonal? Why or why not?

Eigenvectors easy as ABCD

10.5.1 The prescription (10.5.20) for finding general U(2) eigenvectors is powerful and important.

    (a) Write it out in detail for the AB-Hamiltonian in Fig. 10.5.7. Give eigenstates easily. (Recall (10.5.8a)

    (b) Show how a polarization ellipse would evolve and fill a rectangle if x-polarization were fed to this $\mathbf{H}$.

    (c) Do similarly with the Hamiltonian and initial spin shown in Fig. 10.5.8.

Very cross prodots

10.5.2 Using the σ-operator definitions and the Levi-Civita tensor definition

    derive the following. (First prove Levi-Civita rule: $\varepsilon_{abc}\varepsilon_{dec} = \delta_{ad}\delta_{be} - \delta_{ae}\delta_{bd}$)

    (a) $\sigma_a\sigma_b = \delta_{ab} + i\sum_c \varepsilon_{abc}\sigma_c$ (b) $\sigma_a\sigma_b\sigma_a = 2\delta_{ab}\sigma_a - \sigma_b$ (c) $(\boldsymbol{\sigma}\bullet\mathbf{A})(\boldsymbol{\sigma}\bullet\mathbf{B}) = (\mathbf{A}\bullet\mathbf{B}) + i(\mathbf{A}\times\mathbf{B})\bullet\boldsymbol{\sigma}$

Spinor round

10.5.3 Use spectral decomposition to derive three rotation operators(A-C) and base transforms (d-g).

    (a) $\mathbf{R}\left(\theta_{xy}\right) = e^{-i\frac{\theta_{xy}}{2}\sigma_z} = \mathbf{1}\cos\frac{\theta_{xy}}{2} - i\sigma_z\sin\frac{\theta_{xy}}{2} = \begin{pmatrix} e^{-i\theta_{xy}/2} & 0 \\ 0 & e^{i\theta_{xy}/2} \end{pmatrix}$

    (b) $\mathbf{R}\left(\theta_{yz}\right) = e^{-i\frac{\theta_{yz}}{2}\sigma_x} = \mathbf{1}\cos\frac{\theta_{yz}}{2} - i\sigma_x\sin\frac{\theta_{yz}}{2} = \begin{pmatrix} \underline{\quad} & \underline{\quad} \\ \underline{\quad} & \underline{\quad} \end{pmatrix}$

    (c) $\mathbf{R}\left(\theta_{zx}\right) = e^{-i\frac{\theta_{zx}}{2}\sigma_y} = \mathbf{1}\cos\frac{\theta_{zx}}{2} - i\sigma_y\sin\frac{\theta_{zx}}{2} = \begin{pmatrix} \underline{\quad} & \underline{\quad} \\ \underline{\quad} & \underline{\quad} \end{pmatrix}$

    (d) $\mathbf{R}\left(\theta_{ab}\right)\cdot\mathbf{1}\cdot\mathbf{R}^\dagger\left(\theta_{ab}\right) = \mathbf{1}$

    (e) $\mathbf{R}\left(\theta_{ab}\right)\cdot\sigma_a\cdot\mathbf{R}^\dagger\left(\theta_{ab}\right) = \sigma_a\cos\theta_{ab} + \sigma_b\sin\theta_{ab}$

    (f) $\mathbf{R}\left(\theta_{ab}\right)\cdot\sigma_b\cdot\mathbf{R}^\dagger\left(\theta_{ab}\right) = -\sigma_a\sin\theta_{ab} + \sigma_b\cos\theta_{ab}$

    (g) $\mathbf{R}\left(\theta_{ab}\right)\cdot\sigma_c\cdot\mathbf{R}^\dagger\left(\theta_{ab}\right) = \sigma_c$ (Let:ε_{abc}=1)

The Lorentz district

10.5.4 Use spectral decomposition to derive three Lorentz operators (A-C) and base transforms (d-f).

  (a) $\mathbf{L}\left(\theta_{tz}\right) = e^{\frac{\theta_{tz}}{2}\sigma_z} = \mathbf{1}\cosh\frac{\theta_{tz}}{2} + \sigma_z\sinh\frac{\theta_{tz}}{2} = \begin{pmatrix} e^{\theta_{tz}/2} & 0 \\ 0 & e^{-\theta_{tz}/2} \end{pmatrix}$

  (b) $\mathbf{L}\left(\theta_{tx}\right) = e^{\frac{\theta_{tx}}{2}\sigma_x} = \mathbf{1}\cosh\frac{\theta_{tx}}{2} + \sigma_x\sinh\frac{\theta_{tx}}{2} = \begin{pmatrix} \underline{\quad} & \underline{\quad} \\ \underline{\quad} & \underline{\quad} \end{pmatrix}$

(c) $L(\theta_{ty}) = e^{\frac{\theta_{ty}}{2}\sigma_y} = 1\sinh\frac{\theta_{ty}}{2} + \sigma_y\cosh\frac{\theta_{ty}}{2} = \begin{pmatrix} \underline{\quad\quad} & \underline{\quad\quad} \\ \underline{\quad\quad} & \underline{\quad\quad} \end{pmatrix}$

(d) $L(\theta_{ta}) \cdot 1 \cdot L^\dagger(\theta_{ta}) = 1\cosh\theta_{ta} + \sigma_a\sinh\theta_{ta}$

(e) $L(\theta_{ta}) \cdot \sigma_a \cdot L^\dagger(\theta_{ta}) = 1\sinh\theta_{ta} + \sigma_a\cosh\theta_{ta}$

(f) $L(\theta_{ta}) \cdot \sigma_c \cdot L^\dagger(\theta_{ta}) = \sigma_c$ (Let: $\varepsilon_{abc} = 1$)
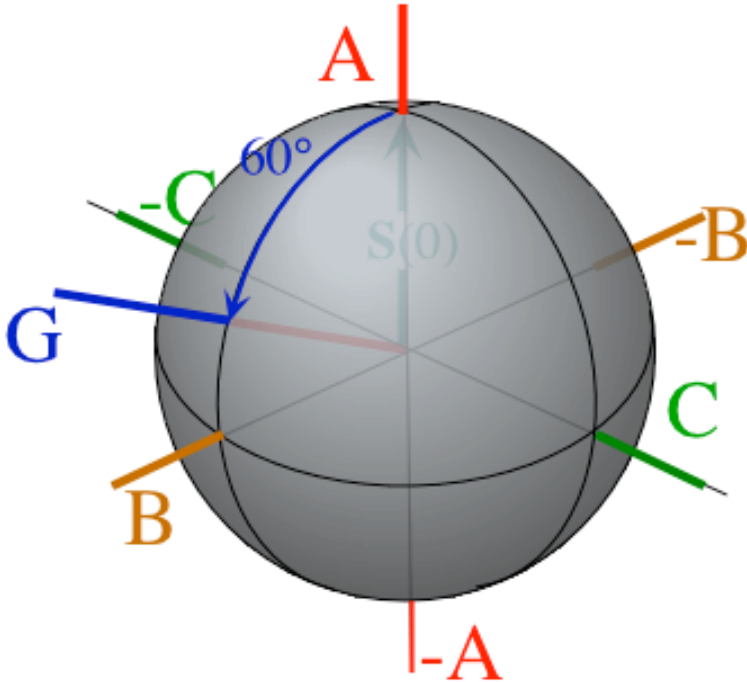
Fig. 1

10.5.5. Suppose an NMR spin system described by Hamiltonian $H = gS \cdot B = {}^g/_2\sigma \cdot B$ is initially in a state

$$\left|\Psi(0)\right\rangle = \frac{\sqrt{3}}{2}\left|\uparrow\right\rangle + \frac{1}{2}\left|\downarrow\right\rangle = \begin{pmatrix} \sqrt{3}/2 \\ 1/2 \end{pmatrix} \qquad (5.1)$$

(a) Write out **H** and its Schrodinger equation using 2-dimensional matrix notation.
(b) Write out **H** and its Bloch equation using 2-dimensional matrix notation.
(c) Define a set of **H** that make state (5.1) stationary. What other state(s) are also stationary.
(d) Find constant Hamiltonian **H** which will drive state (5.1) thru spin-up $\left|\uparrow\right\rangle$ in a given time τ.

$$\left|\left\langle\uparrow|\Psi(\tau)\right\rangle\right|^2 = 1 \quad \text{but:} \ \left|\left\langle\uparrow|\Psi(t)\right\rangle\right|^2 \neq 1 \ \text{ for}: t < \tau \qquad (5.2)$$

A number of **H** satisfy (5.2) but we prefer one which requires the <u>least</u> energy. Explain by describing a set of **H**. (Hint: Does least energy this also mean least angle of spin vector rotation?)
(e) Give the eigenkets and energy eigenvalues of the Hamiltonian resulting from (d) in terms of τ and $\hbar$ and sketch an energy level diagram.
(f) Give a formula for the angular frequency of radiation in terms of τ and $\hbar$ that might be observed as the state (5.1) and Hamiltonian from (d) are allowed to time-evolve.
(g) Indicate where on *Fig. 1* would be the initial spin vector, the driving magnetic **B**-field, and path followed by spin vector.
(h) Let this be the analogous optical polarization problem. Show how the polarization **E** evolves.
         (j) What is the <u>maximum</u> energy or frequency of radiation that can result from (5.1-2) above.

Review Topics & Formulas for Unit 3

Fourier Series Coefficients	*Fourier Integral Transform*	*Fourier C_N Transformation*

$$\langle k_m | \Psi \rangle = \int_{-L/2}^{L/2} dx \langle k_m | x \rangle \langle x | \Psi \rangle \qquad \langle k | \Psi \rangle = \int_{-\infty}^{\infty} dx \langle k | x \rangle \langle x | \Psi \rangle \qquad \langle k_m | \Psi \rangle = \sum_{p=0}^{p=N-1} \langle k_m | x_p \rangle \langle x_p | \Psi \rangle$$

$$\langle k_m | x \rangle = \frac{e^{-ik_m x}}{\sqrt{L}} = \langle x | k_m \rangle^* \qquad Kernal: \langle k | x \rangle = \frac{e^{-ikx}}{\sqrt{2\pi}} = \langle x | k \rangle^* \qquad \langle k_m | x_p \rangle = \frac{e^{-ik_m x_p}}{\sqrt{N}} = \langle x_p | k_m \rangle^*$$

x-Wavefunction $\Psi(x)$ =	*x-Wavefunction $\Psi(x)$ =*	*x-Wavefunction $\Psi(x)$ =*

$$\langle x | \Psi \rangle = \sum_{m=-\infty}^{m=\infty} \langle x | k_m \rangle \langle k_m | \Psi \rangle \qquad \langle x | \Psi \rangle = \int_{-\infty}^{\infty} dk \langle x | k \rangle \langle k | \Psi \rangle \qquad \langle x_p | \Psi \rangle = \sum_{m=0}^{m=N-1} \langle x_p | k_m \rangle \langle k_m | \Psi \rangle$$

Ortho – Completeness   *Ortho – Completeness*   *Ortho – Completeness*

$$\sum_{m=0}^{m=\infty} \langle x | k_m \rangle \langle k_m | x' \rangle = \delta(x - x') \qquad \int_{-\infty}^{\infty} dk \langle x | k \rangle \langle k | x' \rangle = \delta(x - x') \qquad \sum_{m=0}^{m=N-1} \langle x_p | k_m \rangle \langle k_m | x_{p'} \rangle = \delta_{p,p'}$$

$$\int_{-L/2}^{L/2} dx \langle k_m | x \rangle \langle x | k_{m'} \rangle = \delta_{m,m'} \qquad \int_{-\infty}^{\infty} dx \langle k | x \rangle \langle x | k' \rangle = \delta(k - k') \qquad \sum_{p=0}^{p=N-1} \langle k_m | x_p \rangle \langle x_p | k_{m'} \rangle = \delta_{m,m'}$$

Discrete momentum m	*Continuous momentum k*	*Discrete momentum m*
Continuous position x	*Continuous position x*	*Discrete position x_p*

Time Evolution Operator $\mathbf{U}$	*Time Evolution Operator* $\mathbf{U}$	$\mathbf{U}$ *must be Unitary*

$$\left| \Psi(t) \right\rangle = \mathbf{U}(t,0) \left| \Psi(0) \right\rangle \qquad \mathbf{U}(t,0) = e^{-i\,t\,\mathbf{H}/\hbar} \qquad \mathbf{U}^\dagger(t) = \mathbf{U}^{-1}(t) = \mathbf{U}(-t)$$

Hamiltonian Generator $\mathbf{H}$ *Schrodinger t – Equation* $\left(e^{-it\mathbf{H}/\hbar} \right)^\dagger = e^{it\mathbf{H}^\dagger/\hbar} = e^{it\mathbf{H}/\hbar}$

$$i\hbar \frac{\partial}{\partial t} \mathbf{U}(t,0) = \mathbf{H}\,\mathbf{U}(t,0) \qquad i\hbar \frac{\partial}{\partial t} \left| \Psi(t) \right\rangle = \mathbf{H} \left| \Psi(t) \right\rangle \qquad so\ \mathbf{H}\ is\ Hermitiam\ \mathbf{H}^\dagger = \mathbf{H}$$

Schrodinger time-independent energy eigen equation.

$$\mathbf{H} | \omega_m \rangle = \hbar\omega_m | \omega_m \rangle = \varepsilon_m | \omega_m \rangle \tag{9.3.1a}$$

$\mathbf{H}$-eigenvalues use $\mathbf{r}$-expansion (9.2.6) of $\mathbf{H}$ and C_6 symmetry $\mathbf{r}^p$-eigenvalues from (8.2.9).

$$\langle k_m | \mathbf{r}^p | k_m \rangle = e^{-ipk_m a} = e^{-ipm2\pi/N} \quad where:\ k_m = m(2\pi/Na)$$

$$\langle k_m | \mathbf{H} | k_m \rangle = H \langle k_m | \mathbf{1} | k_m \rangle + S \langle k_m | \mathbf{r} | k_m \rangle + T \langle k_m | \mathbf{r}^2 | k_m \rangle + U \langle k_m | \mathbf{r}^3 | k_m \rangle + T^* \langle k_m | \mathbf{r}^4 | k_m \rangle + S^* \langle k_m | \mathbf{r}^5 | k_m \rangle$$

$$= H + S\,e^{-ik_m a} + T\,e^{-i2k_m a} + U\,e^{-i3k_m a} + T^*\,e^{i2k_m a} + S^*\,e^{ik_m a} \tag{9.3.5a}$$

Bloch dispersion relation. And Bohr limit ($k \ll \pi/a$) approxiamtion. *Band group velocity V_{group}*.

$$\hbar\omega_m = E_m = H - 2|S|\,cos(k_m a) = H - 2|S| + |S|(k_m a)^2 + .. \tag{9.3.8}$$

$$V_{group} = \frac{d\omega_m}{dk_m} = 2\frac{|S|}{\hbar} a \sin(k_m a) \quad \left(\cong 2\frac{|S|}{\hbar} k_m a^2 \ ,\ for:\ k_m \ll \pi/a \right) \tag{9.3.10}$$

Effective mass M_{eff} <u>inversely</u> proportional to S. $M_{eff}(0) = \hbar^2/(\,2|S|\,a^2\,)$ (9.3.11a)

Fourier transform of a Gaussian $e^{-(m/\Delta m)^2}$ momentum distribution is a Gaussian $e^{-(\phi/\Delta\phi)^2}$ in coordinate ϕ.

$$\langle m|\Psi\rangle = e^{-(m/\Delta m)^2} \quad \text{implies:} \qquad \langle \phi|\Psi\rangle = e^{-(\phi/\Delta\phi)^2} \qquad (9.3.14)$$

The relation between *momentum uncertainty* Δm and *coordinate uncertainty* $\Delta\phi$ is a *Heisenberg relation*.

$$\Delta m/2 = 1/\Delta\phi \text{ ,or:} \qquad\qquad \Delta m\, \Delta\phi = 2 \qquad\qquad (9.3.15)$$

Bohr wave quantum speed limits

$$V_{group}^{Bohr}(m\leftrightarrow n) = \frac{\omega_m - \omega_n}{k_m - k_n} = \frac{\left(m^2 - n^2\right)h\upsilon_1}{\left(m-n\right)h/L} = (m+n)\frac{L}{\tau_1} = (m+n)V_1 \quad (9.3.16)$$

Predicting fractional revivals: *Farey Sum* $\oplus_F$ of the rational fractions n_1/d_1 and n_2/d_2

$$t_{12-intersection} = \frac{n_2 + n_1}{d_2 + d_1} = \frac{n_2}{d_2} \oplus_F \frac{n_1}{d_1} \qquad\qquad (9.3.18)$$

U(2)-Oscillation and R(3)-Rotation Analogies for 2-Dimension or Spin-1/2 Systems

General U(2) Hamiltonian Matrix

$$\begin{pmatrix} A & B-iC \\ B+iC & D \end{pmatrix} =$$

$$\begin{pmatrix} 2\Omega_0 + \Omega_Z & \Omega_X - i\Omega_Y \\ \Omega_X + i\Omega_Y & 2\Omega_0 - \Omega_Z \end{pmatrix}\frac{1}{2}$$

General U(2) State Vector $|\Psi\rangle =$

$$\begin{pmatrix} \Psi_1 \\ \Psi_1 \end{pmatrix} = \begin{pmatrix} x_1 + i\, p_1 \\ x_2 + i\, p_2 \end{pmatrix}$$

$$= \sqrt{N}\begin{pmatrix} e^{-i\alpha/2}\cos\beta/2 \\ e^{i\alpha/2}\sin\beta/2 \end{pmatrix}e^{-i\frac{\gamma}{2}}$$

Asymmetric Diagonal C_2^A

$$\mathbf{H} = \begin{pmatrix} A & 0 \\ 0 & D \end{pmatrix} = \Omega_0\mathbf{1} + \Omega_A\sigma_A$$

$$= \frac{A+D}{2}\begin{pmatrix} 1 & 0 \\ 0 & 1 \end{pmatrix} + \frac{A-D}{2}\begin{pmatrix} 1 & 0 \\ 0 & -1 \end{pmatrix}$$

Bilateral(Balanced) C_2^B

$$\mathbf{H} = \begin{pmatrix} A & B \\ B & A \end{pmatrix} = \Omega_0\mathbf{1} + \Omega_B\sigma_B$$

$$= A\begin{pmatrix} 1 & 0 \\ 0 & 1 \end{pmatrix} + B\begin{pmatrix} 0 & 1 \\ 1 & 0 \end{pmatrix}$$

Circular, Cyclotron, Curly C_2^C

$$\mathbf{H} = \begin{pmatrix} A & -iC \\ iC & A \end{pmatrix} = \Omega_0\mathbf{1} + \Omega_C\sigma_C$$

$$= A\begin{pmatrix} 1 & 0 \\ 0 & 1 \end{pmatrix} + C\begin{pmatrix} 0 & -i \\ i & 0 \end{pmatrix}$$

Hermitian Hamilton-Jordan-Pauli-Jones ABC or XYZ operator basis for U(2) Hamiltonians

A - Type or Z - Spin Op

$$\frac{iq_Z}{2} = J_Z = S_Z = \frac{\sigma_Z}{2}$$

$$= S_A = \begin{pmatrix} 1 & 0 \\ 0 & -1 \end{pmatrix}\frac{1}{2}$$

B - Type or X - Spin Op

$$\frac{iq_X}{2} = J_X = S_X = \frac{\sigma_X}{2}$$

$$= S_B = \begin{pmatrix} 0 & 1 \\ 1 & 0 \end{pmatrix}\frac{1}{2}$$

C - Type or Y - Spin Op

$$\frac{iq_Y}{2} = J_Y = S_Y = \frac{\sigma_Y}{2}$$

$$= S_C = \begin{pmatrix} 0 & -i \\ i & 0 \end{pmatrix}\frac{1}{2}$$

A − Spin Expectaion Value

$$S_Z = S_A = \langle\Psi|\mathbf{S}_Z|\Psi\rangle$$
$$= N\left(p_1^2 + x_1^2 - p_2^2 - x_2^2\right)/2$$
$$= (N/2)\,\cos\beta$$
$$= \left(\Psi_1^*\Psi_1 - \Psi_2^*\Psi_2\right)/2$$

B − Spin Expectaion Value

$$S_X = S_B = \langle\Psi|\mathbf{S}_X|\Psi\rangle$$
$$= N\left(x_1 x_2 + p_1 p_2\right)$$
$$= (N/2)\,\cos\alpha\,\sin\beta$$
$$= \text{Re }\Psi_1^*\Psi_2$$

C − Spin Expectation Value

$$S_Y = S_C = \langle\Psi|\mathbf{S}_Y|\Psi\rangle$$
$$= N\left(x_1 p_2 - x_2 p_1\right)$$
$$= (N/2)\,\sin\alpha\,\sin\beta$$
$$= \text{Im }\Psi_1^*\Psi_2$$

$U(2)\,Hamiltonian\,Operator\,\mathbf{H}$ $\qquad$ $U(2)$ $\mathbf{H}$ in ABC $notation$

$$\mathbf{H} = \begin{pmatrix} A & B-iC \\ B+iC & D \end{pmatrix}$$

$$\mathbf{H} = \Omega_0\mathbf{1} + \mathbf{\Omega}\bullet\mathbf{S} \,, \quad \mathbf{\Omega}\bullet\mathbf{S} = \qquad \mathbf{H} = \Omega_0\mathbf{1} + \mathbf{\Omega}\bullet\mathbf{S} \,, \quad \mathbf{\Omega}\bullet\mathbf{S} =$$

$$= \Omega_X\mathbf{S}_X + \Omega_Y\mathbf{S}_Y + \Omega_Z\mathbf{S}_Z \qquad = (A-D)\mathbf{S}_A + 2B\mathbf{S}_B + 2C\mathbf{S}_C$$

$$= \Omega_X\frac{\sigma_X}{2} + \Omega_Y\frac{\sigma_Z}{2} + \Omega_Z\frac{\sigma_Z}{2} \qquad = \frac{A-D}{2}\sigma_Z + B\sigma_X + C\sigma_Y$$

$$\Omega_Z = \Omega_A = H_{11} - H_{22} = A-D \qquad \Omega_X = \Omega_B = 2\mathrm{Re}H_{21} = 2B \qquad \Omega_Y = \Omega_C = 2\mathrm{Im}H_{21} = 2C$$

$$= \Omega\,\cos\vartheta \;\; (\mathbf{H}\text{-}Crank\;A\text{-}Component) \qquad = \Omega\cos\varphi\,\sin\vartheta \;\;(\Omega\;B\text{-}Component) \quad = \Omega\sin\varphi\,\sin\vartheta \;\;(\Omega\;C\text{-}Component)$$

Density Operator (Pure 2-state only) $\rho = |\Psi\rangle\langle\Psi| = \begin{pmatrix} \Psi_1 \\ \Psi_2 \end{pmatrix} \otimes \begin{pmatrix} \Psi_1^* & \Psi_2^* \end{pmatrix} = \begin{pmatrix} \Psi_1\Psi_1^* & \Psi_1\Psi_2^* \\ \Psi_2\Psi_1^* & \Psi_2\Psi_2^* \end{pmatrix}$

$$\begin{pmatrix} \rho_{11} & \rho_{12} \\ \rho_{21} & \rho_{22} \end{pmatrix} = \begin{pmatrix} \Psi_1^*\Psi_1 & \Psi_2^*\Psi_1 \\ \Psi_1^*\Psi_2 & \Psi_2^*\Psi_2 \end{pmatrix} = \rho = \frac{N}{2}\,\mathbf{1} + S_X\sigma_X + S_Y\sigma_Y + S_Z\sigma_Z \qquad = N/2\,\mathbf{1} + \mathbf{S}\bullet\mathbf{\sigma}$$

Bloch equations. $\qquad i\hbar\dfrac{\partial}{\partial t}\rho = i\hbar\dot{\rho} = \mathbf{H}\rho - \rho\mathbf{H} = [\mathbf{H},\rho] \quad$ or: $\quad \dfrac{\partial\mathbf{S}}{\partial t} = \dot{\mathbf{S}} = \mathbf{\Omega}\times\mathbf{S}$

Hamilton-Pauli Identities

$$(\mathbf{A}\bullet\mathbf{\sigma})(\mathbf{B}\bullet\mathbf{\sigma}) = \mathbf{A}\bullet\mathbf{B} + i(\mathbf{A}\times\mathbf{B})\bullet\mathbf{\sigma}\,, \qquad\qquad \sigma_\mu\,\sigma_\nu = \delta_{\mu\nu}\mathbf{1} + i\,\varepsilon_{\mu\nu\lambda}\,\sigma_\lambda\,.$$

SU(2) rotation matrix by rotation axis vector $\Theta = \Omega\,t.$ and *Two-state evolution operator*

$$\mathbf{R}[\Theta] = \cos\frac{\Theta}{2}\,\mathbf{1} \;-\; i\sigma_X\,\hat{\Theta}_X\sin\frac{\Theta}{2} \;-\; i\sigma_Y\,\hat{\Theta}_Y\sin\frac{\Theta}{2} \;-\; i\sigma_Z\,\hat{\Theta}_Z\sin\frac{\Theta}{2}$$

$$\begin{pmatrix} \langle 1|\mathbf{R}[\Theta]|1\rangle & \langle 1|\mathbf{R}[\Theta]|2\rangle \\ \langle 2|\mathbf{R}[\Theta]|1\rangle & \langle 2|\mathbf{R}[\Theta]|2\rangle \end{pmatrix} = \begin{pmatrix} \cos\frac{\Theta}{2} - i\hat{\Theta}_Z\sin\frac{\Theta}{2} & -i\sin\frac{\Theta}{2}(\hat{\Theta}_X - i\hat{\Theta}_Y) \\ -i\sin\frac{\Theta}{2}(\hat{\Theta}_X + i\hat{\Theta}_Y) & \cos\frac{\Theta}{2} + i\hat{\Theta}_Z\sin\frac{\Theta}{2} \end{pmatrix} \qquad (10.5.25b)$$

The rotation axis is given by its *polar coordinates* (φ, ϑ) and *angle of turn* $\Theta = \sqrt{\Theta_X^2 + \Theta_Y^2 + \Theta_Z^2} = \Omega\,t.$

$$\Theta = (\Theta_X, \Theta_Y, \Theta_Z) = \Theta\,(\cos\varphi\,\sin\vartheta, \sin\varphi\,\sin\vartheta, \cos\vartheta) = (\Theta_B, \Theta_C, \Theta_A)$$

Unit rotation axis vector $\hat{\Theta} = \vec{\Theta}/|\Theta| = \begin{pmatrix} \hat{\Theta}_X, & \hat{\Theta}_Y, & \hat{\Theta}_Z \end{pmatrix} = \begin{pmatrix} \cos\varphi\sin\vartheta & \sin\varphi\sin\vartheta & \cos\vartheta \end{pmatrix}$

$$\mathbf{R}[\Theta] = \begin{pmatrix} \cos\frac{\Theta}{2} - i\cos\vartheta\sin\frac{\Theta}{2} & -i\sin\frac{\Theta}{2}(\cos\varphi\sin\vartheta - i\sin\varphi\sin\vartheta) \\ -i\sin\frac{\Theta}{2}(\cos\varphi\sin\vartheta + i\sin\varphi\sin\vartheta) & \cos\frac{\Theta}{2} + i\cos\vartheta\sin\frac{\Theta}{2} \end{pmatrix} \qquad (10.5.25c)$$

$$= \mathbf{R}[\varphi\vartheta\Theta] = \begin{pmatrix} \cos\frac{\Theta}{2} - i\cos\vartheta\sin\frac{\Theta}{2} & -ie^{-i\varphi}\sin\vartheta\sin\frac{\Theta}{2} \\ -ie^{i\varphi}\sin\vartheta\sin\frac{\Theta}{2} & \cos\frac{\Theta}{2} + i\cos\vartheta\sin\frac{\Theta}{2} \end{pmatrix} = e^{-i\mathbf{H}t} = e^{-i\mathbf{\Theta}\bullet\mathbf{S}}$$

Hamiltonian generator determines crank rate Ω.

$$\Omega_Z = \Omega_A = H_{11} - H_{22} = A-D \qquad \Omega_X = \Omega_B = 2\mathrm{Re}H_{21} = 2B \qquad \Omega_Y = \Omega_C = 2\mathrm{Im}H_{21} = 2C$$

$$= \Omega\,\cos\vartheta \;\; (\mathbf{H}\text{-}Crank\;A\text{-}Component) \qquad = \Omega\cos\varphi\,\sin\vartheta \;\;(\Omega\;B\text{-}Component) \quad = \Omega\sin\varphi\,\sin\vartheta \;\;(\Omega\;C\text{-}Component)$$

U(2)-R(3) Two-State and Spin-Vector Summary

Hamiltonian **H**	*Hamiltonian* Ω*-vector*	*Eigenvectors* $|\varepsilon\rangle, |\varepsilon'\rangle$ *and*	*Spin expectation* **S**-*vector*
Operator & matrix		*mirror planes (if any) for each eigenvector*	
in $|1\rangle,|2\rangle$-*basis*	*in ABC-space*	*in* $|1\rangle,|2\rangle$-*space*	*in ABC-space*

$$\mathbf{H} = \Omega_0 \mathbf{1} + \boldsymbol{\Omega} \bullet \mathbf{S}$$

$$= \frac{(A+D)}{2}\mathbf{1} + (A-D)\mathbf{S}_A$$
$$+ 2B\mathbf{S}_B + 2C\mathbf{S}_C$$

$$= \begin{pmatrix} A & B - iC \\ B + iC & D \end{pmatrix}$$

$$\vec{\Omega} = \begin{pmatrix} \Omega_A \\ \Omega_B \\ \Omega_C \end{pmatrix} = \begin{pmatrix} A - D \\ 2B \\ 2C \end{pmatrix}$$

$$|\varepsilon\rangle = \begin{pmatrix} x_1 + ip_1 \\ x_2 + ip_2 \end{pmatrix}$$

$$|\varepsilon'\rangle = \begin{pmatrix} x_1' + ip_1' \\ x_2' + ip_2' \end{pmatrix}$$

$$\mathbf{S} = \begin{pmatrix} S_A \\ S_B \\ S_C \end{pmatrix} = \begin{pmatrix} \langle\varepsilon|\mathbf{S}_A|\varepsilon\rangle \\ \langle\varepsilon|\mathbf{S}_B|\varepsilon\rangle \\ \langle\varepsilon|\mathbf{S}_C|\varepsilon\rangle \end{pmatrix}$$

$$= \begin{pmatrix} \dfrac{x_1^2 + p_1^2 - x_2^2 - p_2^2}{2} \\ x_1 x_2 + p_1 p_2 \\ x_1 p_2 - x_2 p_1 \end{pmatrix}$$

A. Asymmetric – Diagonal

$$\mathbf{H}^A =$$
$$\frac{(A+D)}{2}\mathbf{1} + (A-D)\mathbf{S}_A$$
$$= \begin{pmatrix} A & 0 \\ 0 & D \end{pmatrix}$$

$$\vec{\Omega} = \begin{pmatrix} \Omega_A \\ \Omega_B \\ \Omega_C \end{pmatrix} = \begin{pmatrix} A - D \\ 0 \\ 0 \end{pmatrix}$$

$$|\varepsilon_1\rangle = \begin{pmatrix} 1 \\ 0 \end{pmatrix}$$

$$|\varepsilon_2\rangle = \begin{pmatrix} 0 \\ 1 \end{pmatrix}$$

$$\begin{pmatrix} \langle\varepsilon_1|\mathbf{S}_A|\varepsilon_1\rangle \\ \langle\varepsilon_1|\mathbf{S}_B|\varepsilon_1\rangle \\ \langle\varepsilon_1|\mathbf{S}_C|\varepsilon_1\rangle \end{pmatrix} = \begin{pmatrix} 1/2 \\ 0 \\ 0 \end{pmatrix}$$

$$\begin{pmatrix} \langle\varepsilon_2|\mathbf{S}_A|\varepsilon_2\rangle \\ \langle\varepsilon_2|\mathbf{S}_B|\varepsilon_2\rangle \\ \langle\varepsilon_2|\mathbf{S}_C|\varepsilon_2\rangle \end{pmatrix} = \begin{pmatrix} -1/2 \\ 0 \\ 0 \end{pmatrix}$$
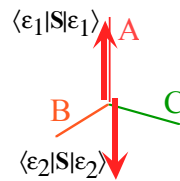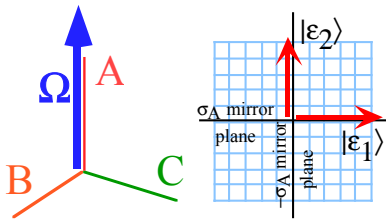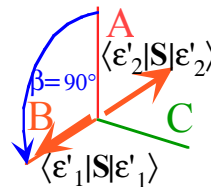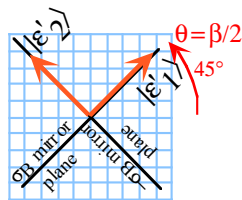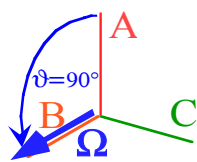

B. Bilateral – Balanced

$$\mathbf{H}^B =$$
$$A \cdot \mathbf{1} + 2B\mathbf{S}_B$$
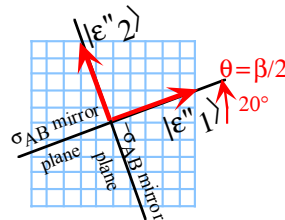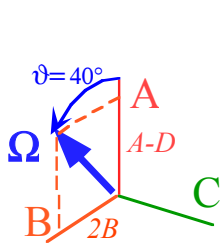$$= \begin{pmatrix} A & B \\ B & A \end{pmatrix}$$

$$\vec{\Omega} = \begin{pmatrix} \Omega_A \\ \Omega_B \\ \Omega_C \end{pmatrix} = \begin{pmatrix} 0 \\ 2B \\ 0 \end{pmatrix}$$

$$|\varepsilon_1'\rangle = \begin{pmatrix} 1/\sqrt{2} \\ 1/\sqrt{2} \end{pmatrix}$$

$$|\varepsilon_2'\rangle = \begin{pmatrix} -1/\sqrt{2} \\ 1/\sqrt{2} \end{pmatrix}$$

$$\begin{pmatrix} \langle\varepsilon_1'|\mathbf{S}_A|\varepsilon_1'\rangle \\ \langle\varepsilon_1'|\mathbf{S}_B|\varepsilon_1'\rangle \\ \langle\varepsilon_1'|\mathbf{S}_C|\varepsilon_1'\rangle \end{pmatrix} = \begin{pmatrix} 0 \\ 1/2 \\ 0 \end{pmatrix}$$

$$\begin{pmatrix} \langle\varepsilon_2'|\mathbf{S}_A|\varepsilon_2'\rangle \\ \langle\varepsilon_2'|\mathbf{S}_B|\varepsilon_2'\rangle \\ \langle\varepsilon_2'|\mathbf{S}_C|\varepsilon_2'\rangle \end{pmatrix} = \begin{pmatrix} 0 \\ -1/2 \\ 0 \end{pmatrix}$$

$$S_B = \frac{1}{2}\begin{pmatrix} 0 & 1 \\ 1 & 0 \end{pmatrix} = \frac{1}{2}\sigma_B$$

AB. Asymmetric − Bilateral

$$\mathbf{H}^{AB} = \frac{(A-D)}{2}\mathbf{1} +$$
$$+ (A-D)\mathbf{S}_A + 2B\mathbf{S}_B$$
$$= \begin{pmatrix} A & B \\ B & D \end{pmatrix}$$

$$\vec{\Omega} = \begin{pmatrix} \Omega_A \\ \Omega_B \\ \Omega_C \end{pmatrix} = \begin{pmatrix} A-D \\ 2B \\ 0 \end{pmatrix}$$

$$\left|\varepsilon_1''\right\rangle = \begin{pmatrix} \cos\theta \\ \sin\theta \end{pmatrix}$$

$$\left|\varepsilon_2''\right\rangle = \begin{pmatrix} -\sin\theta \\ \cos\theta \end{pmatrix}$$

$$\begin{pmatrix} \langle\varepsilon_1''|\mathbf{S}_A|\varepsilon_1''\rangle \\ \langle\varepsilon_1''|\mathbf{S}_B|\varepsilon_1''\rangle \\ \langle\varepsilon_1''|\mathbf{S}_C|\varepsilon_1''\rangle \end{pmatrix} = \frac{1}{2}\begin{pmatrix} \cos\beta \\ \sin\beta \\ 0 \end{pmatrix}$$

$$\begin{pmatrix} \langle\varepsilon_2''|\mathbf{S}_A|\varepsilon_2''\rangle \\ \langle\varepsilon_2''|\mathbf{S}_B|\varepsilon_2''\rangle \\ \langle\varepsilon_2''|\mathbf{S}_C|\varepsilon_2''\rangle \end{pmatrix} = \frac{1}{2}\begin{pmatrix} -\cos\beta \\ -\sin\beta \\ 0 \end{pmatrix}$$
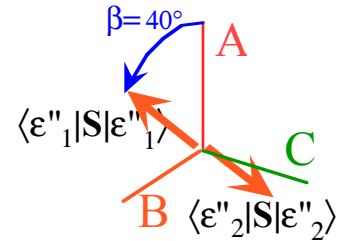
C. Circular − Complex

$$\mathbf{H}^C =$$
$$A\cdot\mathbf{1} + 2C\mathbf{S}_C$$
$$= \begin{pmatrix} A & -iC \\ iC & A \end{pmatrix}$$

$$\vec{\Omega} = \begin{pmatrix} \Omega_A \\ \Omega_B \\ \Omega_C \end{pmatrix} = \begin{pmatrix} 0 \\ 0 \\ 2C \end{pmatrix}$$
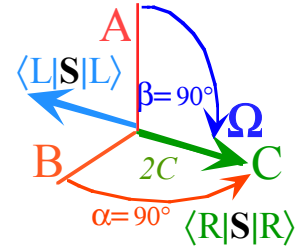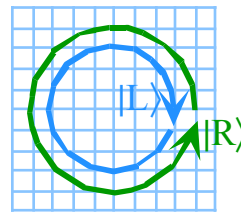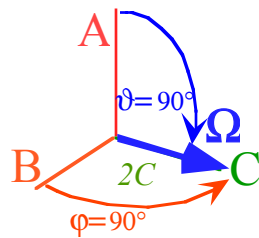
$$\left|R\right\rangle = \begin{pmatrix} 1/\sqrt{2} \\ i/\sqrt{2} \end{pmatrix}$$

$$\left|L\right\rangle = \begin{pmatrix} 1/\sqrt{2} \\ -i/\sqrt{2} \end{pmatrix}$$

$$\begin{pmatrix} \langle R|\mathbf{S}_A|R\rangle \\ \langle R|\mathbf{S}_B|R\rangle \\ \langle R|\mathbf{S}_C|R\rangle \end{pmatrix} = \begin{pmatrix} 0 \\ 0 \\ 1/2 \end{pmatrix}$$

$$\begin{pmatrix} \langle L|\mathbf{S}_A|L\rangle \\ \langle L|\mathbf{S}_B|L\rangle \\ \langle L|\mathbf{S}_C|L\rangle \end{pmatrix} = \begin{pmatrix} 0 \\ 0 \\ -1/2 \end{pmatrix}$$

$$S_C = \frac{1}{2}\begin{pmatrix} 0 & -i \\ i & 0 \end{pmatrix}$$
$$= \frac{1}{2}\sigma_C$$

Polar Angle Descriptions of U(2) Hamiltonian **H** *and its state space* $|\varepsilon\rangle, |\varepsilon'\rangle$...

Crank Axis angles $(\varphi, \vartheta, \Omega)$ $(\Omega = \sqrt{\Omega_X^2 + \Omega_Y^2 + \Omega_Z^2})$ *Spin Vector Euler angles* (α, β, γ)

$$\mathbf{H} = \Omega_0\mathbf{1} + \vec{\Omega}\bullet\mathbf{S} = \frac{1}{2}\begin{pmatrix} 2\Omega_0 + \Omega_Z & \Omega_X - i\Omega_Y \\ \Omega_X + i\Omega_Y & 2\Omega_0 - \Omega_Z \end{pmatrix}$$

$$\vec{\Omega} = \begin{pmatrix} \Omega_A \\ \Omega_B \\ \Omega_C \end{pmatrix} = \begin{pmatrix} A-D \\ 2B \\ 2C \end{pmatrix} =$$

$$\begin{pmatrix} \Omega_Z \\ \Omega_X \\ \Omega_Y \end{pmatrix} = \Omega\begin{pmatrix} \cos\vartheta \\ \cos\varphi\sin\vartheta \\ \sin\varphi\sin\vartheta \end{pmatrix}$$

$$\left|\varepsilon\right\rangle = \begin{pmatrix} e^{-i\alpha/2}\cos\beta/2 \\ e^{i\alpha/2}\sin\beta/2 \end{pmatrix}e^{-i\frac{\gamma}{2}}$$
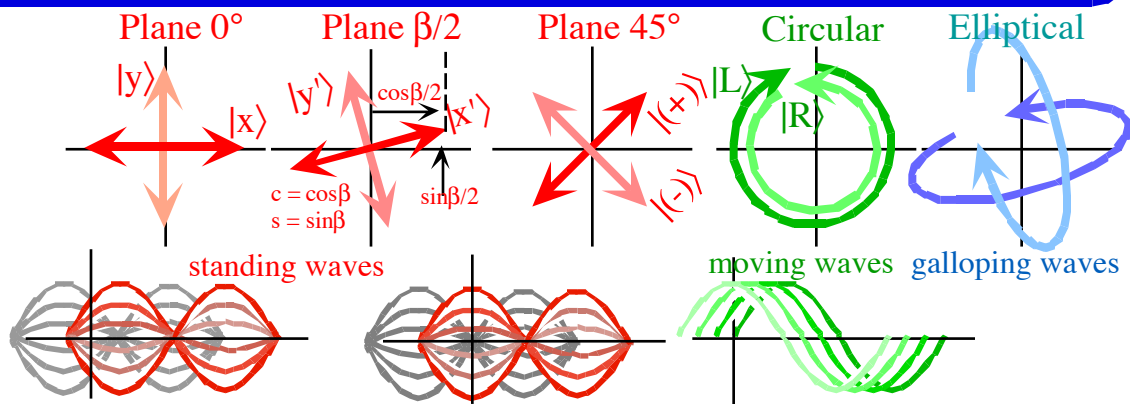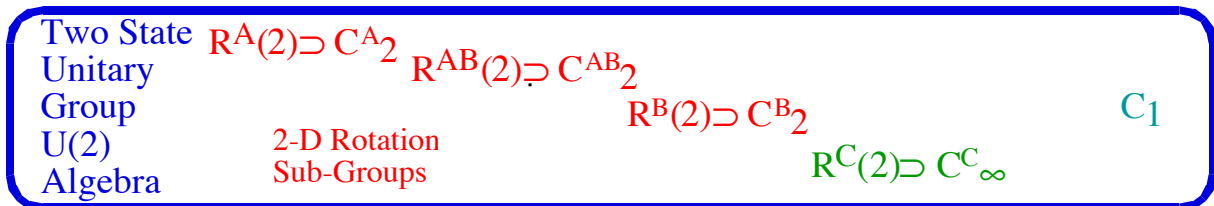
$$\left|\varepsilon'\right\rangle = \begin{pmatrix} -e^{-i\alpha/2}\sin\beta/2 \\ e^{i\alpha/2}\cos\beta/2 \end{pmatrix}e^{-i\frac{\gamma}{2}}$$

$$\mathbf{S} = \begin{pmatrix} S_A \\ S_B \\ S_C \end{pmatrix} = \begin{pmatrix} \langle\varepsilon|\mathbf{S}_A|\varepsilon\rangle \\ \langle\varepsilon|\mathbf{S}_B|\varepsilon\rangle \\ \langle\varepsilon|\mathbf{S}_C|\varepsilon\rangle \end{pmatrix}$$

$$\mathbf{S} = \begin{pmatrix} \cos\beta \\ \cos\alpha\sin\beta \\ \sin\alpha\sin\beta \end{pmatrix}$$
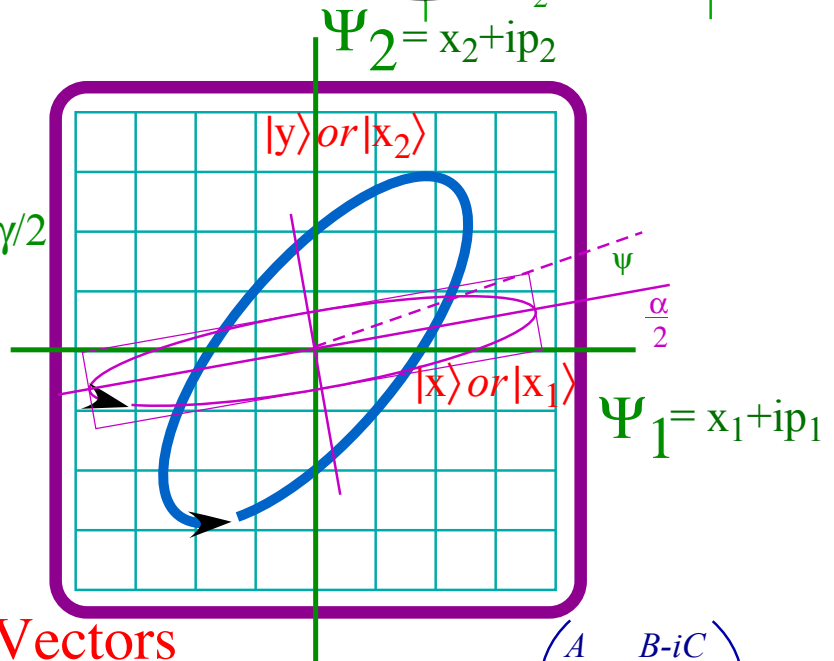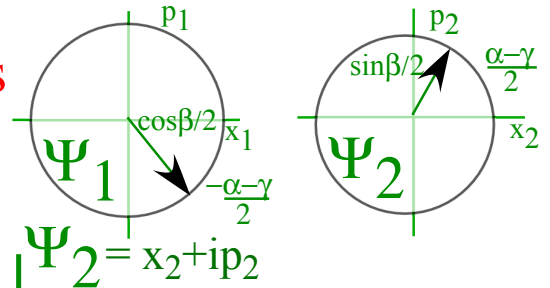
Catalog of Two - State Hamiltonians

	$H_{U(2)} =$	$H_{C_2^A} =$	$H_{C_2^{AB}} =$	$H_{C_2^B} =$	$H_{C_2^C} =$	$H_{C_1} =$
$H = H^\dagger =$	$\begin{pmatrix} A & 0 \\ 0 & A \end{pmatrix}$	$\begin{pmatrix} A & 0 \\ 0 & D \end{pmatrix}$	$\begin{pmatrix} A & B \\ B & D \end{pmatrix}$	$\begin{pmatrix} A & B \\ B & A \end{pmatrix}$	$\begin{pmatrix} A & -iC \\ iC & A \end{pmatrix}$	$\begin{pmatrix} A & B-iC \\ B+iC & D \end{pmatrix}$
Commute with :	$U=$ $\begin{pmatrix} U_{11} & U_{12} \\ U_{21} & U_{22} \end{pmatrix}$	$R(\theta)=$ $\begin{pmatrix} e^{-i\theta} & 0 \\ 0 & e^{i\theta} \end{pmatrix}$	$R(\zeta)=$ $\begin{pmatrix} \cos\zeta \\ -ic\sin\zeta & -is\sin\zeta \\ \\ -is\sin\zeta & \cos\zeta \\ & +ic\sin\zeta \end{pmatrix}$	$R(\chi)=$ $\begin{pmatrix} \cos\chi & -i\sin\chi \\ -i\sin\chi & \cos\chi \end{pmatrix}$	$R(\varphi)=$ $\begin{pmatrix} \cos\varphi & -\sin\varphi \\ \sin\varphi & \cos\varphi \end{pmatrix}$	$\mathbf{1}(\lambda)=$ $e^{i\lambda}\begin{pmatrix} 1 & 0 \\ 0 & 1 \end{pmatrix}$
Generated by :	$e_{11}=\begin{pmatrix} 1 & 0 \\ 0 & 0 \end{pmatrix}$ $e_{12}=\begin{pmatrix} 0 & 1 \\ 0 & 0 \end{pmatrix}$ $e_{21}=\begin{pmatrix} 0 & 0 \\ 1 & 0 \end{pmatrix}$ $e_{22}=\begin{pmatrix} 0 & 0 \\ 0 & 1 \end{pmatrix}$	$G_A=$ $\left.\dfrac{dR(\theta)}{d\theta}\right\|_0=$ $\begin{pmatrix} -i & 0 \\ 0 & i \end{pmatrix}$	$G_{AB}=$ $\left.\dfrac{dR(\zeta)}{d\zeta}\right\|_0=$ $\begin{pmatrix} -ic & -is \\ -is & ic \end{pmatrix}$	$G_B=$ $\left.\dfrac{dR(\chi)}{d\chi}\right\|_0=$ $\begin{pmatrix} 0 & -i \\ -i & 0 \end{pmatrix}$	$G_C=$ $\left.\dfrac{dR(\varphi)}{d\varphi}\right\|_0=$ $\begin{pmatrix} 0 & -1 \\ 1 & 0 \end{pmatrix}$	$G_1=$ $\left.\dfrac{dR(\lambda)}{d\lambda}\right\|_0=$ $\begin{pmatrix} 1 & 0 \\ 0 & 1 \end{pmatrix}$
Spin Operator :	(all)	$\sigma_A=$ $iG_A=$ $\begin{pmatrix} 1 & 0 \\ 0 & -1 \end{pmatrix}$	$\sigma_{AB}=$ $iG_{AB}=$ $\begin{pmatrix} c & s \\ s & -c \end{pmatrix}$	$\sigma_B=$ $iG_B=$ $\begin{pmatrix} 0 & 1 \\ 1 & 0 \end{pmatrix}$	$\sigma_C=$ $iG_C=$ $\begin{pmatrix} 0 & -i \\ i & 0 \end{pmatrix}$	$\sigma_0=$ $\begin{pmatrix} 1 & 0 \\ 0 & 1 \end{pmatrix}$
Symmetry :	$U(2)$	$C_2^A \subset R^A(2)$	$C_2^{AB} \subset R^{AB}(2)$	$C_2^B \subset R^B(2)$	$C_\infty^C \subset R^C(2)$	C_1
H Eigenkets	(Any ket is an eigenvector)	$\|x\rangle$ $\begin{pmatrix} 1 \\ 0 \end{pmatrix}$, $\|y\rangle$ $\begin{pmatrix} 0 \\ 1 \end{pmatrix}$	$\|x'\rangle$ $\begin{pmatrix} \cos\frac{\beta}{2} \\ \sin\frac{\beta}{2} \end{pmatrix}$ $\|y'\rangle$ $\begin{pmatrix} -\sin\frac{\beta}{2} \\ \cos\frac{\beta}{2} \end{pmatrix}$	$\|(+)\rangle$ $\dfrac{\begin{pmatrix} 1 \\ 1 \end{pmatrix}}{\sqrt{2}}$, $\|(-)\rangle$ $\dfrac{\begin{pmatrix} 1 \\ -1 \end{pmatrix}}{\sqrt{2}}$	$\|L\rangle$ $\dfrac{\begin{pmatrix} 1 \\ -i \end{pmatrix}}{\sqrt{2}}$, $\|R\rangle$ $\dfrac{\begin{pmatrix} 1 \\ i \end{pmatrix}}{\sqrt{2}}$	$(\|\varepsilon\rangle$ Depends on $A, B, C,$ and $D)$

Two State Unitary Group U(2) Algebra

$R^A(2) \supset C^A_2$ $R^{AB}(2) \supset C^{AB}_2$

$R^B(2) \supset C^B_2$ C_1

2-D Rotation Sub-Groups

$R^C(2) \supset C^C_\infty$

Plane 0°   Plane β/2   Plane 45°   Circular   Elliptical

$|y\rangle$ $|x\rangle$ $|y'\rangle$ $\cos\beta/2$ $|x'\rangle$ $|(+)\rangle$ $|L\rangle$ $|R\rangle$

$c = \cos\beta$ $s = \sin\beta$ $\sin\beta/2$ $|(-)\rangle$

standing waves   moving waves   galloping waves

U(2) World : Complex 2D Spinors

2-State ket $|\Psi\rangle =$

$$\begin{pmatrix} \Psi_1 \\ \Psi_2 \end{pmatrix} = \begin{pmatrix} \sqrt{N}e^{-i\alpha/2}\cos\beta/2 \\ \sqrt{N}e^{i\alpha/2}\sin\beta/2 \end{pmatrix} e^{-i\gamma/2}$$
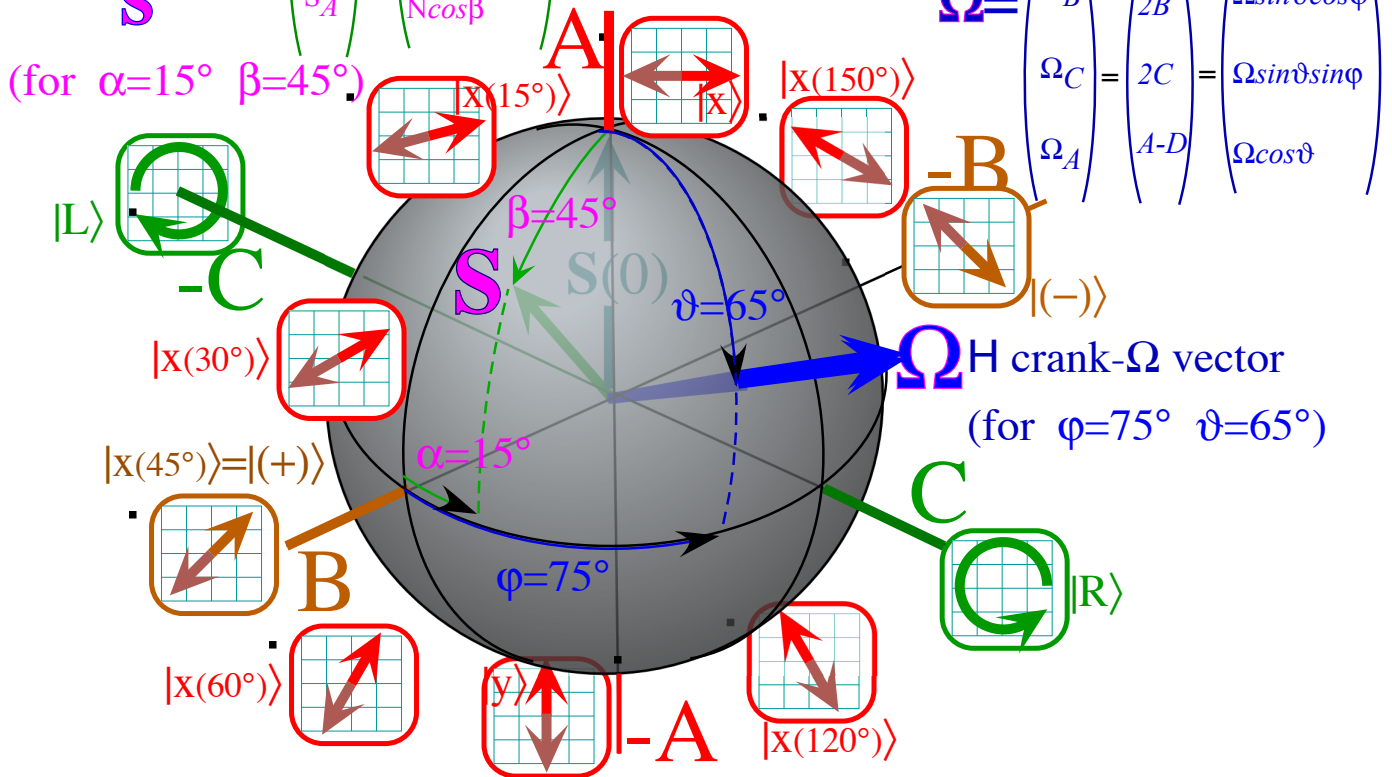
Ψ_1 p_1 $\cos\beta/2$ x_1 $-\frac{\alpha-\gamma}{2}$

Ψ_2 p_2 $\sin\beta/2$ $\frac{\alpha-\gamma}{2}$ x_2

$\Psi_2 = x_2 + ip_2$

$|y\rangle\, or\, |x_2\rangle$

ψ

$\frac{\alpha}{2}$

$|x\rangle\, or\, |x_1\rangle$

$\Psi_1 = x_1 + ip_1$

R(3) World : Real 3D Vectors

$|\Psi\rangle$ State
Spin Vector S

$$\begin{pmatrix} S_B \\ S_C \\ S_A \end{pmatrix} = \begin{pmatrix} N\sin\beta\cos\alpha \\ N\sin\beta\sin\alpha \\ N\cos\beta \end{pmatrix}\frac{1}{2}$$

(for $\alpha = 15°$ $\beta = 45°$)

H-Operator $\begin{pmatrix} A & B-iC \\ B+iC & D \end{pmatrix}$

Angular velocity

$$\Omega = \begin{pmatrix} \Omega_B \\ \Omega_C \\ \Omega_A \end{pmatrix} = \begin{pmatrix} 2B \\ 2C \\ A-D \end{pmatrix} = \begin{pmatrix} \Omega\sin\vartheta\cos\varphi \\ \Omega\sin\vartheta\sin\varphi \\ \Omega\cos\vartheta \end{pmatrix}$$

A

$|x(15°)\rangle$ $|x\rangle$ $|x(150°)\rangle$

$-B$

$|L\rangle$

$-C$

$|x(30°)\rangle$

S $\beta = 45°$ $S(0)$ $\vartheta = 65°$

$|(-)\rangle$

Ω H crank-Ω vector

(for $\varphi = 75°$ $\vartheta = 65°$)

$|x(45°)\rangle = |(+)\rangle$ $\alpha = 15°$

B

$|x(60°)\rangle$ $\varphi = 75°$

$|y\rangle$ $-A$ $|x(120°)\rangle$

C

$|R\rangle$

*Avoided-crossing Hyperbolas. Eigenvalues and eigenstates of AB-symmetry Stark-effects.*

Easy eigensolution and evolution for polarizer-analyzers based on spin-crank allignment

    The behavior of spin-1/2 or optical polarization states inside analyzers is easy to understand and calculate using the polar angles (α,β) of the state spin vector **S** and the polar angles (φ,ϑ) of the analyzer crank Θ. The first eigenstate (own-state) of the analyzer which flies through the <u>upper</u> path unscathed (except for phase shift) is simply one whose **S** angles (α,β) equal the angles (φ,ϑ) of crank Θ , that is, a state whose spin **S** lies <u>along</u> analyzer crank Θ, or α=φ and β=ϑ.The second eigenstate which flies through the <u>lower</u> path is a state whose spin **S** lies <u>opposite</u> to the analyzer crank Θ, so α=φ and β=ϑ−π. Below ϑ=90° and φ=0° so the eigenstates have spin *up-B* (β=90° and α=0°) or else spin *down-B* (β=-90° and α=0°).
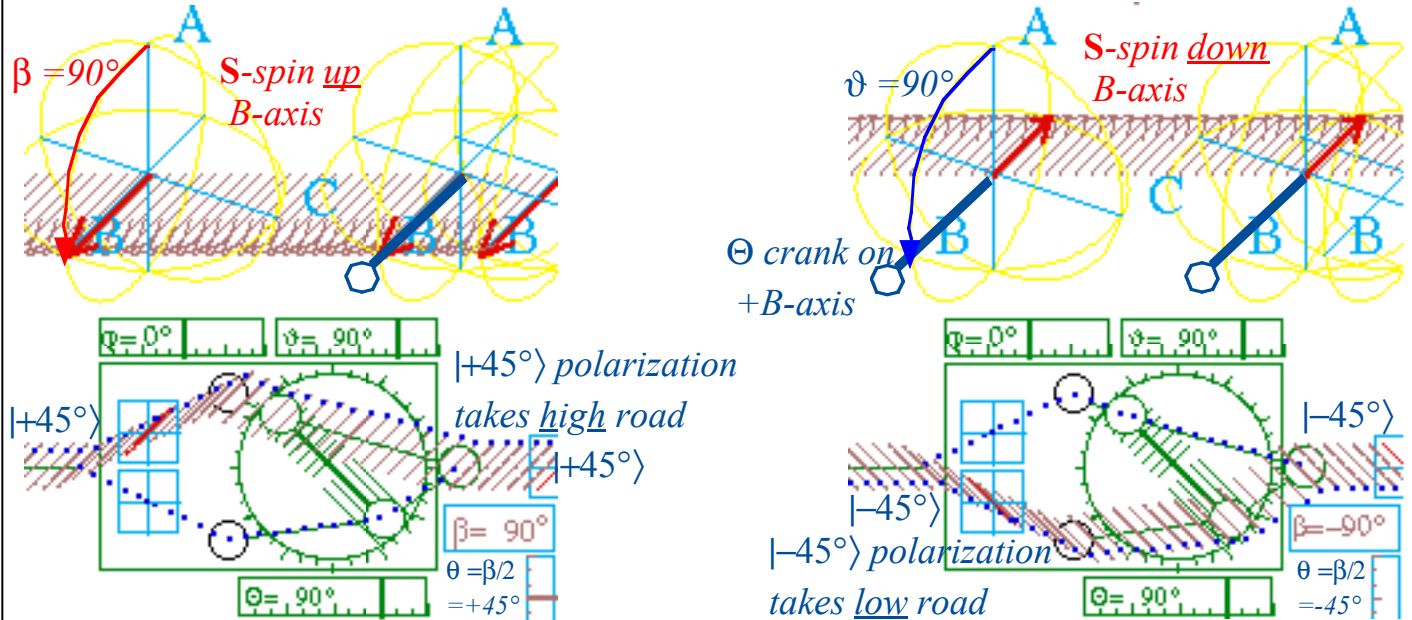
However, other polarization states such as |x⟩ (spin-**S** along the *A*-axis) are changed by going through the analyzer. Now the Θ=90° shift of one path over the other has the effect of rotating the spin vector by Θ=90°. So the first analyzer takes |x⟩ into |L⟩ (left circular or spin *down-C*) and another identical analyzer takes |L⟩ into |y⟩ (vertical or spin *down-A*) . Each of these analyzers acts like a *quarter-wave plate*.

(a) (x_1,x_2) Space

(b) (A,B,C) Space
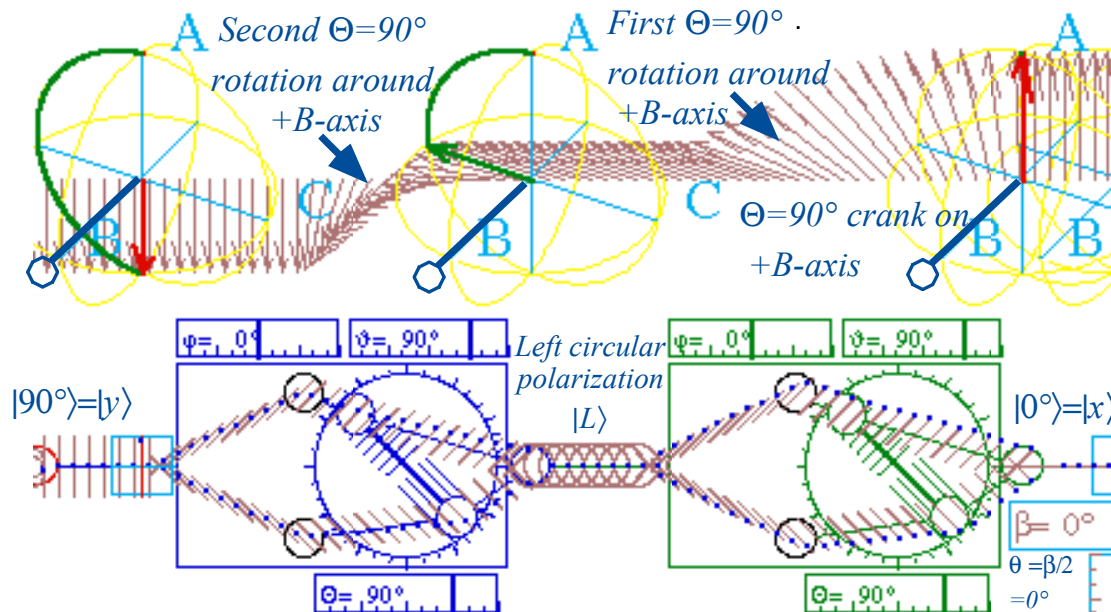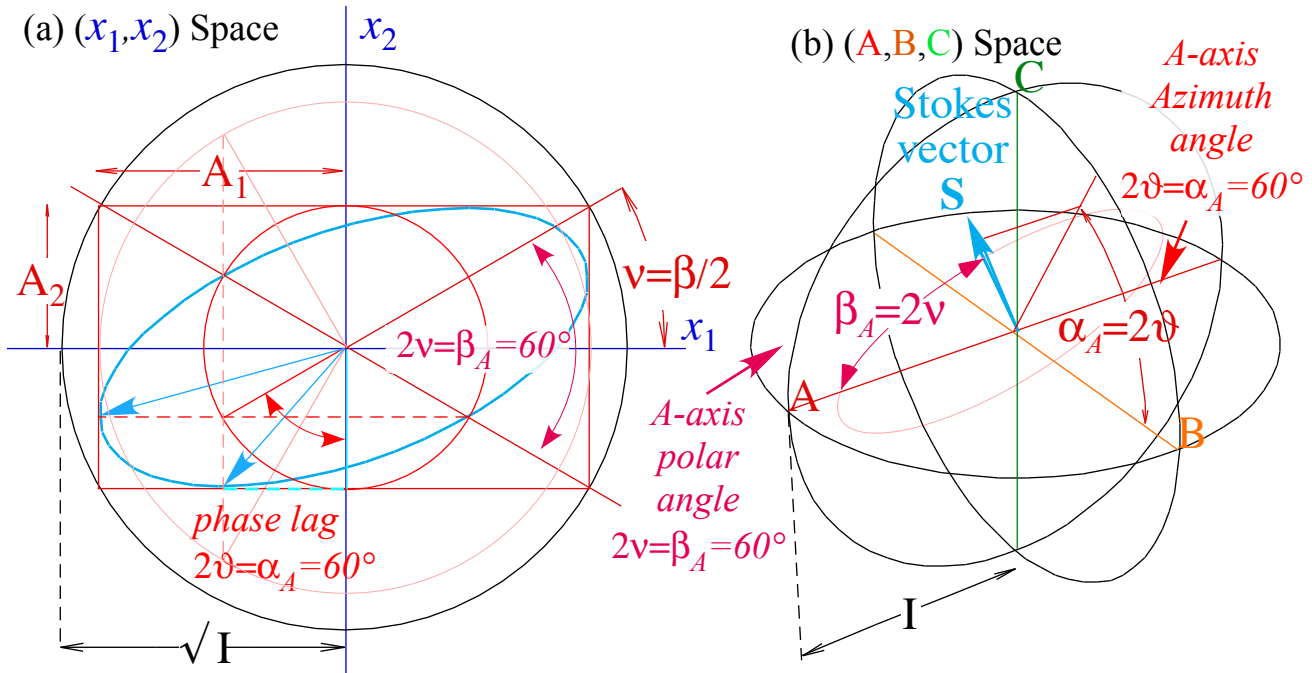
Unit 3 Chapter 10 Appendices A-B: Coordinate Analysis of U(2) States

Appendix 10.A. U(2) Angles and Spin Rotation Operators

Every *U(2)* state $|\Psi(\alpha\beta\gamma)\rangle$ can be obtained from an original base state $|1\rangle$ by doing three rotations shown in Fig. 10.A.1, the first by γ around the *Z* (or *A*) axes, the second by β around *Y* (or *C*) and the third by α around *Z* again. This "favors" the *Z*-axis. Equivalent axial choices are discussed in Appendix 10.B.

$$|\Psi\rangle = \mathbf{R}(\alpha\beta\gamma)|1\rangle = \mathbf{R}(\alpha \text{ around } Z)\ \mathbf{R}(\beta \text{ around } Y)\ \ \mathbf{R}(\gamma \text{ around } Z)\ |1\rangle$$

$$= \begin{pmatrix} e^{-i\frac{\alpha}{2}} & 0 \\ 0 & e^{i\frac{\alpha}{2}} \end{pmatrix} \begin{pmatrix} \cos\frac{\beta}{2} & -\sin\frac{\beta}{2} \\ \sin\frac{\beta}{2} & \cos\frac{\beta}{2} \end{pmatrix} \begin{pmatrix} e^{-i\frac{\gamma}{2}} & 0 \\ 0 & e^{i\frac{\gamma}{2}} \end{pmatrix} \begin{pmatrix} 1 \\ 0 \end{pmatrix}$$

A matrix representation of this gives exactly the original state definition (10.5.8a) with unit norm (*N=1*).

$$\mathbf{R}(\alpha\beta\gamma)|1\rangle = \ \mathbf{R}(\alpha\ 00)\ \mathbf{R}(0\beta\ 0)\ \mathbf{R}(00\gamma) \qquad |1\rangle\ =\ |\Psi\rangle$$

$$= \begin{pmatrix} e^{-i\frac{\alpha+\gamma}{2}}\cos\frac{\beta}{2} & -e^{-i\frac{\alpha-\gamma}{2}}\sin\frac{\beta}{2} \\ e^{i\frac{\alpha-\gamma}{2}}\sin\frac{\beta}{2} & e^{i\frac{\alpha+\gamma}{2}}\cos\frac{\beta}{2} \end{pmatrix} \begin{pmatrix} 1 \\ 0 \end{pmatrix} = \begin{pmatrix} e^{-i\frac{\alpha}{2}}\cos\frac{\beta}{2} \\ e^{i\frac{\alpha}{2}}\sin\frac{\beta}{2} \end{pmatrix} e^{-i\frac{\gamma}{2}} \qquad (10.\text{A}.1\text{a})$$

The resulting *Euler (αβγ)-angle matrix* is simpler in form and construction than the Θ-axis matrix (10.5.25c) using $[\varphi,\vartheta,\Theta]$ angles. Do not confuse the two kinds of angles! We use parentheses () around Euler angles as in $\mathbf{R}(\alpha\beta\gamma)$ while square braces [] are used when a rotation is labeled $\mathbf{R}[\varphi,\vartheta,\Omega t=\Theta]$ by axis-angles. It is important to relate the two. A Hamilton expansion of $\mathbf{R}(\alpha\beta\gamma)$ yields its Θ-axis.

$$\mathbf{R}(\alpha\beta\gamma) = \begin{pmatrix} e^{-i\frac{\alpha+\gamma}{2}}\cos\frac{\beta}{2} & -e^{-i\frac{\alpha-\gamma}{2}}\sin\frac{\beta}{2} \\ e^{i\frac{\alpha-\gamma}{2}}\sin\frac{\beta}{2} & e^{i\frac{\alpha+\gamma}{2}}\cos\frac{\beta}{2} \end{pmatrix} = \cos\frac{\alpha+\gamma}{2}\cos\frac{\beta}{2}\begin{pmatrix} 1 & 0 \\ 0 & 1 \end{pmatrix}$$

$$-i\begin{pmatrix} 0 & 1 \\ 1 & 0 \end{pmatrix}\sin\frac{\gamma-\alpha}{2}\sin\frac{\beta}{2} - i\begin{pmatrix} 0 & -i \\ i & 0 \end{pmatrix}\cos\frac{\gamma-\alpha}{2}\sin\frac{\beta}{2} - i\begin{pmatrix} 1 & 0 \\ 0 & -1 \end{pmatrix}\sin\frac{\alpha+\gamma}{2}\cos\frac{\beta}{2} \qquad (10.\text{A}.1\text{b})$$

We equate $\mathbf{R}(\alpha\beta\gamma)$'s expansion term-by-term to the Θ-axis-angle $\mathbf{R}[\varphi,\vartheta,\Theta]$ expansion (10.5.25a-c).

$$\mathbf{R}[\vec{\Theta}] = \begin{pmatrix} \cos\frac{\Theta}{2} - i\hat{\Theta}_Z\sin\frac{\Theta}{2} & -i\sin\frac{\Theta}{2}(\hat{\Theta}_X - i\hat{\Theta}_Y) \\ -i\sin\frac{\Theta}{2}(\hat{\Theta}_X + i\hat{\Theta}_Y) & \cos\frac{\Theta}{2} + i\hat{\Theta}_Z\sin\frac{\Theta}{2} \end{pmatrix} = \cos\frac{\Theta}{2}\begin{pmatrix} 1 & 0 \\ 0 & 1 \end{pmatrix}$$

$$\textit{(10.5.25a-c)}_{repeated}$$

$$-i\begin{pmatrix} 0 & 1 \\ 1 & 0 \end{pmatrix}\hat{\Theta}_X\sin\frac{\Theta}{2} - i\begin{pmatrix} 0 & -i \\ i & 0 \end{pmatrix}\hat{\Theta}_Y\sin\frac{\Theta}{2} - i\begin{pmatrix} 1 & 0 \\ 0 & -1 \end{pmatrix}\hat{\Theta}_Z\sin\frac{\Theta}{2}$$

The Re-Im 4-D phasor coordinates ($x_j=Re\Psi_j$, $p_j=Im\Psi_j$) show up in the Euler *vs.* Axis angle relations.

$$x_1 = \quad \cos[(\gamma+\alpha)/2]\cos\beta/2 \ = \quad \cos\Theta/2$$
$$-p_2 = \quad \sin[(\gamma-\alpha)/2]\sin\beta/2 \ = \hat{\Theta}_X\sin\Theta/2 = \cos\varphi\ \sin\vartheta\ \sin\Theta/2$$
$$x_2 = \quad \cos[(\gamma-\alpha)/2]\sin\beta/2 \ = \hat{\Theta}_Y\sin\Theta/2 = \sin\varphi\ \sin\vartheta\ \sin\Theta/2 \qquad (10.\text{A}.1\text{c})$$
$$-p_1 = \quad \sin[(\gamma+\alpha)/2]\cos\beta/2 \ = \hat{\Theta}_Z\sin\Theta/2 = \cos\vartheta \qquad \sin\Theta/2$$

Solving these relations yields the following Euler angles in terms of axis angles

$$\alpha = \varphi - \pi/2 + T, \quad \beta = 2\sin^{-1}(\sin\Omega/2 \sin\vartheta), \quad \gamma = \pi/2 - \varphi + T , \qquad (10.A.1d)$$

where; $T = \tan^{-1}(\tan(\Omega/2) \cos\vartheta)$ while the axis-angles in terms of Euler angles are

$$\varphi = (\alpha - \gamma + \pi)/2 , \quad \vartheta = \tan^{-1}[\tan\beta/2/\sin(\alpha+\gamma)/2] , \quad \Omega = 2\cos^{-1}[\cos\beta/2\cos(\alpha+\gamma)/2]. \qquad (10.A.1e)$$

It is important to understand the practical difference between Euler angles ($\alpha\beta\gamma$) and axis angles [φ,ϑ,Θ]. Euler angles ($\alpha\beta\gamma$) are coordinates of rotated <u>states</u> of <u>position</u> while axis-angles [φ,ϑ,Θ] are parameters of rotation <u>operators</u> or angular <u>velocity</u>. Euler angles ($\alpha\beta\gamma$) serve as convenient polar coordinates of spin vectors **S** (Recall Fig. 10.5.2) and for orbiting or spinning bodies as shown below, while axis angles [φ,ϑ,Θ] are the polar coordinates and rotation angle of a crank-axis Ω for an operation. Euler angles ($\alpha\beta\gamma$) label the <u>state</u> and <u>density</u> operator of a *U(2)* system, while axis angles [φ,ϑ,Θ] label its <u>Hamiltonian</u> and <u>time-evolution</u> operator. Euler ($\alpha\beta\gamma$) tell <u>where</u> **S** is; axis [φ,ϑ,Ω] where it's <u>going</u>.

Fig. 10.A.1 shows explicitly how to construct a general spin state or density operator labeled by Euler ($\alpha\beta\gamma$)-angles by illustrating the sequence of rotations: (1) Z-rotation **R**(00γ) by angle γ, followed by (2) Y-rotation **R**(0β0) by angle β, followed by (3) Z-rotation **R**(α00) by angle α. The result is a spin vector **S** pointing with polar angle β or beta (often labeled by its ryhmesake 'theta') and an azimuthal angle α (often labeled with a 'phi'), in exact agreement with (10.5.8c) and Example 7 in Fig. 10.5.4.

One new 'twist' added here is not found in other treatments of *U(2)*. We interpret the third Euler angle γ and overall phase or gauge factor $e^{-i\gamma/2}$ in (10.A.1a) as a twist of a rigid body attached to the spin **S**-vector. Indeed, the first Z-rotation **R**(00γ) by angle γ twists the spin vector as shown in the upper right hand γ-part of Fig. 10.A.1. This means that the overall phase, which got canceled out of the 3D-density - spin-operator formulas involving $\Psi^*\Psi$ quantities, is still present if we consider a 3D spin-<u>body</u> instead of just a spin vector. Twisting a spin vector by γ does nothing if it's just a line, but a solid vector body actually "feels" a twist by γ. Nuclear, molecular and atomic spin rotations all have a twist angle.

A note of caution is in order with respect to exponential operator notation. Axis angle operations were given in (10.5.15) using a single exponential-of-a-sum expression.

$$\mathbf{R}[\vec{\Theta}] = e^{-i\vec{\Theta}\cdot\mathbf{S}} = e^{-i(\Theta_X\mathbf{S}_X + \Theta_Y\mathbf{S}_Y + \Theta_Z\mathbf{S}_Z)} = e^{-i\Theta(\hat{\Theta}_X\mathbf{S}_X + \hat{\Theta}_Y\mathbf{S}_Y + \hat{\Theta}_Z\mathbf{S}_Z)} \qquad (10.A.2a)$$

Euler angle operation (10.A.1a) is a <u>product</u> of three <u>separate</u> single exponentials.
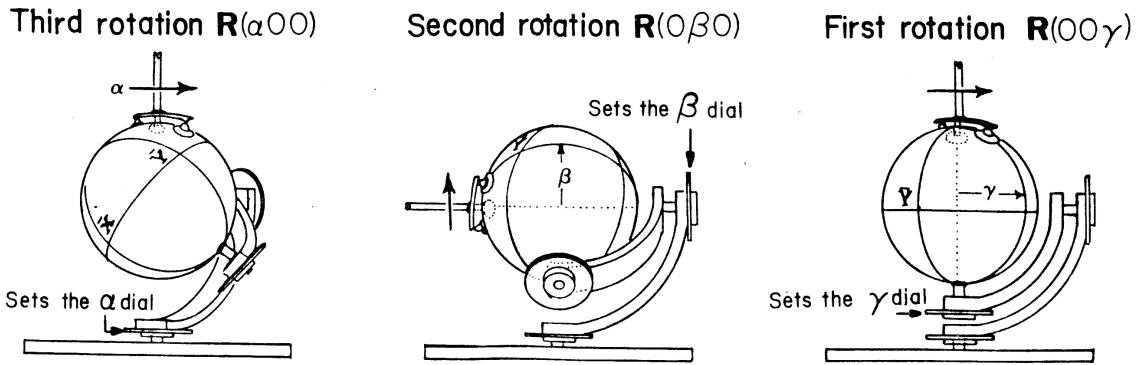
$$\mathbf{R}(\alpha\beta\gamma) = e^{-i\alpha\mathbf{S}_Z} e^{-i\beta\mathbf{S}_Y} e^{-i\gamma\mathbf{S}_Z} \qquad (10.A.2b)$$

Unless operators **A** and **B** commute, you cannot combine $e^{i\mathbf{A}} e^{i\mathbf{B}}$ into $e^{i(\mathbf{A}+\mathbf{B})}$ nor can you factor $e^{i(\mathbf{A}+\mathbf{B})}$. In rare cases (and this is one of them) where two operators commute with their commutator you can write

$$e^{\mathbf{A}} e^{\mathbf{B}} e^{-[\mathbf{A},\mathbf{B}]} = e^{(\mathbf{A}+\mathbf{B})} = e^{\mathbf{B}} e^{\mathbf{A}} e^{[\mathbf{A},\mathbf{B}]} \quad \text{if: } [\mathbf{A},[\mathbf{A},\mathbf{B}]] = 0 = [\mathbf{A},[\mathbf{A},\mathbf{B}]] \qquad (10.A.3)$$

This is the first part of what is known as the *Baker-Campbell-Hausdorf theorem*.

Third rotation R(α00) **Second rotation R**(0β0) **First rotation R**(00γ)

Sets the α dial   Sets the β dial   Sets the γ dial

Sequence **R**(α00)**R**(0 β 0) **R**(00γ) *sets Euler Angle **position state**–|αβγ⟩*

using Z-rotation **R**(α00) *following Y-rotation* **R**(0β 0) *following Z-rotation* **R**(00γ)= **R**(γ00)

S_Z

S

Original
Spin State |1⟩
=|↑⟩

S_X S_Y

(1) Rotate by γ
around Z

γ

S

γ

(2) Rotate by β
around Y

β

S

(3) Rotate by α
around Z

S_Z

α

S

β

S_Y

$S_X = $
$Scosα sinβ$ $S_Y = Ssinα sinβ$

β

S

$S_Z = Scosβ$

General Spin State
|Ψ⟩=**R**(αβγ)|↑⟩

β

S

α

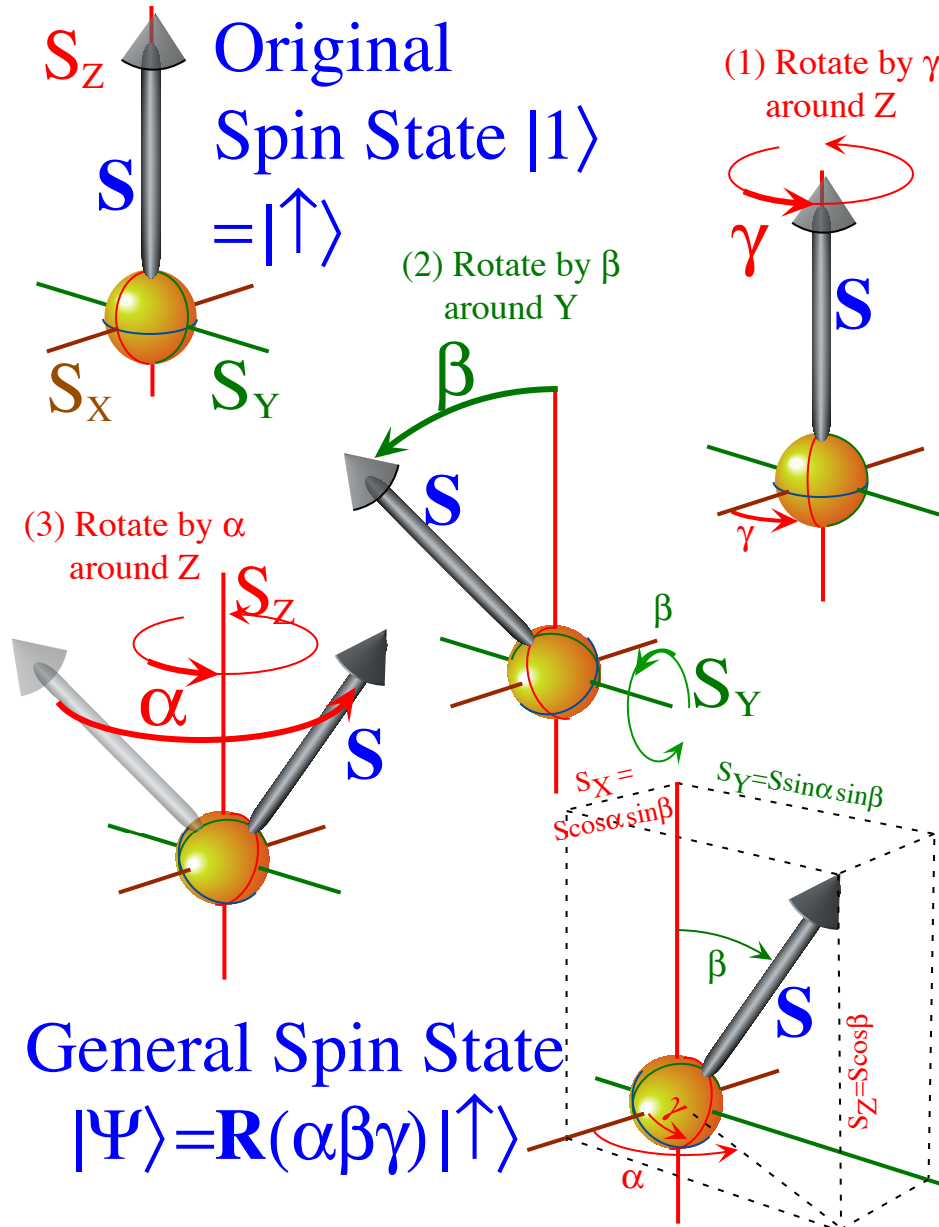*Fig. 10.A.1 The operational definition of Euler (αβγ)-angle coordinates applied to a spin-state.*

(a) Equivalence transformations of rotations

Another way to factor the axis-angle expression (10.A.2a) is to find a transformation $\mathbf{T}$ that builds the rotation $\mathbf{R}[\varphi,\vartheta,\Theta]$ by Θ about an axis Θ at polar angle (φ, ϑ) out of a Z-axis twist rotation $e^{-i\Theta S_Z}$.

$$\mathbf{R}[\varphi,\vartheta,\Theta] = \mathbf{T}\, e^{-i\Theta S_Z}\, \mathbf{T}^\dagger \qquad\qquad (10.A.4)$$

The desired transformation $\mathbf{T}$ is just the Euler operation $\mathbf{R}(\varphi\vartheta 0)$ such as was diagrammed in Fig. 10.A.1, only we leave off the twist γ since it would just cancel out. Effectively, we take the Θ-axis from polar-angle location $[\varphi,\vartheta]$ to the Z-axis with an inverse Euler-op $\mathbf{T}^\dagger = \mathbf{R}^\dagger(\varphi\vartheta 0)$, then do the Z-twist $e^{-i\Theta S_Z}$, and finally, return the axis to its original (φ,ϑ)-position with the Euler rotation (*sans* twist) $\mathbf{T} = \mathbf{R}(\varphi\vartheta 0)$.

$$\mathbf{R}[\varphi,\vartheta,\Theta] = \mathbf{R}(\varphi\vartheta 0)\, e^{-i\Theta S_Z}\, \mathbf{R}^\dagger(\varphi\vartheta 0) = \mathbf{R}(\varphi\vartheta 0)\, \mathbf{R}(00\Theta)\, \mathbf{R}^\dagger(\varphi\vartheta 0) \quad (10.A.5a)$$

Expanding the Euler rotations using (10.A.2b) gives (Note: $\mathbf{R}^\dagger(0\vartheta 0) = \mathbf{R}(0{-}\vartheta 0)$ and $\mathbf{R}^\dagger \mathbf{S}^\dagger = (\mathbf{S}\mathbf{R})^\dagger$)

$$\mathbf{R}[\varphi,\vartheta,\Theta] = \mathbf{R}(\varphi 00)\, \mathbf{R}(0\vartheta 0)\, \mathbf{R}(00\Theta)\, \mathbf{R}(0{-}\vartheta 0)\, \mathbf{R}(-\varphi 00) \qquad (10.A.5b)$$

$$\mathbf{R}[\varphi,\vartheta,\Theta] = e^{-i\varphi S_Z}\ \ e^{-i\vartheta S_Y}\ e^{-i\Theta S_Z}\ e^{+i\vartheta S_Y}\ e^{+i\varphi S_Z} \qquad (10.A.5c)$$

So axis-defined $\mathbf{R}[\varphi,\vartheta,\Theta]$ factors into <u>five</u> monomial exponentials instead of three factors found in the much simpler Euler rotation $\mathbf{R}(\alpha\beta\gamma)$. (Check that this gives the desired 2-by-2 matrix (10.5.25c).) The expression of rotations in terms of just a Y and two Z rotations keeps the matrix arithmetic to a minimum since generally the Z-rotations are diagonal and the Y-rotations, while not diagonal, are generally real. This is very important when we deal with big 201-by-201 spin-100 matrices! But, it helps even with medium-sized 3-by-3, 4-by-4, and 5-by-5 spin-1, spin-3/2, and spin-2 matrices seen later on.

It is important to understand the transformation (10.A.4) as a simple $\mathbf{R}(\varphi\vartheta 0)$-rotation of an operator's crank-vector Θ. The magic-vector of an operator like a rotation $\mathbf{R}$ or a Hamiltonian $\mathbf{H}$ or a time evolution operator $\mathbf{U}$ gets transformed just like the spin vector $\mathbf{S}$ in Fig. 10.A.1, which, after all, is the magic vector of the spin-state density operator ρ. Such a transformation $\mathbf{R'} = \mathbf{T}\,\mathbf{R}\,\mathbf{T}^\dagger$ is called a *similarity* or *equivalence transformation* because the resulting rotation $\mathbf{R'}$ must be similar or equivalent to the original $\mathbf{R}$. In particular, it must have the same trace, determinant, eigenvalues, etc., which means it must rotate by the same angle Θ as the original. So, the crank vector has the same $\Theta =|\Theta|$ length as the original, but, it will be in a different direction $\Theta' = R \cdot \Theta$. Let's see how to quickly calculate a 3-by-3 direction-cosine R-matrix.

(b) Euler equivalence transformations of 3-vectors

The 3-by-3 transformation matrix $R(\alpha\beta\gamma)$ describing an Euler rotation of real 3-vectors is a little more complicated than the 2-by-2 spinor matrix (10.A.1), but simpler than the axis-angle matrix $R[\varphi\vartheta\Theta]$ you will derive later. The triple product rotation $\mathbf{R}(\alpha\beta\gamma)$ made 3-by-3 rotation matrices is

$$\langle R(\alpha\beta\gamma)\rangle = \langle R(\alpha 00)\rangle \qquad \langle R(0\beta 0)\rangle \qquad \langle R(00\gamma)\rangle$$

$$= \begin{pmatrix} \cos\alpha & -\sin\alpha & 0 \\ \sin\alpha & \cos\alpha & 0 \\ 0 & 0 & 1 \end{pmatrix} \begin{pmatrix} \cos\beta & 0 & \sin\beta \\ 0 & 1 & 0 \\ -\sin\beta & 0 & \cos\beta \end{pmatrix} \begin{pmatrix} \cos\gamma & -\sin\gamma & 0 \\ \sin\gamma & \cos\gamma & 0 \\ 0 & 0 & 1 \end{pmatrix} \qquad (10.A.6a)$$

The resulting transformation matrix is

$$\left|\mathbf{e}_{\bar{X}}\right\rangle = R(\alpha\beta\gamma)\left|\mathbf{e}_X\right\rangle \qquad \left|\mathbf{e}_{\bar{Y}}\right\rangle = R(\alpha\beta\gamma)\left|\mathbf{e}_Y\right\rangle \qquad \left|\mathbf{e}_{\bar{Z}}\right\rangle = R(\alpha\beta\gamma)\left|\mathbf{e}_Z\right\rangle$$

$$\langle R(\alpha\beta\gamma)\rangle = \begin{matrix}\langle\mathbf{e}_X| \\ \langle\mathbf{e}_Y| \\ \langle\mathbf{e}_Z|\end{matrix} \begin{pmatrix} \cos\alpha\cos\beta\cos\gamma - \sin\alpha\sin\gamma & -\cos\alpha\cos\beta\sin\gamma - \sin\alpha\cos\gamma & \cos\alpha\sin\beta \\ \sin\alpha\cos\beta\cos\gamma + \cos\alpha\sin\gamma & -\sin\alpha\cos\beta\sin\gamma + \cos\alpha\cos\gamma & \sin\alpha\sin\beta \\ -\cos\gamma\sin\beta & \sin\gamma\sin\beta & \cos\beta \end{pmatrix} \text{(10.A.6b)}$$

The third column contains the Cartesian components of the $\mathbf{R}(\alpha\beta\gamma)$-rotated Z-axis which is labeled

$$\hat{\mathbf{e}}_{\bar{Z}} = \left|\mathbf{e}_{\bar{Z}}\right\rangle = (\cos\alpha\,\sin\beta,\ \sin\alpha\,\sin\beta,\ \cos\beta) \qquad \text{or:} \qquad \mathbf{e}_{\bar{Z}} = \mathbf{e}_X\cos\alpha\sin\beta + \mathbf{e}_Y\sin\alpha\sin\beta + \mathbf{e}_Z\cos\beta$$

It is the same as the polar coordinate components ($\cos\alpha$ $\sin\beta$, $\sin\alpha$ $\sin\beta$, $\cos\beta$) seen in Fig. 10.A.1 or (10.5.8b). The matrix gives the *X, Y, Z-direction cosines* $\mathbf{e}_X \bullet \mathbf{e}_{\bar{X}} = \langle X|\bar{X}\rangle$, $\mathbf{e}_X \bullet \mathbf{e}_{\bar{Y}} = \langle X|\bar{Y}\rangle, \cdots etc.$ so any vector be quickly transformed passively (Recall Fig. 2.2.2) or actively (Recall Fig. 2.2.3).

(c) Euler angle goniometer: Double valued position

Research laboratories which need to orient crystals or X-ray targets or perform angular scattering experiments of any kind must be equipped with some sort of *goniometer* such as is sketched in Fig. 10.A. 1 or Fig. 10.A.2 and photographed there and in Fig. 10.A.3. Theorists, too, would do well to "equip" their minds with such a device since it is a powerful "thought tool" for understanding the *R(3)* and *SU(2)* group properties of Euler angles.

Two metal frames labeled *x′* and *x″*, respectively, are used to connect the laboratory or LAB frame $\{X,Y,Z\}$ to the body or BOD frame $\{\bar{X},\bar{Y},\bar{Z}\}$ through a series of three bearings labeled and measured by dials that keep track of the Euler angles ($\alpha\beta\gamma$). The goniometer shows a number of things immediately.
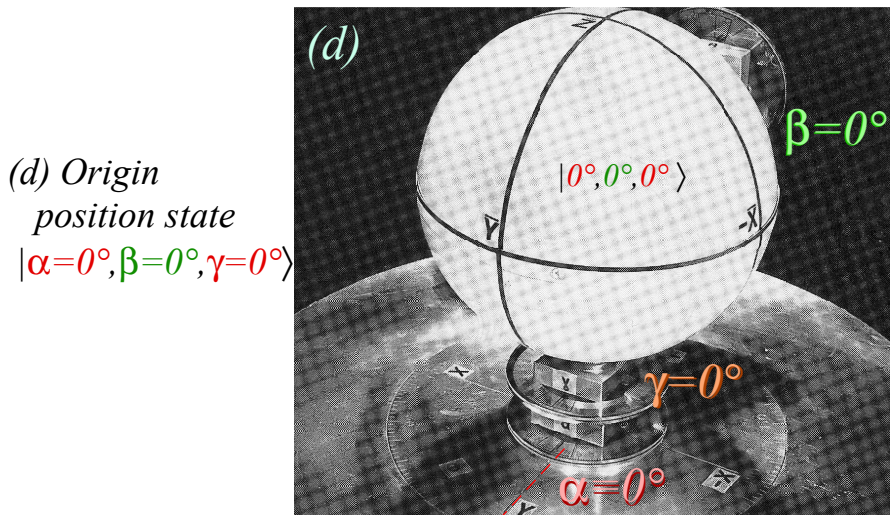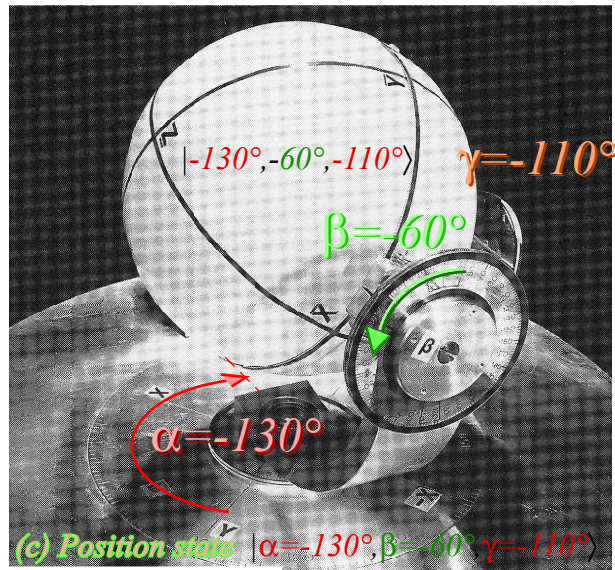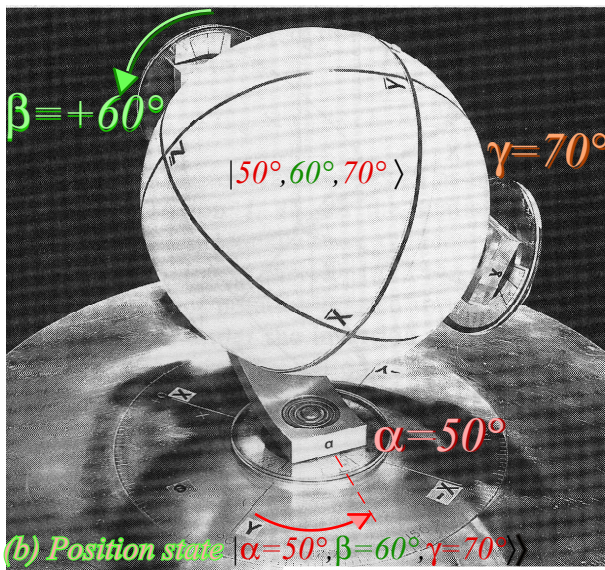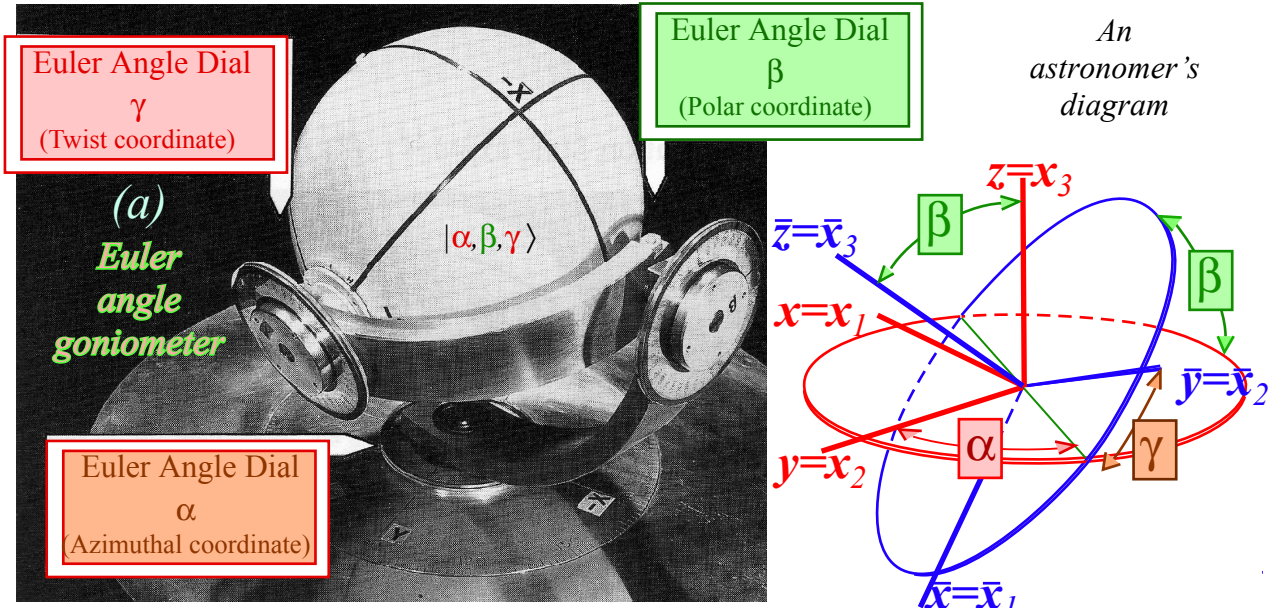
First, it demonstrates clearly that Euler angles are primarily *position coordinates*. While the operator definition given by Fig. 10.A.1 had to be performed in a definite (Z_α), (Y_β), and (Z_γ) order, the dials shown in Fig. 10.A.2 are totally independent of each other. You may set them in any order and the same position state will be obtained and exactly the one obtained by operators in Fig. 10.A.1.

Second, the device shows how Euler angles are natural choices for any laboratory or theoretical problem involving 3D rotation. Indeed, ($\alpha\beta\gamma$) are the same as *yaw (α), pitch (β), and roll (γ)* used by a pilot of space ship, airplane, or submarine to track the bow or $\bar{Z}$ -axis of the craft body relative to Earth or stars.

Third, the convention used in Fig. 10.A.1-2 makes the first two Euler angles (α and β) into azimuth and polar angles of the body zenith $\bar{Z}$. This is the appropriate for atomic and molecular physics where the body zenith $\bar{Z}$ is a symmetry axis, radius vector, or other significant body point.

Fourth, it is seen from Fig. 10.A.2 the second two Euler angles (β and γ), more correctly, their minuses (-β and -γ) are also azimuth and polar angles, but for the LAB zenith Z relative to the body frame. Note that the last row of matrix (10.A.6b) has exactly the polar coordinate form using -β and -γ as azimuth and polar angle, respectively. This is sketched in the upper left hand corner of Fig. 10.A.4.

Fig. 10.A.2 Euler angle device relates body frame to lab frame through a succession of frames and dials.

Euler Angle Dial
γ
(Twist coordinate)

Euler Angle Dial
β
(Polar coordinate)

An astronomer's diagram

(a)
Euler angle goniometer

$|\alpha, \beta, \gamma\rangle$

Euler Angle Dial
α
(Azimuthal coordinate)

$z = x_3$
$\bar{z} = \bar{x}_3$ β
β
$x = x_1$
$\bar{y} = \bar{x}_2$
$y = x_2$ α   γ
$\bar{x} = \bar{x}_1$

β ≡ +60°   γ = 70°
$|50°, 60°, 70°\rangle$
α = 50°
(b) Position state $|\alpha=50°, \beta=60°, \gamma=70°\rangle$

$|-130°, -60°, -110°\rangle$ γ = -110°
β = -60°
α = -130°
(c) Position state $|\alpha=-130°, \beta=-60°, \gamma=-110°\rangle$

(d)
β = 0°
$|0°, 0°, 0°\rangle$
γ = 0°
α = 0°

(d) Origin position state
$|\alpha=0°, \beta=0°, \gamma=0°\rangle$

For β=0°, ball frame holds its position as the α and γ frames swivel by angle ϕ to any state of form
$|\alpha=\phi, \beta=0°, \gamma=-\phi°\rangle$
including origin state
$|\alpha=0°, \beta=0°, \gamma=0°\rangle$.

Other slightly different conventions exist for Euler angles. Indeed, the first were based on astronomical orientation of planetary orbits and celestial stellar tracks. In this case the zenith of an orbit plane is not a measurable or observable point. The azimuth and polar angle of the orbit zenith is useless. Instead the astronomer records the azimuth of the points where the body rises or sets; the so-called *ascending or descending nodes*. These are located exactly *±90°*, respectively, from the azimuth of the orbital zenith so old Euler definitions measure azimuth α from the *±Y*-axis instead of the *X*-axis. The astronomer will also record the *orbital inclination* which is the same as β except, possibly, for a ±-sign.

One should be aware of the fact that Euler angles, and for that matter, any 3D angular coordinates, are intrinsically and fundamentally *double valued*. This is no surprise to us; Fig. 10.5.6 shows that 3D spin vectors went around twice (4π) every time the *U(2)* spinor rotation went around once (2π). However, a mechanical demonstration of this is shown in Fig. 10.A.5b-c. It is easy to see that two different settings, one with positive β (α, β, γ) and another with negative β (π-α, −β, π−γ) leave the body in the same lab-relative position. Calculus texts restrict polar angle θ to being positive to avoid dealing with this.

The case of β=0 (Fig. 10.A.2d) might seem to avoid double valued trouble, but unfortunately, things just get worse there. Then the two remaining α and γ coordinates become *infinite-valued* since the state (α, 0, γ) is the same position as (α−ϕ, 0, γ+ϕ) for all ϕ. This worst of all singularities occurs right at the origin of *R(3)* and *U(2)* group parameter space namely (α=0, β=0, γ=0) or, more likely to be found, (α=ϕ, β=0, γ=−ϕ). There is another such singularity at β=π, too. The singular ϕ−floppiness is a killer, literally; the singularity at (000) corresponds to gyroscopic *gimbal-lock* so dreaded by pilots who fly acrobatic maneuvers that depended upon gyroscopic instruments.

However, the infinite valued rotational origin is a necessary to allow an arbitrary axis-angle rotation **R**[φ,ϑ,Θ] operator to produce the Euler-(αβγ)-angle position states

$$\mathbf{R}(\alpha\beta\gamma)\,|000\rangle = |\alpha\beta\gamma\rangle = \mathbf{R}[\varphi,\vartheta,\Theta]\,|000\rangle = \mathbf{R}[\varphi,\vartheta,\Theta]\,|\varphi-\pi/2, 0, \pi/2-\varphi\rangle \qquad (10.A.7)$$

according to Euler-axis angle relations (10.A.1). The device which demonstrates this is shown attached to the Euler angle goniometer in Fig. 10.A.3. However, gimbal-lock prevents motion from the original position until the goniometer x'-frame is tucked under the axis-angle crank support at azimuth φ, that is, until the origin is reset from (α=0, β=0, γ=0) to (φ−π/2, 0, π/2−φ). Recall, that an azimuth of α puts the x'-frame at α-*90°*. Then, the continuous rotation by axis angle Θ=Ω·t may begin as shown below in in Fig. 10.A.5.
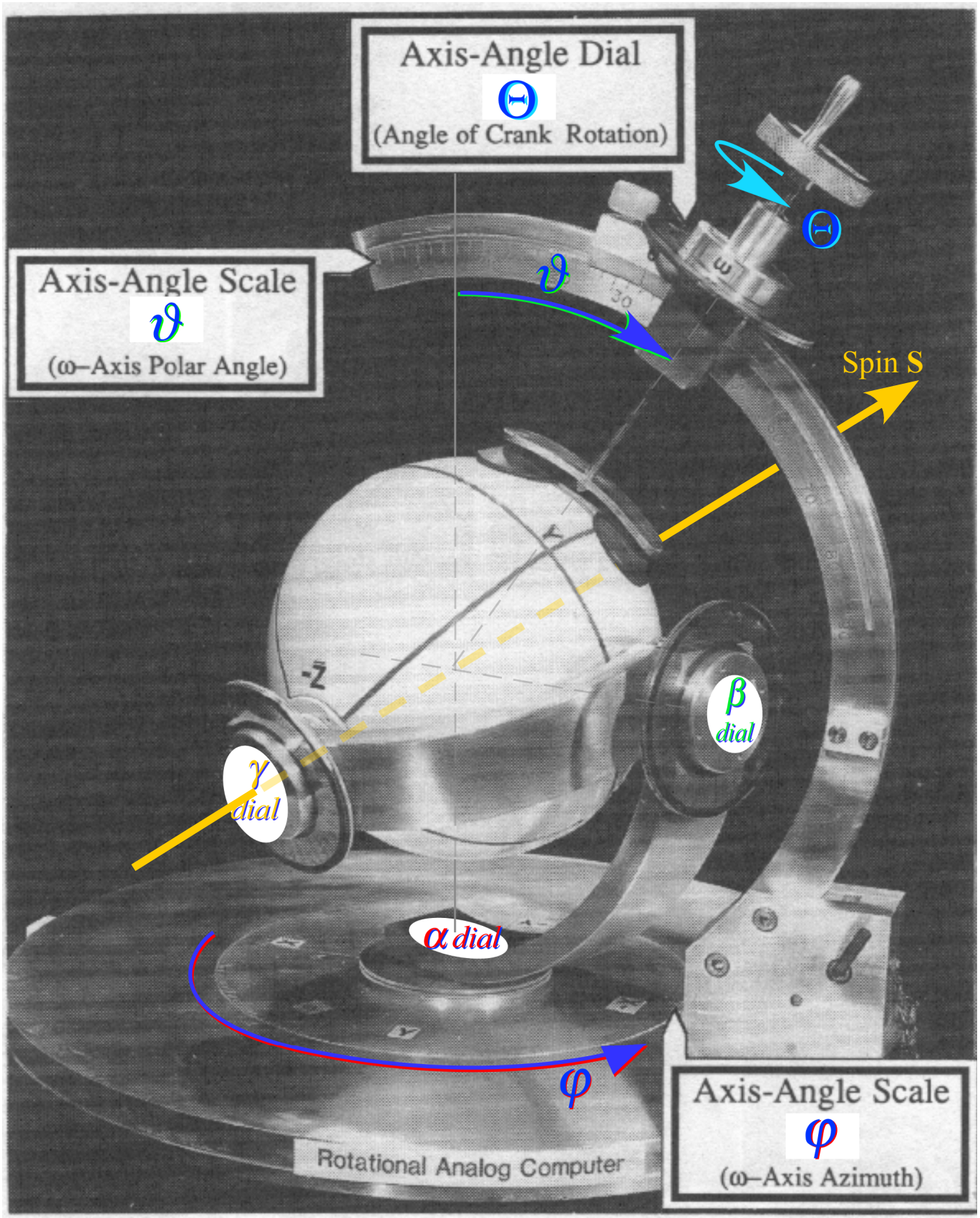
Fig. 10.A.3 Mechanical crank axis angles [φ,ϑ,Θ] operating on sphere having Euler angles (α,β,γ)

BOD frame view
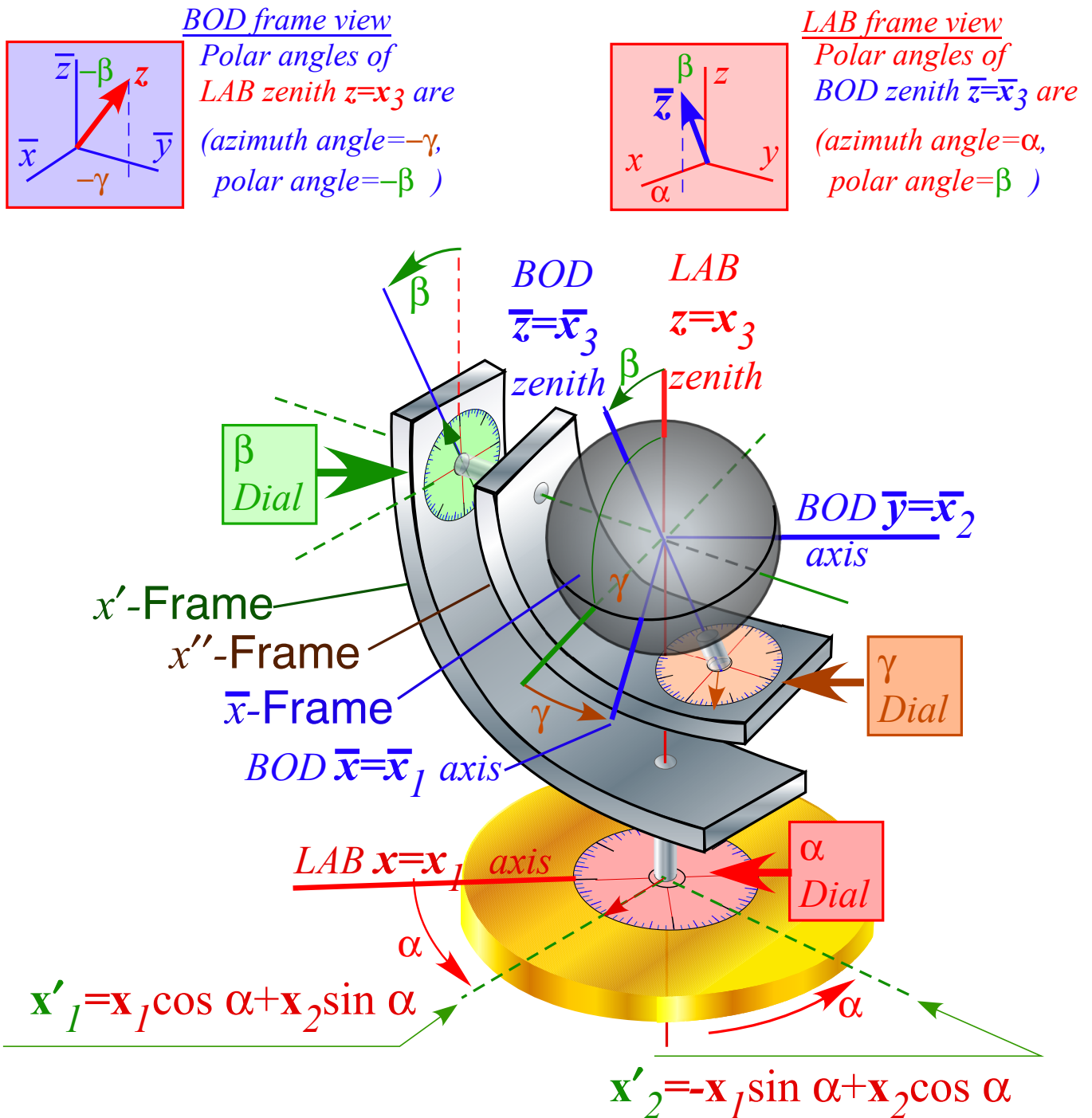*Polar angles of*
LAB zenith $z=x_3$ *are*

(azimuth angle=−γ,
polar angle=−β *)*

LAB frame view
Polar angles of
BOD zenith $\bar{z}=\bar{x}_3$ *are*

*(azimuth angle=*α,
*polar angle=*β *)*

BOD
$\bar{z}=\bar{x}_3$
zenith

LAB
$z=x_3$
zenith

β Dial

β

$BOD\ \bar{y}=\bar{x}_2$
axis

x'-Frame
x''-Frame
$\bar{x}$-Frame

γ Dial

$BOD\ \bar{x}=\bar{x}_1$ *axis*

LAB $x=x_1$ *axis*

α Dial

α

$\mathbf{x'}_1=\mathbf{x}_1\cos\alpha+\mathbf{x}_2\sin\alpha$

α

$\mathbf{x'}_2=-\mathbf{x}_1\sin\alpha+\mathbf{x}_2\cos\alpha$

Fig. 10.A.4 Mechanical device demonstrating Euler angles (α,β,γ) as coordinates of a body BOD-frame relative to a "star-fixed" LAB-frame.

 LAB-frame view sees BOD-$\bar{Z}$ axis with polar angles of azimuth α and polar angle β.
BOD-frame view sees LAB-Z axis with polar angles of azimuth -γ and polar angle -β.
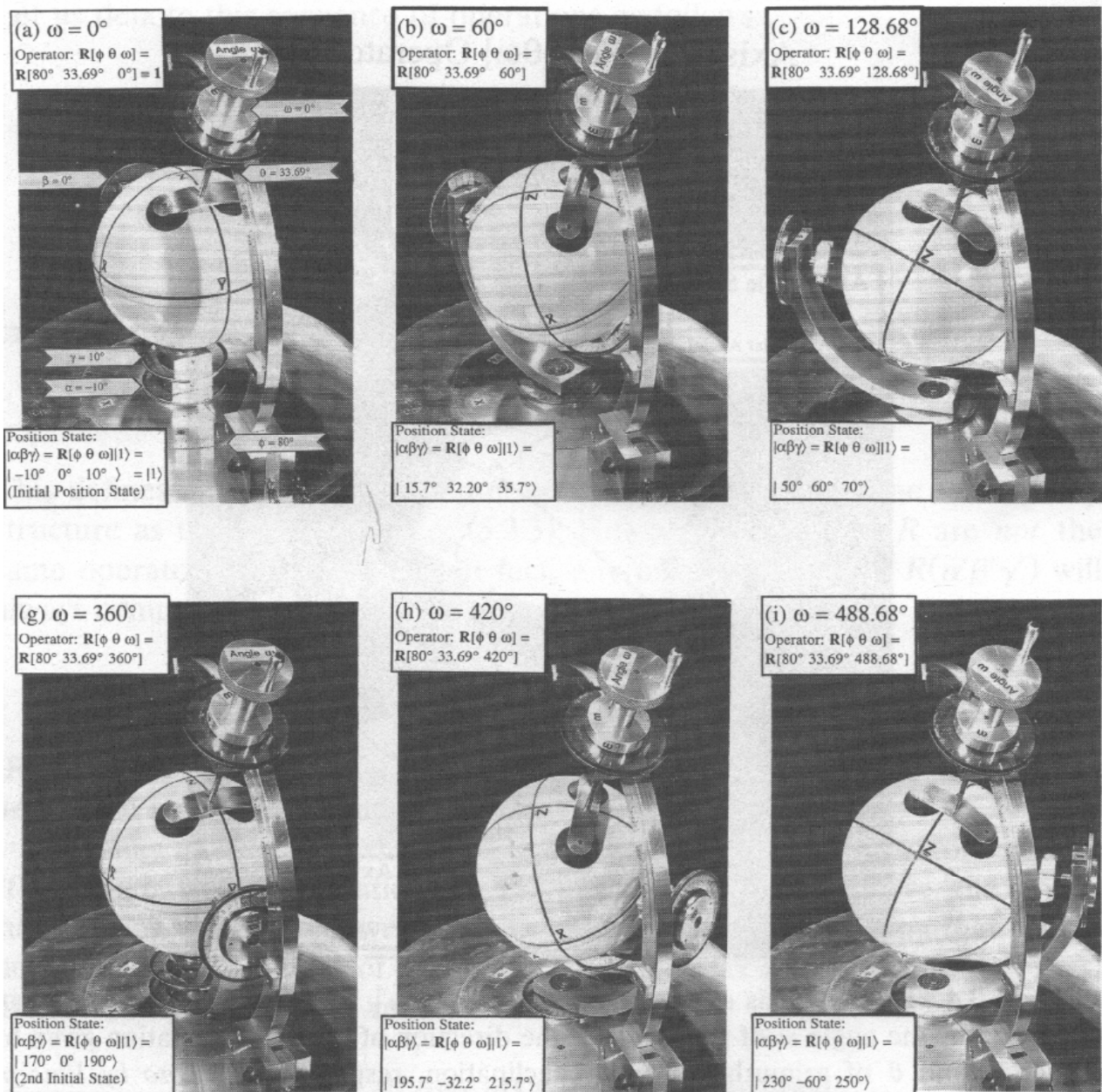
Fig. 10.A.5 Rotational 4π sequence 1ˢᵗ Row: (a) First origin state ω=Θ=0, (b-f) First position states.

(d) Axis angle rotation: Double valued operation

In Fig. 10.A.5 we attempt to follow an entire *720°* or *4π* rotation that connects the two positions shown in Fig. 10.A.2(b-c). First use relations (10.A.1) to derive the axis angles [φ=*80°*, ϑ=*34°*, Θ=*129°*] for the "first" initial Euler position state (α=*50°*, β=*60°*, γ=*70°*) in Fig. 10.A.5(c) and Fig. 10.A.3(a).

$$\mathbf{R}(\alpha=50°, \beta=60°, \gamma=70°)\,|000\rangle = \mathbf{R}[\varphi=80°, \vartheta=34°, \Theta=129°]\,|000\rangle \quad (10.A.8a)$$

It starts from a "first" origin state in Fig. 10.A.5(a). (Note figure notation: φ=φ, θ=ϑ, ω=Θ)

$$|000\rangle = |\varphi-\pi/2, 0, \pi/2-\varphi\rangle = |\alpha=-10°, \beta=0°, \gamma=10°\rangle = \mathbf{R}[\varphi, \vartheta, \Theta=0°]\,|000\rangle \quad (10.A.8b)$$
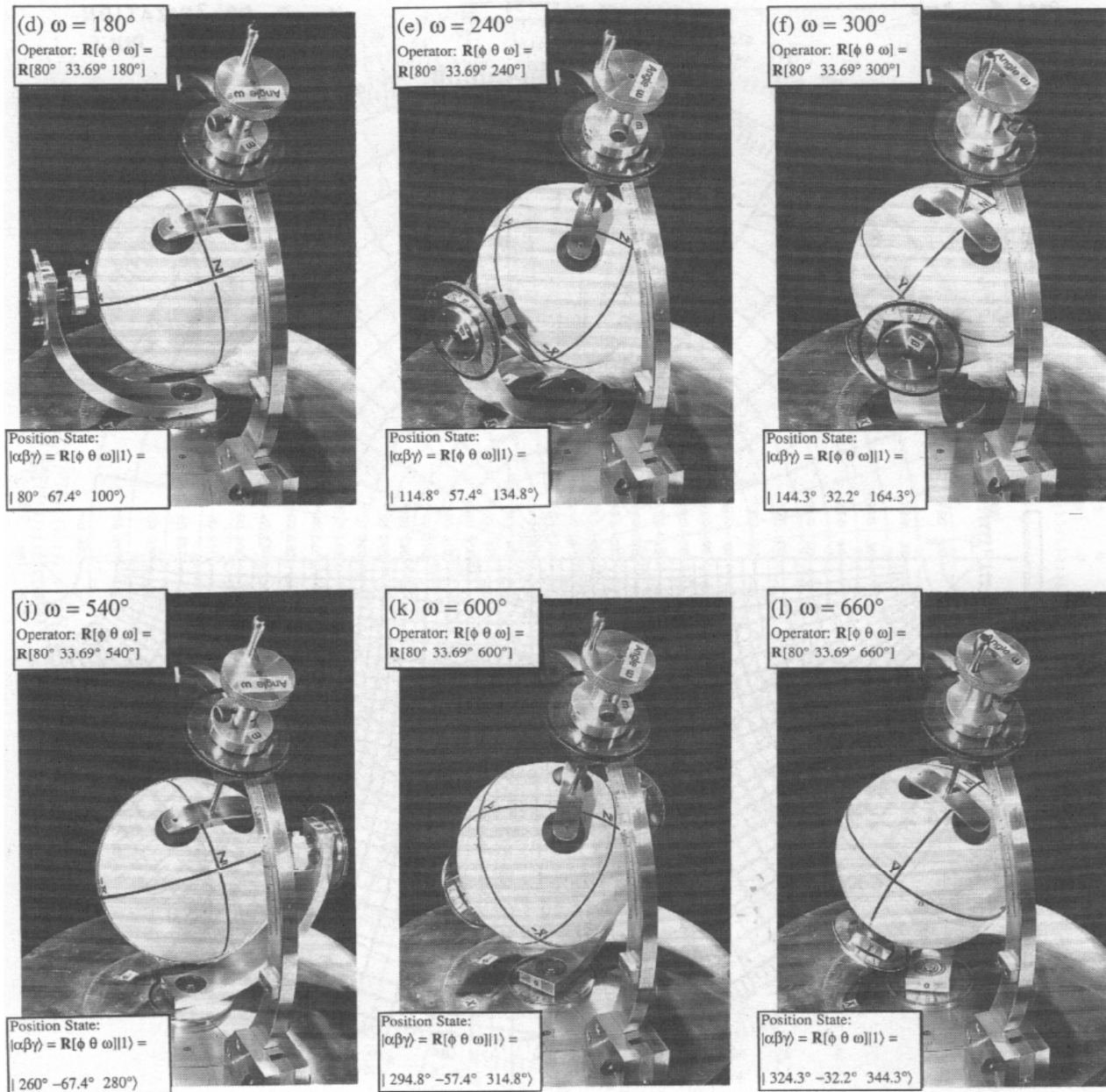
Fig. 10.A.5   2nd Row: (g) 2nd origin state ω=Θ=2π, (h-l) 2nd negative-β position states.

A 2π rotation (a-g) by Θ=ω = *360°* gives the "second" origin state in Fig. 10.A.5(g).

$$\mathbf{R}[\varphi=80°, \vartheta=34°, \Theta=360°] \, |000\rangle = \, |\alpha=170°, \beta=0°, \gamma=190°\rangle \qquad (10.A.8c)$$

The ball "looks" the same in the "second" initial state of Fig. 10.A.5(i) or Fig. 10.A.3(b) as in the "first."

$$\mathbf{R}[\varphi=80°, \vartheta=34°, \Theta=489°] \, |000\rangle = \, |\alpha=230°, \beta=-60°, \gamma=250°\rangle \qquad (10.A.8c)$$

However, "looks" by classical eyes are deceiving in quantum rotations. In fact, the α,γ-Euler angles and the goniometer *x′*-frame for each "second" position in figures 10.A.5(g-l) are π-flipped from those above

them in figures 10.A.5(a-f). Also, β is negative. Another "full" 2π rotation (either way) is needed to finish a full-quantum rotation of *0-modulo-4π* and return apparatus to first initial position in Fig. 10.A.5(c).

There is a double-valued nature of the 3D-space we occupy. It has been noted repeatedly in Chapter 10 comparisons of the real 3-D *R(3)* spin-*vector* world *versus* the complex 2-D *U(2) spinor* world in Fig. 10.5.8. Photon polarization spin-vector **S** goes twice (4π) around *R(3)* space while the polarization **E**-vector or Ψ-spinor goes just once around *U(2)* space in Fig. 10.5.5 and Fig. 10.5.6. Also, spinor reflections only need half the angle of the rotations they accomplish in Fig. 10.3.3. They also provide a more elegant formula and graphical "slide-rule" for rotation group products as we show now.

(1) Combining rotations: U(2) group products

The product of **R**[Θ'] **R**[Θ'] of any two rotations is another rotation operator **R**[Θ"] which can be computed using Hamilton's axis-angle expansion. First we multiply the separate expansions.

$$
\begin{aligned}
\mathbf{R}[\vec{\Theta}']\mathbf{R}[\vec{\Theta}] &= \left(\cos\frac{\Theta'}{2}\ \mathbf{1} - i\sin\frac{\Theta'}{2}\ \hat{\Theta}'\!\cdot\!\boldsymbol{\sigma}\right)\!\left(\cos\frac{\Theta}{2}\ \mathbf{1} - i\sin\frac{\Theta}{2}\ \hat{\Theta}\!\cdot\!\boldsymbol{\sigma}\right) \\
&= \cos\frac{\Theta'}{2}\cos\frac{\Theta}{2}\ \mathbf{1} - i\!\left[\cos\frac{\Theta'}{2}\sin\frac{\Theta}{2}\ \hat{\Theta} + \cos\frac{\Theta}{2}\sin\frac{\Theta'}{2}\ \hat{\Theta}'\right]\!\cdot\!\boldsymbol{\sigma} - \sin\frac{\Theta'}{2}\sin\frac{\Theta}{2}\big(\hat{\Theta}'\!\cdot\!\boldsymbol{\sigma}\big)\big(\hat{\Theta}\!\cdot\!\boldsymbol{\sigma}\big)
\end{aligned}
\tag{10.A.9}
$$

Then the Jordan-Pauli identity (10.5.13) is used to reduce $(\Theta'\!\cdot\!\boldsymbol{\sigma})(\Theta\!\cdot\!\boldsymbol{\sigma})$ to $(\Theta'\!\cdot\!\Theta)\mathbf{1}+(\Theta'\!\times\!\Theta)\boldsymbol{\sigma}$.

$$
\begin{aligned}
\mathbf{R}[\vec{\Theta}']\mathbf{R}[\vec{\Theta}] &= \left(\cos\frac{\Theta''}{2}\right)\mathbf{1}\quad - \quad\quad i\!\left[\sin\frac{\Theta''}{2}\ \hat{\Theta}''\right]\!\cdot\!\boldsymbol{\sigma}\quad\quad = \ \mathbf{R}[\Theta''] \\
&= \left(\cos\frac{\Theta'}{2}\cos\frac{\Theta}{2} - \sin\frac{\Theta'}{2}\sin\frac{\Theta}{2}\hat{\Theta}'\!\cdot\!\hat{\Theta}\right)\mathbf{1} - i\!\left[\!\left[\cos\frac{\Theta'}{2}\sin\frac{\Theta}{2}\ \hat{\Theta} + \cos\frac{\Theta}{2}\sin\frac{\Theta'}{2}\ \hat{\Theta}'\right] + \sin\frac{\Theta'}{2}\sin\frac{\Theta}{2}\hat{\Theta}'\!\times\!\hat{\Theta}\right]\!\cdot\!\boldsymbol{\sigma}
\end{aligned}
\tag{10.A.10a}
$$

It is straightforward to solve for the new product angle Θ" and axis unit vector $\hat{\Theta}''$ of crank Θ".

$$
\begin{aligned}
\left(\cos\frac{\Theta''}{2}\right) &= \left(\cos\frac{\Theta'}{2}\cos\frac{\Theta}{2} - \sin\frac{\Theta'}{2}\sin\frac{\Theta}{2}\hat{\Theta}'\!\cdot\!\hat{\Theta}\right) \\
\left[\sin\frac{\Theta''}{2}\ \hat{\Theta}''\right] &= \left[\cos\frac{\Theta'}{2}\sin\frac{\Theta}{2}\ \hat{\Theta} + \cos\frac{\Theta}{2}\sin\frac{\Theta'}{2}\ \hat{\Theta}' + \sin\frac{\Theta'}{2}\sin\frac{\Theta}{2}\hat{\Theta}'\!\times\!\hat{\Theta}\right]
\end{aligned}
\tag{10.A.10b}
$$

This is the *U(2) group product* formula. Now a simple way to visualize this product is done with mirrors!.

(2) Mirror reflections and Hamilton's turns

In Section 10.3b we noted that *mirror reflection* operations are more fundamental than rotations and are done by real Pauli matrices such as σ_A and σ_B or their combination σ_φ below. Recall Fig. 10.3.3

$$
\sigma_A = \begin{pmatrix} 1 & 0 \\ 0 & -1 \end{pmatrix}, \quad \sigma_B = \begin{pmatrix} 0 & 1 \\ 1 & 0 \end{pmatrix}, \quad \sigma_\phi = \begin{pmatrix} \cos\phi & \sin\phi \\ \sin\phi & -\cos\phi \end{pmatrix} = \sigma_A\cos\phi + \sigma_B\sin\phi
$$

Their action is displayed in Fig. 10.A.6. σ_ϕ reflects through a plane inclined at half-angle φ/2 to the *x*-axis. The product $\sigma_\phi\sigma_A$ is a rotation **R**[φ] by angle φ, while $\sigma_A\sigma_\phi$ is a rotation **R**[-φ] the opposite way (-φ).

$$\sigma_\phi\sigma_X = \begin{pmatrix} \cos\phi & \sin\phi \\ \sin\phi & -\cos\phi \end{pmatrix}\begin{pmatrix} 1 & 0 \\ 0 & -1 \end{pmatrix}, \qquad \sigma_X\sigma_\phi = \begin{pmatrix} 1 & 0 \\ 0 & -1 \end{pmatrix}\begin{pmatrix} \cos\phi & \sin\phi \\ \sin\phi & -\cos\phi \end{pmatrix}$$

$$= \begin{pmatrix} \cos\phi & -\sin\phi \\ \sin\phi & \cos\phi \end{pmatrix}=R[\phi], \qquad\qquad = \begin{pmatrix} \cos\phi & -\sin\phi \\ \sin\phi & \cos\phi \end{pmatrix}=R[-\phi] \qquad (10.A.11)$$
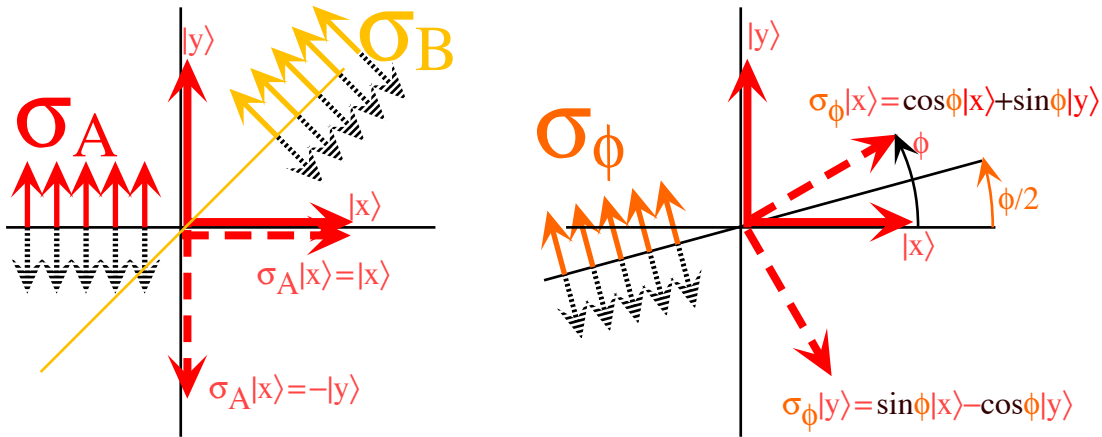
Fig. 10.A.6 Mirror reflections σ_A through xz-plane and σ_ϕ through rotated plane.

Hamilton saw this as a neat way to visualize three-dimensional rotations. Simply install two mirrors so they intersect on a Θ crank vector with half-angle $\Theta/2$ between the first and the second as shown in Fig. 10.A.7. It is like a clothing store mirror which lets you rotate an image of yourself by Θ as you adjust the angle $\Theta/2$ between mirrors. A unit normal vector N_1 and N_2 is constructed from each mirror plane and a $\Theta/2$ arc-vector drawn between the first and second plane normals. This arc is called *Hamilton's turn* vector ($N_1{\to}N_2$). It is these Hamilton turns that can be "added" like vectors to give *U(2)* group products!
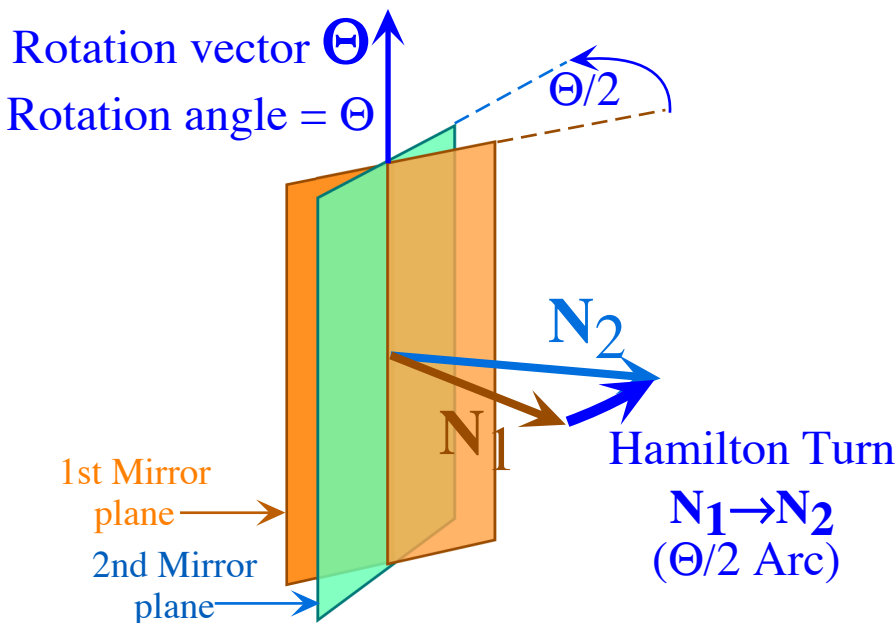

Fig. 10.A.7 Mirror reflection planes, normals, and Hamilton-turn arc vector.

Notice that only the <u>relative</u> angle $\Theta/2$ or $\pi-\Theta/2$ between mirrors is important in defining rotation $\mathbf{R}[\Theta]$; their absolute position is irrelevant. You can swivel the two mirrors anywhere around the Θ-axis. The trick to making products is to swivel the Hamilton turn arc $\mathbf{N_1}\rightarrow\mathbf{N_2}$ for the first rotation $\mathbf{R}[\Theta]$ around so it meets head-to-tail with the Hamilton turn arc $\mathbf{N'_1}\rightarrow\mathbf{N'_2}$ of the second rotation as $\mathbf{R}[\Theta']$ as shown in Fig. 10.A.8.

Then the two mirrors associated with $\mathbf{N_2}$ and $\mathbf{N'_1}$ lie on top of each other and cancel since two reflections by the same mirror is *no reflection*. That leaves only first mirror ($\mathbf{N_1}$) and last mirror ($\mathbf{N'_2}$), and so the resultant Hamilton-turn arc $\mathbf{N_1}\rightarrow\mathbf{N'_2}$ is the arc of the desired product $\mathbf{R}[\Theta'']=\mathbf{R}[\Theta']\mathbf{R}[\Theta]$.
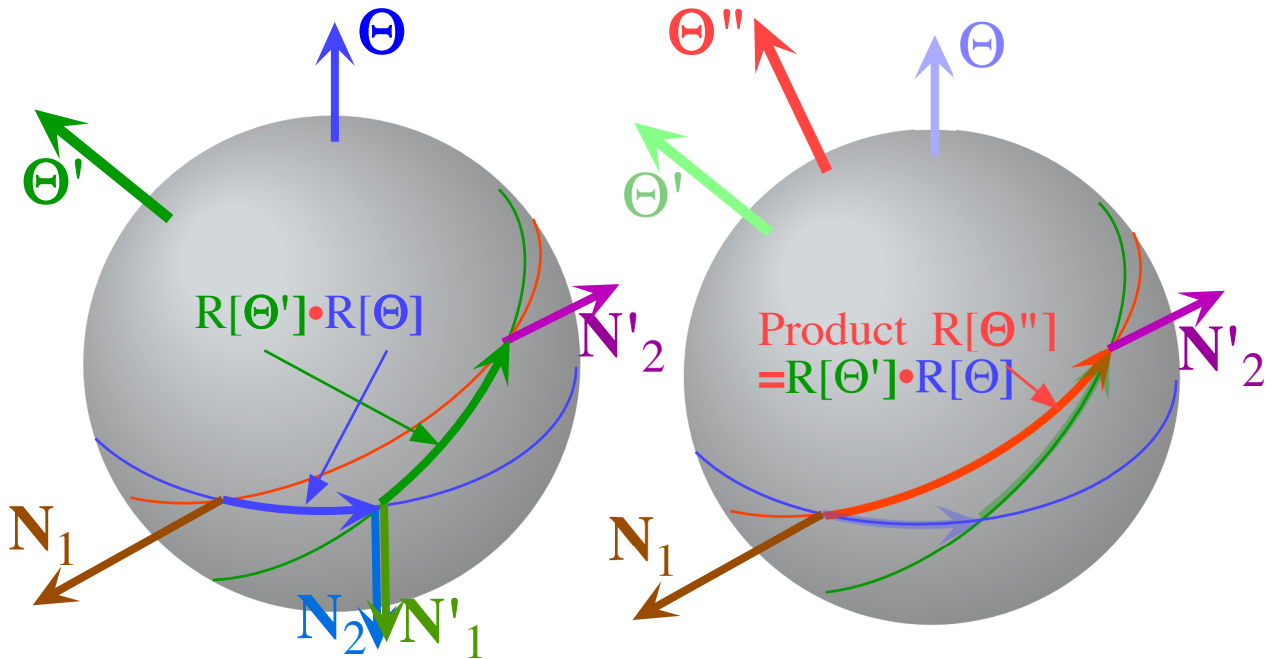

Fig. 10.A.8 Adding Hamilton-turn arcs to compute a U(2) product $\mathbf{R}[\Theta'']=\mathbf{R}[\Theta']\mathbf{R}[\Theta]$.

It is important to note that all Hamilton-turn arcs lie on *great* or *equatorial* circles and slide along the equatorial circles of the rotation axis vector Θ of the rotation $\mathbf{R}[\Theta]$.

Also, note that each Hamilton arc $\Theta/2$, $\Theta'/2$, or $\Theta''/2$ is half of the actual angle Θ, Θ', or Θ'' of rotation $\mathbf{R}[\Theta]$, $\mathbf{R}[\Theta']$, or $\mathbf{R}[\Theta'']$, respectively. That means that an arc $\Theta/2$ between $\mathbf{N_1}$ and $\mathbf{N_2}$ and its supplement angles $(\Theta\pm2\pi)/2=\Theta/2\pm\pi$ between $\mathbf{N_1}$ and -$\mathbf{N_2}$ represent the same <u>classical</u> rotation by Θ. For classical objects, a rotation by $\Theta\pm2\pi$ is the same as one by Θ. However, for a <u>quantum</u> spin-1/2 object, the arc pointing from $\mathbf{N_1}$ to the antipodal normal -$\mathbf{N_2}$ represents a Θ-rotation with an extra π-phase factor $e^{\pm i\pi}$ $= -1$, that is, $-R[\Theta]$. Recall rotation by 2π of the *U(2)* polarization state in Fig. 10.5.6 and Fig. 10.5.7 always comes up the same state, but it's π-out of phase. Hamilton's turns account for this.

(3) Similarity transformation and Hamilton's turns

Finally, the Hamilton-turn "vector addition" on a sphere gives different results if the vectors are added in the reverse order to give $\mathbf{R}[\Theta''']=\mathbf{R}[\Theta]\mathbf{R}[\Theta']$ instead of $\mathbf{R}[\Theta'']=\mathbf{R}[\Theta']\mathbf{R}[\Theta]$. The arc-diagram for

this forms a spherical parallelogram as shown in Fig. 10.A.9. It also shows the effect of a similarity transformation of rotation $R[\Theta'']$ by rotation $R[\Theta]$ to give rotation $R[\Theta''']$.

$$R[\Theta] \, R[\Theta''] \, R[-\Theta] = R[\Theta'''] \quad (10.A.12a) \qquad\qquad R[-\Theta] \, R[\Theta'''] \, R[\Theta] = R[\Theta''] \quad (10.A.12b)$$

As in (10.A.4), a rotation $R[\Theta]$ of a rotation $R[\Theta'']$ is just that. So everything associated with that rotation $R[\Theta'']$ gets rotated by the full angle Θ around axis Θ. This includes its 'crank vector' Θ and now its Hamilton-turn arc which, in Fig. 10.A.9 gets moved by exactly two $R[\Theta]$ Hamilton-turn arcs into path of the $R[\Theta''']$ turn arc below it, that is, two $R[\Theta]$ Hamilton-turn $\Theta/2$ arcs amount to one whole angle Θ. Fig. 10.A.9 shows a similarity transformation of rotation $R[\Theta''']$ by rotation $R[\Theta']$ to gives $R[\Theta'']$.

$$R[\Theta'] \, R[\Theta'''] \, R[-\Theta'] = R[\Theta''] \qquad\qquad (10.A.12c)$$

There are an infinite number of rotations that transform $R[\Theta'']$ into $R[\Theta''']$. Of these, there is one that is by the smallest angle Θ. Can you tell where this one's crank and Hamilton-turn is located in Fig. 10.A.9?
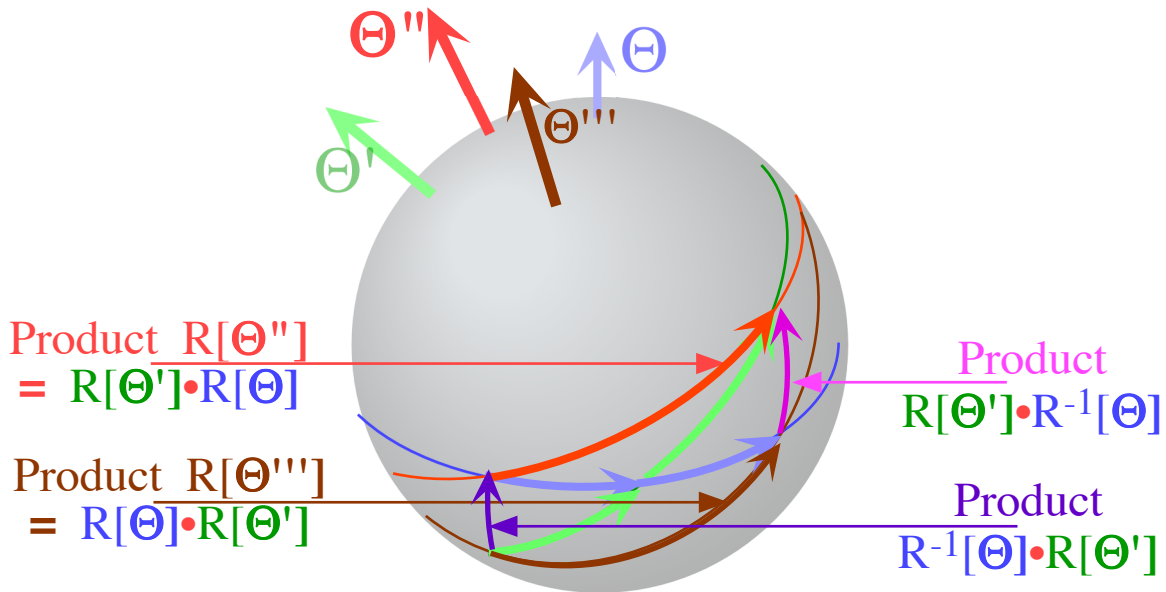

Fig. 10.A.9 Hamilton-turn arc parallelogram with $R[\Theta'']=R[\Theta']R[\Theta]$ and $R[\Theta''']=R[\Theta]R[\Theta']$

(e) Quaternion and spinor algebra (again)

Suppose we rotate a spin ket $|\uparrow\rangle$ or $|\Psi\rangle$ with an operator like the R above to give a new state

$$|\Psi'\rangle = R \, |\Psi\rangle$$

and a new density operator

$$\rho' = |\Psi'\rangle\langle\Psi'| = R \, |\Psi\rangle\langle\Psi| \, R^\dagger = R \, \rho \, R^\dagger \qquad\qquad (10.A.13a)$$

Use (10.5.5) to write $\rho = N/2 \, \mathbf{1} + S\cdot\sigma$ in terms of its S-vector gives

$$\rho' = R \, (N/2 \, \mathbf{1} + S\cdot\sigma) \, R^\dagger = (N/2 \, \mathbf{1} + S\cdot[R \, \sigma \, R^\dagger]) \qquad\qquad (10.A.13b)$$

which is just the same S-vector referred to a rotated spinor basis; in other words an Θ-rotated spin vector. It is important to remember that R acts only on the *U(2)* operators (σ_X, σ_Y, σ_Z) and pays no attention to the scalar component *N/2* or the components of the S-vector. But, the effect is the same as it would be applying the 3-by-3 matrix transformation *R* to the S-vector and leaving the spinor σ's alone.

$$\rho' = R \, (N/2 \, \mathbf{1} + S\cdot\sigma) \, R^\dagger = (N/2 \, \mathbf{1} + \ S'\cdot\sigma) \, , \text{ where: } S'_m = R_{mn}S_n \qquad\qquad (10.A.13c)$$

We will derive the 3-by-3 *R*-matrix by considering each unit base operator (σ_X, σ_Y, σ_Z) in turn. This involves Hamilton's original algebra of quaternions (q_X, q_Y, q_Z) = ($-i\sigma_X$, $-i\sigma_Y$, $-i\sigma_Z$) which satisfies cyclic multiplication rules below along with the negative squares: $q_X q_X = q_Y q_Y = q_Z q_Z = -1$, .

$$q_X q_Y = q_Z = - q_Y q_Z , \qquad q_Z q_X = q_Y = - q_X q_Z , \qquad q_Y q_Z = q_X = - q_Z q_Y . \qquad (10.A.14a)$$

These are summarized using the $\delta_{\upsilon\nu}$ and $\varepsilon_{\lambda\upsilon\nu}$-tensors (Recall $\varepsilon_{\lambda\upsilon\nu...}$ in Appendix 3.A)

$$q_\mu q_\nu = -\delta_{\mu\nu} \mathbf{1} + \varepsilon_{\mu\nu\lambda} q_\lambda \quad \text{or: } \sigma_\mu \sigma_\nu = \delta_{\mu\nu} \mathbf{1} + i \varepsilon_{\mu\nu\lambda} \sigma_\lambda \qquad (10.A.14b)$$

Here, we've written the multiplication rules for Pauli's "σ_μ-quaternions" as well as Hamiltion's $q_\mu = -i\sigma_\mu$.

$\bullet$	1	q_X	q_Y	q_Z
1	1	q_X	q_Y	q_Z
q_X	q_X	-1	q_Z	$-q_Y$
q_Y	q_Y	$-q_Z$	-1	q_X
q_Z	q_Z	q_Y	$-q_X$	-1

$\bullet$	1	σ_X	σ_Y	σ_Z
1	1	σ_X	σ_Y	σ_Z
σ_X	σ_X	1	$i\sigma_Z$	$-i\sigma_Y$
σ_Y	σ_Y	$-i\sigma_Z$	1	$i\sigma_X$
σ_Z	σ_Z	$i\sigma_Y$	$-i\sigma_X$	1

$$(10.A.14c)$$

Also, we need *commutation rules* for Pauli's operators as well as Jordan's spin-ops: $J_\mu = S_\mu = \sigma_\mu/2$.

$$\sigma_\mu\sigma_\nu - \sigma_\nu\sigma_\mu = [\sigma_\mu, \sigma_\nu] = 2i \varepsilon_{\upsilon\nu\lambda} \sigma_\lambda \text{ or: } S_\mu S_\nu - S_\nu S_\mu = [S_\mu, S_\nu] = i \varepsilon_{\mu\nu\lambda} S_\lambda \quad (10.A.14d)$$

The latter are the very important *angular momentum commutation relations* which we will apply later.

Now the application of σ-rules to the derivation of the expression for a general rotation $\mathbf{R}[\Theta]$ of an arbitrary unit 3-vector $\mathbf{e}_L$ or unit spinor σ_L is tricky. But, it's something important that every physicist should do at least once in their life! Therefore we leave the following result as an exercise.

$$\mathbf{R}[\vec{\Theta}]\sigma_L\mathbf{R}[\vec{\Theta}]^\dagger = \left(\cos\frac{\Theta}{2} \mathbf{1} - i\sin\frac{\Theta}{2} \hat{\Theta}_K\sigma_K \right)\sigma_L\left(\cos\frac{\Theta}{2} \mathbf{1} - i\sin\frac{\Theta}{2} \hat{\Theta}_N\sigma_N \right)^\dagger \qquad (10.A.15a)$$
$$= \sigma_L' = \sigma_L \cos\Theta - \varepsilon_{LKM}\hat{\Theta}_K\sigma_M \sin\Theta + (1-\cos\Theta)\hat{\Theta}_L(\hat{\Theta}_N\sigma_N)$$

You should also demonstrate that this is equivalent to the following 3-vector expression.

$$\mathbf{e}_L' = \mathbf{e}_L \cos\Theta - \varepsilon_{LKM}\hat{\Theta}_K\mathbf{e}_M \sin\Theta + (1-\cos\Theta)\hat{\Theta}_L(\hat{\Theta}_N\mathbf{e}_N)$$
$$= \mathbf{e}_L \cos\Theta + \hat{\Theta}\times\mathbf{e}_L \sin\Theta + (1-\cos\Theta)\hat{\Theta}(\hat{\Theta}\bullet\mathbf{e}_L) \qquad (10.A.15b)$$

The 3-vector transformations are a lot more complicated than the 2-spinor ones. But, they do have one simple property; they all use cosines of whole angles Θ of rotation while the *2*-space spinor operations all use half-angles $\Theta/2$ or square-root cosines *cos* $\Theta/2 = \sqrt{[^1/_2 + ^1/_2 cos\ \Theta]}$ of the rotation angle.

Why rotations are such a big deal

In Chapters 8 and 9 we introduced the idea of labeling quantum channels or states using rotational symmetry operators $\mathbf{r}$, $\mathbf{r}^2$,..., and then discovered that the Hamiltonian was made of linear combinations of the $\mathbf{r}^p$'s, as were their projectors which solved the eigenvalue problem. Similar relations apply to 2-state systems. Indeed, all *SU(2)* operators are related to rotations in some way including the grand time evolution operator $\mathbf{U}(t)$. When you have a hammer; everything's a nail!

Appendix 10.B Spin control and ellipsometry

So far, rotational analysis has been referred to the Z-axis or, as we have re-labeled it, the A-axis. This "favors" base states (spin-up-Z, spin-dn-Z) for electrons, (Plane-x, Plane-y) states for photons, and (N-UP, N-DN) for NH_3 shown in Fig. 10.5.1. It favors an A-symmetry (asymmetric-diagonal) Haniltonian in the *U(2)* catalog of Fig. 10.4.2 which begins with A-type base states introduced in Section 10.2(a).

In fact, any axis may be a home base. Three choices A, B, and C (or Z, X, and Y) belong to obvious symmetries. A Hamiltonian near one has archetypical physics. One should be able to quickly relate them.

To begin this, recall the Z-axis or A-type Euler angle (αβγ) definition from (10.A.1).

$$|\Psi\rangle = \mathbf{R}(\alpha\beta\gamma)|1\rangle = \mathbf{R}(\alpha\,00)\,\mathbf{R}(0\beta\,0)\,\mathbf{R}(00\gamma)|1\rangle \quad \substack{represented \\ in\,A-basis \\ by} \quad \begin{pmatrix} e^{-i\frac{\alpha}{2}}\cos\frac{\beta}{2} \\ e^{i\frac{\alpha}{2}}\sin\frac{\beta}{2}\beta \end{pmatrix} e^{-i\frac{\gamma}{2}} \tag{10.B.1}$$

Now we define X or B-type Euler angles (ABG) and Y or C-type Euler angles (abg). A general state is defined by any and all of the following three sets of Euler angles; one set for each choice A, B, or C.

$$|\Psi\rangle = \mathbf{R}_Z(\alpha)\mathbf{R}_Y(\beta)\mathbf{R}_Z(\gamma)|\uparrow Z\rangle = \mathbf{R}_X(A)\mathbf{R}_Z(B)\mathbf{R}_X(G)|\uparrow X\rangle = \mathbf{R}_Y(a)\mathbf{R}_X(b)\mathbf{R}_Y(g)|\uparrow Y\rangle \tag{10.B.2}$$

A main-axis operator Z (for choice-A), X (for choice-B), or Y (for choice-C) sets overall phase of its particular favored number-1 state $|1\rangle$ of spin-up-Z, spin-up-X, or spin-up-Y, respectively.

$$|\Psi\rangle = \mathbf{R}_Z(\alpha)\mathbf{R}_Y(\beta)|\uparrow Z\rangle e^{-i\gamma/2} = \mathbf{R}_X(A)\mathbf{R}_Z(B)|\uparrow X\rangle e^{-iG/2} = \mathbf{R}_Y(a)\mathbf{R}_X(b)|\uparrow Y\rangle e^{-ig/2} \tag{10.B.3}$$

Each gives a *different* algebraic and numerical representation for the *same* general state $|\Psi\rangle$.

$$\substack{represented \\ in\,A-basis \\ by} \begin{pmatrix} e^{-i\frac{\alpha}{2}}\cos\frac{\beta}{2} \\ e^{i\frac{\alpha}{2}}\sin\frac{\beta}{2}\beta \end{pmatrix} e^{-i\frac{\gamma}{2}} \qquad \substack{represented \\ in\,B-basis \\ by} \begin{pmatrix} e^{-i\frac{A}{2}}\cos\frac{B}{2} \\ e^{i\frac{A}{2}}\sin\frac{B}{2} \end{pmatrix} e^{-i\frac{G}{2}} \qquad \substack{represented \\ in\,C-basis \\ by} \begin{pmatrix} e^{-i\frac{a}{2}}\cos\frac{b}{2} \\ e^{i\frac{a}{2}}\sin\frac{b}{2} \end{pmatrix} e^{-i\frac{g}{2}}$$

(10.B.4a)   (10.B.4b)   (10.B.4c)

Relating the three kinds of Euler angles begins by connecting the two spin-vector "polar angles"

$$(\alpha,\beta)\ related\ to\ (a,b)\ related\ to\ (A,B)\cdots$$

We cyclically permute the polar coordinates combinations *(cos_, sin_sin_, sin_cos_)* in (10.5.8c) and solve.

A or Z − based	C or Y − based	B or X − based	
$S_A = S_Z = \cos\beta$	$=S_Z = \sin b\cos a$	$=S_Z = \sin B\sin A$	
$S_C = S_Y = \sin\beta\sin\alpha$	$=S_Y = \cos b$	$=S_Y = \sin B\cos A$	(10.B.5)
$S_B = S_X = \sin\beta\cos\alpha$	$=S_X = \sin b\sin a$	$=S_X = \cos B$	

Fig. 10.B.1a below shows the three sets of (azimuth, polar) angles in the top-down-Z view. Arcs drawn are great circles except for two straight lines that meet the spin vector at the β, b, B triple intersection that are lesser circles at the base of a cone of constant X-polar angle B or constant Y-polar angle b, respectively.

The diagram shows ways to solve a common "spin-erection" problem, finding operations that return an arbitrary initial spin vector to one of the three main axes such as spin-up the Z axis, spin-up the

Y axis, or spin-up the X axis. This also suggests ways to classify and control optical polarization for an arbitrary state of elliptical polarization as will be shown a few pages ahead.
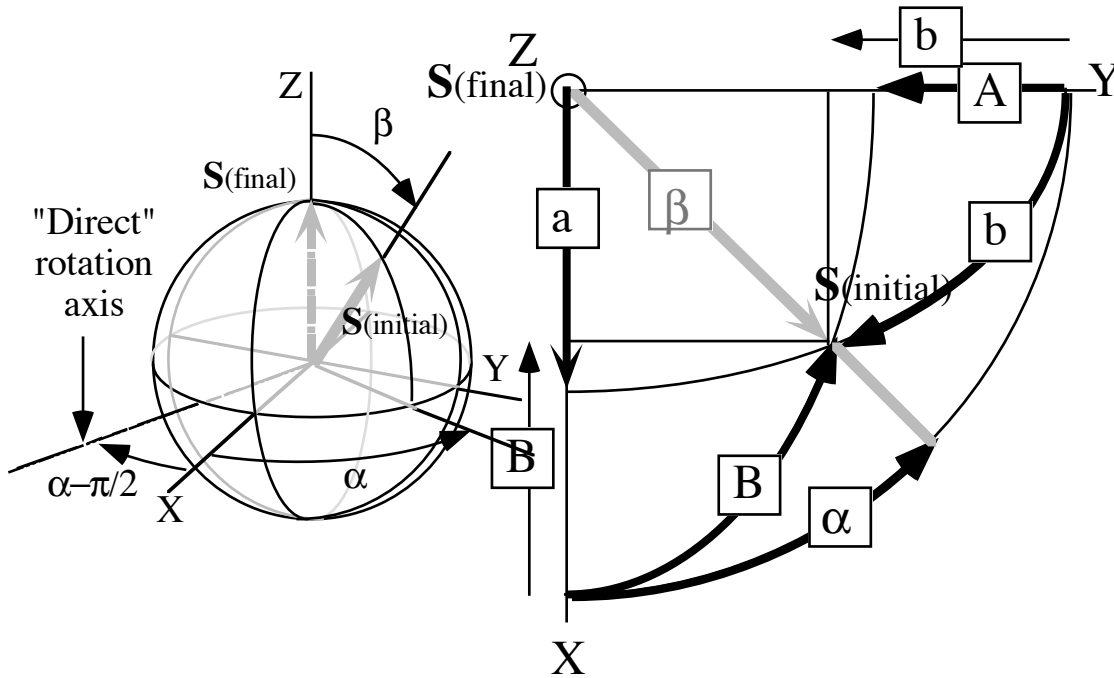

Fig. 10.B.1(a) Map of three different sets of Euler polar angles $(\alpha\beta\gamma)$ *, (abg), and (ABG).*

Three examples of ways to relate a state with an arbitrary spin $S(\alpha,\beta)$ to the state of spin-up-Z are sketched below in Fig. 10.B.1. The paths shown are all done using single or double applications of only X and Y generators $G_X = -iJ_X$ and $G_Y = -iJ_Y$ (or, in the first "direct" case, a linear combination of them) to relate the two states.

$$|S\rangle = R_{direct}[\beta]|\uparrow z\rangle = R_y(a)R_x(b-90°)|\uparrow z\rangle = R_x(A-90°)R_y(90°-B)|\uparrow z\rangle$$

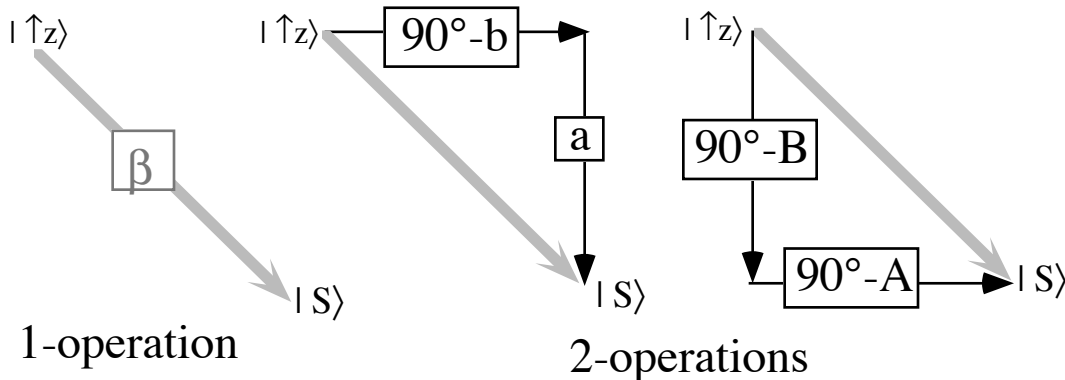1-operation   2-operations

Fig. 10.B.1(b) Map of 1-and 2-op transformations that connect spin-up-Z to an arbitrary spin state.

The "direct" rotation is done using an axis-angle rotation made from a crank vector lying in the *X-Y* plane with an azimuth of $\alpha-\pi/2$ as shown on the left hand side of Fig. 10.B.1a.

$$\mathbf{R}\left[\Theta\right] = \exp^{-i\left(\Theta\cos(\alpha-\pi/2)\mathbf{J}_X + \Theta\sin(\alpha-\pi/2)\mathbf{J}_Y\right)}, \text{ where: } \Theta = \beta \qquad (10.B.6a)$$

The resulting matrix is found from the axis-angle matrix (10.5.15).

$$\mathbf{R}\left[\beta\,direct\right] = \exp^{-i\left(\beta\sin\alpha\mathbf{J}_X - \Theta\cos\alpha\mathbf{J}_Y\right)} = \begin{pmatrix} \cos\dfrac{\beta}{2} & e^{-i\alpha}\sin\dfrac{\beta}{2} \\ -e^{i\alpha}\sin\dfrac{\beta}{2} & \cos\dfrac{\beta}{2} \end{pmatrix} \qquad (10.B.6b)$$

We check that the desired transformation "erects" a general spin state (10.A.1a) back to spin-up-*Z*.

$$\begin{pmatrix} \cos\dfrac{\beta}{2} & e^{-i\alpha}\sin\dfrac{\beta}{2} \\ -e^{i\alpha}\sin\dfrac{\beta}{2} & \cos\dfrac{\beta}{2} \end{pmatrix}\begin{pmatrix} \cos\dfrac{\beta}{2}e^{-i\alpha/2} \\ \sin\dfrac{\beta}{2}e^{i\alpha/2} \end{pmatrix}e^{-i\gamma/2} = \begin{pmatrix} e^{-i\alpha/2} \\ 0 \end{pmatrix}e^{-i\gamma/2} \qquad (10.B.6c)$$

Indeed, it does, and it does not change the phase $\phi = -(\alpha+\gamma)/2$ of the first component. This transformation is "twist-free" in the sense of moving a rigid body attached to spin vector **S** without changing the γ-dial. The other transformations in Fig. 10.B.1b will affect the overall phase differently. One may set a desired state and its overall phase to a particular value by applying the *X* and *Y* rotations <u>three</u> times, following paths like the ones in Fig. 10.B.2. The same can be done by a single operator made up of X, Y, and Z generators such that its crank vector Ω lies in the Z-S bisection plane and has an azimuthal angle measured from the "direct" rotation axis equal to the desired phase. This phase is related to the so-called the "Berry phase" but the geometry behind it goes back to the time of Thales of Miletus around *600 BCE*.
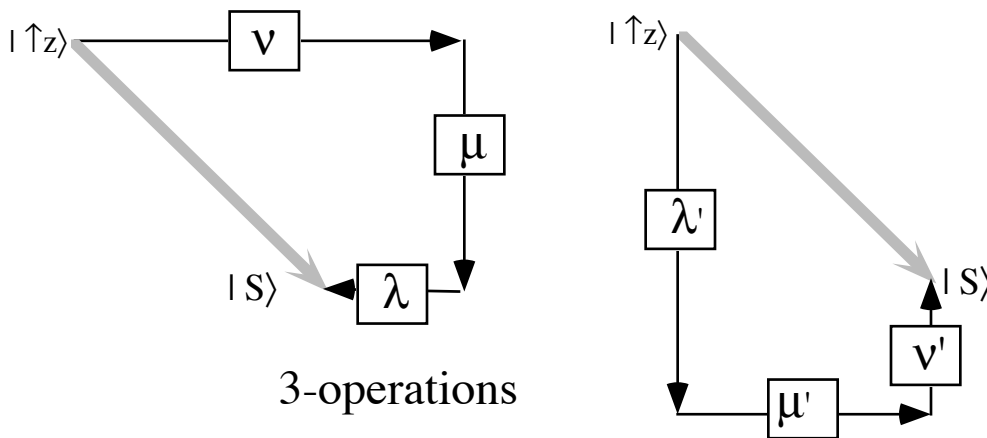

Fig. 10.B.2 Map of 3-op transformations that connect spin-up-Z to an arbitrary spin state and phase.

       A multitude of Euler angles may be used singly or together to give various kinds coordinates for photon polarization states. An (over complete) example is shown in Fig. 10.B.3 in which several competing types of angles are drawn at once to characterize the polarization ellipse. Perhaps, the most commonly used set of coordinates are the Faraday tip angle φ and elliptical shape angle ψ shown in Fig. 10.B.3a. Twice these angles $(2\varphi, 2\psi)$ or more precisely $(a=2\varphi, b=\pi/2-2\psi)$ are Y or *C*-based polar angles in *R(3)* space for the resulting spin vector **S**. In other words $(a=2\varphi, b=\pi/2-2\psi)$ are Euler angles (a,b) measured relative to the *Y*-axis or *C*-type basis of circular polarization states.

No less useful, however, are a set of coordinates $(2\vartheta, 2\nu)$ based upon the *Z*-axis or *A*-type basis of *x* and *y* plane polarization. These are the standard Euler angles (α, β) introduced previously. Not shown in the Fig. 10.B.3 is a third set of angles based upon the bilaterally symmetric *B*-type basis of $\pm 45°$ plane polarization states or NH_3 eigenstates. All these possible coordinates have varying advantages and disadvantages which depend on what Hamiltonian and physics is being studied.

(a)
Stokes Vector
ABC-Space

C

$|R\rangle$

Ω

S

$|y\rangle$

−B

−A

$\beta = 2\psi$

$\alpha = 2\varphi$

A

$|x\rangle$

B

I

$|L\rangle$

(b)
Polarization
xy-Space

$\sqrt{I}$ $|y\rangle$
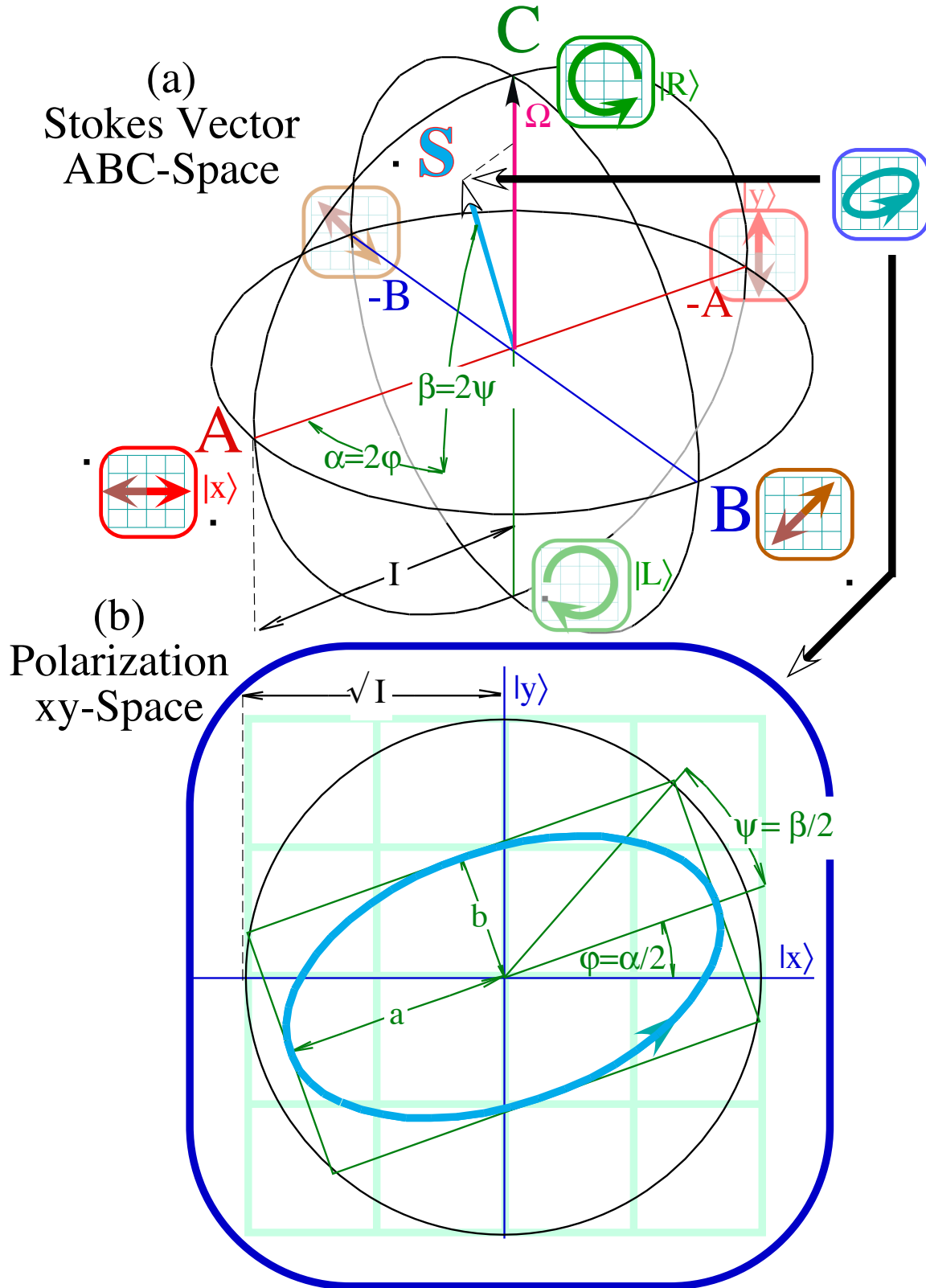
$\psi = \beta/2$

b

$\varphi = \alpha/2$

$|x\rangle$

a

Fig. 10.B.3 Examples of Euler-like coordinates for (a)U(2) polarization ellipse and (b)R(3) spin vector.

(a). Polarization ellipsometry coordinate angles

Optical polarization is analogous to the 2D-harmonic oscillator shown in Section 10.1. Polarization is usually defined by giving the real x and y electric field amplitudes.

$$\text{Re } E_x = \text{Re } \langle x|\Psi\rangle, \qquad\qquad \text{Re } E_y = \text{Re } \langle y|\Psi\rangle. \qquad\qquad (10.B.8)$$

The complex amplitudes $E_x = \langle x|\Psi\rangle$ and $E_y = \langle y|\Psi\rangle$ define the general *U(2)* polarization state.

$$|\Psi\rangle = |x\rangle\langle x |\Psi\rangle + |y\rangle\langle y |\Psi\rangle \qquad\qquad\qquad (10.B.9)$$

Re $\langle x |\Psi\rangle$ and Re $\langle y |\Psi\rangle$ are analogous to oscillator coordinates $x=x_1$ and $y=x_2$ as described by (10.1.1c). For an isotropic oscillator potential $V = k(x^2+y^2)/2$, the general orbit is an ellipse like the one shown in Fig. 10.B.3a. An isotropic oscillator corresponds to the $A=D$ and $B=0=C$ case of *U(2)* symmetry on the extreme left hand table in the catalog of 2-state symmetry of Fig. 10.4.2. Any ellipse or polarization state is an eigenstate of a Hamiltonian **H**$=A\mathbf{1}=D\mathbf{1}$, and any coordinate basis is equally convenient.

However, each lower symmetry case *A, AB, B, C,* or *U(1)* in Fig. 10.4.2 has definite eigenstates and coordinates that are most conveinient for its analysis. For example, $|\Psi\rangle$ can be written three ways

$$|\Psi\rangle = |x\rangle\langle x |\Psi\rangle + |y\rangle\langle y |\Psi\rangle = |+\rangle\langle + |\Psi\rangle + |-\rangle\langle - |\Psi\rangle = |r\rangle\langle r |\Psi\rangle + |\ell\rangle\langle \ell |\Psi\rangle, \qquad (10.B.10)$$

using eigenbasis of *A* (asymmetric diagonal), *B* (bilaterally symmmetric), or *C* (circular) Hamiltonians. The corresponding transformation matrices from plane *A*-type or *(x,y)* polarization are as follows.

$$\begin{pmatrix} \langle x|x\rangle & \langle x|y\rangle \\ \langle y|x\rangle & \langle y|y\rangle \end{pmatrix} = \begin{pmatrix} 1 & 0 \\ 0 & 1 \end{pmatrix} \qquad \begin{pmatrix} \langle x|+\rangle & \langle x|-\rangle \\ \langle y|+\rangle & \langle y|-\rangle \end{pmatrix} = \begin{pmatrix} \frac{1}{\sqrt 2} & \frac{1}{\sqrt 2} \\ \frac{1}{\sqrt 2} & \frac{-1}{\sqrt 2} \end{pmatrix} \qquad \begin{pmatrix} \langle x|r\rangle & \langle x|\ell\rangle \\ \langle y|r\rangle & \langle y|\ell\rangle \end{pmatrix} = \begin{pmatrix} \frac{1}{\sqrt 2} & \frac{1}{\sqrt 2} \\ \frac{i}{\sqrt 2} & \frac{-i}{\sqrt 2} \end{pmatrix}$$

$$\qquad (10.B.11a) \qquad\qquad\qquad (10.B.11b) \qquad\qquad\qquad (10.B.11c)$$

These are introduced in Sections 10.2a, b, and c, respectively. An intermediate case labeled *AB*-type polarization corresponds to plane polarization inclined at angle $\beta/2=\Theta$, as shown in Sec. 10.3 and Fig. 10.1.2ab. *AB*-transformation can be either a rotation matrix $R(\beta/2)=R[\Theta]$ or a reflection matrix $\sigma(\beta/2)$.

$$R(\frac{\beta}{2}) = R[\Theta] = \begin{pmatrix} \langle x|x_{AB}\rangle & \langle x|y_{AB}\rangle \\ \langle y|x_{AB}\rangle & \langle y|y_{AB}\rangle \end{pmatrix} \qquad\qquad \sigma(\frac{\beta}{2}) = \sigma[\Theta] = \begin{pmatrix} \langle x|x_{AB}\rangle & \langle x|\bar y_{AB}\rangle \\ \langle y|x_{AB}\rangle & \langle y|\bar y_{AB}\rangle \end{pmatrix}$$

$$= \begin{pmatrix} \cos\frac{\beta}{2} & -\sin\frac{\beta}{2} \\ \sin\frac{\beta}{2} & \cos\frac{\beta}{2} \end{pmatrix} = \begin{pmatrix} \cos\Theta & -\sin\Theta \\ \sin\Theta & \cos\Theta \end{pmatrix} \qquad = \begin{pmatrix} \cos\frac{\beta}{2} & \sin\frac{\beta}{2} \\ \sin\frac{\beta}{2} & -\cos\frac{\beta}{2} \end{pmatrix} = \begin{pmatrix} \cos\Theta & \sin\Theta \\ \sin\Theta & -\cos\Theta \end{pmatrix}$$

$$\qquad\qquad (10.B.12a) \qquad\qquad\qquad\qquad\qquad\qquad (10.B.12b)$$

The only difference is is the $\pm$-sign of the second column. A rotation has a determinate $det|R|=+1$ while a reflection has $det|\sigma|=-1$. $\sigma(\beta/2)$ belongs to *U(2)* but not *SU(2)*. Rotation $R(\beta/2)$ belongs to both.

Unit-determinant or unimodular *SU(2)* transformations are area or volume-preserving. This is sometimes an advantage, particularly if you are trying to apply $R(\Theta)$ to solid objects in a laboratory! But, light is easier to reflect than to rotate. Transformation (10.B.11b) is a reflection $\sigma[\pi/4]$ through a mirror plane half-way between *x* and *45°*-line. Transformation (10.B.11c) is also a refelection and not in *SU(2)*. From now on we use the following *SU(2) C-toA* transformation. Its phase differs from (10.2.23b).

$$\begin{pmatrix} \langle x|R\rangle & \langle x|L\rangle \\ \langle y|R\rangle & \langle y|L\rangle \end{pmatrix} = \begin{pmatrix} \dfrac{-1}{\sqrt{2}} & \dfrac{1}{\sqrt{2}} \\ \dfrac{-i}{\sqrt{2}} & \dfrac{-i}{\sqrt{2}} \end{pmatrix} \tag{10.B.13}$$

The difference is the sign of the *R*-column. (This is called a Condon-Shortely phase convention.)

(1) Type-A ellipsometry Euler angles

Now we define Euler-angle coordinates (following (10.A.1a)) for A-type linear polarization basis.

$$|\Psi\rangle = (Xe^{-i\vartheta}|x\rangle + Ye^{i\vartheta}|y\rangle)e^{-i\theta} = \sqrt{I}(\cos v\, e^{-i\vartheta}|x\rangle + \sin v\, e^{i\vartheta}|y\rangle)e^{-i\theta} \tag{10.B.14a}$$

Here the magnitudes of the E-field components are defined by an *A* or Z-based Euler polar angle $\beta=2v$.

$$X = \sqrt{I}\cos v = \sqrt{I}\cos \beta/2 = |E_x(\vartheta,v,\theta)| = |\langle x|\Psi\rangle| \tag{10.B.14b}$$

$$Y = \sqrt{I}\sin v = \sqrt{I}\sin \beta/2 = |E_y(\vartheta,v,\theta)| = |\langle y|\Psi\rangle| \tag{10.B.14c}$$

The real E-field components are defined by an *A* or Z-based Euler azimuthal angle $\alpha/2=\vartheta$ and overall phase angle $\gamma/2 = \theta$. (Note: Do not confuse ϑ or φ used below with axis-operator angles defined before.)

$$x_1 = \mathrm{Re}E_x(\vartheta,v,\theta) = \mathrm{Re}\langle x|\Psi\rangle = X\cos(\vartheta+\theta) \tag{10.B.14d}$$

$$x_2 = \mathrm{Re}E_y(\vartheta,v,\theta) = \mathrm{Re}\langle y|\Psi\rangle = Y\cos(\vartheta-\theta) \tag{10.B.14e}$$

Coordinates x_1 and x_2 trace an ellipse in a horizontial *2X*-by-*2Y* box where azimuth $\alpha=2\vartheta$ determines the orientation or shape of the ellipse in the box and overall phase angle $\gamma=2\theta$ ("twist") locates each orbiting point on the ellipse. The enclosing box aspect ratio *X:Y* is fixed by polar angle $\beta=2v$ in (10.B.14b-c).

Fig. 10.B.4 shows three cases which differ only by the angle $\alpha=2\vartheta$ which has value $\alpha=45°=2$ *(22.5°)* in the upper Fig. 10.B.4 and increases to $\alpha=90°$ and then $\alpha=180°$ in the successive lower figures. In each case, the box-diagonal angle $\beta/2 = v$ remains fixed at $v = 30°$ or $\beta=60°$.

The Stokes spin **S**-vector diagram for each polarization ellipse is drawn in ABC space on the right hand side of the figures. Note that polar angle of the **S**-vector remains fixed at $\beta= 2v =60°$ with respect to the A-axis, while the azimuth $\alpha=2\vartheta$ rotates from $\alpha=45°$ to $\alpha=90°$ and finally to $\alpha=180°$.

The α-evolution seen in Fig. 10.B.4 is an *A*-axis rotation similar to that which an *A*-type (asymmetric-diagonal) Hamiltonian would cause. If the precession rate $\Omega =\dot\alpha$ of the **S**-vector is much slower than phase angle "orbit" rate $\dot\gamma/2 = \dot\theta$ around the ellipse, then you can imagine an ellipse changing shape slowly. However, if the precession rate $\Omega=\dot\alpha$ becomes a significant fraction of the overall phase rate $\dot\gamma/2 = \dot\theta$ or actually exceeds it, then each ellipse is not given time to be fully drawn before shape-angle $\alpha=2\vartheta$ changes significantly. Fig. 10.2.2 is an example of such hyper-*A*-rotation.

In most optical polarization experiments so far, the overall phase rate for optical polarization evolution is hundreds of tera-Hertz and many times that of typical precession rates. However, modern experiments may not be so slow in changing the state of polarization.
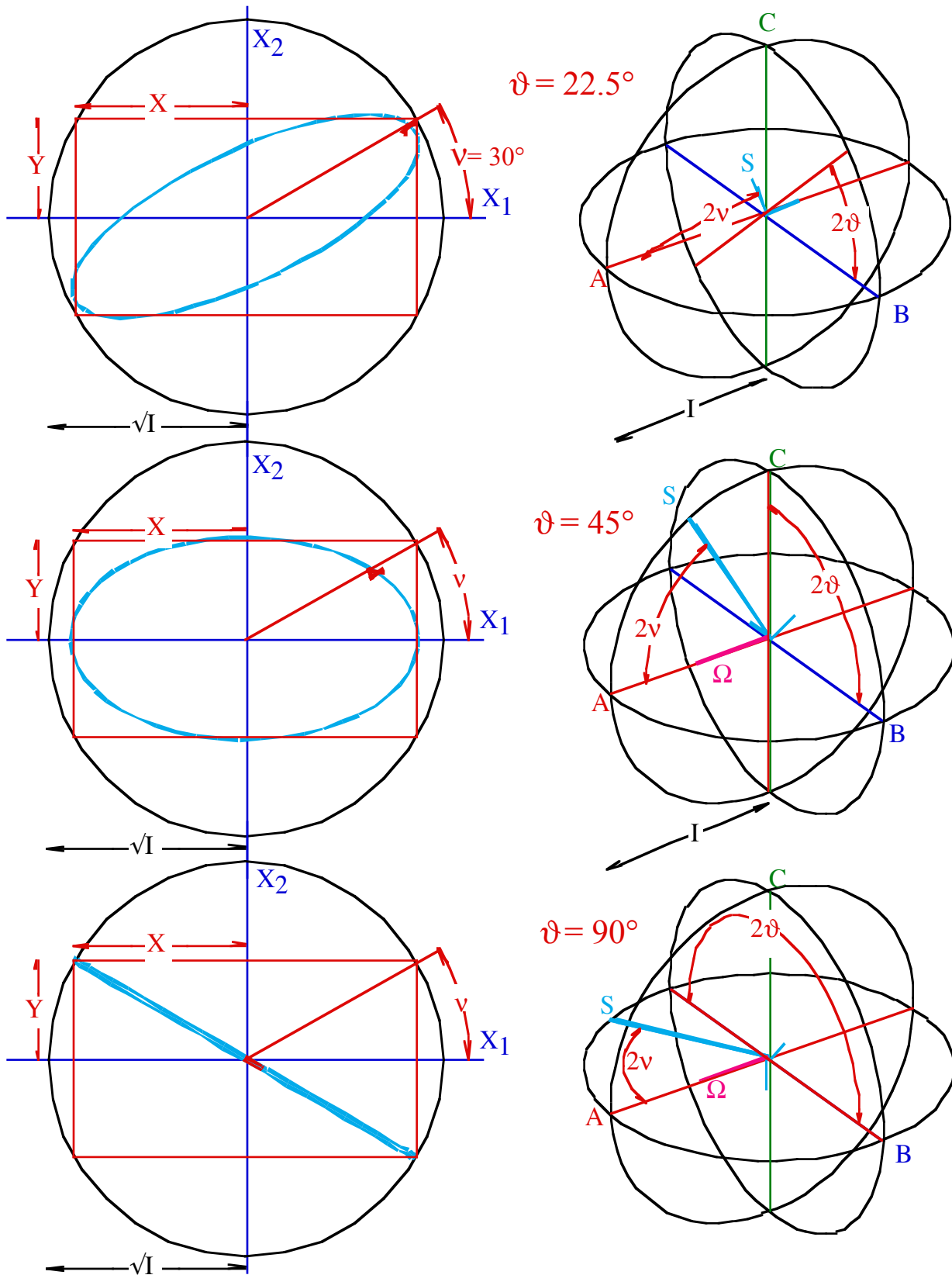
Fig. 10.B.4 A-Type polarization angles ($\alpha=2\vartheta, \beta=2\nu, \gamma=2\theta$) with rotation to $\alpha=45°$, 90°, and 180°.

(2) Type-C ellipsometry Euler angles

Now we define Euler-angle coordinates (following (10.A.1a)) for *C*-type linear polarization basis.

$$|\Psi\rangle = [Re^{-i\phi}|r\rangle + Le^{i\phi}|\ell\rangle]e^{-i\Phi} = [Re^{-i\phi}(|x\rangle+i|y\rangle)+ Le^{i\phi}(|x\rangle-i|y\rangle)]e^{-i\Phi}/\sqrt{2} \quad (10.B.15a)$$

The right and left circular bases $|r\rangle=(|x\rangle+i|y\rangle)/\sqrt{2}$ and $|\ell\rangle=(|x\rangle-i|y\rangle)/\sqrt{2}$ from (10.B.11c) are expanded.

$$|\Psi\rangle = [Re^{-i\phi} + Le^{i\phi}] |x\rangle e^{-i\Phi}/\sqrt{2} \qquad = [(R+L)\cos\phi - i(R-L)\sin\phi] |x\rangle(\cos\Phi-i\sin\Phi)/\sqrt{2}$$

$$+i[Re^{-i\phi} - Le^{i\phi}] |y\rangle e^{-i\Phi}/\sqrt{2} \qquad +i[(R-L)\cos\phi -i(R+L)\sin\phi] |y\rangle(\cos\Phi-i\sin\Phi)/\sqrt{2}$$

Separating the real and imaginary parts gives a ϕ-rotation transformation for each part.

$$|\Psi\rangle =[(R+L)\cos\phi \cos\Phi -(R-L)\sin\phi \sin\Phi - i(R+L)\sin\phi \sin\Phi-i(R-L)\sin\phi \cos\Phi] |x\rangle/\sqrt{2}$$

$$+[(R+L)\sin\phi \cos\Phi+(R-L)\cos\phi \sin\Phi+i(R+L)\cos\phi \cos\Phi-i(R+L)\sin\phi \sin\Phi] |y\rangle/\sqrt{2} \quad (10.B.15b)$$

The real *E*-field (x_1,x_2)-plots in Fig. 10.B.5 are thus given as follows

$$x_1=ReE_x(\phi,\psi,\Phi) = Re \langle x |\Psi\rangle = (a \cos\Phi)\cos\phi \ - \ (b \sin\Phi)\sin\phi \qquad (10.B.15c)$$

$$x_2=ReE_y(\phi,\psi,\Phi) = Re \langle y |\Psi\rangle = (a \cos\Phi)\sin\phi \ + \ (b \sin\Phi)\cos\phi \qquad (10.B.15d)$$

where the ellipse semi-major axis *a* and semi-minor axis *b* are defined using a new angle ψ.

$$a = (R + L)/\sqrt{2} = \sqrt{I} \cos \psi \qquad\qquad (10.B.15e)$$

$$b = (R - L)/\sqrt{2} = \sqrt{I} \sin \psi \qquad\qquad (10.B.15f)$$

The ellipse box aspect ratio *a:b* is defined by ψ, related below to a *C*-based Euler polar angle $b=\pi/2-2\psi$, just as the *X:Y* ratio is defined by an *A*-based Euler polar angle $\beta=2\nu$ in (10.B.14b-c). The real E-field components (x_1,x_2) are defined by a *C*-based Euler azimuthal angle $a=2\phi$ and overall phase angle $g/2=\Phi$. (10.B.15) are analogous to the defininition in (10.B.14d-e) by an *A*-based Euler azimuthal angle $\alpha=2\vartheta$ and an overall phase angle $\gamma/2 =\theta$. Furthermore, *C*-type evolution or *Faraday rotation* in Fig. 10.B.5 is rotation about the *C*-axis by azimuthal angle $a=2\phi$, just as *A*-type evolution in Fig. 10.B.4 was *A*-axial rotation by angle $\alpha=2\vartheta$. The latter is called *birefringence*.

Fig. 10.B.5 shows three cases differing only by the angle $a=2\phi$ which has value $a=30° =2(15°)$ in the upper Fig. 10.B.5 and increases to $a=90°$ and then $a=170°$ in the successive lower figures. In each case, the ellipse-box-diagonal angle $b/2 = \pi/4-\psi$ remains fixed at $\psi= 30°$ or $b=30°$ ($\psi=30°=b$ is just a coincidence!). As we will show, the *C*-axial Euler polar angle of the **S**-vector is $b=\pi/2-2\psi$, in general. The complimentary angle $2\psi=\pi/2-b=b_c$ is a spin polar *elevation* angle or *latitude*, not a polar angle.

As in Fig. 10.B.4, the objects in the real *ABC* **S**-vector 3-space move twice as fast as the ones in the complex $|\Psi\rangle$-spinor or polarization 2-space. Ellipse rotation by ϕ is a rotation of the **S**-vector by $a=2\phi$. The same applies to the overall phase angle Φ which is related by a factor of 2 with the Euler twist or "gauge" angle $g = 2\Phi$ around the **S**-vector axis. Examples of normal *(Φ>>ϕ)* and hyper-Faraday rotation *(Φ~ϕ)* are sketched in Fig. 10.2.10 and Fig. 10.2.11, respectively.

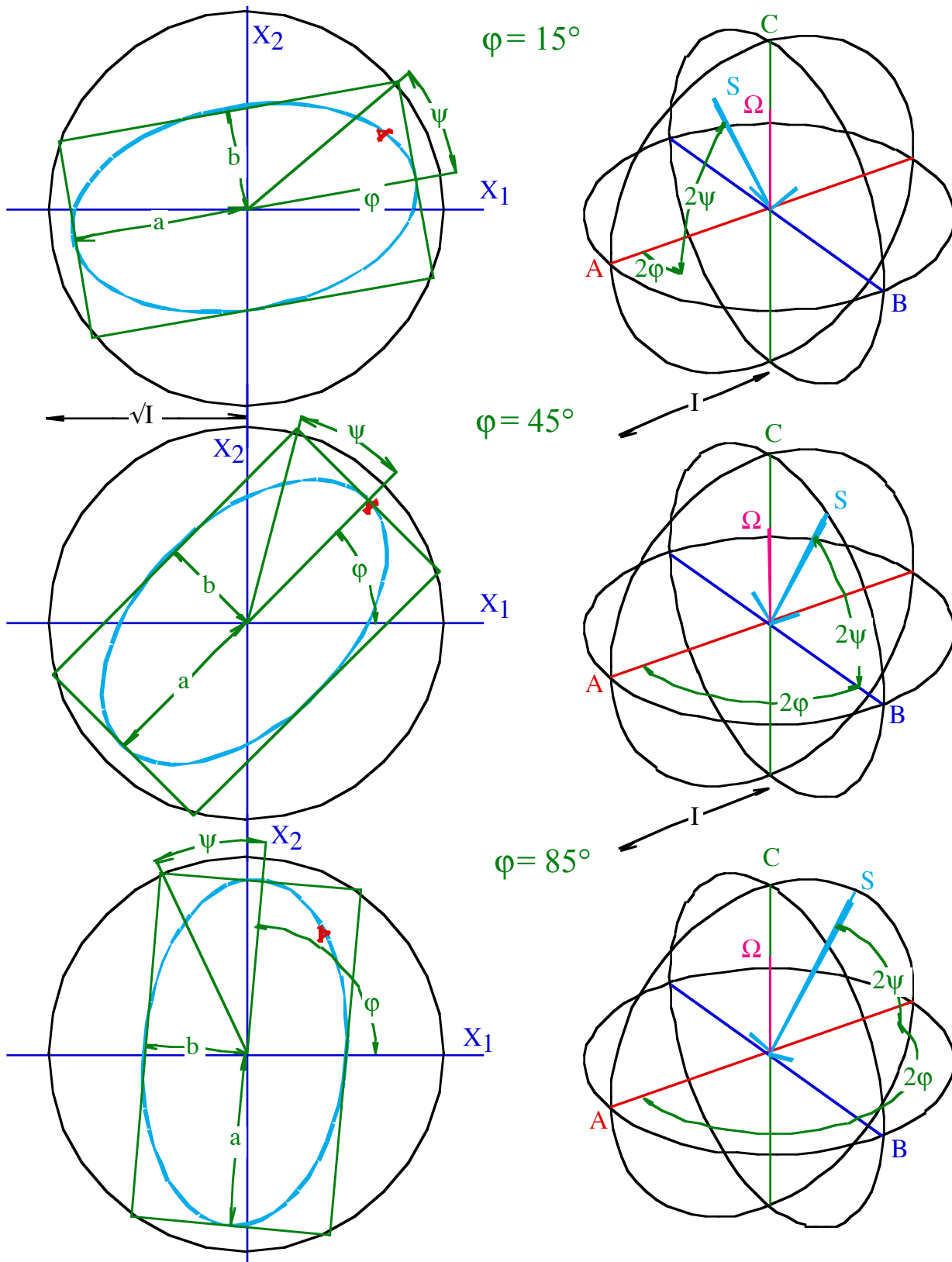*Fig. 10.B.5 C-Type polarization angles (a=2ϕ,b=π/2-2ψ ,g=2Φ) with C-axial rotation to a=30°, 90°, and 170°. Polar angle of S from C-axis is fixed at b=π/2-2ψ=30°.*

$\phi = 15°$

$\phi = 45°$

$\phi = 85°$

Fig. 10.B.5 C-Type polarization angles (a=2φ ,b=π/2-2ψ ,g=2Φ) with C-axial rotation to a=30°, 90°, and 170°. Polar angle of S from C-axis is fixed at b=π/2-2ψ=30°.

To define polar angles of the **S**-vector relative to *A*, *B*, or *C*-axes we can use the transformation relations given by (10.B.5). However, we need to be aware of the base changing transformations behind such shortcuts. For example, suppose we define *C*-axis as our true *Z*-axis of "up" and "down" so that

$$C(\sigma_N) = \begin{pmatrix} \langle r|\sigma_N|r\rangle & \langle r|\sigma_N|\ell\rangle \\ \langle \ell|\sigma_N|r\rangle & \langle \ell|\sigma_N|\ell\rangle \end{pmatrix} \tag{10.B.16}$$

is the following representation of the three Pauli (Hamilton) operators in the *C* (circular) basis $\{|r\rangle, |\ell\rangle\}$.

$$C(\sigma_A) = \begin{pmatrix} 0 & 1 \\ 1 & 0 \end{pmatrix} \quad (10.B.17a) \quad C(\sigma_B) = \begin{pmatrix} 0 & -i \\ i & 0 \end{pmatrix} \quad (10.B.17b) \quad C(\sigma_C) = \begin{pmatrix} 1 & 0 \\ 0 & -1 \end{pmatrix} \quad (10.B.17c)$$

This would be the conventional definition of $(\sigma_X, \sigma_Y, \sigma_Z) = (\sigma_A, \sigma_B, \sigma_C)$ of Pauli operators in that order with the third (σ_Z or σ_C) diagonal. In this text we have had σ_A be the diagonal one. But, in the *A* basis (Asymmetric diagonal or linear) σ_A is diagonal. A basis change by (10.B.11c) proves this as shown below.

$$L(\sigma_N) = \begin{pmatrix} \langle x|\sigma_N|x\rangle & \langle x|\sigma_N|y\rangle \\ \langle y|\sigma_N|x\rangle & \langle y|\sigma_N|y\rangle \end{pmatrix} = \begin{pmatrix} \langle x|r\rangle & \langle x|\ell\rangle \\ \langle y|r\rangle & \langle \ell|\ell\rangle \end{pmatrix} \begin{pmatrix} \langle r|\sigma_N|r\rangle & \langle r|\sigma_N|\ell\rangle \\ \langle \ell|\sigma_N|r\rangle & \langle \ell|\sigma_N|\ell\rangle \end{pmatrix} \begin{pmatrix} \langle r|x\rangle & \langle r|y\rangle \\ \langle \ell|x\rangle & \langle \ell|y\rangle \end{pmatrix}$$
$$= \quad T \cdot C(\sigma_N) \cdot T^\dagger \quad = \begin{pmatrix} 1/\sqrt{2} & 1/\sqrt{2} \\ i/\sqrt{2} & -i/\sqrt{2} \end{pmatrix} \begin{pmatrix} \langle r|\sigma_N|r\rangle & \langle r|\sigma_N|\ell\rangle \\ \langle \ell|\sigma_N|r\rangle & \langle \ell|\sigma_N|\ell\rangle \end{pmatrix} \begin{pmatrix} 1/\sqrt{2} & -i/\sqrt{2} \\ 1/\sqrt{2} & i/\sqrt{2} \end{pmatrix} \tag{10.B.18}$$

The following is the representation of the three operators in the *A* (linear) basis $\{|x\rangle, |y\rangle\}$.

$$L(\sigma_A) = \begin{pmatrix} 1 & 0 \\ 0 & -1 \end{pmatrix} \quad (10.B.19a) \quad L(\sigma_B) = \begin{pmatrix} 0 & 1 \\ 1 & 0 \end{pmatrix} \quad (10.B.19b) \quad L(\sigma_C) = \begin{pmatrix} 0 & -i \\ i & 0 \end{pmatrix} \quad (10.B.19c)$$

This has been the conventional representation for this text, so far. Relative to (10.B.17) it is a cyclic reordering $A \to B \to C \to A$, that is, a *120°* rotation around the [111] axis in *ABC*-space.

    σ_N-expectation values are basis-independent (provided the right representations are used for both the states and the operator!) Consider first the linear *A*-representations using (10.B.19) and (10.B.14).

$$\langle\Psi|\sigma_A|\Psi\rangle = \begin{pmatrix} Xe^{-i\vartheta} & Ye^{i\vartheta} \end{pmatrix}^* \begin{pmatrix} 1 & 0 \\ 0 & -1 \end{pmatrix} \begin{pmatrix} Xe^{-i\vartheta} \\ Ye^{i\vartheta} \end{pmatrix} = X^2 - Y^2 \tag{10.B.20a}$$

$$\langle\Psi|\sigma_B|\Psi\rangle = \begin{pmatrix} Xe^{-i\vartheta} & Ye^{i\vartheta} \end{pmatrix}^* \begin{pmatrix} 0 & 1 \\ 1 & 0 \end{pmatrix} \begin{pmatrix} Xe^{-i\vartheta} \\ Ye^{i\vartheta} \end{pmatrix} = 2XY\cos 2\vartheta \tag{10.B.20a}$$

$$\langle\Psi|\sigma_C|\Psi\rangle = \begin{pmatrix} Xe^{-i\vartheta} & Ye^{i\vartheta} \end{pmatrix}^* \begin{pmatrix} 0 & -i \\ i & 0 \end{pmatrix} \begin{pmatrix} Xe^{-i\vartheta} \\ Ye^{i\vartheta} \end{pmatrix} = 2XY\sin 2\vartheta \tag{10.B.20b}$$

Now do the same values in the circular *C*-representations using (10.B.17) and (10.B.15).

$$\langle\Psi|\sigma_A|\Psi\rangle = \begin{pmatrix} Re^{-i\varphi} & Le^{i\varphi} \end{pmatrix}^* \begin{pmatrix} 0 & 1 \\ 1 & 0 \end{pmatrix} \begin{pmatrix} Re^{-i\varphi} \\ Le^{i\varphi} \end{pmatrix} = 2RL\cos 2\varphi = (a^2 - b^2)\cos 2\varphi \tag{10.B.21a}$$

$$\langle\Psi|\sigma_B|\Psi\rangle = \begin{pmatrix} Re^{-i\varphi} & Le^{i\varphi} \end{pmatrix}^* \begin{pmatrix} 0 & -i \\ i & 0 \end{pmatrix} \begin{pmatrix} Re^{-i\varphi} \\ Le^{i\varphi} \end{pmatrix} = 2RL\sin 2\varphi = (a^2 - b^2)\sin 2\varphi \tag{10.B.21b}$$

$$\langle\Psi|\sigma_C|\Psi\rangle = \begin{pmatrix} \text{R}e^{-i\varphi} & Le^{i\varphi} \end{pmatrix}^* \begin{pmatrix} 1 & 0 \\ 0 & -1 \end{pmatrix} \begin{pmatrix} \text{R}e^{-i\varphi} \\ Le^{i\varphi} \end{pmatrix} = R^2 - L^2 = 2ab \qquad (10.B.21c)$$

Equating A-defined and C-defined **S**-vector components $S_N = \langle\Psi|\sigma_N|\Psi\rangle$ relates A-based and C-based Euler angles. Use A-definitions (10.B.14) and C-definitions (10.B.15) as follows.

S-vector	A	Linear Basis	C	Circular Basis
$\langle\Psi|\sigma_A|\Psi\rangle =$	$X^2 - Y^2$ $=$	$I\cos 2v$	$= 2RL\cos 2\varphi =$	$(a^2 - b^2)\cos 2\varphi = I\cos 2\psi \ \cos 2\varphi$
$\langle\Psi|\sigma_B|\Psi\rangle =$	$2XY\cos 2\vartheta$ $= I\cos 2\vartheta \ \sin 2v$		$= 2RL\sin 2\varphi =$	$(a^2 - b^2)\sin 2\varphi = I\cos 2\psi \ \sin 2\varphi$
$\langle\Psi|\sigma_C|\Psi\rangle =$	$2XY\sin 2\vartheta$ $= I\sin 2\vartheta \ \sin 2v$		$= R^2 - L^2$ $=$	$2ab$ $= I\sin 2\psi$
$\langle\Psi|1|\Psi\rangle =$	$X^2 + Y^2 =$	I	$= R^2 + L^2$ $=$	$a^2 + b^2$

(10.B.22)

First notice how the polar coordinates for the C-basis are defined in the right-most column of (10.B.22). The C-azimuth plane projection is *(I cos2ψ cos2φ, I cos2ψ sin2φ)* while the main C-axial projection is *I sin2ψ* . This is different from the A-basis defined in the middle column of (10.B.22) with A-azimuth plane projection is *(I sin2v cos2ϑ, I sin2v sin2ϑ)* while the main A-axial projection is *I cos2v* .

For A-bases angle $\beta = 2v$ is a true polar angle measured from the main A-axis as shown in Fig. 10.B.4. For C-bases angle $b_C = 2\psi$ is an elevation angle or complement $b_C = \pi/2 - b$ of a true polar angle $b = \pi/2 - 2\psi$ measured from the main C-axis as shown in Fig. 10.B.5. This is consistent with (10.B.5) which relates Euler polar angles β, b, and B.

The C-component of the **S**-vector is an oscillator or *"photon" angular momentum* component

$$S_C = I(xp_y - yp_x) = I(x_1 p_2 - x_2 p_1) = 2ab = R^2 - L^2 \qquad (10.B.23)$$

according to fundamental definitions (10.5.8c). Comparing this to (10.B.22) above shows that S_C is proportional to the area πab of the polarization ellipse. This makes the C-axis or Z-axis the important one in angular momentum theory which will be treated in later chapters. Given the importance of *U(2)>R(3)* isotropy and the quantum theory of angular momentum in atomic and nuclear physics, this probably explains why the Pauli representation (10.B.17) is the most widely accepted convention.

However, for anisotropic condensed matter the A-axis (which we have up to now called the Z-axis) has an important *anisotropy* or *Stark-Splitting* component.

$$S_A = I(x_1^2 + p_1^2 - x_2^2 - p_2^2) = X^2 - Y^2 \qquad (10.B.24)$$

Maximum or minimum values of the A-component correspond to pure x or pure y polarization just as maximum or minimum values of the C-component correspond to pure R or pure L polarization. Development of the bilateral or B-component and coordination is left as an exercise.

Transformations which change the bases-of-choice or quantization axis from A to B or C belong to a dual or "external" *U(2)* group that commutes with the *U(2)* group from which Hamiltonian and evolution operators are made. Dual symmetry is an important topic which will be introduced in Chapter 15 and applied again in Chapters 24, 25, and 30.

(b) Beam evolution of polarization

Evolution of optical polarization is often a function of distance z along a propagating beam. The evolution is described classically by Maxwell's equations which are second order in position.

$$\nabla^2\mathbf{E} - \nabla\left(\nabla\bullet\mathbf{E}\right) = \frac{1}{c^2}\frac{\partial^2\mathbf{E}}{\partial t^2} + \frac{1}{c^2\varepsilon_0}\frac{\partial^2\mathbf{P}}{\partial t^2} \qquad \text{where: } \mathbf{P} = \varepsilon_0\tilde{\alpha}\bullet\mathbf{E} \qquad (10.\text{B}.25)$$

This simplifies if all field $\mathbf{E}$ and polarization vectors $\mathbf{P}$ are in the x-y direction transverse to beam line z. The *polarizability* α-*tensor* relation is then two-dimensional.

$$\mathbf{P} = \varepsilon_0\tilde{\alpha}\bullet\mathbf{E} \qquad \text{becomes: } \frac{1}{\varepsilon_0}\begin{pmatrix} P_x \\ P_y \end{pmatrix} = \begin{pmatrix} \alpha_{xx} & \alpha_{xy} \\ \alpha_{yx} & \alpha_{yy} \end{pmatrix}\begin{pmatrix} E_x \\ E_y \end{pmatrix} \qquad (10.\text{B}.26)$$

Furthermore, we assume single frequency vector amplitudes depend on the z-coordinate only

$$\mathbf{P}(z,t) = \mathbf{P}(z)e^{-i\omega t}, \qquad\qquad \mathbf{E}(z,t) = \mathbf{E}(z)e^{-i\omega t}$$

Maxwell's equations simplify under the preceding conditions.

$$\frac{\partial^2}{\partial z^2}\begin{pmatrix} \langle x|\phi(z)\rangle \\ \langle y|\phi(z)\rangle \end{pmatrix} = -\frac{\omega^2}{c^2}\begin{pmatrix} 1+\alpha_{xx} & \alpha_{xy} \\ \alpha_{yx} & 1+\alpha_{yy} \end{pmatrix}\begin{pmatrix} \langle x|\phi(z)\rangle \\ \langle y|\phi(z)\rangle \end{pmatrix}, \qquad (10.\text{B}.27\text{a})$$

where the complex polarization field is related to the real E-field.

$$\text{Re}\begin{pmatrix} E_x(z) \\ E_y(z) \end{pmatrix} = \text{Re}\begin{pmatrix} \langle x|\phi(z)\rangle \\ \langle y|\phi(z)\rangle \end{pmatrix} \qquad (10.\text{B}.27\text{b})$$

The forward propagating wave solutions are used in the simplest beam approximation.

$$\begin{pmatrix} \langle x|\phi(z)\rangle \\ \langle y|\phi(z)\rangle \end{pmatrix} = e^{iz\begin{pmatrix} k_{xx} & k_{xy} \\ k_{yx} & k_{yy} \end{pmatrix}}\begin{pmatrix} \langle x|\phi(0)\rangle \\ \langle y|\phi(0)\rangle \end{pmatrix} \qquad (10.\text{B}.28\text{a})$$

A *wave-vector matrix* $\mathbf{k}$ is the doubly-positive (++) square root of the *susceptability tensor* $\chi = 1+\alpha$..

$$\begin{pmatrix} k_{xx} & k_{xy} \\ k_{yx} & k_{yy} \end{pmatrix} = \frac{\omega}{c}\begin{pmatrix} 1+\alpha_{xx} & \alpha_{xy} \\ \alpha_{yx} & 1+\alpha_{yy} \end{pmatrix}^{1/2}_{(+,+)} = \frac{\omega}{c}\left(+\sqrt{\chi_1}\mathbf{P}_{\chi_1} + \sqrt{\chi_2}\mathbf{P}_{\chi_2}\right) \qquad (10.\text{B}.28\text{b})$$

In the absence of absorption or gain the eigenvalues (χ_1,χ_2) of χ are assumed positive-real while the matrix $\mathbf{k}$ and the projectors $\mathbf{P}_{\chi_1}$ and $\mathbf{P}_{\chi_2}$ of χ and $\mathbf{k}$ are assumed all to be Hermitian. $(\mathbf{k}^\dagger = \mathbf{k})$

$$P_{\chi_1} = \frac{\begin{pmatrix} \chi_{xx} - \chi_2 & \chi_{xy} \\ \chi_{yx} & \chi_{yy} - \chi_2 \end{pmatrix}}{\chi_1 - \chi_2}, \qquad P_{\chi_2} = \frac{\begin{pmatrix} \chi_{xx} - \chi_1 & \chi_{xy} \\ \chi_{yx} & \chi_{yy} - \chi_1 \end{pmatrix}}{\chi_2 - \chi_1} \qquad (10.B.28c)$$

In this approximation the spatial *z*-evolution (10.B.28a) due to e^{ikz} proceeds quite analogously with the temporal *t*-evolution due to a Hamiltonian $e^{-iHt/\hbar}$ discussed previously. One difference is that a positive **k** will correspond to a negative or *clock*wise $\Omega = -|\Omega|$ crank motion in *ABC*-space. (As you move down the beam you are effectively "undoing" time ωt and looking at what has already passed you.) Also, time enters here as a simple overall $e^{-i\omega t}$ phase contribution to give a polarization wave operator $e^{ikz-i\omega t}$. The opposite moving wave $e^{-ikz-i\omega t}$ is assumed zero. Interference of counter-propagating waves is studied in the next unit.

Problems for Appendix 10.A and B

Euler Can Canonize
10.A.1 An 2D-oscillator canonical phase state-(x_1, p_1, x_2, p_2) and a spin-state-$|\alpha, \beta, \gamma\rangle$ are both defined by the Euler angles (α, β, γ) through (10.A.1a-b) as well as by axis angles $[\varphi, \vartheta, \Theta]$ through (10.A.1c). (First, verify all parts of (10.A.1).) If rotation-axis-Θ polar angles $[\varphi, \vartheta]$ are fixed while rotation angle $\Theta = \Omega t$ varies uniformly with time, Euler angles (α, β, γ) and phase point (x_1, p_1, x_2, p_2) trace spin and oscillator trajectories, respectively. Verify this for the following cases by discussing plots requested below.
(a) $[\varphi=0, \vartheta=0]$, (b) $[\varphi=0, \vartheta=\pi/2]$, (c) $[\varphi=\pi/2, \vartheta=\pi/2]$, (d) $[\varphi=0, \vartheta=\pi/4]$, (e) $[\varphi=\pi/2, \vartheta=\pi/4]$.
For each case sketch 2D-paths -p_1 vs. x_1 and x_2 vs. x_1 and sketch $\hat{\Theta} \sin\Theta/2$ in a 3D (-p_2,x_2,-p_1)-space which should also have paths for –p_2 vs. x_2 and x_2 vs. -p_1 etc. Also, indicate the paths followed by the tip of the **S**-spin-vector (10.5.8c) in 3D-spin space (S_X, S_Y, S_Z) and characterize as A-type, B-type, or C-type motion, etc., in each case.

Invariantipodals
10.A.2 When an Euler sphere is rotated from origin $|1\rangle$ state $(0=\alpha=\beta=\gamma)$ to some angles (α, β, γ), there are always points on the sphere which end up exactly where they were before the rotation. Verify this and express the polar-coordinates (ϕ,θ) of all such invariant points in terms of (α, β, γ).

Spinor-Vector-Rotor
10.A.3 Prove and develop the result (10.A.15) as described below.

$$\mathbf{R}[\vec{\Theta}]\sigma_L \mathbf{R}[\vec{\Theta}]^\dagger = \left(\cos\frac{\Theta}{2}\mathbf{1} - i\sin\frac{\Theta}{2}\hat{\Theta}_K\sigma_K\right)\sigma_L\left(\cos\frac{\Theta}{2}\mathbf{1} - i\sin\frac{\Theta}{2}\hat{\Theta}_N\sigma_N\right)^\dagger$$

$$= \sigma_L' = \sigma_L\cos\Theta - \varepsilon_{LKM}\hat{\Theta}_K\sigma_M\sin\Theta + (1-\cos\Theta)\hat{\Theta}_L\left(\hat{\Theta}_N\sigma_N\right)$$

(a) Using the σ-product definitions and the Levi-Civita tensor identity
$$\varepsilon_{abc}\varepsilon_{dec} = \delta_{ad}\delta_{be} - \delta_{ae}\delta_{bd} \quad \text{(Prove this, too!)}$$
to derive the above result. (Equation (10.A.15))
(b) Check if the above result (Eq. (10.A.15a)) yields Eq. (10.A.15b) and sketch the resulting vectors Θ and $\mathbf{e}_L$ (before rotation) and $\mathbf{e'}_L$ (after rotation) for a rotation of $\mathbf{e}_z$ by $\Theta=120°$ around an axis with polar angle $\vartheta=54.7° = arcos(1/\sqrt{3})$ and azimuthal angle $\varphi=45°$. (As is conventional, we measure polar angles off the *Z*(or *A*) axis and azimuthal angles from the *X*(or *B*) axis counter clockwise in the *XY* (or *BC*) plane. What semi-famous-name axis is this Θ? Give Cartesian coordinates.)
(b) Use the above to write down a general 3-by-3 matrix in terms of axis angles $[\varphi, \vartheta, \Theta]$, and test it using angles in (b).

(c) Derive the Euler angles (α, β, γ) for this rotation matrix.
(d) Compare formulas and numerics for 3-by-3 R(3) matrices to the corresponding 2-by-2 U(2) matrices for the same rotations.
(e) Find 3-by-3 R(3) and 2-by-2 U(2) matrices for rotation $\mathbf{R}_y$ by 90° around *Y* (or *C*)-axis.
(f) Do products $\mathbf{R}_y\mathbf{R}[\varphi, \vartheta, \Theta]$ and $\mathbf{R}[\varphi, \vartheta, \Theta]\mathbf{R}_y$ numerically and check with product formula (10.A.10). Describe results.

_____

Spinor-Vector-Rotor Polarized

10.B.1. Suppose a Hamiltonian **H** has an Ω-vector pointing along the Θ-vector in a preceding problem 10.A.3b. Here we will let $\hbar=1$, and let $\Theta=\Omega t$ with $\Theta=2\pi/3$ at $t=1$.

    (a) Write down the 2-by-2 Hamiltonian matrix **H**.

    (b) Give at least two sets of values for Euler angles which give an eigenstate of **H**.

    (c) Write out the corresponding complex *U(2)* eigenstates of **H** obtained using (b) and sketch their polarization ellipse-orbit (the real spinor space picture), U(2) phasor picture, and **S**-vectors.

    (d) Describe what happens to the initial A-state $|\Psi(t=0)\rangle = |x\rangle$ (x-polarization or spin-up) given this Hamiltonian **H**. Does $|\Psi(t)\rangle$ ever return 100% to $|x\rangle$?

    (e) Does x-polarization ever get close to y-(-A)-polarization? …45°-(B)-polarizaton? …R-(C)-polarizaton? How long does it take to get from $|\Psi(t=0)\rangle$ to the closest approach to each?

Spin erection. Does it phase U(2)?

10.B.2. The following general problem may certainly become relevant if the mythical quantum computer materializes. It involves erecting an arbitrary state with spin vector **S** to the spin-up Z (or A) position with a particular overall phase Φ. In each case make the description of your solution as simple as possible as though you needed to explain it to engineers.

    (a) For a state of 0-phase with spin on the X (or B), describe a single operator that does the above.

    (b) For a state of 0-phase with spin at β in the XZ (or AB) plane, describe a single operator that does the above.

The trouble with ϑ

10.B.3. The polarization angle ϑ defies placement in the U(2) diagram of Fig. 10.B.3. (That is, it's not there!) Is it easier to locate if $\nu=45°=\varphi$? Discuss contact points on XY box. Let a cardboard cut-out ellipse of a given I and ν rotate 360° on the floor in the corner of a room always tangent to two walls. What simple curve does its center describe? Does it change radically as $\nu\to0$? (It's a lot easier to answer this using U(2) ellipse geometry than by algebraic machination.)

Strange susceptibility

10.B.4. A solid has an xy-susceptibility tensor $\dfrac{\omega^2}{c^2}(1+\ddot{\alpha}) = \begin{pmatrix} 1.8 & -0.9+0.9i \\ -0.9-0.9i & 2.7 \end{pmatrix}$ for a z-beam.

    (a) Derive (φ,ψ) and sketch ellipses for all polarization states whose ellipses go unchanged.

    (b) A circular $|R\rangle$-state $(\nu=45°)$ enters at z=0. Discuss its z-evolution. How far is a "π-pulse" (Half-wave plate or π rotation of **S**)?

To B or not

10.B.5. A B-axial description applies to NH_3 states or a $\pm45°$ polarization eigenvector medium. First, write the form of the B-type (bilaterally symmetric) Hamiltonian or xy-susceptability tensor.

    (a) Given an algebraic description of U(2) bases and R(3) spin vectors using B-type Euler angles (A,B,G).

    (b) Give a geometric sketch of U(2) ellipses and R(3) spin vectors like Fig. 10.B.4-5 as they might evolve under a B-type Hamiltonian or susceptibility tensor. Start with the case $(\varphi=45°, \psi=30°, \Phi=0°)$ in center of Fig. 10.B.5, convert it to (A,B,G) angles, then sketch result of subsequent 45°, 90°, and 180° rotations of **S** around B-axis.